

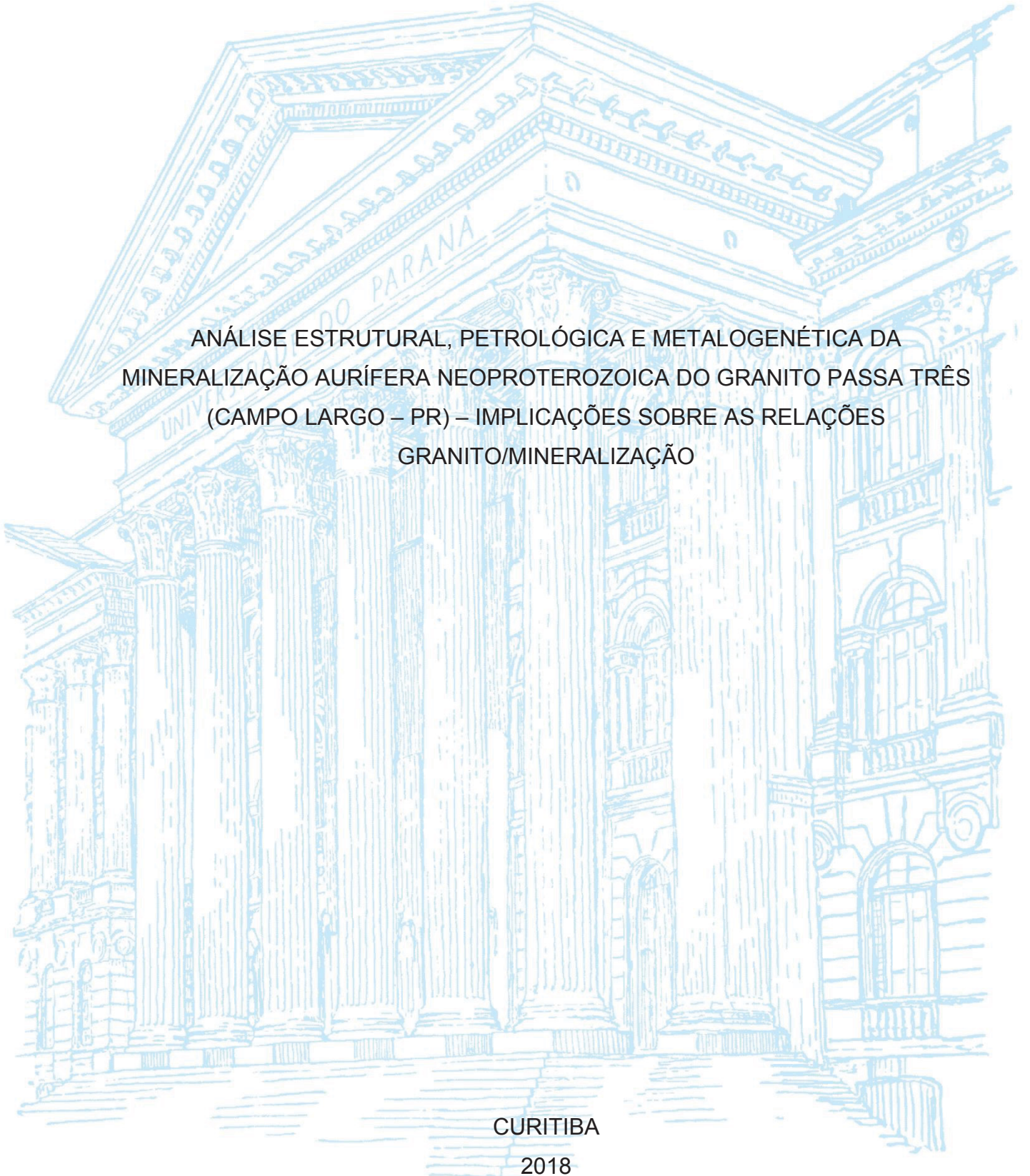
UNIVERSIDADE FEDERAL DO PARANÁ

BÁRBARA CAROLINA DRESSEL

ANÁLISE ESTRUTURAL, PETROLÓGICA E METALOGENÉTICA DA
MINERALIZAÇÃO AURÍFERA NEOPROTEROZOICA DO GRANITO PASSA TRÊS
(CAMPO LARGO – PR) – IMPLICAÇÕES SOBRE AS RELAÇÕES
GRANITO/MINERALIZAÇÃO

CURITIBA

2018



BÁRBARA CAROLINA DRESSEL

ANÁLISE ESTRUTURAL, PETROLÓGICA E METALOGENÉTICA DA
MINERALIZAÇÃO AURÍFERA NEOPROTEROZOICA DO GRANITO PASSA TRÊS
(CAMPO LARGO – PR) – IMPLICAÇÕES SOBRE AS RELAÇÕES
GRANITO/MINERALIZAÇÃO

Tese apresentada como requisito parcial ao grau de Doutora em Geologia, no curso de Pós-Graduação em Geologia, área de concentração em Geologia Exploratória, Setor de Ciências da Terra, Universidade Federal do Paraná

Orientadores: Profª Drª Barbara Trzaskos
Pesquisador Dr. Alain Chauvet

CURITIBA

2018

Catálogo na Fonte: Sistema de Bibliotecas, UFPR
Biblioteca de Ciência e Tecnologia

D773a

Dressel, Bárbara Carolina

Análise estrutural, petrológica e metalogenética da mineralização aurífera neoproterozoica do Granito Passa Três (Campo Largo – PR) – implicações sobre as relações granito/mineralização [recurso eletrônico] / Bárbara Carolina Dressel. – Curitiba, 2018.

Tese - Universidade Federal do Paraná, Setor de Ciências da Terra, Programa de Pós-Graduação em Geologia, 2018.

Orientador: Barbara Trzaskos – Coorientador: Alain Chauvet.

1. Alteração hidrotermal. 2. Quartzo. 3. Granito Passa Três (PR). I. Universidade Federal do Paraná. II. Trzaskos, Barbara. III. Chauvet, Alain. IV. Título.

CDD: 551.71098162

Bibliotecário: Elias Barbosa da Silva CRB-9/1894

TERMO DE APROVAÇÃO

Os membros da Banca Examinadora designada pelo Colegiado do Programa de Pós-Graduação em GEOLOGIA da Universidade Federal do Paraná foram convocados para realizar a arguição da tese de Doutorado de **BARBARA CAROLINA DRESSEL** intitulada: **ANÁLISE ESTRUTURAL, PETROLÓGICA E METALOGENÉTICA DA MINERALIZAÇÃO AURÍFERA NEOPROTEROZOICA DO GRANITO PASSA TRÊS (CAMPO LARGO - PR) - IMPLICAÇÕES SOBRE AS RELAÇÕES GRANITO/MINERALIZAÇÃO**, após terem inquirido a aluna e realizado a avaliação do trabalho, são de parecer pela sua APROVAÇÃO no rito de defesa.

A outorga do título de doutor está sujeita à homologação pelo colegiado, ao atendimento de todas as indicações e correções solicitadas pela banca e ao pleno atendimento das demandas regimentais do Programa de Pós-Graduação.

CURITIBA, 27 de Julho de 2018.



BÁRBARA TRZASKOS
Presidente da Banca Examinadora



MANUEL MUNOZ
Avaliador Externo



LENA VIRGÍNIA SOARES MONTEIRO
Avaliador Externo



CARLOS EDUARDO DE MESQUITA BARROS
Avaliador Interno



PHILIPPE GONÇALVES
Avaliador Externo



ALAIN CHAUVET
Avaliador Externo

AGRADECIMENTOS/REMERCIEMENTS

Gostaria de agradecer primeiramente pelo apoio e pela compreensão da minha família, por aceitar minha ausência em muitos momentos. Agradeço ao meu pai, minha mãe, meus irmãos e minhas cunhadas, minha avó, que me escutaram muito ao longo dos quatro anos da tese.

Agradeço também à Mineração Tabiporã, pelo apoio de campo e disponibilidade de pesquisa na Mina do Morro, em especial ao Seu Alfredo e ao Luiz. Gostaria de agradecer também ao Clóvis e, especialmente, aos geólogos José Bazille e Sandro Villanova, pelo apoio essencial em todas as fases desse projeto, e pelas ricas discussões e pelo conhecimento e experiência compartilhados.

Na Universidade Federal do Rio Grande do Sul (UFRGS), gostaria de agradecer ao Prof. Dr. Edinei Koester, do Laboratório de Geologia Isotópica, e à Prof. Maria de Fátima Bittencourt, pelas conversas iniciais sobre deformação submagmática. Agradeço também ao Marcelo e à Denise, e, especialmente a Daiane Francis, que já mudou de continente, mas se dispôs a uma semana de preparação de amostras no moinho de discos em Porto Alegre!

Na UFPR, muitas pessoas me auxiliaram em várias fases desse projeto. Gostaria de agradecer ao pessoal do Labap (Danielle Schemiko, Amanda Carvalho, Renata Zanella, Fábio Berton, Coxinha, Thammy, Aurora, Mérolyn, Ronaldo), pelas conversas nos intervalos e palavras de incentivo, em especial ao Fernando Vesely pelo apoio principalmente no início do processo de cotutela. Ao pessoal da pós, agradeço a Camila, Mayara e Rhander, pelas conversas e companheirismo!!

Agradecimento especial ao Lamir, pelo apoio essencial em diversas fases desse trabalho. Gostaria de agradecer, a Elisiane, Rodrigo, Keiji, Francielle, Isis, Bruno Titon, Jéssica Oste, Annelise Bahniuk, Ivan, Roberto, Daniel, Larissa, Lara, Veleda, que auxiliaram de diversas formas ao longo do projeto, tanto como apoio técnico, como com palavras de incentivo. Em especial Eleonora Vasconcelos e Leonardo Cury pela disponibilidade do laboratório, e ao Guilherme Fedalto, pelo companheirismo, palavras de incentivo e auxílio indispensável com as inclusões fluidas e com a Linkam.

No Programa de Pós-graduação em Geologia – UFPR, gostaria de agradecer ao Kazu, Maria Cristina, Cadu, e ao programa pelo apoio. Ao Departamento de Geologia e à Capes, pela bolsa durante a estadia no Brasil e pela bolsa de doutorado-sanduiche (Capes-PDSE Processo n. 99999.006489/2015-00; CAPES, Ministério da Educação, Brasília - DF, 70.040-020).

Agradeço também aos meus amigos, que estiveram por perto durante as várias fases dessa jornada, são eles: Marcell Besser, Guto, Pedro Vogt, Ana Pires, Alessandra Faresin, Verônica Velloso, Marília Boldorini, Aline Faraco, Stake, Francine Schroeder, Filipe Delmonego, Polyana Roberta, Diógenes, Fabrise Semmer e Edgar Silva. Em especial, à Lili Zacharia, quem esteve presente e disponível em absolutamente todos os momentos em que precisei, com seus

conselhos e reflexões essenciais para a continuação do meu caminho, o qual ficou muito mais florido!!!

Gostaria de agradecer em especial ao Guilherme Fedalto (Lamir) e ao André Pestilho (Cenpes/Petrobras) pelo apoio, auxílio e discussões imprescindíveis para o meu estudo de inclusões fluidas. Sem vocês, certamente não teria conhecido e compreendido esse mundo fascinante das bolhas...

Agradeço imensamente à Ariadne Borgo, quem me ajudou muito com a cotutela de tese, pelas dicas, auxílios, apoio e companheirismo durante todas as fases desse doutorado. Durante minha estadia na França, conheci alguns brasileiros muito legais, aos quais gostaria de agradecer o apoio e companheirismo, principalmente no fim de 2015: Francisca, Matheus, Priscila, Allan e Annete. Obrigada, queridos!!!

À l'Université de Montpellier, je voudrais remercier le chaleureux accueil reçu par l'équipe bassins : Michel Lopez, Roger Soliva, Michel Seranne, Flavia Girard, Jean-Jacques Cornée. Je remercie aussi à Jeff, Bernard Boyer (microsonde), Christophe Nevado et Doriane Dolmas (laboratoire de litholamellage), Frederique (MEB), Dominique et Amélie de l'administration. Et aussi à l'Université de Montpellier, à l'école doctoral GAIA et au Laboratoire Géosciences Montpellier.

À Montpellier, je remercie à tous mes amies et les autres doctorants par son accueil et amitié : Sofia, Laure, Maxime, Julie, Santiago, Enora, Romain, Alizia, Anaïs, Gaétan, Remi, Camille, Amélie, Samuel, Natalie, Anneka et, spécialement à : Séverine Furst, Lise Petit-Jean, Manon Dubois, Benjamin Fores, Cyprien Astoury, Guenolé, Audrey Taillefer, Carlotta Ferrando, Anita et Olivier Rodriguez. Mon séjour en France était super et n'aurait pas été le même sans vous tous. Je suis très heureuse de vous avoir rencontré !!!

En France, je voudrais remercier aussi à Miguel Lopez, le référant dans les comités de thèse, et, en Suisse, à Kalin Kouzmanov, par les discussions et suggestions sur les inclusions fluides et les altérations hydrothermales. Du côté des encadrants, je remercie à Patrick Monié et Olivier Bruguier par les analyses et les discussions sur la géochronologie. Et, finalement, je remercie mon directeur de thèse, qui m'a très bien accueilli à Montpellier et m'a beaucoup aidé et, avec qui, j'ai vachement appris sur la géologie, la culture de la France et la vraie langue française, Alain Chauvet.

Em Curitiba, agradeço finalmente a João Carlos Biondi, principalmente no início do projeto, e à minha orientadora Barbara Trzaskos, pelo apoio, auxílio, sugestões e discussões sempre muito realistas e práticas. Muito obrigada!!!

Por fim, agradeço ao meu amado Chris, quem me acompanhou nesses últimos 6 meses de tese, sempre com muito bom humor, otimismo e companheirismo! Obrigada pelas excelentes sugestões nas últimas semanas da redação e pela parceria na véspera da entrega da tese...

Instructions for freedom

1. *Life's metaphors are God's instructions.*
2. *You have just climbed up and above the roof. There is nothing between you and the Infinite. Now, let go.*
3. *The day is ending. It's time for something that was beautiful to turn into something else that is beautiful. Now, let go.*
4. *Your wish for resolution was a prayer. Your being here is God's response. Let go, and watch the stars come out – on the outside and on the inside.*
5. *With all your heart, ask for grace, and let go.*
6. *With all your heart, forgive him, forgive yourself, and let him go.*
7. *Let your intention be freedom from useless suffering. Then, let go.*
8. *Watch the heat of day pass into the cool night. Let go.*
9. *When the karma of a relationship is done, only love remains. It's safe. Let go.*
10. *When the past has passed from you at last, let go. Then climb down and begin the rest of your life. With great joy.*

Eat, Pray, Love – Elizabeth Gilbert

RESUMO

O Granito Passa Três situa-se à Leste do Estado do Paraná, no Sul do Brasil, e é alongado segundo a direção NNE-SSW. Está intrudido em rochas metapelíticas mesoproterozoicas do Grupo Açungui (Cinturão Ribeira, Província Mantiqueira), entre as falhas transcorrentes de Morro Agudo e Lancinha, de direção N040°E. A mineralização aurífera do Granito Passa Três constitui-se de veios centimétricos a métricos de quartzo com quantidades variáveis de fluorita, sulfetos e carbonatos. Os principais objetivos dessa tese abrangem i) compreender o modelo de formação dos sistemas de veios mineralizados considerando as relações entre magmatismo, hidrotermalismo, deformação e mineralogia de forma espacial e temporal; ii) caracterização da natureza, fonte e condições dos fluidos mineralizadores; e iii) a caracterização do modelo metalogenético desse depósito bastante singular. Para atingir tais objetivos, os métodos utilizados incluem, além da geologia estrutural e de campo: petrografia, geocronologia U-Pb em zircão (LA-ICP-MS) e ^{40}Ar - ^{39}Ar em muscovita, microscopia eletrônica de varredura (MEV), microsonda eletrônica, fluorescência de raios-X (XFR), análise isotópica de enxofre ($\delta^{34}\text{S}$) e análise microtermométrica e Raman de inclusões fluidas. Os dados estruturais demonstraram a coexistência de dois sistemas principais de filões mineralizados, um N-S e o outro E-W, com mergulho de 60-75°W e 45-70°S, respectivamente. Os dois sistemas são interpretados como contemporâneos e conjugados. Os corpos mineralizados formam geometrias sigmoidais que resultam da abertura de pull-aparts devido ao movimento ao longo dos planos de deslizamento de baixo mergulho. As estruturas mineralizadas com mergulhos mais altos representam o envelope global formado pela sucessão dos pull-aparts. O sistema mineralizado foi formado em quatro etapas mineralógicas: fase 1 [quartzo 1 + fluorita], fase 2a [quartzo 2 + pirita 2a ± ouro ± calcopirita ± aikinita ± fluorita ± esfalerita ± muscovita], fase 2b [quartzo 2 + pirita 2b + ouro + calcopirita + aikinita + anquerita ± esfalerita ± fluorita ± muscovita] e fase 3 [quartzo 3 + anquerita + calcita + molibdenita ± aikinita ± muscovita ± fluorita]. O ouro se encontra na forma invisível e como ouro nativo em fraturas que afetam as piritas 2a e 2b, geralmente associado com a calcopirita e a aikinita. A alteração hidrotermal associada à mineralização inclui as assembleias compostas por muscovita/quartzo/pirita/calcopirita/K-feldspato (alteração do tipo greisen) e sericita/anquerita/rutilo/siderita/clinocloro/calcita (alteração filíca). O estudo das inclusões fluidas sugere um fluido mineralizador de composição H_2O - CO_2 - NaCl , com salinidades moderadas (de 0.2 a 12.84 wt.% NaCl eq.) e temperaturas de homogeneização de 400 a 150°C. Os valores isotópicos $\delta^{34}\text{S}$ dos cristais de pirita (de -0.1‰ a 1.1‰) indicam que o enxofre pode ter uma origem magmática. Essa hipótese está de acordo com a observação sistemática, nas porções superiores do granito (sondagem e níveis superiores da mina), de estruturas típicas de transição magmato-hidrotermal, como aplito-pegmatitos, veios de quartzo com borda de feldspato potássico, concentrações de quartzo do tipo stockscheider e estruturas de solidificação unilaterais (UST). Os resultados de geocronologia absoluta confirmam tal hipótese com as idades U-Pb em zircão (611.9±4.7 et 611.9±5.6 Ma) para o granito equigranular médio (GEM) e para o microgranito (GEF) e ^{40}Ar - ^{39}Ar em muscovita (veios com borda de K-feldspato: 612.9±2 a 608.8±2 Ma ; veios mineralizados: 611.7±2 a 608.8±2 Ma ; veios de quartzo precoces : 608.4±2 Ma) muito próximas. Essas idades obtidas indicam que a colocação do granito, a exsolução do fluido magmato-hidrotermal e a formação dos veios de quartzo auríferos ocorreram num intervalo de tempo de 5 Ma, entre 613 e 610 Ma. A mineralização (611 a 608 Ma) contemporânea à cristalização do granito (612 a 610 Ma), a associação do ouro com minerais de bismuto (aikinita), o controle estrutural na formação dos veios e as evidências de transição magmato-hidrotermal em zona de cúpola granítica mostram que o depósito do Granito Passa Três compartilha diversas semelhanças com os depósitos do tipo intrusion-related, mais especificamente com o tipo granite-hosted, o qual será discutido na conclusão dessa tese.

Palavras-chave: transição magmato-hidrotermal. Veio de quartzo. Sistema distensivo. « *Intrusion-related gold deposit* ». Granito Passa Três, Brasil, Neoproterozoico.

ABSTRACT

The Passa Três Granite is situated in southern Brazil (Paraná State) and presents a NNE-SSW elongated shape. This intrusion is emplaced within metapelites of the Mesoproterozoic Açungui Group (Ribeira Belt, Mantiqueira Province), between the N40E trending Morro Agudo and Lancinha faults. Gold mineralisation is composed of centimetric to metric quartz veins with fluorite, sulphides and carbonates. The main objectives of this work are i) to understand the model of formation of the mineralised veins systems taking into account the relationships between magmatism, hydrothermalism, deformation and mineralogy in space and time; ii) the characterization of the nature, source and emplacement conditions of the ore fluids; and iii) the characterization of a metallogenic model for this singular deposit. In order to reach these purposes, the methods to be applied include, beyond the structural geology and field works: petrography, U-Pb zircon (LA-ICP-MS) and ^{40}Ar - ^{39}Ar muscovite geochronology, scanning electron microscopy (SEM), electron-microprobe analyses (EPMA), X-ray fluorescence (XRF), isotopic analysis of sulphur ($\delta^{34}\text{S}$), and microthermometric and Raman analysis of fluid inclusions. Structural data showed the coexistence of two major normal mineralised vein systems, one N-S and the other one E-W, with dips of 60-75°W and 45-70°S, respectively. Both systems are interpreted to be contemporaneous and conjugated. Orebodies form sigmoidal geometries that resulted of the opening of pull-aparts as a consequence of the normal movements along low-angle fault planes. High-angle dip of the global mineralised structures is explained by the succession of the pull-aparts. Four mineralogical stages resulted in the formation of the mineralised system: phase 1 [quartz 1 + fluorite], phase 2a [quartz 2 + pyrite 2a ± gold ± chalcopyrite ± aikinite ± fluorite ± sphalerite ± muscovite], phase 2b [quartz 2 + pyrite 2b + gold + chalcopyrite + aikinite + ankerite ± sphalerite ± fluorite ± muscovite] and phase 3 [quartz 3 + ankerite + calcite + molybdenite ± aikinite ± muscovite ± fluorite]. Gold occurs as invisible gold and as native grains within fractures that affect pyrite 2a and 2b, commonly associated with chalcopyrite and aikinite. Alteration related to the mineralisation includes muscovite/quartz/pyrite/chalcopyrite/K-feldspar (greisen type alteration) and sericite/ankerite/rutile/siderite/clinochlore/calcite (phyllic alteration) assemblages. Fluid inclusion study suggests a fluid with H₂O-CO₂-NaCl composition, with moderate salinities (from 0.2 to 12.84 %wt. NaCl eq.) and homogenization temperatures from 400 to 150°C. The $\delta^{34}\text{S}$ values of pyrite crystals (from -0.1‰ to 1.1‰) indicate that the sulphur in this deposit may have a magmatic origin. This hypothesis agrees with the systematic observation, within the upper part of the granite (drill holes and superior levels of the mine), of structures typical of magmatic-hydrothermal transition such as aplite-pegmatite systems, quartz veins with K-feldspar border, quartz concentration of stockscheider type and unilateral solidification textures (UST). Geochronological data confirm this hypothesis with U-Pb zircon ages (611.9±4.7 and 611.9±5.6 Ma for medium grained granite facies (GEM) and microgranite (GEF), respectively) and ^{40}Ar - ^{39}Ar muscovite dating (veins with K-feldspar border: 612.9±2 to 608.8±2 Ma; mineralised veins: 611.7±2 to 608.8±2 Ma; barren vein: 608.4±2 Ma), that are very close. These ages indicate that the granite emplacement, the magmatic-hydrothermal fluid release and the formation of gold-bearing quartz veins occur during a time lapse of approximately 5 Ma, between 613 and 608 Ma. The mineralisation (611 to 608 Ma) coeval to granite crystallization (612 to 610 Ma), the association of gold with Bi minerals (aikinite), the strong structural control for veins and magmatic-hydrothermal transition features at the roof of a small granitic intrusion suggest that the Passa Três gold deposit shares several similarities with intrusion-related gold deposits, more specifically with granite-hosted gold deposit type, that will be discussed intensively within the conclusion of this thesis.

Keywords: Magmatic-hydrothermal transition. Quartz vein. Extensional system. Intrusion-related gold deposit. Passa Três granite, Brazil, Neoproterozoic.

RÉSUMÉ

Le Granite Passa Três est situé à l'Est de l'Etat du Paraná, au Sud du Brésil, et est allongé selon une direction NNE-SSW. Sa mise en place se fait au cœur des métapelites mesoprotérozoïques du Groupe Açungui (Ceinture Ribeira, Province Mantiqueira), entre les failles décrochantes de Morro Agudo et Lancinha, de direction N040°E. La minéralisation d'or du Granite Passa Três est composée par des veines centimétriques à métriques de quartz contenant des quantités variables de fluorite, sulfures et carbonates. Les objectifs principaux de ce travail de thèse sont i) de comprendre le modèle de formation du système de veines minéralisées en prenant en compte les relations entre magmatisme, hydrothermalisme, déformation et minéralogie à la fois dans l'espace et dans le temps ; ii) la caractérisation de la nature, de la source et des conditions de dépôt des fluides ; et iii) la caractérisation du modèle métallogénique de ce gisement singulier. Pour arriver à ces objectifs, les méthodes utilisées seront, en sus de la géologie structurale et de terrain : la pétrographie, la géochronologie U-Pb (LA-ICP-MS) sur zircon et ^{40}Ar - ^{39}Ar sur muscovite, la microscopie électronique à balayage (MEB), la microsonde électronique, la fluorescence X (XFR), l'analyse isotopique du soufre ($\delta^{34}\text{S}$) et l'analyse microthermométrique et RAMAN des inclusions fluides. Les données structurales ont montré la coexistence de deux systèmes principaux de filons minéralisés, l'un N-S et l'autre E-W, avec des pendages de 60-75°W et 45-70°S, respectivement. Les deux systèmes sont interprétés comme contemporains et conjugués. Les corps minéralisés forment des géométries sigmoïdales qui résultent de l'ouverture en pull-aparts résultant de mouvements en faille normale le long de plans de glissement à faible pendage. Le fort pendage des structures minéralisées s'explique par l'enveloppe globale formée par la succession des pull-aparts. Quatre étapes minéralogiques sont à l'origine de la formation du système minéralisé : phase 1 [quartz 1 + fluorite], phase 2a [quartz 2 + pyrite 2a ± or ± chalcopryrite ± aikinite ± fluorite ± sphalérite ± muscovite], phase 2b [quartz 2 + pyrite 2b + or + chalcopryrite + aikinite + ankérite ± sphalérite ± fluorite ± muscovite] et phase 3 [quartz 3 + ankérite + calcite + molybdénite ± aikinite ± muscovite ± fluorite]. L'or se trouve dans la forme d'or invisible et d'or natif dans des fractures qui affectent les pyrites des phases 2a et b, systématiquement associé avec la chalcopryrite et l'aikinite. L'altération associée à la minéralisation inclue des assemblages composés par muscovite/quartz/pyrite/chalcopryrite/feldspath potassique (altération du type greisen) et séricite/ankérite/rutile/sidérite/clinochlore/calcite (altération phyllique). L'étude des inclusions fluides suggèrent un fluide de composition H_2O - CO_2 - NaCl , avec des salinités modérées (de 0.2 à 12.84 wt. % NaCl eq.) et des températures d'homogénéisation de 400 à 150°C. Les valeurs $\delta^{34}\text{S}$ des pyrites (de -0.1‰ à 1.1‰) indiquant que le soufre du dépôt peut être d'origine magmatique. Cette hypothèse est en accord avec l'observation systématique, dans les parties supérieures du granite (sondage et niveaux supérieurs de la mine), de structures caractéristiques de transition magmatique-hydrothermale comme des systèmes aplo-pegmatitiques, des veines de quartz à bordure de feldspath potassique, des concentrations de quartz de type stockscheider et des textures de solidification unilatérales (UST). Les résultats de géochronologie absolue confirment cette hypothèse avec des âges U-Pb sur zircon (611.9±4.7 et 611.9±5.6 Ma pour le granite à grain moyen (GEM) et le microgranite (GEF) et ^{40}Ar - ^{39}Ar sur muscovite (veines à bordure de K-feldspath : 612.9±2 à 608.8±2 Ma ; veines minéralisées : 611.7±2 à 608.8±2 Ma ; veines de quartz précoces : 608.4±2 Ma) très proches. Ces âges obtenus indiquent que la mise-en-place du granite, l'exsolution du fluide magmatique-hydrothermal et la formation des veines de quartz aurifères ont été réalisées pendant un écart de temps de 5 Ma, entre 613 et 608 Ma. La minéralisation (611 à 608 Ma) contemporaine de la cristallisation du granite (612 à 610 Ma), l'association de l'or avec des minéraux de bismuth (aikinite), la démonstration du contrôle structural sur la formation des veines et les évidences de transition magmatique-hydrothermale en domaine de coupole granitique montrent que le dépôt d'or du Granite Passa Três partage plusieurs similitudes avec les dépôts du type *intrusion-related*, plus spécifiquement avec le type *granite-hosted*, ce qui sera discuté en conclusion de la thèse.

Mots-clés : Transition magmatique-hydrothermale, Veine de quartz, Système extensif, « Intrusion-related gold deposit », Granite Passa Três, Brésil, Néoprotérozoïque.

RÉSUMÉ ETENDU EN FRANCAIS

1 INTRODUCTION

1.1 PREAMBULE ET CADRE DE L'ETUDE

Cette thèse de doctorat résulte d'une cotutelle entre les Universités Fédéral du Paraná (UFPR, Curitiba, Brésil) et de Montpellier (UM, Montpellier, France). La thèse a débuté au Brésil en août 2014 et a comporté un séjour d'un an en France, au sein du laboratoire Géosciences Montpellier, entre septembre 2015 et septembre 2016. Cette cotutelle a été développée dans le cadre de la complémentarité scientifique et thématique d'abord entre les deux directeurs de thèse mais aussi sur le plan des moyens analytiques disponibles sur les deux sites.

Le Granite Passa Três, objet central de l'étude, est situé à l'Est de l'État du Paraná, Sud du Brésil, et est allongé selon une direction NNE-SSW. Sa mise en place se fait au cœur des métapelites paléoprotérozoïques du Groupe Açungui (Ceinture Ribeira, Province Mantiqueira), entre les failles décrochantes de Morro Agudo et Lancinha, qui forment le couloir décrochant Lancinha, de direction N040°E (Figure 1). La minéralisation d'or du Granite Passa Três est composée par veines centimétriques à métriques de quartz contenant des quantités variables de fluorite, sulfures et carbonates. Ces corps minéralisés montrent des textures internes variables, comme des textures massives, rubanées, cisillées et/ou bréchiques. Les données structurales indiquent l'existence de deux systèmes principaux de failles et de filons, N-S et E-W, avec des pendages de 60-75°W et 45-70°S, respectivement.

Au cœur du Granite Passa Três, il existe plusieurs systèmes de veines qui se nomment, en fonction de leur découverte successive : Mineiros, G-2 - Cleiton, Colnaghi, Urbano, Diogo, Diogo 2, Pacheco et la Faixa do Barreiro. De tous ces sites, la « Faixa do Barreiro » représente la zone principale et est actuellement exploitée par l'entreprise minière Tabiporã depuis les années 1980 avec le développement de 5 niveaux souterrains. Dans ce contexte, nos travaux de recherche seront réalisés par l'étude et la visite des 5 niveaux de la mine souterraine mais aussi des rares affleurements de surface et surtout la description de nombreux sondages, mis à notre disposition par l'entreprise Tabiporã.

Le Granite Passa Três et sa minéralisation aurifère ont fait déjà l'objet de nombreux travaux (SOARES ; GÓIS, 1987 ; PIEKARZ, 1992 ; PICANÇO, 2000 ; TURINI NETO, 2012), qui ont abordé le granite, l'altération hydrothermale, la minéralisation, et permis la suggestion de modèles sur la formation du gisement. Cependant, malgré ces contributions scientifiques, quelques points restent encore mal compris comme, par exemple, la relation entre le magmatisme, l'hydrothermalisme, la déformation et la minéralisation mais aussi la compréhension du modèle métallogénique du gisement. Ceci étant, une relation génétique entre

la formation de la minéralisation et son granite encaissant a toujours été soupçonnée mais jamais démontrée.

1.2 PROBLEMATIQUE SCIENTIFIQUE

Le développement du modèle IRGD (LANG ; BAKER, 2001) et la description de plusieurs dépôts du type *intrusion-hosted deposit* ont ouvert de nouvelles possibilités pour la compréhension du modèle de minéralisation du Granite Passa Três. Ainsi, de nombreux dépôts d'or composés par des veines de quartz mises en place au cœur d'un granite ont pu être étudiés et discutés dans le débat entre les caractéristiques des dépôts orogéniques ou Intrusion-related. De surcroît, ce type de gisement, c'est-à-dire composé par des veines de quartz de grande échelle (métrique) mises en place au sein d'une intrusion granitique reste relativement rare et peu décrit (e.g. MALOOF et al., 2001 ; STEPHENS et al., 2004). Ainsi, la minéralisation d'or du Granite Passa Três représente un cas d'étude particulièrement intéressant notamment dans le cadre de l'importance du contrôle structural sur la formation de ce type de gisement mais également de son intégration dans le débat sur la formation des gisements lors de la transition magmatique-hydrothermale (LANG ; BAKER, 2001 ; HART, 2007).

Les objectifs scientifiques de cette thèse sont donc :

- Compréhension de la géométrie des veines minéralisées et de leur évolution structurale ;
- Compréhension des relations entre magmatisme, hydrothermalisme, déformation et minéralisation à la fois dans l'espace et dans le temps (terrain en galeries de mines, description de carottes de sondages, description des lames-minces, etc...) ;
- Datation des facies magmatiques, hydrothermaux et minéralisés (âge U-Pb sur zircons, Ar-Ar sur micas) ;
- Caractérisation de la nature, de la source et des conditions de dépôt des fluides minéralisateurs par géochimie isotopique et étude des inclusions fluides ;
- Caractérisation du modèle métallogénique du gisement, notamment dans le contexte des IRGDs (*intrusion-related gold deposit*) en espérant des retombées économiques par une optimisation de l'exploitation actuelle du dépôt.

Une collaboration publique-privée entre l'UFPR et l'entreprise minière brésilienne Tabiporã a rendu possible la réalisation de cette recherche. Cette entreprise détient les droits miniers sur le site d'étude qui a été exploré depuis les années 1980. Au cours de cette période, plus de 45.000 mètres de carottes de sondage ont été récupérés. Cette base de données a permis une bonne compréhension de la composition lithologique du gisement, les types d'altération hydrothermale et la distribution de la minéralisation.

1.3 MATERIAUX ET METHODES

Une analyse structurale et de terrain a été réalisée en premier lieu et surtout consisté en une analyse des veines minéralisées en galeries souterraines au regard que la région étudiée ne montre que très peu d'affleurements corrects. Un échantillonnage complet a pu être réalisé lors de cette étude à cinq différents niveaux de la mine (Figure 2) et sur les carottes de sondage dans le but de confectionner des lames-minces orientées lorsque ceci a été possible. 92 lames minces ont été réalisées dont 17 polies et 10 lames épaisses polies double face pour l'étude des inclusions fluides.

L'analyse pétrographique-structurale a été réalisée par l'étude de 68 lames-minces orientées au microscope à lumière réfléchiée et transmise (UFPR et GM/UM) et a impliqué la caractérisation des roches granitiques, des textures et des paragenèses des veines de quartz. En complément, des analyses au microscope électronique de balayage (MEB) ont été effectués sur un FEI Quanta 200 FEG SEM avec un détecteur Silicon Drift (SDD) – X-Max^N pour les analyses EDS (GM/UM). Des analyses de chimie minérale ont été analysées sur une microsonde électronique de minéraux (*electron-microprobe analyses* – EPMA) Cameca SX100 Electron Microprobe Microanalyzer avec spectrométrie de dispersion (*wavelength dispersion spectrometry*) (UM/GM). Les analyses ont été faites avec un courant de 20 kV (*cup reading*) de 10nA, avec les lignes de rayons-X suivantes : S K α , Fe K α , Cu K α , Au L α , Mo L α , Pb L α , Ag L α , Zn L α , Ti K α , As L α , Bi L α (minéraux métalliques) et F K α , Al K α , Si K α , Ti K α , Na K α , Mg K α , Mn K α , Fe K α , K K α and Ca K α (silicates et carbonates).

L'âge de cristallisation du granite a été établi par analyses U-Pb sur zircon par LA-ICP-MS (GM/UM), tandis que les datations ⁴⁰Ar/³⁹Ar sur micas hydrothermaux (muscovite et séricite essentiellement, GM/UM) des roches encaissantes altérées et des veines de quartz ont aidé à déterminer l'âge de formation de la minéralisation.

Pour l'analyse U-Pb, des grains de zircon ont été séparés par techniques conventionnelles. Après l'écrasement et le tamisage, les grains lourds ont été concentrés par un « *gold panning kit - three sizes* » et ensuite isolés par séparation magnétique sur un séparateur Frantz au Laboratoire de Géologie Isotopique, à l'Université Fédéral du Rio Grande do Sul (UFRGS, Porto Alegre, Brésil). Les grains de zircon ont été choisis visuellement à la loupe binoculaire à partir de la fraction 1.5 A d'intensité et les grains ont été mis sur un ruban adhésif et inclus dans résine epoxy. Les données U-Pb ont été acquies à l'Université de Montpellier avec un « *single collector, sector field ICP-MS (Element XR) coupled to a GEOLAS 193 nm excimer laser system (AETE-ISO regional facility of the OSU OREME)* ». Les analyses ont été exécutées en utilisant un spot de 26 μ m, taux de répétition de 4 Hz et densité d'énergie de 12 J/cm². Pour plus de détails sur les procédures analytiques, voir Bruguié et al. (2017) et Bosch et al. (2011). Pour les analyses concordantes, les âges des zircons ont été exprimés en rapports ²⁰⁷Pb/²⁰⁶Pb

(grains plus vieux que 1 Ga) ou rapports $^{206}\text{Pb}/^{238}\text{U}$ (grains d'âge Néoprotérozoïque). Des âges moyens et par régression linéaire ont été calculés avec le logiciel Isoplot (Ludwig, 2012). Les erreurs indiquées sont de 2σ .

Pour les analyses Ar-Ar, les muscovites de 10 échantillons ont été séparées à partir des veines minéralisées, veines avec bordure de feldspath potassique et veines de quartz stériles (voir définition dans le chapitre « Résultats »). Les échantillons ont été écrasés et tamisés et chaque cristal de muscovite a été sélectionné manuellement à l'aide d'une loupe binoculaire. Les grains séparés ont été lavés à plusieurs reprises dans un bain à ultrasons avec eau distillée et acétone. Ensuite, les échantillons ont été irradiés pendant 40 heures dans un réacteur à Pavia (Italie). Les analyses $^{40}\text{Ar}/^{39}\text{Ar}$ classiques (chauffage par étape) ont été faites sur un multi-collecteur Argus VI (Thermo Scientific). Les grains séparés ont été chauffés par laser infrarouge (CO_2 , $\lambda = 10.600 \mu\text{m}$, $P = 30 \text{ W}$), et les sections polies ont été attaquées (ablation laser) avec un laser ultra-violet (Spectron Laser Systems, $\lambda = 266\text{nm}$, $P = 240 \text{ mJ}$). Le logiciel ArArCalc software© v. 2.5.2 par Koppers (2002) a été utilisé pour calculer les âges et faire les schémas. Le critère utilisé pour définir un âge plateau a été fixé à au moins 50% du ^{39}Ar libéré sur trois ou plus de mesures consécutives. Les erreurs sont de deux σ .

La caractérisation géochimique des échantillons de granite a été faite essentiellement par analyse quantitative des éléments majeurs par spectrométrie de masse (XRF) (Unige, Suisse). Des analyses complémentaires QemScan ont été réalisées afin d'obtenir une image des éléments majeur et traces par fluorescence de rayons-X (XRF) avec un PANalytical AXIOS MAX et un tube anode de Rhodium de 4 W à l'Université de Genève. Les standards SY-2, BHVO, NIM-N and NIM-G ont été utilisés pour le contrôle de qualité. L'analyse isotopique de soufre $\delta^{34}\text{S}$ des sulfures a été fait dans 5 échantillons de pyrites des veines minéralisées, lesquelles ont été envoyées pour analyse au Laboratoire Actlab (Canada).

Enfin, pour l'étude des inclusions fluides, dix lames-minces double-polies ont été fabriquées à Géosciences Montpellier, à l'Université de Montpellier, et cinq ont été sélectionnées pour l'analyse microthermométrie. Les mesures ont été faites sur une platine Linkam avec stage de réchauffement et refroidissement, avec une gamme de température entre -180°C et $+600^\circ\text{C}$, au Laboratoire Lamir de l'Université Fédéral du Paraná, Brésil.

2 CADRE GÉOLOGIQUE RÉGIONAL

La partie Est de l'état du Paraná est composée par quatre *terranes* probablement mis en contact au Néoprotérozoïque. Ces *terranes* sont, du Nord vers le Sud : les blocs Apiaí, Curitiba, Luís Alves et Paranaguá (Figure 1). La collision de ces quatre terrains compose maintenant la portion Sud de la ceinture plissée Ribeira (HEILBRON et al., 2004). Le Granite Passa Três s'est mis en place au sein des roches du Groupe Votuverava (Terrain Apiaí), d'âge Mésoprotérozoïque

et composé par une succession de roches meta-pélitiques (schiste à séricite, phyllites, ardoise), avec des intercalations de meta-grès, de roches carbonatées et de meta-basaltes (BASEI et al., 2010).

Des différentes études ont montré que la partie sud du Terrain Apiaí est déformée et affectée par des événements à la fois chevauchant et décrochant (FIORI, 1992 ; CAMPANHA ; SADOWSKI, 1999 ; SIGA JR. et al., 2009 ; BASEI et al., 2010). Ces événements ont été produits par la collision oblique entre les cratons San Francisco, Congo et Paraná pendant le Néoprotérozoïque (FRAGOSO CESAR, 1993 ; CAMPOS NETO ; FIGUEIREDO, 1995 ; ROGERS et al., 1995), collision à l'origine de la déformation et du métamorphisme de la séquence sédimentaire dans des conditions faibles à modérées (CAMPANHA ; SADOWSKI, 1999).

En fait, plusieurs auteurs sont maintenant d'accord avec l'existence de trois événements principaux qui ont affectés les roches des terrains Précambriens situés à l'Est de l'état du Paraná. Le premier est lié à un chevauchement (Système de Chevauchement Açungui), le deuxième s'appelle Système de Plissage Apiaí, et le troisième est associé à la déformation décrochante (Système de Cisaillement Lancinha, Figure 1), lequel forme la limite Sud-Est du Terrain Apiaí (FIORI et al., 1987 ; FIORI, 1992, 1994 ; FASSBINDER, 1996 ; KAULFUSS, 2001 ; CURY et al., 2002). Proche du Granite Passa Três, le troisième événement tectonique est représenté par les failles Morro Grande et Lancinha, entre lesquelles le Granite Passa Três s'est mis en place (Figure 1).

Deux épisodes principaux de magmatisme ont été décrit. Le premier, entre 700 et 600 Ma, est lié à la formation de l'arc magmatique (du type Cordilleran) et la production de plutonisme calco-alcalin représenté par des granites du type I. La mise-en-place de la plupart des intrusions syn à post-tectoniques (par exemple, les batholithes Cunhaporanga et Três Córregos) est attribuée à ce premier événement (CAMPANHA ; SADOWSKI, 1999 ; GIMENEZ FILHO et al., 2000 ; PRAZERES FILHO, 2000 ; JANASI et al., 2001 ; PRAZERES FILHO et al., 2003a). A partir de 600 Ma, l'océan Adamastor a été consommé et la majorité des blocs continentaux ont été collée. La tectonique qui a suivie voit alors le développement de zones de cisaillement décrochantes associées à la collision oblique (« Escape tectonics », Système de Cisaillement Lancinha). Dans ce contexte, des bassins du type *pull-apart* ont été développés et remplis par les séquences molassiques, et les unités régionales ont été intrudées par des granites post-tectoniques associés à un deuxième événement entre 590 et 560 Ma (magmatisme du type A – granites du Cerne, Passa Três, Piedade, Morro Grande et Varginha – Figure 1 ; CAMPANHA ; SADOWSKI, 1999 ; PRAZERES FILHO et al., 2003b).

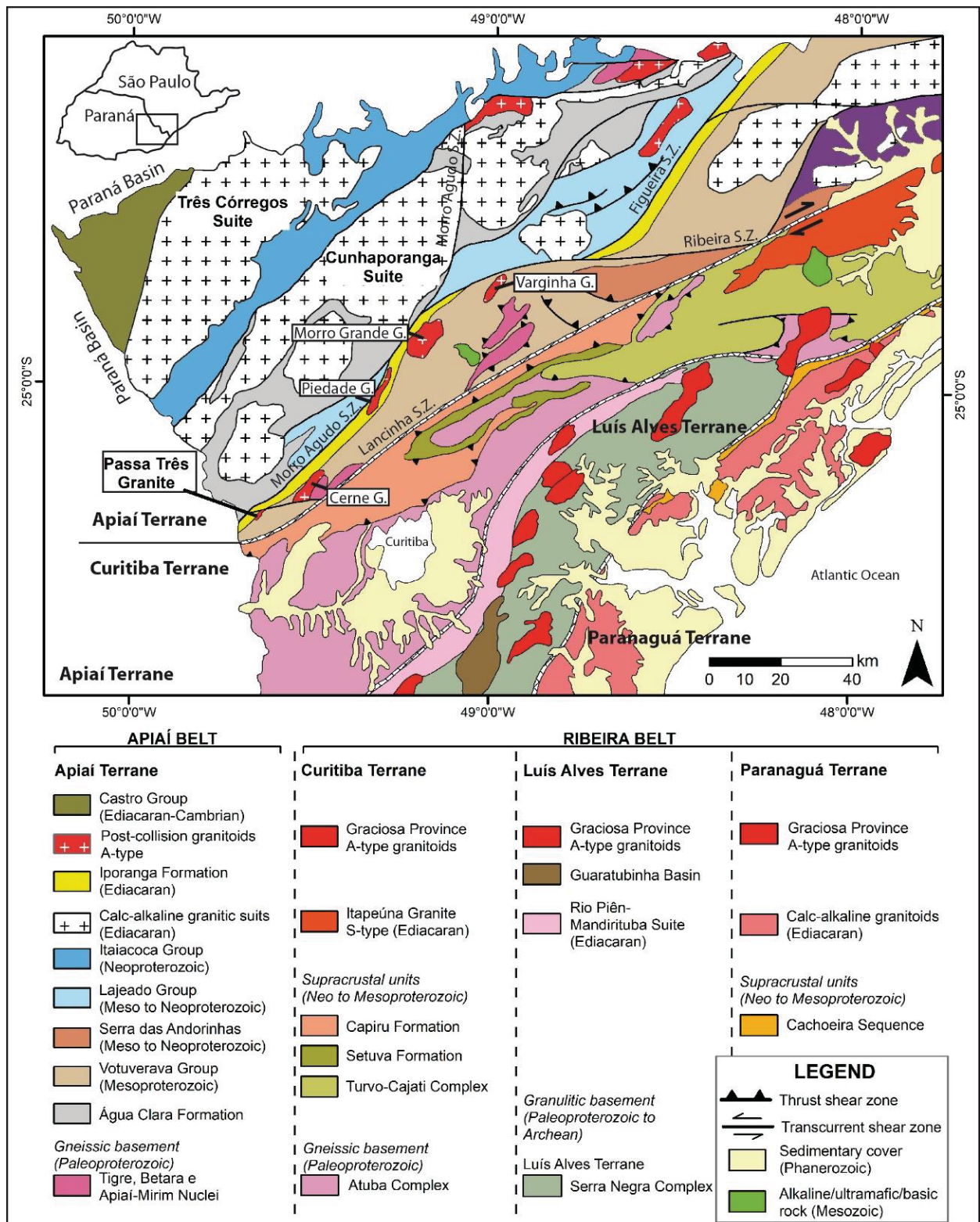


Figure 1 - Carte géologique régionale montrant la localisation du Granite Passa Três entouré par ses roches encaissantes. Les terrains Apiaí, Curitiba, Luís Alves et Paranaguá sont indiqués. (Adapté de FALEIROS, 2008)

3 GÉOLOGIE LOCALE

Le Granite Passa Três est une intrusion allongée et orientée selon la direction NE-SW, avec une surface totale d'environ 5 km² (Figure 2). Ce pluton est essentiellement constitué de syenogranites, monzogranites et quartz syénites. Il est classé dans les granites de type I par son caractère métalumineux et une association minérale composée par magnétite, titanite, apatite, amphibole, biotite, et l'absence des minéraux très alumineux (PIEKARZ, 1992). Il a également été considéré comme un granite hybride par son caractère métalumineux, caractérisé par une anomalie négative en éléments REE lourds par rapport aux REE légers, et pas d'anomalie négative en Eu (PIEKARZ, 1992). En plus, les concentrations en Nd (de -13 à -16), en Sr (120-72), les hautes teneurs de Ba et de Sr suggèrent une contribution crustale significative (CURY, 2003). La mise en place du Granite Passa Três a eu lieu dans un contexte orogénique tardif à post-collisionnel lié à l'arc magmatique Néoprotérozoïque Três Córregos-Cunhaporanga (SOARES ; GÓIS, 1987 ; CHIODI FILHO et al., 1989 in PIEKARZ, 1992 ; PIEKARZ, 1992), et syntectonique à tardif par rapport aux zones de cisaillement décrochantes (e.g., the Zone de cisaillement Lancinha ; FIORI, 1985b ; CURY, 2003).

Les veines de quartz minéralisées avec de l'or sont très irrégulières et présentent des dimensions variables, avec des épaisseurs de quelques millimètres à quelques mètres, et des longueurs pouvant aller jusqu'à 200 mètres. La principale zone de minéralisation s'appelle « Faixa do Barreiro » et se trouve au cœur du granite. La gangue est composée par du quartz avec de quantités variables de fluorite, chalcopyrite, feldspath potassique, carbonate et muscovite (PIEKARZ, 1992 ; PICANÇO, 2000). La paragenesis métallique est formée par la pyrite, la chalcopyrite, des sulfosels de Bi-Cu et d'or natif (PIEKARZ, 1992), avec des quantités moins importantes de bornite, sphalérite, galène et molybdénite (PICANÇO, 2000). Parmi les altérations hydrothermales qui ont été identifiées et décrites, on rencontre l'altération potassique, phyllique, une silicification, carbonatation et une altération argileuse (PIEKARZ, 1992 ; PICANÇO, 2000 ; TURINI NETO, 2012), mais aussi une altération à épidote et saussuratization (CURY, 2003).

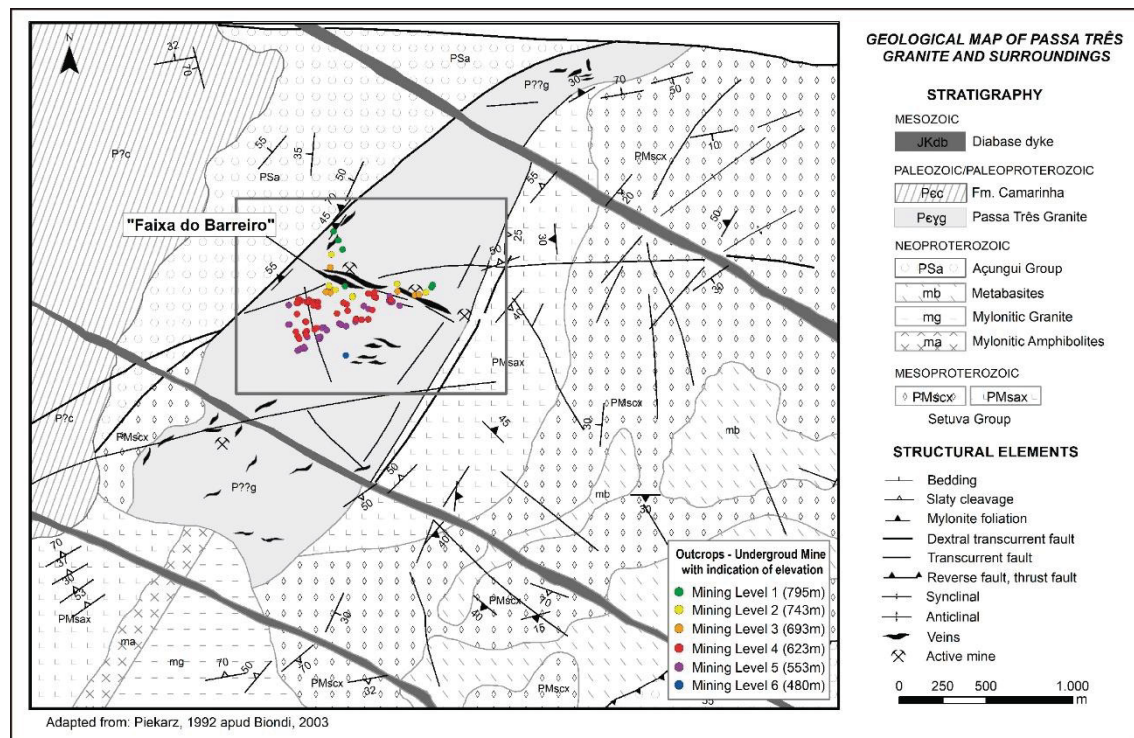


Figure 2 - Carte géologique du granite Passa Três et de ses unités encaissantes. Les différentes couleurs représentent la profondeur en mine des minéralisations. Les structures qui contiennent le minerai ont donc majoritairement des pendages vers le sud avec une valeur moyenne de 40 à 60° (Modifié de PIEKARZ, 1992 in BIONDI, 2003)

4 RÉSULTATS

4.1 FACIES MAGMATIQUES ET ALTERATION HYDROTHERMALE

Dans le Granite Passa Três, trois faciès granitiques différents ont été identifiés (Figure 3a-e) : le granite à grain moyen (GEM), le microgranite (GEF) et le granite blanc (GEB) ainsi que des zones et dykes d'aprites et de pegmatites. Les faciès GEF et GEM sont majoritaires (Figure 3a, b) et supposé contemporains alors que le GEB n'a été observé que dans les carottes de sondage et reste minoritaire.

Le faciès GEM a été classé dans le secteur des syénogranites et présente une texture isotrope (Figure 3c). Il est composé de microcline, plagioclase, quartz et biotite, avec des minéraux accessoires comme le zircon et l'apatite. Le faciès GEF est le même granite (syénogranites), mais avec une texture plus fine mais toujours isotrope (Figure 3d). La composition minéralogique est identique avec en plus la fluorite comme minéral accessoire. Les faciès GEM et GEF présentent de nombreuses fractures submagmatiques (BOUCHEZ et al., 1992) (Figure 3e). Le faciès GEB est un monzogranite, composé par du plagioclase, microcline et quartz, avec une texture moyenne et isotrope. Les minéraux accessoires sont le zircon, l'apatite et la titanite.

4.1.1 Altérations hydrothermales

À partir de la description des carottes de sondage, la présence des altérations hydrothermales suivantes a été établie : altération rouge de haute température (affecte tous les faciès du granite de Passa Très à l'exception du faciès GEB), altération du type *greisen* et altération phyllique. Dans les plans de faille, on observe parfois la présence de gouge, associée à un envahissement tardif par des argiles et des sulfures.

L'altération rouge est interprétée comme une altération de haute température qui affecte tout le corps du granite. Cette altération est caractérisée par la présence de magnétite et d'hématite dans les cristaux de feldspath potassique. Elle est antérieure à la minéralisation et peut être considérée comme une altération potassique.

L'altération du type *greisen* se produit dans les bordures de certaines veines de quartz moins épaisses, probablement un peu précoces par rapport aux structures minéralisées, mais toujours localisées aux alentours des veines minéralisées, souvent proches des aplites. Cette altération est composée par l'assemblage suivant : muscovite + quartz + chalcopyrite ± pyrite ± feldspath potassique.

L'altération phyllique est d'intensité faible et est associée aux plans de failles liés à la minéralisation. Elle a été clairement observée dans les carottes de sondage, et est caractérisée par l'assemblage : séricite + quartz + ankérite + rutile + sidérite + clinochlore ± pyrite ± calcite.

Finalement, il y a également la gouge de faille (associée à des sulfures) dans les failles principales, interprétées comme les plans principaux de glissement normal contrôlant la formation des *pull-aparts* minéralisés. Ces plans sont très importants au niveau de la mine souterraine, et les géologues de la mine les utilisent comme guides de prospection pour trouver les corps minéralisés.

4.2 TRANSITION MAGMATIQUE-HYDROTHERMALE

Dans les affleurements de mine et dans les carottes de sondage, on a pu identifier clairement la présence roches, textures et structures qui sont caractéristiques de la transition magmatique-hydrothermale (Figure 3f-j), comme des poches d'aplites/pegmatites, UST (*Unidirectional Solidification Texture*, HÖNIG et al., 2010 ; SHAFAROU DI et al., 2015 ; YANG et al., 2016), des veines de quartz bordées de feldspath potassiques (veines hydrothermales préliminaires) et des environnements de *stockscheider*. Tous ces structures sont très développées dans la partie supérieure du granite et sont décrites en détail ci-dessous.

Les aplites sont composées par le quartz, le feldspath potassique, le plagioclase et la titanite, sans texture cristalline visible (Figure 3f). Elles sont souvent au contact des corps minéralisés (Figure 3b) ou spatialement associés aux poches de pegmatites. Des structures de

déformation ductile/fragile comme par exemple, des feldspaths fracturés (structures submagmatiques) et la formation de subgrains autour des quartz sont observées. Le quartz, magmatique, hydrothermal ou les deux (magmatique-hydrothermal) est en remplissage des fractures. Les pegmatites sont composées par des poches de quartz avec feldspath potassique, plagioclase, fluorite et hématite (Figure 3l). Parfois, on observe des niveaux de transition entre les pegmatites et les aplites.

Des veines hydrothermales préliminaires sont composées par quartz, molybdénite, pyrite, chalcopryrite, muscovite et fluorite (Figure 4g), et sont caractérisées par des cristaux de feldspath potassique rencontrés le long des bordures (Figure 4h). Des textures du type UST sont composées par des alternances entre niveaux de quartz et de feldspath potassique (HÖNIG et al., 2010 ; SHAFAROUDI et al., 2015 ; YANG et al., 2016) (Figure 4j). Des veines à remplissage de quartz seul sont également observés (Figure 4d). Elles sont abondantes proche des corps minéralisés, et sont fréquemment entourées par le halo d'altération du type *greisen*. Enfin, des secteurs apparentés comme proche des zones à *stockscheider* (NESEN, 1980 ; CERNY, 1991) ont été suspectées dans les niveaux proches de la surface de la mine souterraine (Figure 4e). Ainsi, avec les autres témoins de transition magmatique-hydrothermale, ces observations indiquent que certains niveaux de la minéralisation se trouvent dans une zone de coupole du granite.

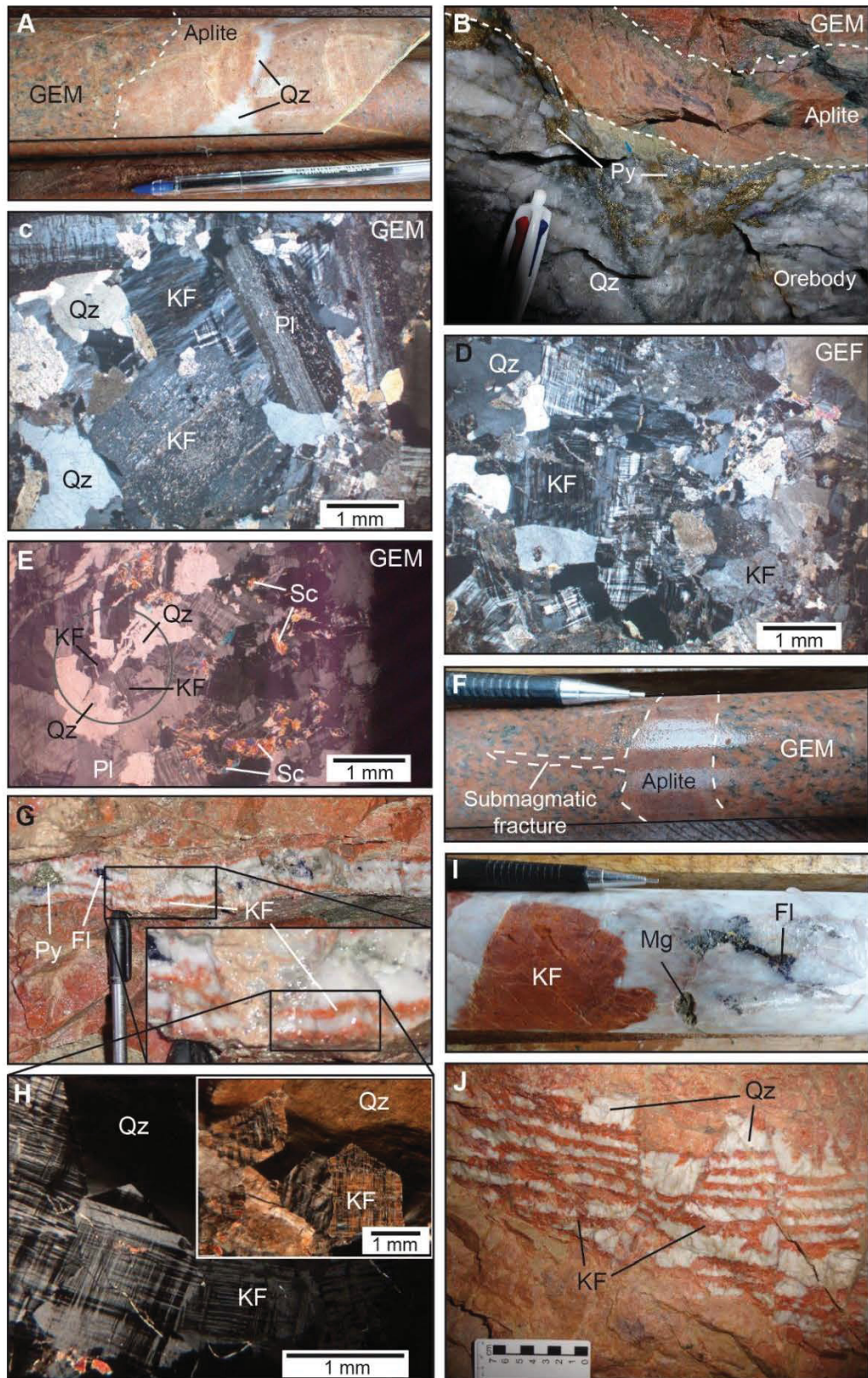


Figure 3 - Illustrations des faciès principaux du Granite Passa Très, et des textures de la transition magmatique-hydrothermale. A) Transition entre le faciès GEM, l'aplite et des poches de quartz, le tout étant interprété comme témoin de la transition magmatique-hydrothermale ; B) Filon d'aplite en bordure d'une veine minéralisée ; C) Aspect du faciès GEM en lame mince ; on reconnaît l'altération à séricite qui affecte les cristaux de plagioclase et de feldspath potassique ; D) Photomicrographie du faciès microgranite (GEF) ; E) Cristal de feldspath potassique avec fracture submagmatique remplie par du quartz (faciès GEM) ; F) Aplite en remplissage d'une fracture submagmatique affectant le faciès GEM, en carotte de sondage ; G) Veine intermédiaire montrant une bordure de feldspath potassique et composée de quartz, fluorite,

chalcopyrite, pyrite et molybdénite ; image de détail des bandes de feldspath potassique et de quartz ; H) Image en microscopie des cristaux de feldspath potassique présents sur les bordures des veines transitionnels (ou intermédiaires); I) Poche de pegmatite riche en quartz, avec du feldspath potassique, fluorite et magnétite ; J) Texture du type UST dans les niveaux supérieures de la mine, proche de la surface. GEM : granite à grain moyen, Fl : fluorite, KF: feldspath potassique, Mg : magnétite, Mu : muscovite, Pl : plagioclase, Qz : quartz, Py : pyrite, Sc : séricite.

4.3 CORPS MINERALISES – TEXTURE ET PARAGENESE

La minéralisation aurifère du Granite Passa Très est composée par des veines de quartz d'épaisseur centimétrique à métrique, contenant en plus du quartz comme gangue, des sulfures (pyrite, chalcopyrite, aikinite, molybdénite), fluorite, chlorite, muscovite, séricite, ankérite, calcite et barytine (Figure 4). Ces corps minéralisés sont très segmentés et présentent différentes textures internes, comme des textures massives, cisillées (Figure 4b) et/ou bréchifiées. Deux systèmes principaux de failles normales et de veines ont été identifiés, N-S et E-W, avec des pendages de 60-75° W et 45-70° S, respectivement. Les observations de terrain indiquent que les deux systèmes de veines (E-W et N-S) sont contemporains (même allure, même taille, même géométrie, même texture interne). Les veines minéralisées sont piégées dans les sites d'ouverture de ces systèmes de failles, interprétés comme des *pull-aparts* extensifs (Figure 4a). Cette configuration est observée à différentes échelles, depuis celle de l'affleurement jusqu'à celle de la lame-mince (Figure 4a, c, g).

L'étude pétrographique (avec la contribution des analyses microsonde et MEB et de terrain) indique que les veines minéralisées ont été formées lors de quatre évènements successifs en plus de la phase initiale magmatique [développement des plans de cisaillement qui servent de guides et mise en place des aplites et des autres structures de la transition magmatique-hydrothermale], phase 1 [remplissage principal des veines à quartz 1 + fluorite], phase 2a [quartz 2 + pyrite 2a ± or ± chalcopyrite ± aikinite ± fluorite ± sphalérite ± muscovite], phase 2b [quartz 2 + pyrite 2b + or + chalcopyrite + aikinite + ankérite ± sphalérite ± fluorite ± muscovite] (Figure 4h) et phase 3 [quartz 3 + ankérite + calcite + molybdénite + aikinite + muscovite + fluorite], qui présente une cinématique inverse (Figure 4f).

L'or se trouve principalement comme remplissage des fractures et des sites d'ouverture des pyrites 2a, même s'il est parfois observé en inclusions primaires dans ce même minéral. Les analyses microsonde indiquent aussi que l'or se trouve également sous la forme d'or invisible dans la pyrite 2a. Dans tous les cas, il est également fréquemment associé à la chalcopyrite, la pyrite 2b et l'aikinite.

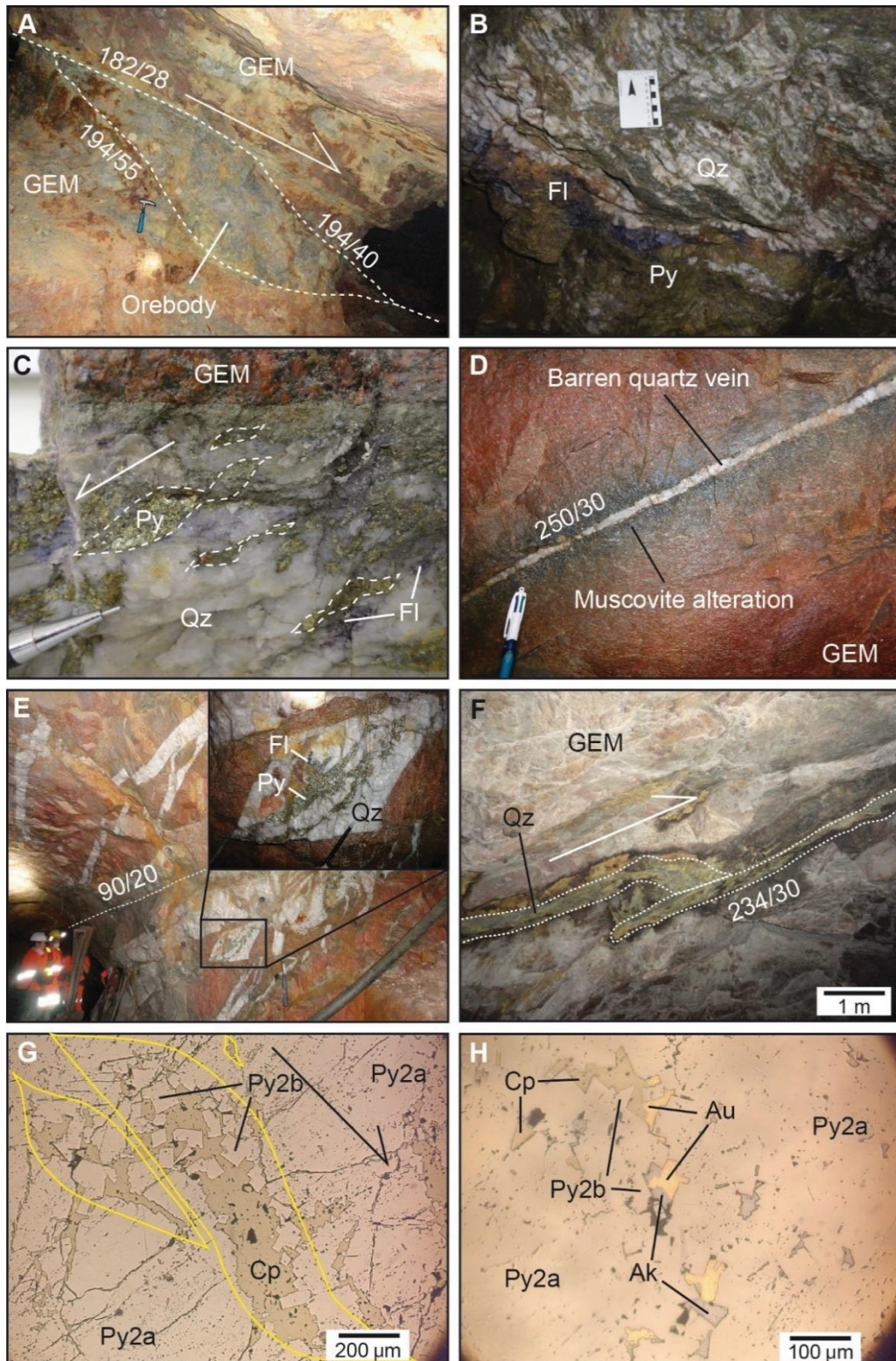


Figure 4 - Textures et structures des veines aurifères du gisement de Passa Três. A) Corps minéralisé de forme sigmoïdale interprétée comme un pull-apart extensif ; B) Veine minéralisée avec une texture interne cisailée ; C) Veine minéralisée contenant un micro pull-apart extensif à remplissage de pyrite ; D) Veine de quartz préliminaire observée dans les niveaux supérieures de la mine, présentant un halo d'altération centimétrique (altération de type greisen) ; E) Système intensif de veines de quartz indicateur d'un environnement de *stockscheider* avec pyrite et fluorite ; détail de géométrie en pull-apart extensif à remplissage de pyrite et fluorite ; F) Veine minéralisée affectée tardivement par une faille inverse ; G) Site d'ouverture interprétée comme un pull-apart rempli par la paragenèse aurifère composée de chalcopryrite, or, aikinite et pyrite 2b ; H) Paragenèse économique à or, aikinite et chalcopryrite. Ak : aikinite, An : ankérite, Au : or, Cp : chalcopryrite, FI : fluorite, GEM : granite à grain moyen, Py : pyrite, Py2a : pyrite 2a, Py2b : pyrite 2b, Qz : quartz.

4.4 GÉOCHRONOLOGIE

Afin de contraindre entre les stades hydrothermaux et magmatiques et d'apporter un argument supplémentaire à la question posée sur le lien magmatique-hydrothermal, des analyses géochronologiques ont été menées pour déterminer l'âge du magmatisme (U-Pb, zircon) et de l'hydrothermalisme (Ar-Ar sur feldspath potassique et muscovite). Les âges du granite par la méthode U-Pb (LA-ICP-MS) ont été déterminés pour les trois faciès granitiques préalablement définis, à savoir : le faciès GEM (granite à grain moyen), le faciès GEF (microgranite) et le faciès GEB (leucogranite). Les faciès principaux, GEM et GEF, donnent respectivement des âges de 611.9 ± 4.7 et 611.9 ± 5.6 Ma, alors que le faciès GEB un âge plus jeune de 592.8 ± 7.1 Ma (Figure 5). Les analyses Ar-Ar ont donné les âges suivants (Figure 5) :

- muscovites dans les veines avec bordure de feldspath potassique : 612 ± 2 à 608 ± 2 Ma ;
- muscovites dans les veines minéralisées : 611 ± 2 à 608 ± 2 Ma ;
- muscovites dans les veines non-minéralisées : 608 ± 2 Ma.

La marge très réduite entre l'âge obtenu de cristallisation du Granite Passa Très et ceux des minéraux des veines minéralisées représente un résultat très important quant à la réponse sur le lien magmatisme-hydrothermalisme et minéralisation. Ce résultat semble confirmer que les fluides hydrothermaux responsables de la minéralisation peuvent évoluer dans un délai de temps très court depuis les fluides magmatiques, hypothèse qui reste à être confirmée par les résultats de l'analyse isotopique ($\delta^{34}\text{S}$ des sulfures)

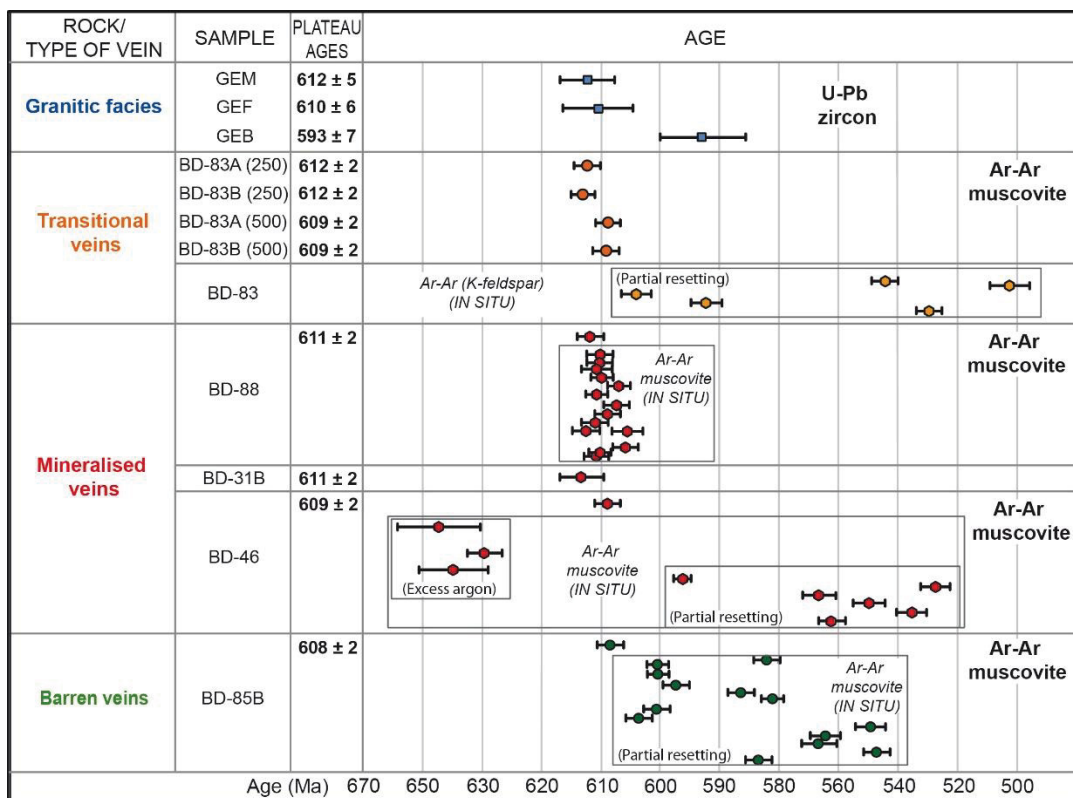


Figure 5 - Tableau de distribution des âges Ar-Ar et U-Pb obtenus pendant cette étude sur le Granite Passa Très et sa minéralisation aurifère.

4.5 LES ISOTOPES DE SOUFRE ($\delta^{34}\text{S}$)

Pour vérifier l'origine du gisement, des analyses isotopiques de soufre ont été menées sur cinq échantillons de pyrite et un échantillon de barytine. Les échantillons ont été envoyés au Laboratoire Actlab, au Canada. Les pyrites montrent des valeurs isotopiques $\delta^{34}\text{S}$ entre -0.1 et 1.1 ‰, valeurs cohérentes avec une origine magmatique pour les sulfures, et possiblement mantéllique, ce qui indiquerait une source assez profonde.

4.6 INCLUSIONS FLUIDES

Pour l'étude des inclusions fluides, dix échantillons ont été sélectionnés parmi le granite, les aplites et les veines minéralisées. Dans tous les cas, les inclusions analysées sont contenues dans des minéraux de quartz, minéral omniprésent et surtout très représentatif de la gangue des veines minéralisées. A partir des analyses pétrographiques et microthermométriques, quatre types d'inclusions ont été identifiés (Figure 6) :

- type I (origine primaire), rencontré uniquement dans le quartz du granite ; ces inclusions sont composées par une phase liquide et une phase vapeur (H_2O liquide + CO_2 vapeur) et sont donc des inclusions $\text{H}_2\text{O}-\text{CO}_2-\text{NaCl}$.
- type II (origine secondaire), de formes très irrégulières et avec des rapports vapeur/liquide très variables ; ces inclusions sont triphasées et présentent une phase vapeur (vapeur CO_2) et deux phases liquides (H_2O liquide + CO_2 liquide) ; elles peuvent être riches en liquide ou en vapeur ; elles sont observées dans le quartz du granite, de l'aplite et des veines minéralisées.
- type IIIa ; inclusions de forme arrondie qui se trouvent en plans et qui présentent une phase vapeur (H_2O vapeur) et une phase liquide (H_2O liquide) ; elles sont donc biphasées, secondaires et de composition $\text{H}_2\text{O}-\text{NaCl}$.
- type IIIb (origine secondaire), inclusions monophasées (H_2O liquide) qui se trouvent dans le quartz 3, en association avec la paragenèse aurifère.

Les salinités calculées pour les inclusions fluides du type I varient entre 0.04 et 10.63 wt.% NaCl eq. (Avec une valeur moyenne de 3.65 wt.% NaCl eq.), et les densités calculées varient entre 0.74 et 0.87 g/cm³ (avec une valeur moyenne de 0.87 wt.% NaCl eq.). Pour les inclusions du type II, les salinités calculées varient entre 0.04 et 9.77 wt.% NaCl eq. (Avec une valeur moyenne de 2.45 wt. % NaCl eq.), et les densités calculées varient entre 0.62 et 1.02 g/cm³ (avec une valeur moyenne de 0.89 wt.% NaCl eq.). Pour les inclusions du type IIIa, les salinités calculées varient entre 0.35 et 12.84 wt.% NaCl eq. (Avec une valeur moyenne de 4.61 wt.% NaCl eq.), et les densités calculées varient entre 0.81 et 1.01 g/cm³ (avec une valeur moyenne de 0.90 wt.% NaCl eq.). Finalement, les inclusions du type IIIb présentent des salinités calculées entre 2.4 et 9.7 wt.% NaCl eq. (Avec une valeur moyenne de 4.88 wt.% NaCl eq.).

Les températures d'homogénéisation (T_h -tot) du type I sont très variables et oscillent entre 430 et 180°C (valeur moyenne de 330°C). Celles du type II sont comprises entre 450 et 140°C (valeur moyenne de 276°C), et celles du type IIIa entre 250 et 130°C (valeur moyenne de 198°C).

	Type I (H ₂ O-CO ₂ -NaCl) <i>Primary inclusions</i>	Type II (H ₂ O-CO ₂ -NaCl) <i>Related to Q1</i>	Type III (H ₂ O-NaCl) <i>Related to Q3</i>
GRANITE			
APLITE			
MINERALISED VEIN			

Figure 6 - Dessin schématique des différents types d'inclusions fluides observés et de leur distribution respective. Les inclusions primaires (type I) sont observées dans le quartz magmatique du granite ; les inclusions fluides de type II sont rencontrées dans le granite, les aplites et dans les veines minéralisées ; les types IIIa et IIIb sont observés dans le granite et dans les veines minéralisées.

5 INTERPRÉTATION

À l'échelle de la mine, il y a deux systèmes de failles normales développés selon deux directions orthogonales, N-S et E-W, observés dans la mine souterraine. Des évidences de transition magmatique-hydrothermale sont observées dans la partie supérieure des carottes de sondage et aussi dans les niveaux supérieurs de la mine souterraine, en indiquant une transition entre les phases magmatiques (granite), tardi-magmatiques (aplités, pegmatites, veines de transitions avec bordure de feldspath potassique, *stockscheider*), jusqu'aux phases hydrothermales (veines de quartz seul et veines de quartz minéralisées) (Figure 7).

MINERAL	Late magmatic stages				Early hydrothermal stages		Hydrothermal stages - Mineralisation Normal movement			Post-mineralisation	
	UST	Aplite	Pegmatite	Stockscheider	Vein (FK border)	Barren quartz veins	Stage 1	Stage 2 Phase 2a	Stage 2 Phase 2b	Stage 3	Reverse movement
Plagioclase											
K-Feldspar (magm.)											
Quartz (magm.)											
Muscovite											
Ankerite											
Fluorite											
Quartz 1 (hydr.)											
Illite											
Sericite											
Quartz 2 (hydr.)											
Pyrite 2a											
Pyrite 2b											
Chalcopyrite											
Gold											
Aikinite											
Sphalerite											
Molybdenite											
Calcite											
Quartz 3 (hydr.)											

Figure 7 - Évolution paragenétique globale du dépôt d'or du Granite Passa Très, montrant les différents stades de minéralisation en rapport avec l'évolution magmatique-hydrothermale tardive du granite. L'or est associé au stade 2a en tant que minéraux inclus invisible et au stade 2b sous la forme d'or natif. Les minéraux associés sont donc la pyrite 2a, la pyrite 2b, la chalcopryrite, l'aikinite et la sphalérite. Les minéraux d'altération ne sont pas indiqués.

Les données indiquent que le Granite Passa Très a été affecté par la formation de deux plans de faille produits en réponse à une tectonique extensive pendant et après sa mise en place, comme cela est indiqué par la présence d'aprites parallèles et contrôlées par ces plans de mouvement. Les critères d'extension sont abondants, représentés principalement par la formation des sites d'ouverture en *pull-aparts* extensifs contrôlés par le système de failles normales et remplis par les différents assemblages minéralogiques (Figure 8). Pendant le premier stade, le quartz 1 et la fluorite constitue le remplissage principal et primaire des *pull-aparts*. Le deuxième stade se divise en stades 2a et 2b. Le stage 2a crée des *pull-aparts* plus petits développés dans les *pull-aparts* du premier stade et est associée au quartz 2, pyrite 2a, ± or, ± chalcopryrite, ± aikinite, ± fluorite, ± sphalérite et ± muscovite. Le stade 2b a été observé seulement dans des *pull-aparts* plus petits et des fractures créées dans les *pull-aparts* du stade 2a. Ce stade contient des grains d'or et présente l'assemblage suivant : quartz 2 + pyrite 2b + or + chalcopryrite + aikinite + ankérite ± sphalérite ± fluorite ± muscovite. Le dernier stade (3), est caractérisé par l'assemblage suivant : quartz 3 + ankérite + calcite + molybdénite + aikinite + muscovite + fluorite. A l'encontre de tous les autres stades, ce dernier stade est associé à une cinématique inverse.

Ainsi, le dépôt, dans sa globalité, est formé par une succession de *pull-aparts* extensifs d'échelles métrique contrôlé par deux systèmes de failles orthogonaux, ce qui explique le pendage global des corps minéralisés vers le Sud et vers le Est.

Deux altérations hydrothermales principales ont été identifiés comme associés à la minéralisation : altération du type *greisen* et altération phyllique. L'altération du type *greisen* se présente comme des halos de couleur gris à la bordure des veines de quartz stériles et est définie

par la paragenèse muscovite + quartz + chalcopryrite ± pyrite ± feldspath potassique. L'altération phyllique est représentée par une coloration verte et est composée par l'assemblage séricite + quartz + ankérite + rutile + sidérite + clinochlore ± pyrite ± calcite. Cette altération est directement associée au système minéralisé et se rencontre surtout en bordure des veines aurifères sous la forme de halo d'altération parallèle. Ceci est particulièrement visible dans le carottes de sondage. En plus de ces deux altérations principales, il existe aussi une argilisation tardive que l'on rencontre systématiquement le long des plans de mouvement et surtout dans les parties à faible pendage. La présence d'altération potassique a été suspectée mais sans être démontrée. Elle serait de toute manière antérieure à la minéralisation et interprétée comme du meta-somatisme de haute température liée à l'histoire tardive du granite.

Les données d'isotope de soufre ($\delta^{34}\text{S}$) indiquent une origine magmatique pour les sulfures.

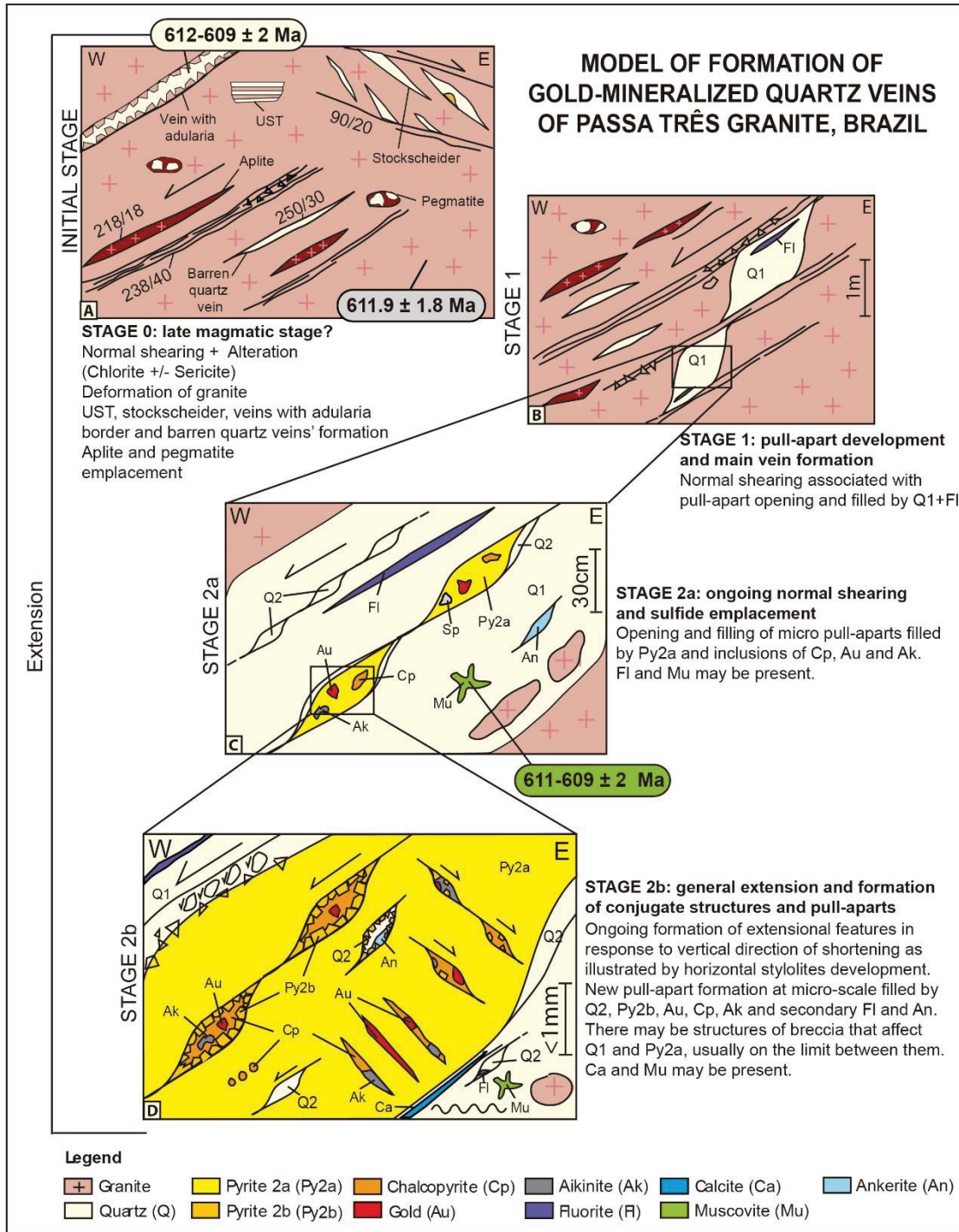


Figure 8 - Modèle de formation des veines minéralisées du Granite Passa Três en trois stades considérés comme contemporains au regard des données géochronologiques de ce travail (âges zircon et muscovite). Le quatrième stade, interprété comme inverse et mineur, n'est pas représenté.

6 DISCUSSION

6.1 ROLE DE LA TRANSITION MAGMATIQUE-HYDROTHERMALE ET RELATIONS TEMPORELLES ET SPATIALES

La transition magmatique-hydrothermale est un processus clé dans la formation de dépôts minéraux liés aux intrusions granitiques, et sa caractérisation est ainsi très importante pour comprendre ces dépôts (GLOAGEN et al., 2014 ; ZENG et al., 2016). Ainsi, le lien entre le magmatisme et la minéralisation représente un point clé de cette étude. Dans le Granite Passa Três, la présence des cristaux de feldspath potassique en bordure de certaines veines hydrothermales, les « *sills* » d'aplite parallèles aux veines minéralisées, la présence de nombreuses poches d'aplite et de pegmatites dans les parties supérieures de la mine et des carottes de sondage, et les textures UST sont des arguments très forts d'abord pour justifier que le dépôt est situé en coupole du granite et en lien avec l'histoire tardive magmatique-hydrothermale du pluton.

Bien qu'aucune variation latérale n'ait été observée comme dans beaucoup « *d'Intrusion-related gold deposits* » où les veines aurifères sont aux abords du granite, (McCOY et al., 1997 in THOMPSON et al., 1999 ; Timbarra, Australia, MUSTARD, 2001 ; Fort Knox, Alaska, USA ; BAKKE, 1995 in MUSTARD, 2001), nous observons dans notre cas une localisation singulière de la minéralisation au cœur du granite, ce qui reste un cas peu répandu. Toutefois, de nombreux arguments comme, par exemple, la présence de cristaux de feldspath potassique en bordures des veines hydrothermales minéralisées illustrent bien la transition de la phase magmatique jusqu'à la phase hydrothermale (avec de fluorite et des sulfures), en montrant que la minéralisation n'est pas entièrement postérieure au stade magmatique, mais intimement associée. De la même manière, les relations temporelle et spatiale très proches entre les fluides magmatiques et hydrothermaux suggèrent une relation génétique entre la minéralisation et la fin de la cristallisation du pluton.

Les caractéristiques du dépôt du Granite Passa Três (nombreuses occurrences d'aprites, pegmatites, UST's, veines de quartz avec bordure de feldspath potassique, *stockscheider*) sont observées dans les niveaux supérieurs de la mine souterraine. Selon Pirajno (2009), ces types de structures se produisent dans la zone de coupole dans un corps granitique qui représente l'endroit le plus favorable pour la création des dépôts minéralisés et particulièrement d'or, comme déjà identifié dans d'autres dépôts aurifères (Timbarra, Australie, MUSTARD, 2001 ; dépôt d'or associé à syénite, *greenstone belt* d'Abitibi, Canada, ROBERT, 2001).

Dans le Granite Passa Três, la relation temporelle entre la cristallisation du granite et la minéralisation est surtout vérifiée par les données géochronologiques obtenues pendant cette étude. A part pour le faciès du granite blanc (GEB), les deux autres faciès (GEM et GEF) ont des

âges contemporains entre eux mais surtout avec la minéralisation aurifère. Ce résultat permet d'ajouter, en plus de la relation spatiale, une relation temporelle claire. De cette façon, la combinaison des évidences de transition magmatique-hydrothermale et des données de datation confirme le lien entre le magmatisme, l'hydrothermalisme et la minéralisation, et confirme l'assurance d'un *continuum* entre les phases tardi-magmatiques et les veines hydrothermales.

Sur la base des observations de terrain et des données géochronologiques, la séquence de formation suivante est ainsi proposée : mise en place du granite (faciès GEM et GEF : 611.9 ± 3.6 Ma), phases tardi-magmatiques (aplite, pegmatite), veines hydrothermales de transition avec bordure de feldspath potassique (612.9 ± 2 à 608.8 ± 2 Ma), veines de quartz aurifères (611.7 ± 2 à 608.8 ± 2 Ma) et veines de quartz seules (608.4 ± 2 Ma). Ainsi, on peut considérer que l'intervalle de temps existant entre 613 et 608 Ma, soit 5 Ma, soit suffisant pour la formation de ce dépôt. En outre, ces données sont en accord avec les âges proposés par Picanço (2000) pour l'âge final de cristallisation du granite (616 ± 36 Ma, Sm-Nd fluorite) et les processus tardi-magmatiques (604 ± 11 Ma, K-Ar muscovite en pegmatite).

Outre le Granite Passa Três, plusieurs dépôts aurifères en lien avec des intrusions présentent une différence de quelques millions d'années entre la mise-en-place du granite et la formation de la minéralisation associée (VIGNERESSE, 2007 ; LI et al., 2011). Cette situation a été observée dans les cas suivants : dépôt de Sn-Be-F de Jiepailing (Chine) (Ar-Ar, minéralisation: 92.1 ± 0.7 Ma ; U-Pb zircon, granite : 90.5 ± 0.9 Ma) (YUAN et al., 2015), dépôt de W-Sn de Xitian, Sud de la Chine (U-Pb zircon, granite : 152 ± 1.4 Ma ; Re-Os molybdénite, minéralisation : 149.7 ± 0.9 Ma ; Ar-Ar, *greisen* minéralisé: 149.5 ± 1.5 Ma ; LIANG et al., 2016), le granite Mine au Maroc (Ar-Ar, Granite Mine: 286 ± 0.4 Ma ; Re-Os molybdénite, W-Mo minéralisation : 285 ± 0.5 Ma) (MARCOUX et al., 2015), Fort Knox (Alaska, USA) (U-Pb zircon: 92.5 ± 0.2 Ma ; Re-Os molybdénite : 92.4 ± 1.2 Ma) (e.g., McCOY et al., 1997 in SELBY et al., 2002).

6.2 FLUIDE MINERALISATEUR : COMPOSITION, SOURCE ET ALTERATIONS HYDROTHERMALES

L'étude des inclusions fluides, des altérations et des isotopes du soufre a été entreprise dans le but de mieux caractériser la nature et la source du fluide minéralisateur

Les analyses microthermométriques et de spectroscopie Raman indiquent que les inclusions fluides appartiennent à un système fluide de température moyenne à basse, de faible salinité et de composition H₂O-CO₂-NaCl. Les inclusions du type II et III caractérisent le stade minéralisateur. Les inclusions du type II sont liées au quartz 1 et les types IIIa et IIIb sont associés au quartz 3, en association avec la minéralisation économique. Entre les stades I et III, les salinités varient généralement entre 0 et 4 wt.% NaCl eq., localement avec salinité entre 9 et 12

wt.% NaCl eq., comme identifié dans quelques inclusions. Cette variation de salinité peut être expliquée par un processus global de décompression peut-être associé à des phénomènes de valve-sismique (discuté au-dessous).

Les analyses microthermométriques indiquent aussi un fluide avec des inclusions primaires de composition H₂O-NaCl-CO₂ dans le quartz magmatique (Type I, Th-tot ~420°C). Cette composition était dominante pendant le premier stade de formation des veines (Type II, Th-tot~420 à 150°C). Pendant le stage 2b, l'or se trouve associé à la chalcopyrite et l'aikinite, et le fluide présente alors une composition H₂O-NaCl et des températures plus basses (Th-tot ~240 à 180°C). Ainsi, le fluide minéralisateur appartiendrait à un système H₂O-CO₂-NaCl développé à des températures plus modérées et associé à un enrichissement en CO₂ et une salinité plus basse. Ensuite, pendant le stade 2b, le fluide présente une composition H₂O-NaCl, avec des températures plus basses, des salinités également plus basses et l'absence de CO₂. Il faut noter que la présence de SO₂ a été suspectée dans les inclusions de types II et IIIa par spectroscopie Raman. Attention, toutes les températures discutées dans ce paragraphe sont les températures minimales de piégeage correspondant aux températures d'homogénéisation mesurées.

Ces données sont en cohérence avec les résultats de Piekarz (1992) pour le même dépôt, où il considère des températures entre 265 et 280°C et des pressions au tour de 1240 bars comme conditions de formation des corps minéralisés. Les données de notre étude peuvent également être comparées à celles des dépôts aurifères de Yukon (e.g. Fort Knox, Dublin Gulch, Scheelite Dome et Clear Creek, GOLDFARB et al., 2007 ; HART, 2007), même si ces dépôts ne présentent que deux types d'inclusions fluides de basse et haute salinité (HART, 2007). Toutefois, pour la minéralisation du Granite Passa Três, il n'a été observé que des inclusions de basse salinité.

Les valeurs $\delta^{34}\text{S}$ en pyrite de la « Faixa do Barreiro » (Granite Passa Três) sont entre - 0.1‰ et 1.1‰, et correspondent aux valeurs des systèmes magmatiques (HEDENQUIST ; LOWERSTERN, 1994 ; ASSUNÇÃO ; KLEIN, 2014 ; BIONDI, 2015). La combinaison entre ces données, la présence d'un fluide du système H₂O-CO₂-NaCl et les évidences de transition magmatique-hydrothermal indiquent que les fluides minéralisateurs sont certainement en lien avec les fluides magmatiques du Granite Passa Três (HEDENQUIST ; LOWERSTERN, 1994 ; AUDÉTAT et al., 2008 ; WEN et al., 2016).

Sans toutefois évoqué de l'or magmatique, on peut penser que l'or ait été dissous et transporté sous la forme de bi-sulfures [Au(HS)₀, Au(HS)₂-] ou de chlorure [AuCl₂-] (PIRAJNO, 2009 ; BIONDI, 2015 ; WEN et al., 2016) et ce, sous l'influence de fluides chauds d'origine magmatique. Dans le cas du Granite Passa Três, la relation de l'or avec les sulfures dans les corps minéralisés et sa composition (H₂O-CO₂-NaCl et salinités basses à modérées) sont des évidences qui suggèrent un transport de l'or par un complexe bi-sulfuré (LI et al., 2013 ; WEN et al., 2016).

Deux types majeurs d'altération hydrothermales associées à la minéralisation ont été reconnus : altération du type *greisen* (liée aux veines de quartz stériles) et du type phyllique (liée aux veines minéralisées), sans oublier la possible altération potassique, considérée de haute température (meta-somatisme) et antérieure à la minéralisation. En fait, les altérations de type *greisen* et de type phyllique sont très discrètes, et les données indiquent que le fluide minéralisateur soit en lien avec un fluide magmatique sans en être directement issu. Par conséquent, on peut considérer que le processus d'altération soit endogène dans le système magmatique-hydrothermale. La présence de zones d'altération très faibles a été notée dans d'autres types de dépôts d'or (e.g. Emerald Lake, BAKER ; LANG, 2001 ; Dublin Gulch, MALOOF et al., 2001) et la caractéristique des enveloppes discrètes, en lien avec la longueur des veines a été considérée comme des preuves de systèmes aurifères de type *intrusion-related* (BAKER ; LANG, 2001 ; STEPHENS, 2004 ; HART, 2007).

6.3 CONTROLE STRUCTURAL ET PROCESSUS DE FORMATION DE LA MINERALISATION

Dans les systèmes d'or « *intrusion-related* », les gisements économiques peuvent être le résultat de l'action de différents processus complexes qui peuvent être, par exemple, la participation d'une chambre magmatique, la cristallisation fractionnée de magmas felsiques et mafiques, l'exsolution de fluides aqueux et leur canalisation vers un site piège confiné, l'immiscibilité vapeur-saumure, le mélange de magmas, et enfin le processus de refroidissement en lien avec la précipitation du minerai (HEDENQUIST ; LOWERSTERN, 1994 ; FOURNIER, 1999 ; HART, 2007 ; PIRAJNO, 2007 ; AUDÉTAT et al., 2008).

Dans le cas du Granite Passa Três, le modèle structural suggère la formation de veines minéralisées dans un contexte extensif associé au développement de deux systèmes de failles normales, lesquels ont créé des poches d'ouverture (*pull-aparts*). La présence des deux systèmes perpendiculaires et contemporains peut être interprété dans le cadre d'un système extensif dominant avec une direction de raccourcissement verticale. Le contrôle structural des corps minéralisés a été observé et mis en avant dans plusieurs dépôts aurifères, comme Scheelite Dome, Clear Creek et Dublin Gulch (Yukon, Canada) (STEPHENS et al., 2004), et on considère les structures d'échelle régionale et d'échelle locale comme responsable de ce contrôle. De surcroît, les zones de coupole dans un système magmatique sont souvent le site de développement d'instabilité mécanique qui peuvent facilement devenir le site de concentrations métalliques structuralement contrôlées (GLOAGEN et al., 2014). Dans ce contexte, des évidences de déformation submagmatique comme le développement de failles normales et des *pull-aparts* suggèrent un contexte extensif prépondérant pour les veines aurifères du Granite Passa Três, développé dans les conditions de la transition magmatique-hydrothermale.

Ainsi, la composition des fluides serait modifiée à partir des inclusions primaires, hébergées par quartz magmatiques, jusqu'à la première et la troisième phase de minéralisation. Ce changement peut se produire en cas d'immiscibilité et/ou par l'interaction avec les roches encaissantes (FOURNIER, 1999 ; WILKINSON, 2001 ; HURAI et al., 2015). Comme dans notre cas, l'altération hydrothermale semble faible et de nature endogène, il est possible que le processus d'immiscibilité (*unmixing*) soit à l'origine de la formation du dépôt même si cela reste discutable à notre stade. Dans les échantillons analysés, la coexistence d'inclusions fluides biphasés riches en liquide et d'autres riches en vapeur avec des températures d'homogénéisation variables et un comportement drastiquement différent pendant l'homogénéisation, peut suggérer le piégeage hétérogène de fluides immiscibles (*unmixing*), au moins localement (FAN et al., 2005 in DENG et al., 2015). Dans la phase principale de la minéralisation, les inclusions fluides sont dominées par une composition H₂O-NaCl-CO₂ (première phase), suivi par une composition H₂O-NaCl (troisième phase), ce qui pourrait être le résultat de cette immiscibilité (*unmixing*) à partir d'un même fluide parental (FALEIROS et al., 2014). Les inclusions de type II sont représentées par des inclusions avec des différences de salinités, de densités, de températures d'homogénéisation et des rapports vapeur/liquide variables, possiblement associés à une décompression progressive et à la formation de vapeur (FOURNIER, 1999 ; WILKINSON, 2001 ; HURAI et al., 2015). Cela serait vérifié par le diagramme d'isochores qui montre une évolution vers les basses températures entre les isochores des inclusions du type II et type IIIa. Les variations de pression observées pour le même type d'inclusions pourraient être expliquées par l'intervention possible de processus de valve-sismique (BOULLIER ; ROBERT, 1992 ; SIBSON, 2000 ; FAMIN et al., 2005 ; FALEIROS et al., 2014).

Ainsi, le contrôle structural de la minéralisation, sa localisation (dans une zone de coupole) et l'étude d'inclusions fluides, peuvent suggérer un contexte de décompression associée à la déformation, possiblement lié au processus de valve-sismique dans un contexte extensif et le développement des failles normales, en impliquant un changement de pression lithostatique pour pression hydrostatique (BOULLIER ; ROBERT, 1992 ; SIBSON, 2000 ; FAMIN et al., 2005 ; FALEIROS et al., 2014). Dans ce contexte, les changements brusques de pression entre lithostatique et hydrostatique (plus importante) pourraient conduire à l'exsolution de fluides sous forme de vapeur pendant une transition fragile-ductile et ce, à des profondeurs de 2 à 3 km (phénomène d'ébullition, FOURNIER, 1999). Cependant, l'absence de *stockwork* dans les dépôts de type *intrusion-hosted* s'explique par une mise en place à des niveaux plus profonds (5-9 km, BAKER ; LANG, 2001), et dans ce cas, on considère que l'augmentation de la pression de confinement prévient l'exsolution rapide et l'explosion, expliquant ainsi l'absence de *stockwork* et favorisant le contrôle structural des corps minéralisés dans la zone de carapace du pluton (FOURNIER, 1999 ; STEPHENS et al., 2004) et sa mise en place dans les failles normales. Les dépôts du type *intrusion-related* sont fréquemment estimés comme mis en place à des pressions

de 1 et 2 kbars correspondant à des profondeurs de 3 à 9 km (GOLDFARB et al., 2007 ; HART, 2007). Ainsi, le refroidissement associé au processus de valve-sismique et de décompression peut être considéré comme responsable de la formation de la minéralisation (FOURNIER, 1999; BAKER ; LANG, 2001), mais aussi de la canalisation des fluides dans les structures associées, comme les failles normales. Ainsi, on considère qu'une profondeur de 3,5 à 4 km et des pressions 1.240 Kbars est raisonnable pour la formation du dépôt du Granite Passa Três (Figure 9).

**METALLOGENIC MODEL OF FORMATION OF THE
PASSA TRÊS GRANITE'S GOLD DEPOSIT**

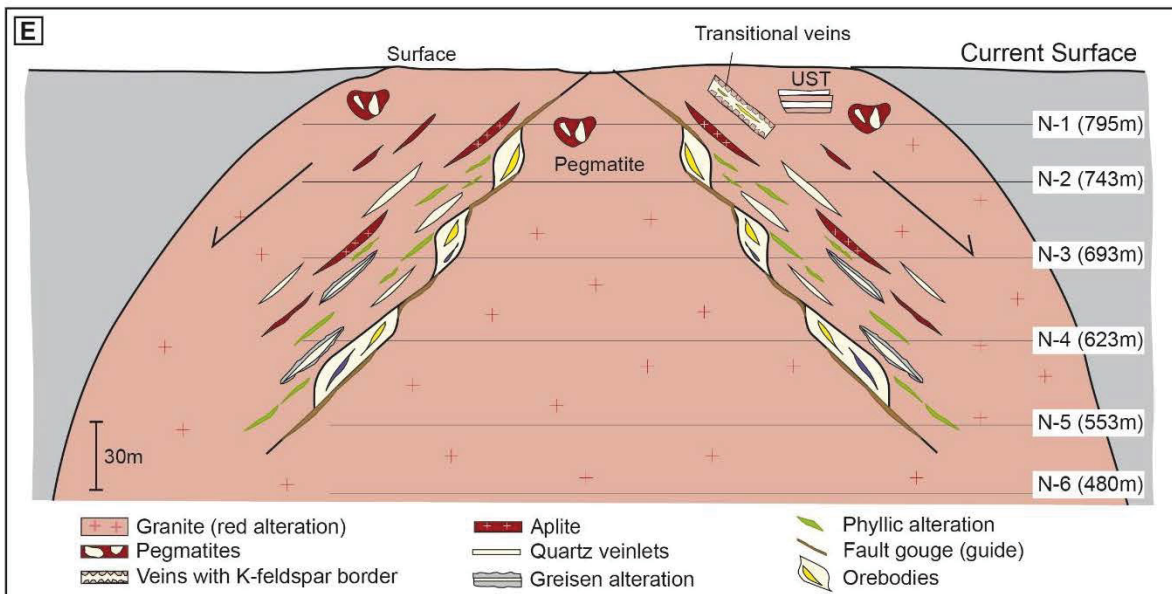
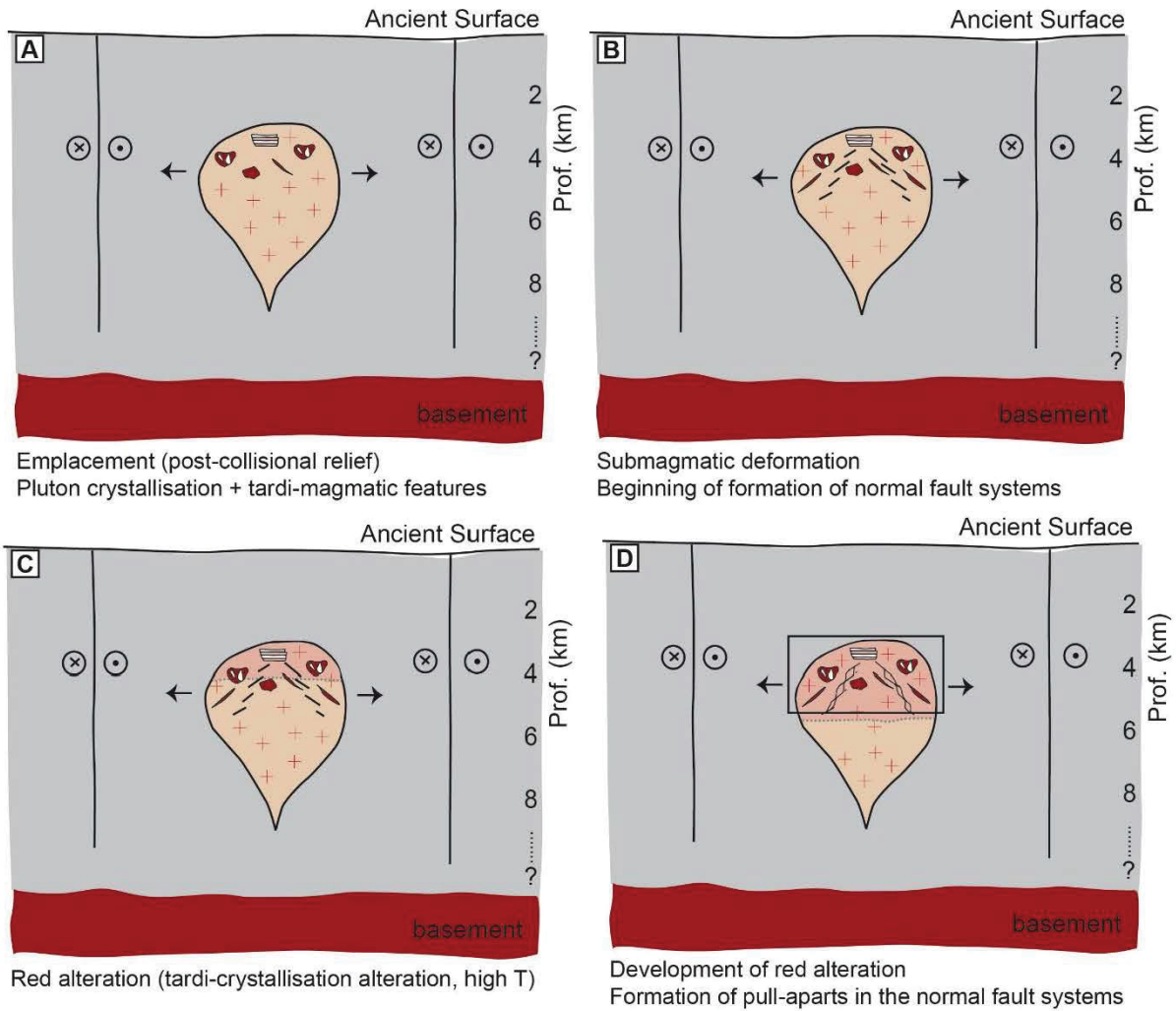


Figure 9 - Modèle métallogénique et structural de la formation de la minéralisation aurifère du Granite Passa Três.

6.4 MODELE METALLOGENIQUE ET COMPARAISON AVEC *INTRUSION-RELATED GOLD SYSTEMS*

La minéralisation d'or du Granite Passa Très présente des caractéristiques compatibles avec les dépôts classifiés comme *intrusion-related*. Le lien avec les structures de transition magmatique-hydrothermale et surtout l'association de l'or avec des minéraux de cuivre et de bismuth (paragenèse composée par l'or + chalcopryrite + aikinite) sont les arguments principaux. D'autres caractéristiques comme la minéralisation (611 à 608 Ma) contemporaine ou très proche de l'âge du granite (612 à 610 Ma), la faible teneur en sulfure, le contrôle structural de formation des veines minéralisées, la nature du système fluide avec des inclusions riches en CO₂ et de faible salinité et enfin la faiblesse de l'altération sont des arguments supplémentaires pour ce modèle (THOMPSON et al., 1999 ; LANG ; BAKER, 2001 ; GOLDFARB et al., 2007 ; HART, 2007).

7 CONCLUSIONS

Les principaux résultats de cette étude peuvent être résumés par les points suivants :

- Le Granite Passa Très est formé par un faciès très homogène associé à une altération de couleur rouge (faciès GEM et GEF) liée à la présence d'inclusions d'hématite dans le réseau microcristallin des cristaux de feldspath potassique. Un faciès de granite plus clair a été rencontré seulement en carottes de sondage (faciès GEB). Il est interprété comme plus tardif;
- La minéralisation d'or dans le Granite Passa Très est associée à deux systèmes de failles normales, de directions N-S et E-W. Les deux systèmes de veines présentent les mêmes paragenèses et les mêmes phases de déformation. Le piégeage des fluides minéralisateurs est contemporain de la déformation et du remplissage de nombreux *pull-aparts* extensifs, et ce, à toutes les échelles d'observation ;
- Les veines contiennent la paragenèse aurifère qui se décompose en quatre stades. L'or est associé aux stades II et III, associé à la cristallisation de pyrite + chalcopryrite + or + aikinite + ankérite + quartz + sphalérite ;
- Plusieurs témoins de transition magmatique-hydrothermale ont été rencontrés dans les carottes de sondage et dans les affleurements de la mine. Ces structures sont, par ordre d'abondance, des poches de pegmatite avec du quartz hydrothermal, des veines de quartz avec bordure de feldspath potassique, des textures « UST », des veines de quartz stériles et des veines d'aplite ;
- Les données de la géochronologie absolue indiquent pour le Granite Passa Très un âge de cristallisation de 611.9 ± 4.7 et 611.9 ± 5.6 Ma (faciès GEM et GEF, respectivement), par contre le faciès GEB a un âge plus jeune de 592.8 ± 7.1 Ma. Les analyses Ar-Ar des cristaux

de muscovite collectés dans les structures intermédiaires et hydrothermales ont donné des âges de 612.9 ± 2 à 608.8 ± 2 Ma pour les veines intermédiaires à bordure de feldspath potassique, 611.7 ± 2 à 608.8 ± 2 Ma pour les veines minéralisées et de 608.4 ± 2 Ma pour les dernières veines de quartz ;

- Dans le granite Passa Três, trois types d'altération hydrothermale ont été identifiés : altération potassique, représentée par le granite rouge (facies GEM et GEF, stage magmatique) ; altération du type *greisen*, liée aux veines de quartz stériles (pendant la transition magmatique-hydrothermale) ; et une altération du type phyllique, très faible, mais associée à la formation du stade minéralisé (stade hydrothermale) ;
- Les valeurs $\delta^{34}\text{S}$ obtenues à partir de cristaux de pyrites sont très similaires à celles caractéristiques des systèmes magmatiques et suggèrent ainsi une origine magmatique pour le soufre de ce dépôt ;
- Des données pétrographiques et microthermométriques indiquent que les inclusions fluides dans le dépôt d'or du Granite Passa Três sont représentées par un fluide minéralisateur de composition $\text{H}_2\text{O}-\text{CO}_2-\text{NaCl}$, avec des températures d'homogénéisation fortes à modérées (entre 400 et 180°C), et des salinités plutôt faibles à modérées (0.04 à 12.84 wt.% NaCl eq.);
- Le fluide minéralisateur résulterait d'une dérivation du fluide magmatique, avec de la silice et concentration de métaux dans les stades tardi-magmatiques (aplites, pegmatites, UST, *stockscheider*), suivi par les stages hydrothermaux préliminaires (veines hydrothermales préliminaires avec bordure de feldspath potassique, veines de quartz stériles), avec la concentration du minerai dans les stages hydrothermaux (veines de quartz minéralisées). Cette évolution accompagnerait des processus de décompression, de refroidissement et peut-être d'immiscibilité, considérés responsables de la formation du gisement et associés à un contexte tectonique extensif.

La minéralisation (611 à 608 Ma) serait contemporaine de la cristallisation du granite (612 à 610 Ma), l'association de l'or avec des minéraux de bismuth, le contrôle structural des veines et les évidences de transition magmatique-hydrothermale dans la zone de coupole d'un petit corps granitique suggèrent que le dépôt d'or du granite de Passa Três partage plusieurs similitudes avec les dépôts d'or du type *intrusion-related*, plus spécifiquement avec le type *granite-hosted gold deposit*.

LISTA DE FIGURAS

Figura 1.1 - Mapa geológico com indicação do Granito Passa Três, com terrenos Apiaí, Curitiba, Luís Alves e Paranaguá. Adaptado de: FALEIROS, 2008.	47
Figura 1.2 - Limites do Granito Passa Três e localização dos veios de quartzo mineralizados. Fonte: TURINI NETO, 2012.	48
Figura 2.1 - Localização dos pontos de afloramentos na Faixa do Barreiro. As cores são relativas aos níveis da mina: verde - nível 1, amarelo - nível 2, alaranjado - nível 3, vermelho - nível 4 e violeta - nível 5.	52
Figura 2.2 - Detalhe da localização dos pontos de afloramento de acordo com os diferentes níveis na Mina Tabiporã.	53
Figura 3.1 - Mapa geológico com indicação do Granito Passa Três cercado pelas rochas encaixantes dos grupos Setuva e Açungui (MINEROPAR, 2006).	58
Figura 3.2 - Modelo esquemático da posição dos veios auríferos proposto por Piekarz (1992).	64
Figura 3.3 - Esboço de seção N-S do granito sugerida por Turini Neto (2012), onde se observa tendência de mergulhos dos veios para sul. Fonte: TURINI NETO, 2012.	65
<i>Figure 4.1 - Geological map with location of the Passa Três granite surrounded by its host rocks. The Apiaí, Curitiba, Luís Alves and Paranaguá terranes are also indicated. (Adapted from FALEIROS, 2008)</i>	<i>70</i>
<i>Figure 4.2 - Geologic map of the Passa Três granite and surrounding units. Different colours represent underground exposures of the mineralisation at different mine levels thus implying that gold-bearing structures dip southwards with moderate to high angles (40 to 60°). (Modified from PIEKARZ, 1992 in BIONDI, 2003)</i>	<i>72</i>
<i>Figure 4.3 - Photographs of the three main facies of the Passa Três granite. A) Red coloured "medium grained granite" facies (GEM); B) Photomicrograph of the GEM facies; note sericitic alteration on plagioclase and K-feldspar crystals; C) K-feldspar with a submagmatic fracture filled by quartz (GEM); D) Photomicrograph of the microgranite facies (GEF); E) "White granite" facies (GEB); F) Photomicrograph of the GEB facies; note the absence of sericitic alteration. Sc: sericite; Qz: quartz; KF: K-feldspar; Pl: plagioclase.</i>	<i>75</i>
<i>Figure 4.4 - Macroscopic and microscopic magmatic-hydrothermal transition features. A) Transition from GEM facies to aplite and quartz pockets interpreted as magmatic-hydrothermal transition; B) Mineralised vein hosted by granite (GEM facies) and bordered by aplite; C) Aplite filling a submagmatic fracture in GEM facies, in borehole drill; D) Aplite photomicrograph showing a K-feldspar crystal affected by a submagmatic fracture and filled by quartz (polarized light); E) Quartz-rich pegmatite pocket composed of quartz, K-feldspar, fluorite and magnetite; F) Plagioclase crystal with submagmatic fractures filled by quartz in pegmatite pocket (polarized light); G) Transitional vein with K-feldspar borders composed of quartz, fluorite, chalcopyrite, pyrite and molybdenite; and image showing in detail the K-feldspar and quartz bands; H) Details of K-feldspar crystals in the border of the transitional veins; I) UST-type texture observed at upper underground mine level, close to the surface. GEM: medium grain granite, Fl: fluorite, KF: K-feldspar, Mg: magnetite, Mu: muscovite, Pl: plagioclase, Qz: quartz, Py: pyrite.</i>	<i>77</i>
<i>Figure 4.5 - Unidirectional Solidification Texture (UST) illustrated by photomicrographs mosaic (natural light) in A, photomicrographs mosaic (polarized light) in B and a schematic drawing in C. The texture is composed of alternating quartz and K-feldspar bands. Growing direction is indicated by K-feldspar grain shape and is downwards (indicated by arrows). This texture is affected by fractures filled by fluorite, pyrite and chalcopyrite, and affected by alteration-related minerals (illite and sericite).</i>	<i>78</i>
<i>Figure 4.6 - Different textures and structures exhibited by the gold-mineralised veins: A) Orebody with a sigmoidal shape (i.e., extensional pull-apart); B) Mineralised vein with a sheared</i>	

internal texture; C) Mineralised vein with pull-apart filled by pyrite at hand specimen scale; D) Earlier quartz vein with “en-échelon” fractures showing a very low-angle normal motion (Even if the normal motion is unclear, the quartz vein plane dip toward the south and the motion is toward the South); E) Early low-angle quartz veins observed within upper level of underground mine, with a centimetre-scale alteration halo; F) Intensive quartz vein system development indicator of a stockscheider environment and exhibiting pyrite and fluorite minerals. Focus on an extensional pull-apart geometry associated with the emplacement of pyrite and fluorite; G) Low-angle faults filled by clay minerals posterior to the quartz veins, indicative of late argillic alteration; H) Reverse fault affecting a mineralised vein. Fl: fluorite, GEM: medium grain granite, Qz: quartz, Py: pyrite. 80

Figure 4.7 - Global paragenetic evolution of the Passa Três gold deposit and relationships with different stages of the magmatic-hydrothermal transition. Gold occurs at Stage 2a as inclusions and at Stage 2b as native grain, forming an ore paragenesis with pyrite 2a, pyrite 2b, chalcopyrite, aikinite and rare sphalerite. Alteration minerals are not represented. 81

Figure 4.8 - Microscopic and SEM aspects of ore paragenesis. A) Supposed pull-apart site filled by ore paragenesis composed of chalcopyrite, gold, aikinite and pyrite 2b; B) Fractures associated to the main ore phase filled by chalcopyrite; C) Ore paragenesis composed of gold, aikinite and chalcopyrite; D) Pull-apart filled by quartz 2 in a pull-apart filled with pyrite 2a, next to quartz 1; E) Differences between pyrite 2a and pyrite 2b. Pyrite 2a presents inclusions and pyrite 2b is euhedral, with no inclusions. These images show the transitional limit between the two pyrites, indicating a progressive change of fluid composition and thus justifying their association within the same second event; F) Aikinite (white mineral) in equilibrium with chalcopyrite and pyrite 2b (light grey). Note the occurrence of ankerite and quartz as fracture infilling and related to the ore paragenesis (phase 2b). Ak: aikinite; An: ankerite; Au: native gold; Cp: chalcopyrite; Py2a: pyrite 2a; Py2b: pyrite 2b; Qz: quartz. 83

Figure 4.9 - Example of large scale gold-bearing pull-apart structure. A) The vein exhibits a banded structure underlined by pyrite (Py), fluorite (Fl) and portions of brecciated granite. The yellow squares indicate the location of Figures 4.9B, C, D, E and F; B) Extensional pull-apart filled with pyrite; C) Quartz 1 microtexture with pull-apart formed by recrystallized new grains and associated with normal movement; D) Pyrite layers affected by extensional fractures parallel to vein dipping; E) Breccia with fracture filled by pyrite, next to quartz 1 (orebody); F) Limit between granite and orebody marked by brecciated granite affected by alteration (sericite, carbonate) next to quartz 1 and pyrite (orebody). Fl: fluorite, GEM: medium grain granite, Py: pyrite, Qz: quartz. Orientations are indicated next to the structures in Figure A; Figures B, C, D, E, F are displayed in the same orientation in relation to the exposure view in Figure A. 84

Figure 4.10 - U-Pb Concordia diagrams of two different facies of the Passa Três granite: GEM (red colour, medium texture) and GEF (red colour, microgranite). 87

Figure 4.11 - U-Pb Concordia diagram of the white granite (GEB - Branco) facies of the Passa Três granite. 88

Figure 4.12 - ^{40}Ar - ^{39}Ar age spectra of muscovite crystals from transitional, mineralised and barren veins. 90

Figure 4.13 - ^{40}Ar - ^{39}Ar in situ ages of three muscovite samples and one K-feldspar sample. Ages older than 620 Ma for sample BD-46 are due to excess of argon. Ages younger than 600 Ma (samples BD-46 and BD-85b - muscovite, sample BD-88 - K-feldspar) are interpreted as partial resetting. 91

Figure 4.14 - Table showing the distribution of ^{40}Ar - ^{39}Ar and U-Pb ages obtained during this study for the Passa Três granite and gold mineralisation. 92

Figure 4.15 - Model of formation of the mineralised quartz veins of Passa Três granite, with the three stages considered as occurring within the errors of the zircon and muscovite ages (the fourth stage, interpreted as a reverse one, is not represented). 94

<i>Figure 4.16 - Block-diagram of the Passa Três granite gold deposit with stereograms of the two normal fault systems (N-S and E-W) and ages for the granite facies, transitional veins, mineralised veins and non-mineralised veins. N-S stereogram: n=45, maximum density at 105/68 (pole), main plane at 285/22; E-W stereogram: n=54, maximum density at 12/63 (pole), main plane at 192/27.</i>	95
<i>Figure 5.1 - Geological map with localisation of the Passa Três granite surrounded by its host rocks. The Apiaí, Curitiba, Luís Alves and Paranaguá terranes are also indicated. (Adapted from FALEIROS, 2008)</i>	105
<i>Figure 5.2 - A) Photograph of the orebody composed mainly of quartz, sulphides (pyrite, chalcopyrite) and fluorite; B) Detail of the ore paragenesis with two pyrite phases (Py2a, Py2b, see Dressel et al., submitted - Chapter 4), chalcopyrite, aikinite and gold in a pull-apart site.</i>	108
<i>Figure 5.3 – SEM images of the ore paragenesis. Figures A and C show backscattering images, with indication of pyrite 2a, pyrite 2b, chalcopyrite, aikinite and gold. Figures B and D display the same images, but with an EDS chemical mapping, evidencing the presence of Cu, Pb and Bi.</i>	109
<i>Figure 5.4 - EPMA analysis in gold next to pyrite 2a, pyrite 2b, chalcopyrite and aikinite.</i>	110
<i>Figure 5.5 - EPMA analysis in crystals of aikinite, displaying its composition of Pb, Cu and Bi.</i>	110
<i>Figure 5.6 - Trace elements distribution by LA-ICP-MS analysis (Appendix 5.A) on the following minerals: pyrite 2a, pyrite 2b, chalcopyrite, aikinite and native gold. One may observe the concentration variation (ppm) of Co, Ni, Cu, Zn, As, Mo, Ag, Sb, Te, Au, Pb, Bi and Se. Concentration are displayed in logarithmic scale.</i>	111
<i>Figure 5.7 - Schematic sketch of the section showing the distribution of main alteration zones and veins near the main mineralisation at the “Faixa do Barreiro” pit.</i>	113
<i>Figure 5.8 - Red granite’s photographs (A, B), photomicrographs (C, D), SEM images (E, F) and SEM/EDS analyses (G). A and B) Red granite with medium isotropic texture; biotite crystals are altered to chlorite; photograph in the underground mine (A) and in borehole (B); C) and D) Red granite with biotite crystal with chlorite alteration, in a medium isotropic texture; E) SEM image displaying hematite crystals in porous of a K-feldspar crystal; F) Hematite crystals in a K-feldspar pores and EDS analyses indicating presence of Fe. Bt: biotite, Ch: chlorite, FeO: Fe-oxide, Qz: quartz, KF: K-feldspar, Plag: plagioclase.</i>	115
<i>Figure 5.9 - A) QemScan map of the red granite. Distribution maps of X-ray elemental map of Na (B), Si (C), Mg (D), Ca (E) and Fe (F).</i>	116
<i>Figure 5.10 - Photographs of the greisen-type alteration related to the gold mineralisation. A) Greisen-type alteration in the border of a barren quartz vein, underground mine; B) Greisen-type alteration in borehole; the grey colour is very characteristic; C) Muscovite crystals as alteration of K-feldspar and plagioclase crystals, in a medium isotropic texture; D) Two fault planes with concentration of muscovite crystals.</i>	117
<i>Figure 5.11 - Aspects of the phyllic-type alteration in the Passa Três deposit. A) Phyllic-type alteration in borehole; this alteration produces a greenish colour; B) Phyllic-type alteration in the border of an orebody (borehole); C) Phyllic-type alteration with sericite planes affecting the texture of the granite; D) Ankerite planes associated to the phyllic-type alteration; E to H) Phyllic-alteration superimposed to breccia (red granite) at the border of the orebody with details of normal faulting (E), fractured K-feldspar crystal (F) and strong alteration and py levels (G, H). Carb: carbonate, KF: K-feldspar, Mu: muscovite, Qz: quartz, Plag: plagioclase, Py: pyrite.</i>	119
<i>Figure 5.12 - A) QemScan map of the phyllic alteration. Distribution maps of X-ray elemental map of Na (B), Si (C), Mg (D), Ca (E) and Fe (F).</i>	120
<i>Figure 5.13 - Photograph of alteration minerals analysed in EPMA of red granite alteration and phyllic alteration in the thin sections. A) Chlorite crystals as alteration of biotite crystal, red granite alteration; B) Mafic aggregate in red granite formed by biotite, and possibly amphibole;</i>	

<i>as alteration minerals; analyses points indicate the presence of clinocllore, siderite, ankerite, calcite; quartz and albite are also identified; C) Localised alteration was observed in the red granite sample, with the presence of ankerite and siderite; D) Ancient titanite crystal altered by siderite, muscovite, ankerite and rutile, phyllic alteration; E) K-feldspar with Fe-oxide alteration; analysis spots indicate the strong presence of FeO; F) Phyllic alteration with indication of the analysed spots.</i>	121
<i>Figure 5.14 - Classification diagram for Fe-Mg chlorites proposed by Bailey (1988). Plotted points indicate the presence of clinocllore crystals, associated to the red alteration.</i>	123
<i>Figure 5.15 - Diagrams for mass balance calculations for greisen-type and phyllic-type alteration. Values that are greater than diagram boundaries are indicated next to the element.</i>	135
<i>Figure 5.16 - Sulphur isotopic composition histograms of pyrite and barityne minerals from the Passa Três gold deposit.</i>	137
<i>Figure 5.17 - Fluid inclusions in gold mineralisation in the Passa Três gold deposit. A) Primary H₂O-NaCl-CO₂ (type I) in growing planes in magmatic quartz and secondary H₂O-NaCl (type IIIa) as a trail, GEM facies; B) Detail of type IIIa fluid inclusions (liquid H₂O); C) Type II fluid inclusions showing different shapes and vapor/liquid rates, in granite sample; D) Type II fluid inclusions showing different shapes and vapor/liquid rates, in aplite sample; E) Type II fluid inclusions in quartz 1, mineralised vein; F) Detail of a type II fluid inclusion (liquid H₂O + vapor CO₂); G) Type IIIa fluid inclusions occurring in cluster in quartz 1, mineralised vein; H) Type IIIb fluid inclusions in quartz 3 near pyrite crystals, mineralised vein.</i>	139
<i>Figure 5.18 - Sketch of the different types of fluid inclusions. Primary fluid inclusions (type I) are found in magmatic quartz in the granite; type II fluid inclusions occur in the granite, in the aplites, as well as in the mineralised vein; types IIIa and IIIb are observed in the granite and in the mineralised vein.</i>	140
<i>Figure 5.19 – A) Diagram with T_{fm} vs. salinity values for the fluid inclusions of the Passa Três gold deposit; B) Temperature (total homogenisation) vs. salinity plot of the fluid inclusions; C) Diagram with T_{fm} vs T_{h-tot} of various types of fluid inclusions of the Passa Três gold deposit. T_h (tot): total homogenisation temperature, T_{fm}: temperature of first melting, T_m ice: temperature of final ice melting.</i>	142
<i>Figure 5.20 - A) Frequency histogram of salinities of the fluid inclusions types observed in the Passa Três deposit; B) Frequency histogram of total homogenisation temperatures (T_{h-tot}).</i>	142
<i>Figure 5.21 - P-T diagram based on fluid inclusion data (isochore) of the different types of fluid inclusions.</i>	143
<i>Figure 5.22 - Representative Raman spectra of fluid inclusions in the Passa Três deposit. A, B and C show the spectra of type II fluid inclusions, with the indication of the presence of CO₂, SO₂ and H₂O in vapor and liquid phases. Images D, E and F display spectra of type IIIa fluid inclusions and evidence the presence of SO₂ and minor presence of CO₂ in vapor and liquid phases.</i>	144
<i>Figure 5.23 - Paragenetic sequence for the hydrothermal minerals of the Passa Três gold deposit. The widths of the solid lines denote relative abundance of minerals.</i>	145
<i>Figure 5.24 - Schematic sketch of a drill hole with the distribution of main alteration zones and mineralised veins. Different stages represent chronological order of events. The insert is a schematic lithostratigraphic column revealed in the Borehole 401/402.</i>	146
<i>Figura 6.1 - Paragêneses esquemáticas dos tipos e associações minerais associadas ao sistema típico RIRGS. Assim como o tempo, o eixo inferior poderia representar também a distância a partir da fonte granítica, tanto que os veios de As, Sb e Pb-Zn-Ag estão praticamente fora do plúton. (HART, 2007)</i>	162
<i>Figura 6.2 - Modelo metalogenético proposto para a mineralização aurífera do Granito Passa Três.</i>	164

LISTA DE TABELAS

<i>Table 5.1 - EPMA analysis and calculated structural formula for feldspars of granite (GEM facies, K-feldspar), transitional veins (K-feldspar), red granite alteration (albite) and phyllic alteration (albite).</i>	124
<i>Table 5.2 - EPMA results of white mica of transitional vein, greisen-type alteration and phyllic alteration.</i>	125
<i>Table 5.3A - Chlorite analysis related to red granite alteration and phyllic alteration (Part A).</i>	126
<i>Table 5.3B - Chlorite analysis related to red granite alteration and phyllic alteration (Part B).</i>	127
<i>Table 5.4 - EPMA analysis and calculated structural formula for biotite crystals (GEM facies).</i>	128
<i>Table 5.5 - EPMA ankerite analysis related to the red granite alteration.</i>	129
<i>Table 5.6 - EPMA ankerite analysis associated with the phyllic alteration.</i>	130
<i>Table 5.7 - EPMA calcite analysis related to the red granite and to the phyllic alterations.</i>	130
<i>Table 5.8 - EPMA siderite analysis related to the red granite and phyllic alterations.</i>	131
<i>Table 5.9 - Major oxides (wt.%) and trace elements (ppm) for the Passa Três granite and altered samples.</i>	132
<i>Table 5.10 - Calculated gains and losses for the different alteration zones.</i>	133
<i>Table 5.11 - Sulphur isotopic data of sulphides from different pyrite and one of barityne crystals of Passa Três gold mineralisation.</i>	136
<i>Table 5.12 - Microthermometric results of fluid inclusions in the Passa Três gold deposit.</i>	141

LISTA DE QUADROS

Quadro 6. 1 - Comparação entre os modelos de depósitos do tipo <i>intrusion-related</i> (conforme proposto por LANG; BAKER, 2001; THOMPSON et al., 1999) e o depósito aurífero do Granito Passa Três.....	166
-----------------------------------------------------------------------------------------------------------------------------------------------------------------------------------------------------------	-----

SUMÁRIO

1 INTRODUÇÃO	46
1.1 JUSTIFICATIVA	50
1.2 OBJETIVO	51
2 MATERIAIS E MÉTODOS	52
2.1 MICROSCÓPIO ELETRÔNICO DE VARREDURA (MEV).....	54
2.2 MICROSSONDA ELETRÔNICA (EPMA)	54
2.3 GEOCROLOGIA U-PB EM ZIRCÕES (LA-ICP-MS).....	54
2.4 GEOCROLOGIA AR-AR EM MUSCOVITA	55
2.5 ANÁLISES DE ELEMENTOS TRAÇOS (LA-ICP-MS)	55
2.6 ANÁLISES DE INCLUSÕES FLUIDAS.....	55
2.7 ANÁLISE DE ISÓTOPO DE ENXOFRE E QEMSCAN	56
3 GEOLOGIA REGIONAL	57
3.1 O GRANITO PASSA TRÊS	61
3.1.1 Modelos de formação da mineralização	62
4 THE PASSA TRÊS LODGE GOLD DEPOSIT (PARANÁ STATE, BRAZIL): AN EXAMPLE OF STRUCTURALLY-CONTROLLED MINERALISATION FORMED DURING MAGMATIC-HYDROTHERMAL TRANSITION AND HOSTED WITHIN GRANITE.....	66
ABSTRACT	66
4.1 INTRODUCTION	67
4.2 GEOLOGICAL SETTING.....	68
4.2.1 The Passa Três granite	70
4.3 METHODS	72
4.4 GEOLOGY OF THE DEPOSIT	73
4.4.1 Magmatic facies and alteration	73
4.4.2 Magmatic-hydrothermal transition.....	75
4.4.3 Orebodies macroscopic features	79
4.4.4 Microstructures and internal texture.....	81
4.5 GEOCHRONOLOGY.....	85
4.5.1 U-Pb zircon dating	85
4.5.2 Muscovite Ar-Ar dating	88
4.5.3 Geochronology integration.....	91
4.6 INTERPRETATION	92
4.7 DISCUSSION	95
4.7.1 Structural model	95
4.7.2 Timing of granite emplacement and gold-mineralisation	96
4.7.3 Magmatic-hydrothermal transition.....	98
4.7.4 Implications for intrusion-related gold systems	100

4.8 CONCLUSIONS	100
5 HYDROTHERMAL EVOLUTION AND ORE GENESIS OF THE PASSA TRÊS' GRANITE GOLD MINERALISATION, NEOPROTEROZOIC: CONSTRAINTS FROM S ISOTOPE, FLUID INCLUSIONS AND HYDROTHERMAL ALTERATION.....	102
5.1 INTRODUCTION	102
5.2 GEOLOGICAL SETTING.....	103
5.2.1 Regional geology.....	103
5.2.2 Local geology and characteristics of the Passa Três gold deposit	106
5.3 SAMPLING AND ANALYTICAL TECHNIQUES.....	107
5.4 GOLD-MINERALISATION	108
5.4.1 Mineral chemistry (EPMA, LA-ICP-MS)	109
5.4.2 Fault gouge	112
5.5 MINERALISATION RELATED HYDROTHERMAL ALTERATIONS.....	112
5.5.1 Red Granite	113
5.5.2 Greisen-type alteration	116
5.5.3 Phyllic-type alteration	117
5.5.4 Mineral chemistry (EPMA)	120
5.6 BULK-ROCK GEOCHEMISTRY AND MOBILIZATION OF ELEMENTS.....	132
5.6.1 Greisen-type alteration	134
5.6.2 Phyllic-type alteration	134
5.6.3 Summary.....	135
5.7 SULFUR ISOTOPES DATA	136
5.8 FLUID INCLUSIONS	137
5.8.1 Petrography of fluid inclusions	137
5.8.2 Microthermometry.....	140
5.8.3 Laser Raman spectroscopy	143
5.9 DISCUSSION	144
5.9.1 Paragenetic sequence of alteration and mineralisation.....	144
5.9.2 Ore fluid composition.....	147
5.9.3 Sources of ore-forming fluids and materials.....	148
5.9.4 Possible fluid processes	149
5.9.5 Implications for ore formation in the Passa Três gold deposit.....	150
5.10 CONCLUSIONS	151
ACKNOWLEDGEMENTS.....	152
6 DISCUSSÕES.....	153
6.1 TRANSIÇÃO MAGMATO-HIDROTERMAL E RELAÇÃO TEMPORAL.....	154
6.2 FLUIDO MINERALIZADOR: COMPOSIÇÃO, FONTES E ALTERAÇÕES HIDROTERMAIS	156
6.3 CONTROLE ESTRUTURAL E PROCESSOS DE FORMAÇÃO DA MINERALIZAÇÃO ...	159

6.4 SÍNTESE DOS PROCESSOS DE FORMAÇÃO DO DEPÓSITO	163
6.5 MODELO METALOGENÉTICO E COMPARAÇÃO COM SISTEMAS DO TIPO <i>INTRUSION-RELATED</i> (IRGD)	165
7 CONCLUSÕES	167
REFERÊNCIAS.....	169
APÊNDICES	177

1 INTRODUÇÃO

O Granito Passa Três localiza-se no leste do Estado do Paraná, no município de Campo Largo, e contém mineralização aurífera na forma de veios, sendo a principal localidade de exploração a jazida aurífera de São João do Povinho (Figura 1.1). Esse granito aflora com formato alongado orientado NE e ocorre alojado em rochas metapelíticas mesoproterozoicas do Grupo Açungui e nos litotipos do Grupo Setuva (Cinturão Ribeira, Província Mantiqueira), entre as falhas transcorrentes de Morro Agudo e Lancinha, que formam o Sistema Transcorrente Lancinha, de direção N040E. O Granito Passa Três contém mineralização aurífera constituída por veios de quartzo de dimensões centimétricas a métricas, com quantidades variáveis de fluorita, sulfetos e carbonatos, de diferentes aspectos, incluindo estruturas maciça, bandada, cisalhada e/ou brechada. Contidos no Granito Passa Três, os veios auríferos apresentam arranjo complexo, onde os filões principais apresentam direção preferencial de tendência N-S e E-W, e mergulhos de 60-75°W e 45-70°S, respectivamente. Estes veios, mineralizados ou não, apresentam diversas ramificações com diferentes direções secundárias, aparentemente com disposição caótica, representando um arcabouço estrutural que ainda não havia sido totalmente compreendido.

No Granito Passa Três há vários agrupamentos de veios que foram expostos pela atividade garimpeira, sendo que alguns foram posteriormente explorados por atividade subterrânea, sendo eles: Mineiros, G-2 - Cleiton, Colnaghi, Urbano, Diogo, Diogo 2, Pacheco e a Faixa do Barreiro (Figura 1.2). A Faixa do Barreiro representa a principal zona mineralizada do Granito Passa Três, e é atualmente minerada pela Mineração Tabiporã, que atua desde a década de 1980, tendo desenvolvido cinco níveis de galerias com painéis de lavra. Nesse contexto, a pesquisa concentrou-se nos corpos mineralizados subterrâneos da Faixa do Barreiro, e contou com trabalhos de superfície e descrição de testemunhos de sondagem, disponibilizados pela Mineração Tabiporã.

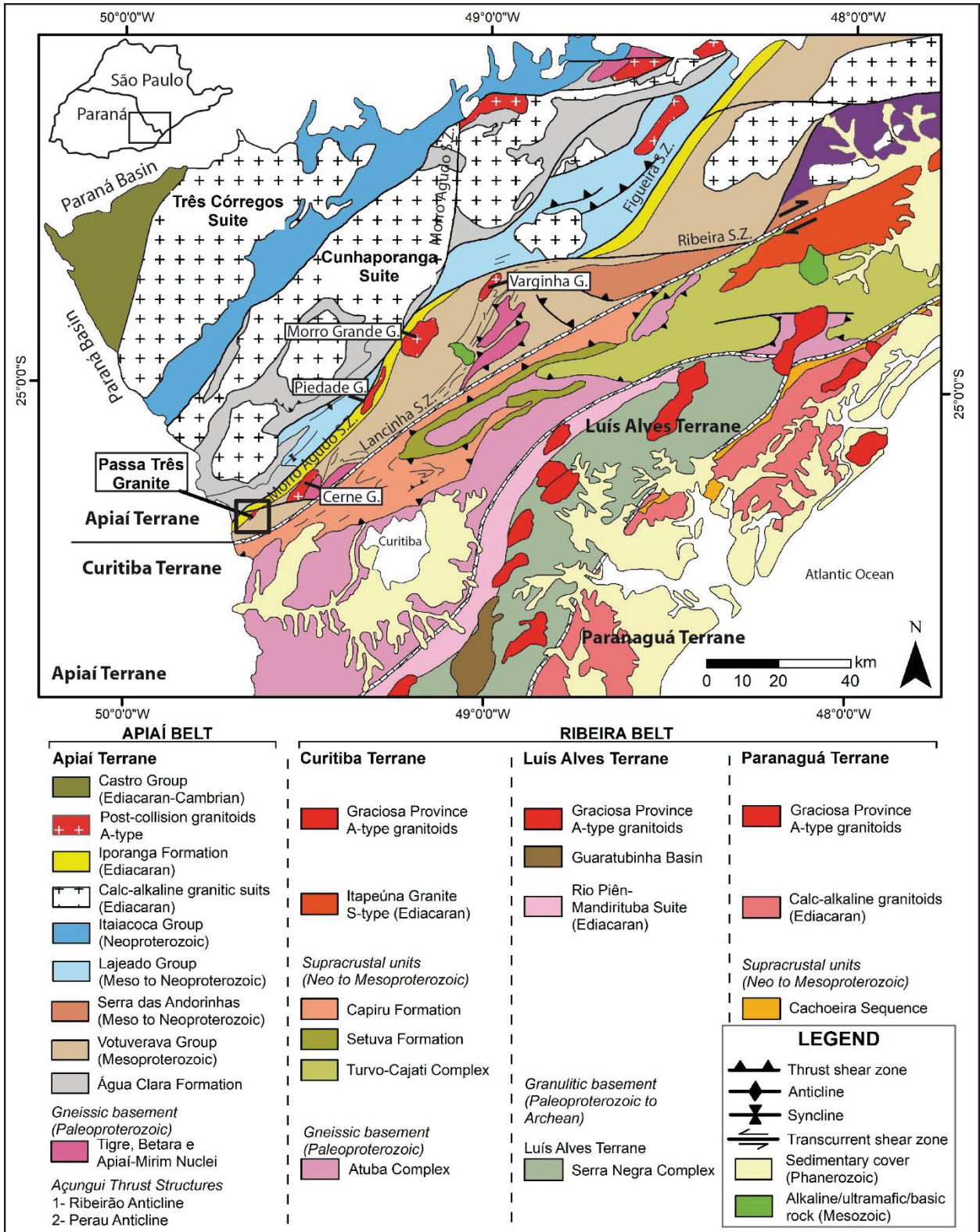


Figura 1.1 - Mapa geológico com indicação do Granito Passa Três, com terrenos Apiaí, Curitiba, Luís Alves e Paranaguá. Adaptado de: FALEIROS, 2008.

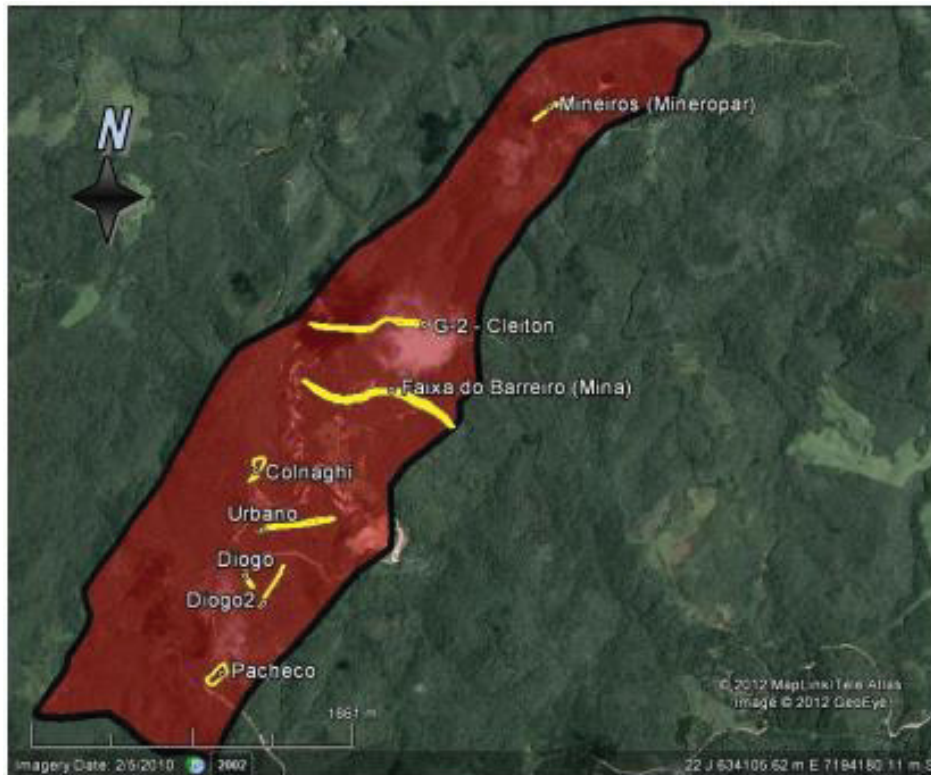


Figura 1.2 - Limites do Granito Passa Três e localização dos veios de quartzo mineralizados. Fonte: TURINI NETO, 2012.

Essa tese de doutorado beneficiou-se de um convênio entre a Universidade Federal do Paraná (Curitiba, PR) e a Universidade de Montpellier (UM, Montpellier, França), e foi desenvolvida em regime de cotutela. O doutorado foi iniciado no Brasil em agosto de 2014 com período de um ano na França, no Laboratório Géosciences Montpellier, na Universidade de Montpellier, entre setembro de 2015 e setembro de 2016. A tese não apenas foi desenvolvida dentro do quadro de complementariedade científica e temática entre os orientadores de ambas as universidades, mas também em virtude dos recursos analíticos disponíveis em cada uma das instituições. A pesquisa também foi possibilitada através da parceria público-privada entre a UFPR e Mineração Tabiporã. Além de deter os direitos minerários da jazida, a mineração possui uma base de dados consistente, baseada inclusive em mais de 45 mil metros de testemunhos de sondagem, perfurados ao longo das últimas quatro décadas. A base de dados disponibilizada pela empresa, assim como os quase dois mil metros de testemunhos de sondagem descritos, permitiu uma boa compreensão sobre as feições do depósito, tipos de alteração hidrotermal e distribuição da mineralização.

O Granito Passa Três foi estudado por diversos trabalhos (SOARES; GÓIS, 1987; PIEKARZ, 1992; PICANÇO, 2000; TURINI NETO, 2012), os quais abordaram aspectos da descrição e classificação do corpo granítico, alteração hidrotermal, estudos sobre a mineralização, e propuseram modelos de formação para a mineralização aurífera contida no Granito Passa Três. Entretanto, apesar dessas contribuições, alguns aspectos sobre a

mineralização ainda careciam de compreensão, como, por exemplo, a relação entre o magmatismo, hidrotermalismo, deformação e mineralização. Dessa forma, suspeitava-se da relação genética entre a formação da mineralização e o granito, mas ainda faltavam evidências para confirmar tal hipótese, assim como um modelo metalogenético do depósito. De fato, a classificação de diversos depósitos de ouro compostos por veios de quartzo alojados em corpos graníticos foi discutida quanto ao modelo de depósito por diversos autores (SOARES; GÓIS, 1987; PIEKARZ, 1992; PIKANÇO, 2000), como o modelo de ouro em zona de cisalhamento (ou orogênico) ou se relacionado ao granito, e se sim, qual a sua relação com a intrusão granítica.

Nesse contexto, a descrição de vários depósitos classificados como *intrusion-related* e o desenvolvimento do modelo *intrusion-related gold systems* (IRGD - SILLITOE; THOMPSON, 1998; THOMPSON et al., 1999; LANG; BAKER, 2001) trouxeram nova luz para o estudo do Granito Passa Três. Como a mineralização aurífera nesse granito apresenta feições de controle estrutural e evidências de transição magmato-hidrotermal, esse depósito representou um estudo de caso absolutamente interessante. Assim sendo, esse trabalho teve como objetivos apresentar e discutir novos dados estruturais, petrográficos, mineralógicos, geocronológicos, isotópicos e de inclusões fluidas sobre o Granito Passa Três e sua mineralização aurífera associada. Esse estudo foi desenvolvido com a finalidade de compreender a formação e a geometria do depósito; contribuir para a exploração da mineração; e esclarecer a relação entre os processos magmáticos, hidrotermais e tectônicos que possivelmente contribuíram para a formação desse depósito bastante específico, e que difere dos modelos clássicos. Para tanto, os dados de geologia estrutural, petrografia e de geocronologia foram integrados e apresentados na forma do artigo intitulado: “*The Passa Três lode gold deposit (Paraná State, Brazil): An exemple of structurally-controlled mineralization formed during magmatic-hydrothermal transition and hosted within granite*”, o qual compõe o primeiro capítulo de resultados dessa tese (capítulo 4). Esse artigo foi submetido ao periódico *Ore Geology Reviews*, em 06 de fevereiro de 2018 e se encontra em fase de correção após a avaliação dos revisores. Os dados relativos às alterações hidrotermais, isótopos de enxofre ($\delta^{34}\text{S}$) e de inclusões fluidas foram integrados e são apresentados também na forma de artigo, compondo o segundo capítulo de resultados (capítulo 5). Em seguida, o capítulo de discussões (capítulo 6) abrange a integração e discussão dos dados apresentados nos dois artigos.

Em função do regime de cotutela, os trabalhos foram divididos em três períodos principais:

Entre agosto/2014 e setembro/2015, as atividades foram feitas no Brasil, envolvendo a participação de disciplinas cursadas no Programa de Pós-graduação em Geologia (UFPR) e a realização de estágio de docência. Quanto às atividades de pesquisa, essas envolveram atividades de campo, tanto na mina subterrânea, quanto descrição de testemunhos de sondagem, coleta de amostras e planejamento da pesquisa. Além disso, foram selecionadas as

amostras, seguidas de sua preparação, para as análises previstas para terem sido realizadas na etapa seguinte.

No período de setembro/2015 a setembro/2016, a pesquisa foi desenvolvida no Laboratório Géosciences Montpellier, na Universidade de Montpellier, França. Durante esse período, foram realizadas análises petrográficas em microscópio de luz transmitida e refletida; análise em microscópio eletrônico de varredura (MEV); análises geocronológicas de U-Pb em zircão LA-ICP-MS em 3 amostras, e Ar-Ar em 8 amostras; e análise de química mineral em microsonda eletrônica. Além disso, ocorreu a publicação de resumos e a participação em eventos científicos, como o *Resources and Innovative Geology* (RIG, Montpellier, abril/2016), *Journée des Doctorants* (Montpellier, abril/2016), *European Geosciences Assembly* (EGU, Vienna, Áustria, abril/2016) e *École thématique du CNRS – Ressources Minérales*, (Toulouse, França, 07-09/junho/2016).

Por fim, entre setembro/2016 e julho/2018, de volta ao Brasil, a pesquisa contemplou análises geoquímicas e petrográficas (alterações hidrotermais), de isótopo de enxofre ($\delta^{34}\text{S}$) e de inclusões fluidas, com o apoio fundamental do Laboratório de Análise de Minerais e Rochas (Lamir, UFPR). Nesse período, houve também a participação em eventos científicos com o envio de resumos e apresentação dos trabalhos no Congresso Brasileiro de Geologia (Porto Alegre, outubro/2016) e no Simpósio Sul-brasileiro de Geologia (Curitiba, junho/2017). Esse período abrangeu também a redação do exame de qualificação, dos dois artigos científicos, e da tese. A submissão do segundo artigo está prevista para após a defesa da tese.

1.1 JUSTIFICATIVA

Apesar dos estudos previamente realizados sobre a mineralização do Granito Passa Três, a geometria do corpo mineralizado e seu arcabouço estrutural, assim como os processos metalogenéticos responsáveis pela formação do depósito mineral ainda não haviam sido completamente compreendidos, gerando diversas questões ainda a serem respondidas, tais como: qual é o modelo geométrico, a textura interna dos veios e as deformações associadas, assim como as características do fluido e a caracterização final do modelo metalogenético.

Considerando que a Jazida de São João do Povinho é um dos poucos depósitos minerais de ouro no sul do Brasil, o último ainda em atividade, e que sua geometria e processos de venulação, mineralização e de deformação ainda não haviam sido totalmente compreendidos, o seu estudo e caracterização podem contribuir com o avanço acerca da compreensão de depósitos de ouro em corpos graníticos. Com a compreensão sobre os processos estruturais e mineralizadores atuantes, esse estudo pode também contribuir para o avanço da prospecção dentro do próprio depósito mineral.

1.2 OBJETIVO

O objetivo principal desse projeto de pesquisa foi elaborar o modelo metalogenético da mineralização do Granito Passa Três.

De forma específica, os objetivos parciais foram definidos da seguinte forma:

- Compressão da geometria dos veios e evolução estrutural do depósito;
- Compreensão das relações entre magmatismo, hidrotermalismo, deformação e mineralização no espaço e no tempo;
- Datação das fácies magmáticas, hidrotermais e veios mineralizados;
- Caracterização da natureza, fonte e evolução dos fluidos mineralizadores.

Com o auxílio desses novos dados, esperou-se contribuir para a compreensão do modelo de depósitos de ouro do tipo “*granite-hosted*” e, em particular, com o caso específico representado pelo depósito do Granito Passa Três, onde os veios de quartzo encontram-se mineralizados somente no interior do granito, não sendo observados nas rochas encaixantes. Ao final da pesquisa, foram respondidas as seguintes perguntas:

- Qual é a geometria dos corpos mineralizados e seu contexto estrutural de formação?
- Qual é a ligação entre os processos magmáticos e a mineralização?
- Idade e duração dos eventos – geocronologia absoluta?
- Qual é a distribuição das zonas hidrotermais e quais são as características dos fluidos mineralizadores?

2 MATERIAIS E MÉTODOS

O trabalho de campo foi constituído de duas etapas principais, a primeira realizada entre setembro e novembro de 2014, a qual abrangeu a descrição de mais de 90 afloramentos em todos os setores subterrâneos abertos da Mina Tabiporã, totalizando 14 dias de trabalho subterrâneo (Figuras 2.1 e 2.2). A segunda etapa foi realizada no período de 20 a 28 de janeiro de 2015 e contou com a presença do orientador Dr. Alain Chauvet (Universidade de Montpellier). Houve ainda uma terceira etapa de campo, entre os dias 16 e 25 de fevereiro de 2017, contando com a presença de ambos os orientadores. Na Figura 2.1 pode-se observar a distribuição dos pontos de afloramento descritos na mina subterrânea, os quais abrangem todos os setores abertos da mina em todos os níveis existentes (Túneis Base 1, 2, 3, 4 e 5). Na Figura 2.2 pode-se observar a distribuição dos pontos de acordo com os níveis da mina.

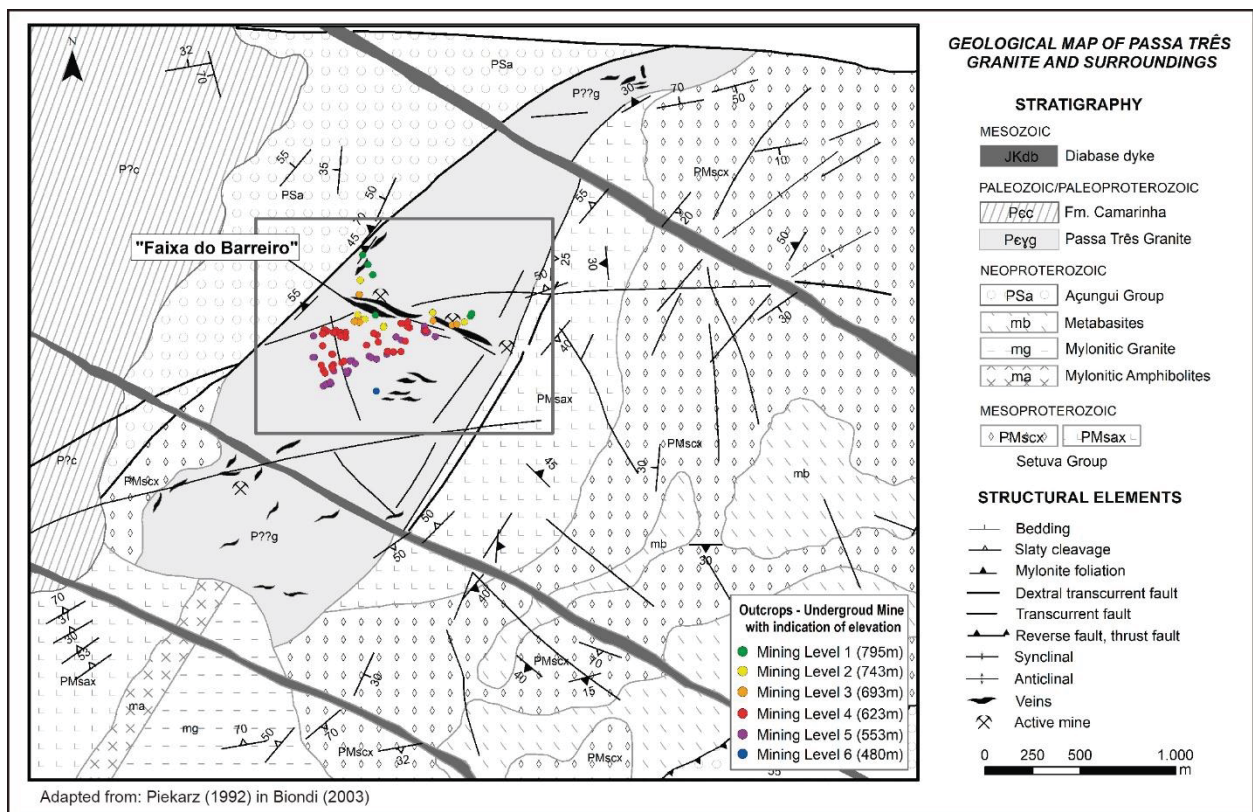


Figura 2.1 - Localização dos pontos de afloramentos na Faixa do Barreiro. As cores são relativas aos níveis da mina: verde - nível 1, amarelo - nível 2, alaranjado - nível 3, vermelho - nível 4 e violeta - nível 5.

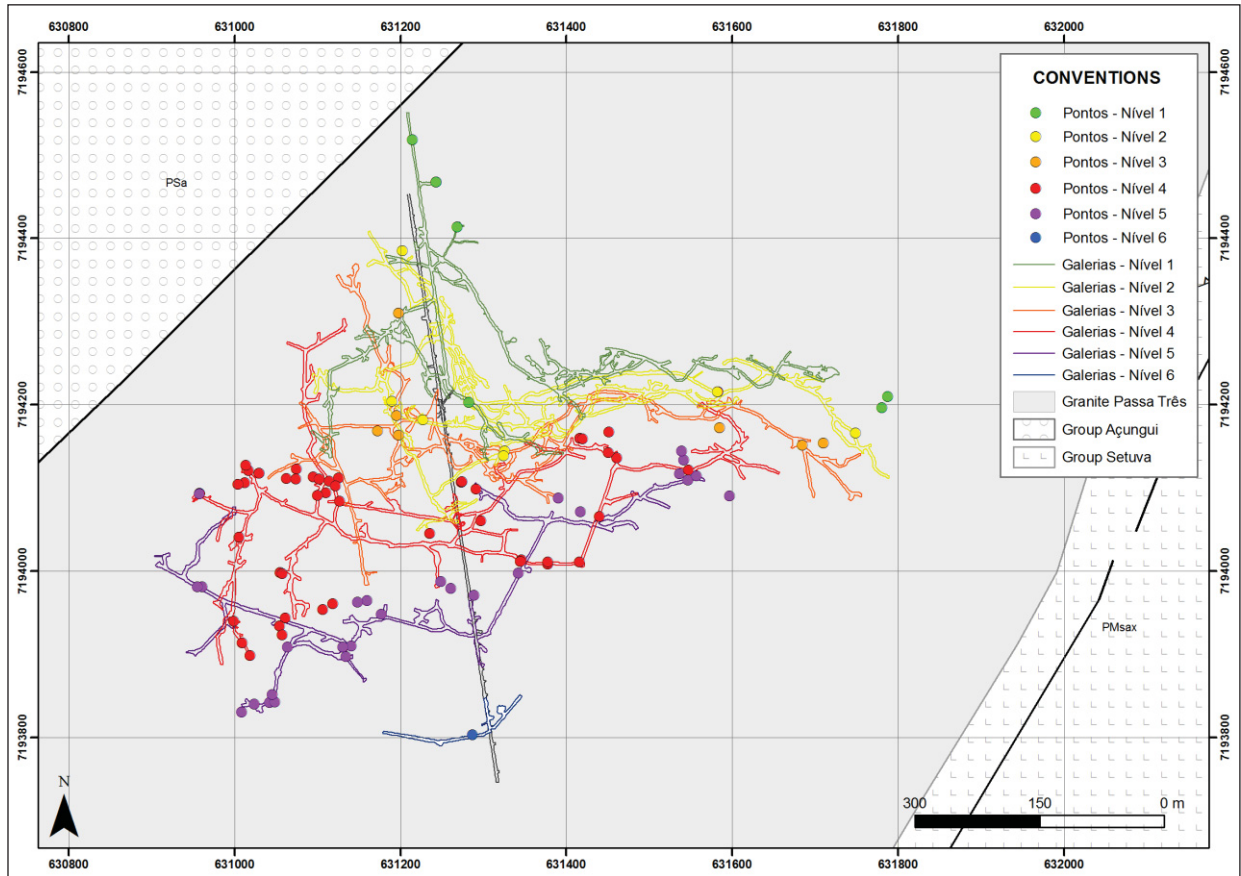


Figura 2.2 - Detalhe da localização dos pontos de afloramento de acordo com os diferentes níveis na Mina Tabaporã

Ao total, cerca de 300 kg de amostras foram coletados visando as análises de laboratório (petrografia, análises estruturais, análises químicas, análises de inclusões fluidas e geocronologia: U-Pb, Ar-Ar e Re-Os). Além das descrições de campo, foram descritos 1.815 metros de testemunhos de sondagem e mais de 150 amostras.

Os estudos petrográficos foram feitos no Laboratório Géosciences Montpellier, na Universidade de Montpellier (França) em 68 lâminas representativas dos veios mineralizados, assim como das diferentes fácies graníticas. Outras técnicas utilizadas no mesmo laboratório incluíram microscopia eletrônica de varredura (MEV), microsonda eletrônica (EPMA), espectrometria de massa induzida por *laser ablation* (LA-ICP-MS) para as datações U-Pb (zircão) e análise de elementos traços e espectrometria de massa por multicoletor para as datações Ar-Ar (muscovita). As análises realizadas no Brasil incluíram análise petrográfica, microtermométrica e espectroscopia Raman para o estudo das inclusões fluidas, análises litogeoquímicas (elementos maiores, traços, elementos terras raras - ETR - e metais preciosos) e isotópicas ($\delta^{34}\text{S}$ em sulfetos). Detalhes sobre os métodos aplicados serão apresentados em seguida.

2.1 MICROSCÓPIO ELETRÔNICO DE VARREDURA (MEV)

As análises foram realizadas em microscópio eletrônico de varredura FEI Quanta 200 FEG acoplado a detector Silicon Drift X-Max^N para análises EDS, no Laboratório Géosciences Montpellier, na Universidade de Montpellier, França.

2.2 MICROSSONDA ELETRÔNICA (EPMA)

As análises de química mineral foram realizadas em microsonda Cameca SX100 por espectrometria de dispersão de comprimento de onda, no Laboratório Géosciences Montpellier, na Universidade de Montpellier, França. As aquisições foram feitas em 20 kV com corrente de 10 nA, utilizando-se das seguintes linhas de raios-X para os minerais metálicos: S K α , Fe K α , Cu K α , Au L α , Mo L α , Pb M α , Ag L α , Zn L α , Ti K α , As L α , Bi L α , e, para silicatos e carbonatos: F K α , Al K α , Si K α , Ti K α , Na K α , Mg K α , Mn K α , Fe K α , K K α e Ca K α . No total foram analisados cerca de 132 pontos, incluindo cristais de pirita, calcopirita, ouro nativo, aikinita, muscovita, carbonato, biotita, clorita e K-feldspato.

2.3 GEOCRONOLOGIA U-PB EM ZIRCÕES (LA-ICP-MS)

A fim de se determinar a idade do corpo granítico, foram analisados cristais de zircão por U-Pb (LA-ICP-MS) de três fácies graníticas: granito equigranular médio (GEM), granito equigranular fino (GEF) e granito branco (GEB). Para a concentração dos zircões, foram coletados cerca de 8,0 kg de rocha de cada fácies. O procedimento para concentração de zircões foi realizado no Laboratório de Geologia Isotópica - UFRGS, em Porto Alegre (RS) e incluiu os seguintes passos: britagem; moagem em moinho de discos; peneiramento e separação em duas frações: 500 e 250 mesh; concentração dos minerais pesados com o auxílio de bateias; separador magnético Frantz em quatro intervalos: 0,4, 0,8, 1,2, 1,8 A; e, por fim, catação dos zircões em placa de Petri com auxílio de microscópio estereoscópico. Os cristais de zircão foram selecionados na fração não-magnética separada no intervalo de 1,5 A, organizados sobre fita adesiva, e impregnados em resina epóxi no Laboratório Géosciences Montpellier, na Universidade de Montpellier, França. Os dados U-Pb foram adquiridos na mesma universidade num ICP-MS (Element XR) acoplado ao sistema de laser GEOLAS de 193 nm. As condições do laser foram as seguintes: densidade de energia de 12 J/cm², com *spot* de 26 μ m e taxa de repetição de 4 Hz.

2.4 GEOCRONOLOGIA AR-AR EM MUSCOVITA

Para auxiliar na determinação da idade de venulação, foram selecionados cristais de muscovita em dez amostras abrangendo veios mineralizados, não-mineralizados e veios transicionais. O procedimento para preparação das amostras de muscovita para análise Ar-Ar foi realizado na seguinte ordem: britagem das amostras brutas; peneiramento nas frações 500 e 250 mesh; pré-seleção de cristais com o auxílio da lupa (cerca de 15 a 20 cristais); limpeza dos cristais com auxílio do aparelho de vibração ultrassônica com o auxílio de mini béqueres (cinco a seis minutos no álcool e três minutos na água); secagem em estufa (cerca de 70°C); e, por fim, seleção dos cristais com o auxílio de lupa. As amostras foram irradiadas por 40 horas na cidade de Pávia, Itália. As análises ^{40}Ar - ^{39}Ar foram obtidas pela técnica da fusão por etapas (*step heating*) foram realizadas no Laboratório Géosciences Montpellier, na Universidade de Montpellier, França, e a aquisição dos isótopos de Ar foram feitas no espectômetro de massa multicoletor Argus IV (Thermo Scientific). Os cristais separados de muscovita foram aquecidos por laser infravermelho (CO_2 , $\lambda = 10.600 \mu\text{m}$, $P = 30 \text{ W}$). Por fim, os dados foram tratados no *software* ArArCalc v. 2.5.2 criado por Koppers (2002). Critérios para geração de espectro de idades contínua e constante, definida como homogênea (ou *plateau*) envolveram pelo menos 50% do ^{39}Ar liberado por três ou mais *steps* consecutivos.

2.5 ANÁLISES DE ELEMENTOS TRAÇOS (LA-ICP-MS)

A fim de estudar a composição dos elementos traços das diferentes gerações de pirita, foram realizadas análises em ICP-MS (Element XR) acoplado ao sistema de *laser* GEOLAS 193 nm. Vinte e cinco pontos foram analisados em cristais de pirita 1, pirita 2, calcopirita, aikinita e ouro nativo com *spot* de tamanho 15 μm . O padrão utilizado foi o MASS1 (WILSON et al., 2002).

2.6 ANÁLISES DE INCLUSÕES FLUIDAS

Para o estudo das inclusões fluidas, foram confeccionadas dez lâminas bipolidas no Laboratório Géosciences Montpellier, na Universidade de Montpellier. Entre tais lâminas, cinco foram selecionadas para análise microtermométrica. As análises de microtermometria foram feitas em fragmentos de lâminas polidas (100 μm) em equipamento Linkam com estágios de aquecimento e resfriamento (de -180°C a +600°C) no Laboratório Lamir, na Universidade Federal do Paraná, Curitiba (PR).

Análises de espectroscopia Raman foram efetuadas em equipamento Raman Confocal Witec alpha 300R. Esse equipamento possui resolução lateral de 200 nm e vertical de 500 nm,

e comprimento de onda utilizado foi 532 e 633 nm. Essas análises foram realizadas no Centro de Microscopia Eletrônica (CME), na Universidade Federal do Paraná.

2.7 ANÁLISE DE ISÓTOPO DE ENXOFRE E QEMSCAN

As análises de isótopo de enxofre foram realizadas em cinco amostras pulverizadas de pirita, coletadas nos principais veios mineralizados da Faixa do Barreiro, e foram efetuadas no Laboratório Actlab em Ancaster, Canadá, em frações de 5 g. Os detalhes do procedimento analítico estão descritos em Borgo (2017), e os resultados estão exibidos em por mil (‰) em relação ao padrão internacional Troilita Canyon Diablo (CDT).

Análises do tipo QemScan determinaram os teores de elementos maiores e traços por fluorescência de raios-X com o auxílio do equipamento PANalytical AXIOS MAX com ânodo de ródio em 4W, na Universidade de Lausanne, Suíça. Os seguintes padrões foram utilizados para controle de qualidade: SY-2, BHVO, NIM-N e NIM-G.

3 GEOLOGIA REGIONAL

O Granito Passa Três é uma intrusão alongada e orientada segundo NE-SW, com aproximadamente 5 km² de área. As rochas encaixantes do Granito Passa Três são representadas pelos grupos Setuva e Açungui (Figura 3.1). Subordinados à Província Mantiqueira, os grupos Açungui e Setuva localizam-se na porção sul do Domínio Apiaí, de idade mesoproterozoica, constituindo parte do Cinturão Ribeira (HEILBRON et al., 2004). A Província Mantiqueira, ou Sistema Orogênico Mantiqueira, forma uma faixa NE-SW, paralela à costa atlântica do sudeste e sul do Brasil. Essa unidade faz limite com as províncias Tocantins, São Francisco e Paraná, e faz contato a leste com as bacias de margem continental, do Espírito Santo, Campos, Santos e Pelotas. É constituída pelos segmentos setentrional (Orógeno Araçuaí), central (Orógeno Ribeira), a zona de interferência entre os orógenos Brasília e Ribeira, terrenos Apiaí, São Roque e Embu, e pelo segmento meridional (orógenos Dom Feliciano e São Gabriel) (HEILBRON et al., 2004). Subordinado ao Cinturão Apiaí, o Grupo Açungui é formado por metapelitos, metapsamitos e metacarbonatos, sendo que a Formação Votuverava é constituída por metapelitos (sericita xistos, filitos, ardósias), com intercalações subordinadas de meta-arenitos, rochas carbonáticas e meta-basitos (BASEI et al., 2010).

Diversos estudos demonstraram que na porção sul do Terreno Apiaí, grandes compartimentos tectônicos foram deformados e justapostos por cisalhamento distensivo, envolvendo zonas de empurrão e de transcorrência (FIORI, 1992; CAMPANHA; SADOWSKI, 1999; SIGA JR. et al., 2009; BASEI et al., 2010) relacionadas à colisão oblíqua entre os crátons São Francisco, Congo e Paraná durante o Mesoproterozoico (FRAGOSO CESAR, 1993; ROGERS et al., 1995; CAMPOS NETO; FIGUEIREDO, 1995), resultando em deformação e metamorfismo em condições de baixo a médio grau metamórfico (CAMPANHA; SADOWSKI, 1999).

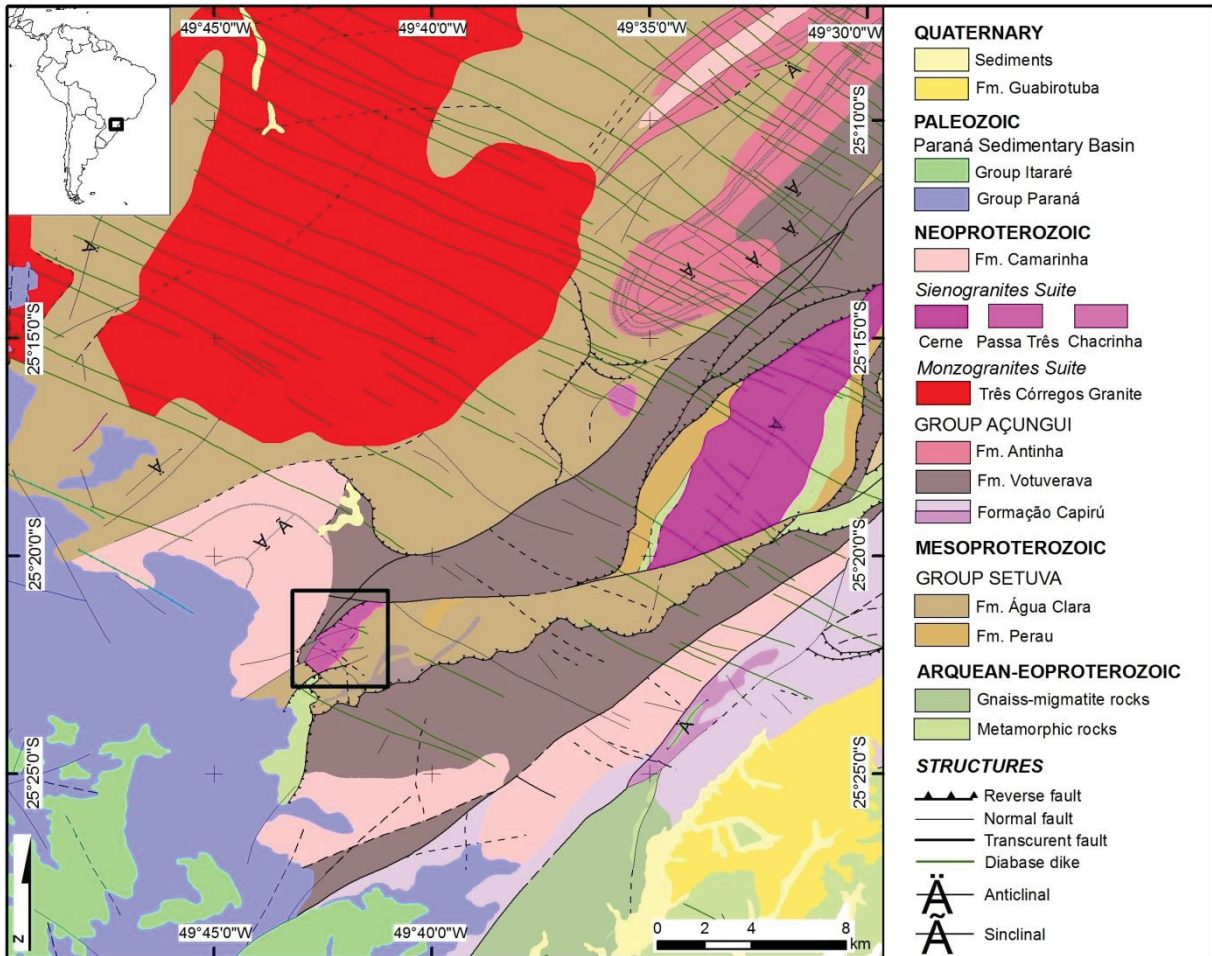


Figura 3.1 - Mapa geológico com indicação do Granito Passa Três cercado pelas rochas encaixantes dos grupos Setuva e Açungui (MINEROPAR, 2006).

Vários autores concordam com a existência de três eventos tectônicos principais que afetaram as rochas da Bacia Açungui (e os terrenos pré-cambrianos do Leste do Estado do Paraná), sendo o primeiro associado a um evento de empurrão (Sistema de Cavalgamento Açungui); o segundo a uma fase intermediária, denominada de Sistema de Dobramento Apiaí; e o terceiro associado a sistemas de cisalhamento transcorrentes (Sistema de Transcorrência Lancinha), o qual delimita o contato sudeste do Terreno Apiaí (FIORI, 1985a; FIORI et al., 1987; SOARES; REIS NETO, 1987; FIORI, 1992; SALAMUNI et al., 1992; FIORI, 1994; FASSBINDER, 1996; KAULFUSS, 2001; CURY et al., 2002; CURY et al., 2008). Entre esses, o Sistema de Transcorrência Lancinha apresenta cinemática dextral e superpõe os primeiros dois sistemas (Sistema de Cavalgamento Açungui e Sistema de Dobramento Apiaí), dividindo as rochas da região em três grandes blocos. Esse sistema é composto principalmente pelas falhas da Lancinha e de Morro Agudo, ambas de direção N40E, e entre as quais se localiza o Granito Passa Três (Figura 1.1).

De acordo com Cury et al. (2008), há uma foliação de baixo ângulo de caráter regional nas unidades pré-cambrianas, chamada de S1 e definida por planos de muscovita e biotita, e

paralela a subparalela ao acamamento sedimentar reliquiar. Essa estrutura é afetada por uma foliação de baixo ângulo (S2), presente nas áreas de cavalgamento. Nas formações Betara e Votuverava, próximo aos granitos do Cerne, Passa Três e Rio Abaixo e do Sienito Rabo de Galo, ambas as estruturas (S1 e S2) apresentam comportamento similar. No entanto, próximo às zonas de cisalhamento do Cerne, Morro Agudo e Lancinha, tais estruturas se mostram com alto ângulo e são afetadas, podendo estar crenuladas, pela foliação S3.

Segundo Sadowski e Motidome (1987), esse sistema está relacionado à falha regional Cubatão-Além Paraíba, resultando em áreas anastomosadas por deformação rúptil a dúctil dentro do sistema de cisalhamento, dificultando a compreensão da compartimentação tectônica e das relações estratigráficas entre as várias subunidades do Supergrupo Açungui.

Segundo Siga Jr. (2009), o magmatismo e a sedimentação dessas áreas estão relacionados a processos distensionais durante o fim do Paleoproterozoico (1750-1700 Ma) e Mesoproterozoico (1600-1450 Ma), e estresses compressivos teriam prevalecido durante o Neoproterozoico (~600 Ma). Em torno de 700 a 600 Ma, um arco magmático (tipo cordilheirano) se formou devido à evolução de uma zona de subducção localizada possivelmente a Sul do Cráton Luís Alves, produzindo um distensivo plutonismo alcalino na região, o que levou à geração de suítes graníticas tardi e pós-tectônicas. A tectônica neoproterozoica é responsável pela deformação, metamorfismo e colocação de plútons do tipo I, como os batólitos de Cunhaporanga e Três Córregos (Figura 1.1), representantes dos arcos magmáticos (PRAZERES FILHO, 2000) formados no Domínio Apiaí, sendo que ambas as unidades são intrudidas por *stocks* tardi-tectônicos (PRAZERES FILHO et al., 2003a). Esses batólitos apresentam grande quantidade de fenocristais de K-feldspato em matriz grossa, isotrópica a fracamente foliada (THEODOROVICZ et al., 1988; WERNICK et al., 1990; REIS NETO, 1994; GIMENEZ FILHO et al., 1995; CAMPANHA; SADOWSKI, 1999), idades U-Pb zircão entre 630 e 600 Ma (GIMENEZ FILHO et al., 2000; PRAZERES FILHO, 2000; JANASI et al., 2001), e são consideradas também como suítes sin a tardi-tectônicas por Campanha e Sadowski (1999).

Entre 600 e 450 Ma, a maior parte dos blocos continentais foi amalgamada a sudeste durante o fechamento do Oceano Adamastor e ocorreu o desenvolvimento de zonas de cisalhamento destrais relacionadas à colisão oblíqua e/ou tectônica de escape (por exemplo, Sistema de Cisalhamento Lancinha). Nesse contexto, bacias *pull-apart* foram criadas e preenchidas por sequências molássicas, e as unidades regionais foram intrudidas por granitos pós-tectônicos (CAMPANHA; SADOWSKI, 1999). A suíte pós-tectônica é considerada como pós-colisional ou anorogênica, e abrange os granitos do Cerne, Piedade, Morro Grande e Varginha (Figura 1.1). Esses plútons são geralmente compostos por álcali-feldspato granitos e quartzo sienitos, de tendência alcalina (CAMPANHA; SADOWSKI, 1999). De acordo com Prazeres Filho et al. (2003b), os *stocks* graníticos intrudidos no Domínio Apiaí, como os

granitos do Cerne, Piedade, Morro Grande e Varginha, apresentam idade entre 590 e 560 Ma, e assinatura do tipo A. Dados U-Pb, Rb-Sr e K-Ar de rochas vulcânicas em bacias *pull-apart* e resfriamento regional indicam idades entre 600 e 500 Ma (SIGA JR., 1995; CAMPANHA; SADOWSKI, 1999).

Rochas encaixantes

A leste e sudeste do Granito Passa Três, os litotipos da Formação Água Clara (Figura 3.2) podem ser divididos em duas associações litológicas principais, denominadas de “Scx” e “Sax”, contendo corpos de metabasitos intercalados (PIEKARZ, 1992). A associação “Scx” foi metamorfisada em fácies xisto verde e é formada por cálcio-xistos e por granada-muscovita/biotita-quartzo xistos com intercalações de quartzitos micáceos a quartzo xistos, xistos carbonosos, sericita-plagioclásio xistos e quartzo-clorita xistos (PIEKARZ, 1992). De acordo com Turini Neto (2012), ocorrem *boudins* de quartzo leitoso nesses xistos, os quais podem apresentar sulfetos (pirita, galena, esfalerita e calcopirita) com baixo teor de ouro. Esses veios geralmente apresentam espessuras desde milimétricas até métricas com extensiva turmalinização e biotitização nos xistos encaixantes com os quais fazem contato. Já a associação “Sax” foi descrita por Piekarz (1981 in PIEKARZ, 1992) como uma sequência calciossilicática, a qual forma uma faixa alongada NE bordejando o Granito Passa Três. As rochas metabásicas apresentam textura subofítica e são constituídas por anfibólio, plagioclásio e minerais opacos (PIEKARZ, 1992; TURINI NETO, 2012). Segundo Turini Neto (2012) as rochas metassedimentares exibem estruturas de bandamento fino e clivagem S1 em plano axial com atitudes entre N30E e E-W com mergulho de 10° a 70° com vergência para sudeste e sul (TURINI NETO, 2012).

A noroeste, o Granito Passa Três é limitado por uma zona de cisalhamento transcorrente, colocando-o em contato com as rochas metassedimentares da Formação Votuverava (Grupo Açungui, Figura 3.1) (PIEKARZ, 1992), as quais são representadas por metargilitos e metassiltitos com intercalações de metacalcários com estruturas de clivagem ardósiana (S1) em geral paralelas ao acamamento original (S0) (TURINI NETO, 2012). Próximo ao contato, esses litotipos se encontram silicificados e intensamente deformados por cisalhamento transcorrente com o desenvolvimento de estrias sub-horizontais presentes em planos de foliação subverticais (PIEKARZ, 1992). Essa zona de falha se estende para nordeste até infletir e acompanhar a Falha do Cerne, com direção leste-oeste, a qual apresenta as mesmas características deformacionais (PIEKARZ, 1992). Por sua vez, Turini Neto (2012) observa próximo ao contato uma foliação cisalhante de baixo ângulo (<45°), a qual representaria o contato tectônico do plúton com as rochas encaixantes.

A sudoeste encontram-se milonitos e blasto-milonitos, incluindo ainda xistos aluminosos a WNW separados de milonito-granitos a E-SSE por uma faixa de milonito-anfibolitos com indicações cinemáticas destrais (PIEKARZ, 1992). Nessa região, ocorre cataclase generalizada e basculamento de blocos com ocorrência de brechas, interpretado por Piekarz (1992) como uma falha normal nesse contato. Cury (2003) também cita a ocorrência de rochas deformadas com termos cataclásticos e subordinadamente protomiloníticos de forma restrita e associada a zonas de cisalhamento de alto ângulo, no contato com as encaixantes.

3.1 O GRANITO PASSA TRÊS

O Granito Passa Três é constituído principalmente por sienogranitos, podendo apresentar também fácies quartzo sieníticas (PIEKARZ, 1992). Esse plúton pode ser classificado como shoshonito, pertencente à série da magnetita, e considerado como granito de tipo I devido ao caráter metaluminoso e ao tipo de mineralização associada (PIEKARZ, 1992; PIKANÇO, 2000). Em relação à origem do magma, é considerado como híbrido, e é interpretado como tendo sido alojado em condições tardi-orogênicas ou tardi a pós-colisionais em relação ao arco magmático Três Córregos - Cunhaporanga (SOARES; GÓIS, 1987; CHIODI FILHO et al., 1989 in PIEKARZ, 1992; PIEKARZ, 1992), e em mesmo contexto que os granitos Varginha, Morro Grande, Piedade e Cerne. A colocação do Granito Passa Três também pode ser considerada como sin a tardi-transcorrências (CURY, 2003), tais como o Sistema de Transcorrência Lancinha, por exemplo (FIORI, 1985a).

A mineralização do Granito Passa Três é formada por veios de quartzo auríferos, os quais apresentam formatos irregulares, sendo tabulares ou em forma de lentes com espessuras milimétricas a métricas. A principal zona mineralizada no Granito Passa Três é representada pela Faixa do Barreiro, a qual foi focada pelo presente estudo. A paragênese não metálica abrange quantidades variáveis de fluorita, K-feldspato, carbonato e muscovita (PIEKARZ, 1992; PIKANÇO, 2000), enquanto que a paragênese metálica é constituída por pirita, calcopirita, sulfossais de Bi-Cu e ouro nativo (PIEKARZ, 1992), incluindo bornita, galena e molibdenita (PIKANÇO, 2000). Além desses minerais, Picanço (2000) também identificou a presença de covelita, calcocita, digenita, aikinita, arsenopirita, óxidos de ferro e argilo-minerais, tais como illita, vermiculita e esmectita.

Alterações hidrotermais foram observadas por diversos autores e abrangem alterações de biotitas e anfibólios, microclinização, sericita e muscovita, alteração argílica, alteração carbonática, silicificação (PIEKARZ, 1992; PIKANÇO, 2000), alteração potássica e alteração fílica (TURINI NETO, 2012), além de alteração de epidoto e saussuritização (CURY, 2003).

3.1.1 Modelos de formação da mineralização

Estudos anteriores sugerem diferentes modelos metalogenéticos para a mineralização do Granito Passa Três (SOARES; GÓIS, 1987; PIEKARZ, 1992; PICANÇO, 2000). Esses modelos apresentam consenso quanto à mineralização filoneana de ouro estar ligada à atividade de hidrotermalismo e associada a estruturas do Sistema de Transcorrência Lancinha. A relação da mineralização com a zona de cisalhamento do Cerne é considerada por Mesquita et al. (2002 in BIONDI, 2003), embora alguns autores considerem que a mineralização aurífera teria sido introduzida nas fases magmáticas finais (BIONDI, 1991 in PICANÇO, 2000; PIEKARZ, 1992; CHIODI FILHO et al., 1989 in PICANÇO, 2000). Entretanto, a possibilidade de ocorrência de mineralização do tipo pórfiro ainda é discutida devido ao quimismo do granito, os tipos, a sequência do hidrotermalismo e a provável origem magmática para o ouro e para o enxofre (CHIODI FILHO et al., 1989 in PICANÇO, 2000; PIEKARZ, 1992).

De acordo com o modelo de Soares e Góis (1987), a colocação do Granito Passa Três teria se dado na terminação sintética transpressional da Zona de Cisalhamento do Cerne, após ter ocorrido fraturamento tardi-magmático associado à formação de aplitos, pegmatitos e veios quartzo-feldspáticos, e com o desenvolvimento de hidrotermalismo (microclinização, greisenização e silicificação), além dos veios de quartzo com sulfetos. Posteriormente, teria ocorrido superimposição do sistema transtraccional rúptil (pós-magmático) representada pela deformação dos veios com direção principal N50E, e com alterações hidrotermais de epidotização e argilização com a deposição de ouro e calcopirita no interior de fraturas da pirita anteriormente formada.

O modelo proposto por Picanço (2000) considera a estrutura de empurrão da Falha do Boa Vista e as zonas de cisalhamento transcorrentes regionais (Falha do Cerne e Falha de Morro Agudo) como grandes condutoras regionais de fluidos, com energia proveniente do calor dos processos finais de metamorfismo regional representados por essas estruturas. Com a área aquecida e com intensa circulação de fluidos nas zonas de cisalhamento regionais, os fluidos com ouro teriam sido depositados em zonas tracionais regionais, representadas pela denominada Zona de Cisalhamento do Barreiro (Faixa do Barreiro) (PICANÇO, 2000). Nesse local, a situação deformacional e de hidrotermalismo facilitariam a entrada assim como a percolação de fluidos, bem como a reação com as encaixantes. Dessa forma, a deposição do ouro teria ocorrido através do processo de decompressão e abaixamento de temperaturas devido ao acúmulo de fluidos seguido de alívio. Ou seja, o ouro teria sido depositado por processo de imiscibilidade de fluidos devido ao contínuo abaixamento de tensões.

Em seu modelo, Picanço (2000) considera as zonas metassedimentares e de embasamento como área fonte dos solutos, cujos fluidos seriam transportados por zonas de

cisalhamento regionais com deposição em área tracionais. O minério seria concentrado em zonas permeáveis com rochas já hidrotermalmente alteradas, as quais teriam gerado condições de deposição de minérios e da paragênese sulfetada, a partir do rebaixamento de temperaturas e pressões.

A partir de análises geocronológicas, Picanço (2000) limitou o intervalo da idade da mineralização entre 510 e 527 Ma a partir de dados K-Ar em sericita de zona de falha (528 ± 10 Ma), Rb-Sr da encaixante mineralizada (526 ± 23 Ma) e de lixiviados de pirita (510 ± 13), ou seja, posterior à idade de colocação do granito interpretada pela isócrona de idade 616 ± 36 Ma pelo método Sm-Nd, com o período tardimagmático posicionado próximo a 600 Ma, sugerido pelo método K-Ar em muscovita e sericita.

Quanto ao arranjo estrutural, Pontes (1986 in PIEKARZ, 1992) descreveu três sistemas de veios: a) veios N50-60E, contidos em zonas de falhas; b) veios N-S, mais raros e menos cisalhados associados a fraturas; e c) filões E-W, precoces no sistema e com teores mais baixos a estéreis. Já Piekarz (1992) defendeu que os veios auríferos estariam controlados por zona de cisalhamento transcorrente dextral, a qual teria deformado o granito em estado rúptil com veios em posições antitéticas (N77W), sintéticas (N58E), distensionais (E-W) e pressionais (N29E), com a principal zona mineralizada (Faixa do Barreiro) alojada em zona de cisalhamento antitética dentro do granito (Figura 3.2). Picanço (2000) defende que a direção principal dos veios de quartzo-sulfetos seria próxima de N60W com caimento para sul. Segundo esse autor, os veios estariam colocados de acordo com o sistema de Riedel regional, onde as direções N40E representariam as direções principais do sistema de falhas, enquanto que as direções ao redor de N70E a E-W representariam as direções sintéticas. Por fim, as direções principais de ocorrência de veios mineralizados correspondem a direções tensionais, ao redor de N60W e N30W, que são as estruturas antitéticas verificadas por Picanço (2000).

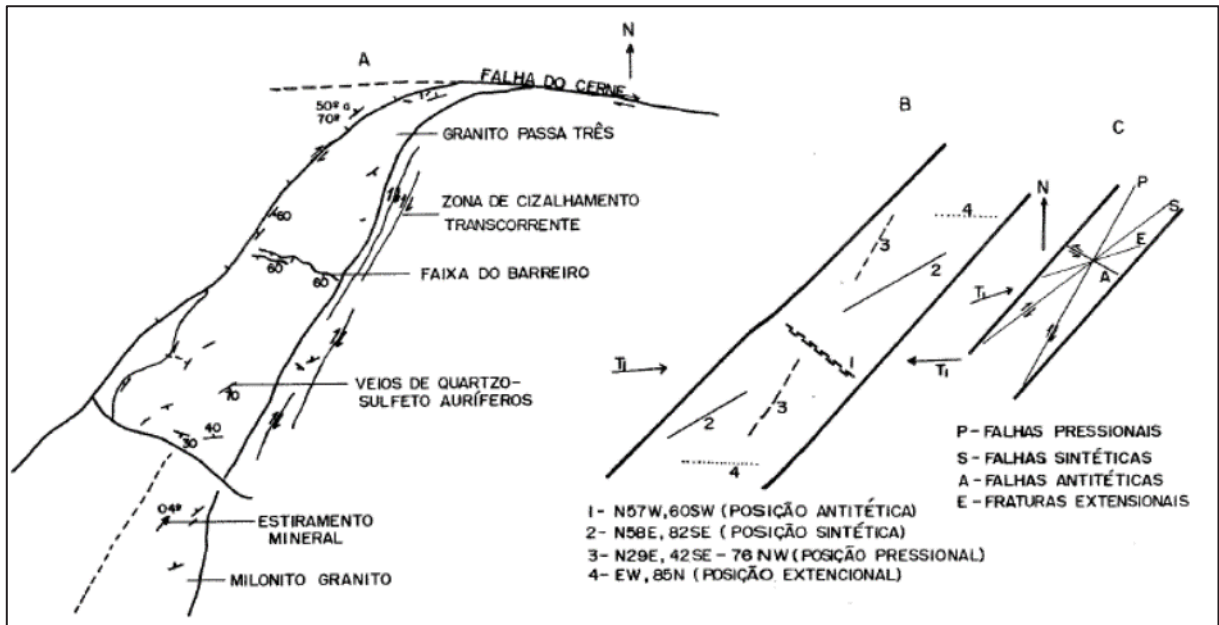


Figura 3.2 - Modelo esquemático da posição dos veios auríferos proposto por Piekarz (1992).

De acordo com Piekarz (1992), os veios de quartzo-sulfetos auríferos apresentam-se extremamente cisalhados e cataclasados, constituindo estrutura brechoide coesiva. Nos veios que ocorrem na Faixa do Barreiro, são comuns estreitas zonas de cisalhamento dentro dos veios, com recristalização dinâmica do quartzo após o seu estiramento, mostrando que houve condições locais de temperatura e pressão suficientes para ocasionar sua ductilidade.

Piekarz (1992) considera que as mineralizações estão associadas à evolução do hidrotermalismo, e com base na disposição estrutural dos filões auríferos e dos tipos de alterações hidrotermais, distingue dois tipos de veios, os quais são denominados de T1 e T2. Nesse contexto, o tipo T1 ocorreria em sistemas de falhas com expressiva argilização acompanhando a mineralização, associado à alteração fílica nas encaixantes, enquanto que o tipo T2 estaria preenchendo fraturas distensionais no granito, não estando associado a movimentos relativos de blocos ou argilização, havendo apenas alteração fílica.

Posteriormente, Turini Neto (2012) publicou esboço da seção N-S com as principais formas e atitudes dos veios mineralizados, onde sugere esforços de empurrão de sul para norte e deformações causadas por esforços de NW para SE (Figura 3.3).

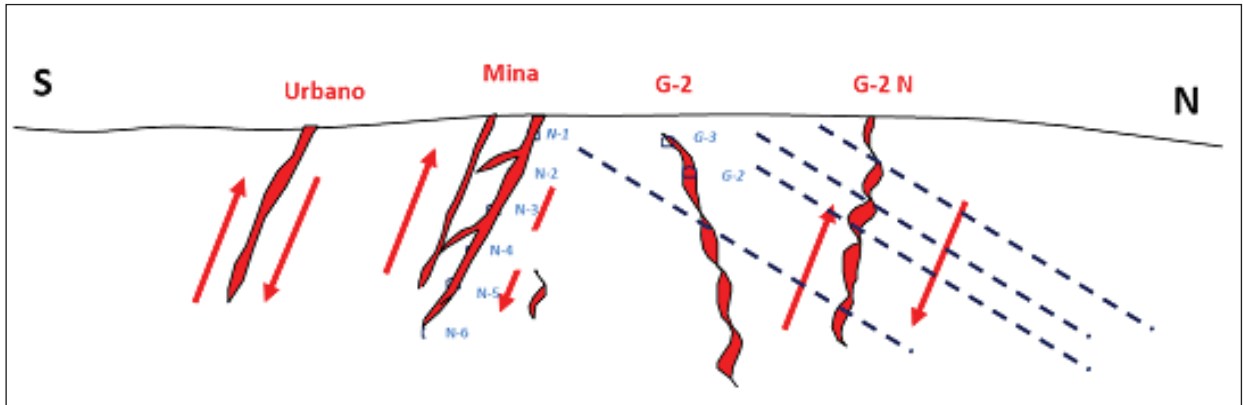


Figura 3.3 - Esboço de seção N-S do granito sugerida por Turini Neto (2012), onde se observa tendência de mergulhos dos veios para sul. Fonte: TURINI NETO, 2012.

4 THE PASSA TRÊS LODE GOLD DEPOSIT (PARANÁ STATE, BRAZIL): AN EXAMPLE OF STRUCTURALLY-CONTROLLED MINERALISATION FORMED DURING MAGMATIC-HYDROTHERMAL TRANSITION AND HOSTED WITHIN GRANITE

Bárbara Carolina Dressel* ^{1,2,4}; Alain Chauvet ¹; Barbara Trzaskos ²; João Carlos Biondi ²; Olivier Bruguier ¹; Patrick Monié ¹; Sandro Notto Villanova ³; José Bazille Newton ³

¹ CNRS-UMR 5243, Géosciences Montpellier, Université de Montpellier, cc60, 34095 Montpellier Cedex 5, France.

² Federal University of Paraná, Post-Graduation Program in Geology, Geology Department, Av. Coronel Francisco Heráclito dos Santos, 210, 81531-970, Curitiba – PR, Brazil.

³ Mineração Tapirorã, Rua Maria Aparecida de Oliveira, 803 - Lt. São Gerônimo, 83606-177, Campo Largo – PR, Brazil.

⁴ Capes-PDSE Scholarship Process n. 99999.006489/2015-00. CAPES Foundation, Ministry of Education of Brazil, Brasília - DF, 70.040-020, Brazil

*Corresponding author

Full postal address: Federal University of Paraná, Post-Graduation Program in Geology, Geology Department, Av. Coronel Francisco Heráclito dos Santos, 210, 81531-970, Curitiba - PR, Brazil

E-mail addresses: barbara.geologia@gmail.com, barbara.dressel@gm.univ-montp2.fr (Dressel, B.C.); alain.chauvet@gm.univ-montp2.fr (Chauvet, A.); barbaratzaskos@ufpr.br (Trzaskos, B.); jcbiondi@ufpr.br (Biondi, J.C.); olivier.bruguier@gm.univ-montp2.fr (Bruguier, O.); patrick.monie@gm.univ-montp2.fr (Monié, P.); notto@tabipora.com.br (Villanova, S.N.); josebazille@hotmail.com (Newton, J.B.)

ABSTRACT

The Passa Três granite is a NNE-SSW elongated shape intrusion located in the Paraná State (southern Brazil). This intrusion was emplaced within metapelites of the Mesoproterozoic Votuverava Group, which are part of the N040°E trending Lancinha Shear Zone. Gold mineralisation within the Passa Três granite is held by meter-scale quartz veins forming orebodies with variable massive, banded, sheared and/or brecciated internal textures. Structural data indicate the existence of two orthogonal directions of structures, N-S and E-W, dipping 60-75°W and 45-70°S respectively. Mineralised veins contain, in addition to the quartz of the gangue, and in chronological order: fluorite, pyrite, chalcopyrite, gold, aikinite, molybdenite, muscovite, carbonate and baryte. Gold occurs as native grains within fractures that affect pyrite, commonly associated with chalcopyrite and aikinite. Quartz veins are sometimes bordered by aplitic dikes. Additionally, some of the veins exhibit a thin margin of K-feldspar minerals that could represent the early stage of vein formation. These observations, the presence of Unidirectional Solidification Textures (UST), along with abundant expression of pegmatite-rich pockets within granite that crops out close to the surface allow the reconstruction of the granite architecture in terms of late magmatic evolution, magmatic-hydrothermal transition and position of the cupola. N-S and E-W systems are interpreted to be contemporaneous and conjugate. Normal displacements are predominant and main

mineralised veins are essentially located within extensional pull-apart structures. The structural model suggests that the normal faults were initiated along former low-angle planes associated with aplite and/or early quartz veins that subsequently controlled the opening of the pull-apart structures that represent the economic orebodies. Zircon from the granite and muscovite grains from mineralised veins were dated by U-Pb and Ar-Ar methods, respectively. Zircons from the main facies (medium grained: GEM and microgranite: GEF) provided undistinguishable ages which were pooled to give an age of 611.9 ± 3.6 Ma. A less abundant, leucocratic facies (“white granite”: GEB) yielded a significantly younger age of 592.8 ± 7.1 Ma. Muscovites from quartz veins gave Ar-Ar ages of 612.9 ± 2 to 608.8 ± 2 Ma (transitional vein with a K-feldspar border), 611.7 ± 2 to 608.8 ± 2 Ma (mineralised veins) and 608.4 ± 2 Ma (barren quartz vein). Thus, the Passa Três granite and its gold mineralisation appear to represent a unique example of an intrusion-related gold system in which the mineralisation concentrates in the core of the magmatic intrusion in the form of meter-scale veins strongly controlled by tectonics.

Keywords: Gold-bearing quartz, Extensional pull-apart, Neoproterozoic.

4.1 INTRODUCTION

Intrusion-related gold deposit (IRGD) models were developed by several authors during the last decades (e.g., LANG; BAKER, 2001; MUSTARD, 2001; SILLITOE; THOMPSON, 1998; THOMPSON et al., 1999), improving the classification of many gold deposits worldwide. While the contribution of granite to gold mineralisation is frequently suggested, its role in the formation of what is called “orogenic gold deposits” has been underestimated (GOLDFARB et al., 2001; GROVES et al., 1998). The intrusion-related gold deposit classification includes intrusion-hosted, proximal and distal deposit styles. However, it is still challenging to distinguish deposits in this classification from orogenic gold deposits, as already highlighted by several authors (BAKER; LANG, 2001; GROVES et al., 1998; HART, 2007; LANG; BAKER, 2001; MARCOUX et al., 2015; THOMPSON et al., 1999). In the literature, several studies described mineralisations with different styles, including disseminations, skarns, stockworks, replacements and veins (GOLDFARB et al., 2001; HART, 2007; LANG; BAKER, 2001; MALOOF et al., 2001). Among these, intrusion-hosted sheeted veins are described in many deposits, thus considering the granite formation and the mineralisation as coeval (LANG; BAKER, 2001; LIANG et al., 2016; MARCOUX et al., 2015; MALOOF et al., 2001, among others). In these cases, sheeted veins frequently form a regular network of thin, flat veins concentrated within the granite cupola, mostly associated with wolfram and tin deposits and

present an association with a magmatic-hydrothermal transition history of the crystallizing pluton (BAKER; LANG, 2001; THOMPSON et al., 1999).

Case studies in which gold deposits, and only gold-bearing ones, occur inside the granite in the form of large-scale quartz-rich veins (horizontal length from 100 to 200 meters) have been debated in the literature and sometimes the classification as intrusion-related gold deposits has been considered for former orogenic lode gold types. During 40 years of exploration of the Passa Três gold deposit, this intrusion and its gold mineralisation have been studied by several projects (SOARES; GÓIS, 1987; PIEKARZ, 1992; PIKANÇO, 2000; TURINI NETO, 2012). These projects focused on describing the granitic body and its facies, the hydrothermal alteration, granite classification, and the mineralisation, producing some models about the formation of the deposit. However, despite their contribution, several aspects of the gold deposit are not yet fully understood, such as the relation between magmatism, hydrothermalism, deformation and mineralisation. Therefore, a genetic relation between the formation of the mineralisation and the granite was suspected, but evidence to confirm this hypothesis is still lacking, as is a definition or an understanding about the metallogenic model of the deposit.

The development of the IRGD model (LANG; BAKER, 2001) and the description of several deposits as intrusion-hosted opened up the possibility of shedding new light on the Passa Três gold deposit. Because the Passa Três gold mineralisation (Paraná State, Brazil) is characterized by a structural-related deposit developed during the magmatic-hydrothermal transition, this deposit represents an interesting case-study. Hence, this paper aims to present and discuss new structural, petrological, mineralogical and geochronological data on the Passa Três granite and associated gold mineralisation. This pluridisciplinary study was undertaken with two main objectives: i) to understand the genesis and the geometry of this deposit in order to contribute to exploitation procedures, and ii) to unravel the combination of magmatic, hydrothermal and tectonic processes that potentially played a role in the formation of this very specific deposit and that may explain why it differs drastically from classical models. Moreover, this contribution will provide additional and interesting arguments to the general discussion of Intrusion-related gold deposits, in particular on the issues of i) the link between granite and mineralisation and ii) the localization of the mineral deposit with respect to the granitic body.

4.2 GEOLOGICAL SETTING

The Eastern Paraná state (Southern Brazil) is composed of four terranes presumably amalgamated during the Neoproterozoic, which include, from North to South, the Apiaí, Curitiba, Luís Alves and Paranaguá terranes (Figure 4.1), all representative of the Southern

portion of the large-scale Ribeira Mobile Belt (HEILBRON et al., 2004). The Passa Três granite crops out within host rocks that mainly comprise the Mesoproterozoic Votuverava Group, of the Apiaí Terrane (Figure 4.1). The Votuverava Group is composed of a monotonous succession of meta-pelitic rocks (sericite schists, phyllites, slates), with subordinate intercalations of meta-arenites, rare carbonate rocks and meta-basites (BASEI et al., 2010).

Several studies demonstrated that the Southern part of the Apiaí Terrane is deformed and affected by extensive shearing events, involving thrust and strike-slip shear zones (BASEI et al., 2010; CAMPANHA; SADOWSKI, 1999; FIORI, 1992; SIGA JR. et al., 2009). These events were related to the oblique collision between the San Francisco, Congo and Paraná cratons during the Neoproterozoic (CAMPO NETO; FIGUEIREDO, 1995; FRAGOSO CESAR, 1993; ROGERS et al., 1995). This resulted in deformation of the sedimentary sequence under low to medium grade metamorphism (CAMPANHA; SADOWSKI, 1999).

Several authors agree on the existence of three main tectonic events that affected the rocks of the Precambrian terranes located in Eastern Paraná State. The first one is related to the thrust event (Açungui Thrust System), the second one is called the Apiaí Folding System, and the third one is associated to transcurrent shear deformation (dextral Lancinha Shear System, Figure 4.1) that delimitates the South-eastern contact of the Apiaí Terrane (CURY et al., 2002; FIORI, 1992, 1994; FIORI et al., 1987; FASSBINDER, 1996; KAULFUSS, 2001). Near the Passa Três granite, the third tectonic event is well illustrated by the Morro Grande and Lancinha faults, with the Passa Três granite being emplaced between these two structures (Figure 4.1).

Two main episodes of magmatism have been described. The first one, from 700 to 600 Ma, reflects the formation of a magmatic arc (Cordilleran type) and the production of extensive calc-alkaline plutonism represented by I-type granites. Syn- to post-tectonic plutons were emplaced between 630 and 600 Ma (i.e., Cunhaporanga and Três Córregos batholiths) and are attributed to this first event (CAMPANHA; SADOWSKI, 1999; GIMENEZ FILHO et al., 2000; JANASI et al., 2001; PRAZERES FILHO, 2000; PRAZERES FILHO et al., 2003a). From 600 Ma onward, the Adamastor Ocean was completely consumed and most continental blocks were amalgamated. The tectonics was then characterized by the development of dextral shear zones related to some oblique collision and/or escape tectonics (e.g., Lancinha Shear System). In this context, pull-apart basins were created, filled by molasse sequences, and the regional units were intruded by post-tectonic granites that formed the second event between 590 and 560 Ma (A-type magmatism developing the Cerne, Passa Três, Piedade, Morro Grande and Varginha granites - Figure 4.1; CAMPANHA; SADOWSKI, 1999; PRAZERES FILHO et al., 2003b).

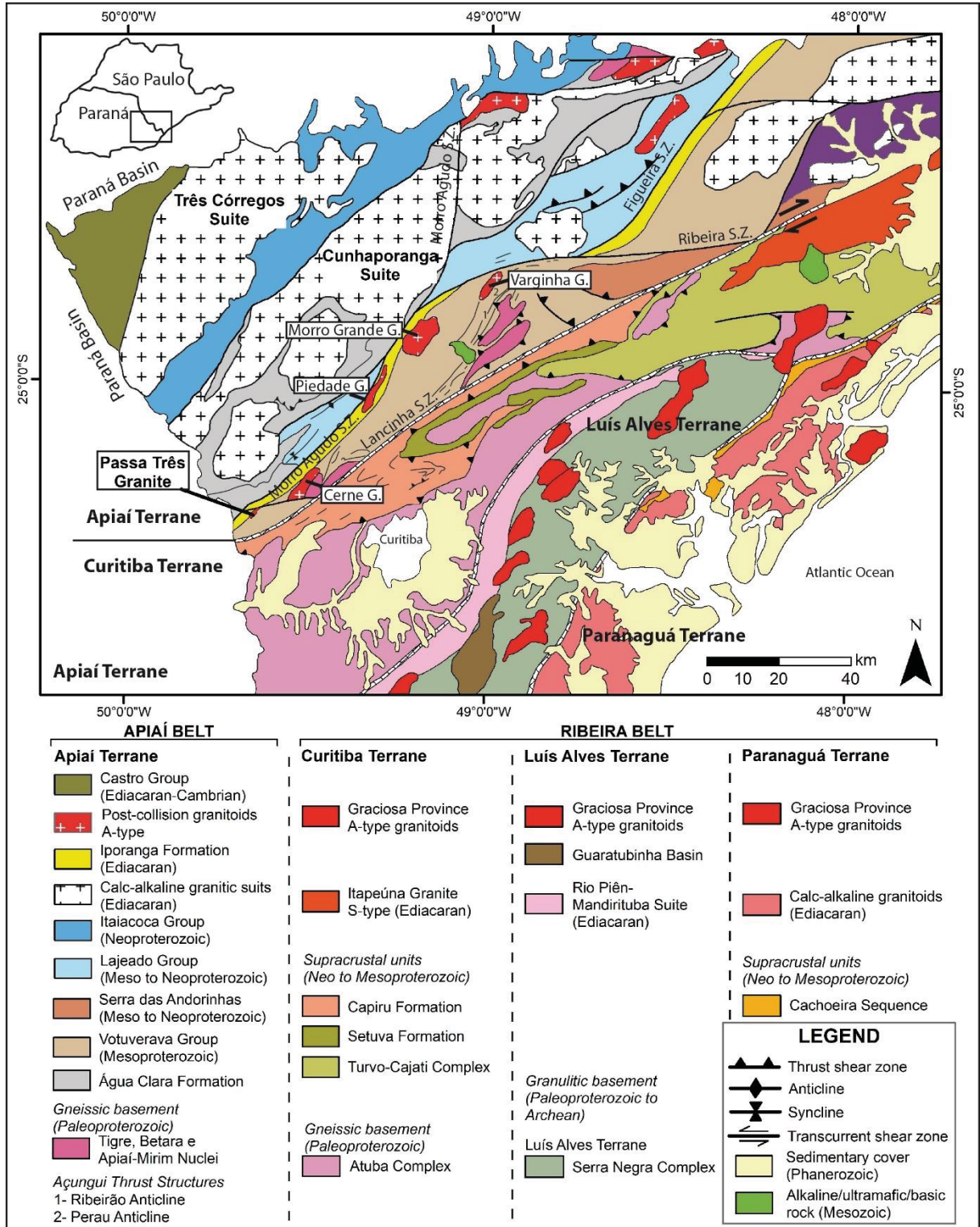


Figure 4.1 - Geological map with location of the Passa Três granite surrounded by its host rocks. The Apiaí, Curitiba, Luís Alves and Paranaguá terranes are also indicated. (Adapted from FALEIROS, 2008)

4.2.1 The Passa Três granite

The Passa Três granite is an elongated NE-SW oriented intrusion, with a surface area of approximately 5 km². This intrusion consists mainly of syenogranites, monzogranites and

quartz syenites, and is classified as an I-type granite due to its metaluminous character and its mineralogical association comprising magnetite, titanite, apatite, amphibole, biotite but lacking aluminous minerals (PIEKARZ, 1992). It has been classified as a shoshonite belonging to the magnetite-granite series (PICANÇO, 2000; PIEKARZ, 1992), and interpreted as a post-collisional intrusion, like the Varginha, Morro Grande, Piedade and Cerne granites, occurring within the same area (Figure 4.1). It is considered as a hybrid granite (crust and mantle origins) because of the metaluminous character, rare earth elements (REE) pattern with heavy REE more depleted than light REE, and no negative Eu anomaly (PIEKARZ, 1992). Additionally, isotopic data of epsilon Nd (from -13 to -16) and epsilon Sr (120-72), and also high Ba and Sr grades suggest a strong crustal contribution (CURY, 2003). The Passa Três granite is thought to have been intruded during a late-orogenic to post-collisional context related to the Neoproterozoic Três Córregos-Cunhaporanga magmatic arc (CHIODI FILHO et al., 1989 in PIEKARZ, 1992; PIEKARZ, 1992; SOARES; GÓIS, 1987), and its emplacement has been also considered as syn- to late-shearing regarding the shear zones (e.g., the Lancinha Shear Zone; CURY, 2003; FIORI, 1985a).

Gold-bearing quartz veins present irregular shapes, frequently occurring in the form of lenses of millimetric to metric dimensions. These dimensions are very variable, but in general widths vary from a few millimetres to three meters, and lengths from 10 to several meters, up to 200 meters. Gold mineralisation mainly developed in the central part of the intrusion within a zone called the “Faixa do Barreiro” (Figure 4.2). Non-metallic paragenesis has been described as made of quartz with varying amounts of fluorite, K-feldspar, carbonate and muscovite (PICANÇO, 2000; PIEKARZ, 1992). Metallic minerals consist of pyrite, chalcopyrite, Bi-Cu sulphosalts and native gold (PIEKARZ, 1992), including subordinate bornite, sphalerite, galena and molybdenite (PICANÇO, 2000). Picanço (2000) also identified the presence of covellite, chalcocite, digenite, aikinite, arsenopyrite, iron oxides and clay minerals such as illite, vermiculite and smectite. Unfortunately, no information regarding ore reserves is available for this deposit; however, personal communication from the mine staff established an average grade of 6 ppm for the gold mineralisation.

Numerous hydrothermal alterations have been described and comprise potassic alteration, phyllic alteration, epidote alteration, saussuritization, silicification, carbonation (CURY, 2003; PICANÇO, 2000; PIEKARZ, 1992; TURINI NETO, 2012) and argillic alteration (related to the fault zones and considered as a hypogene alteration by Piekarz, 1992).

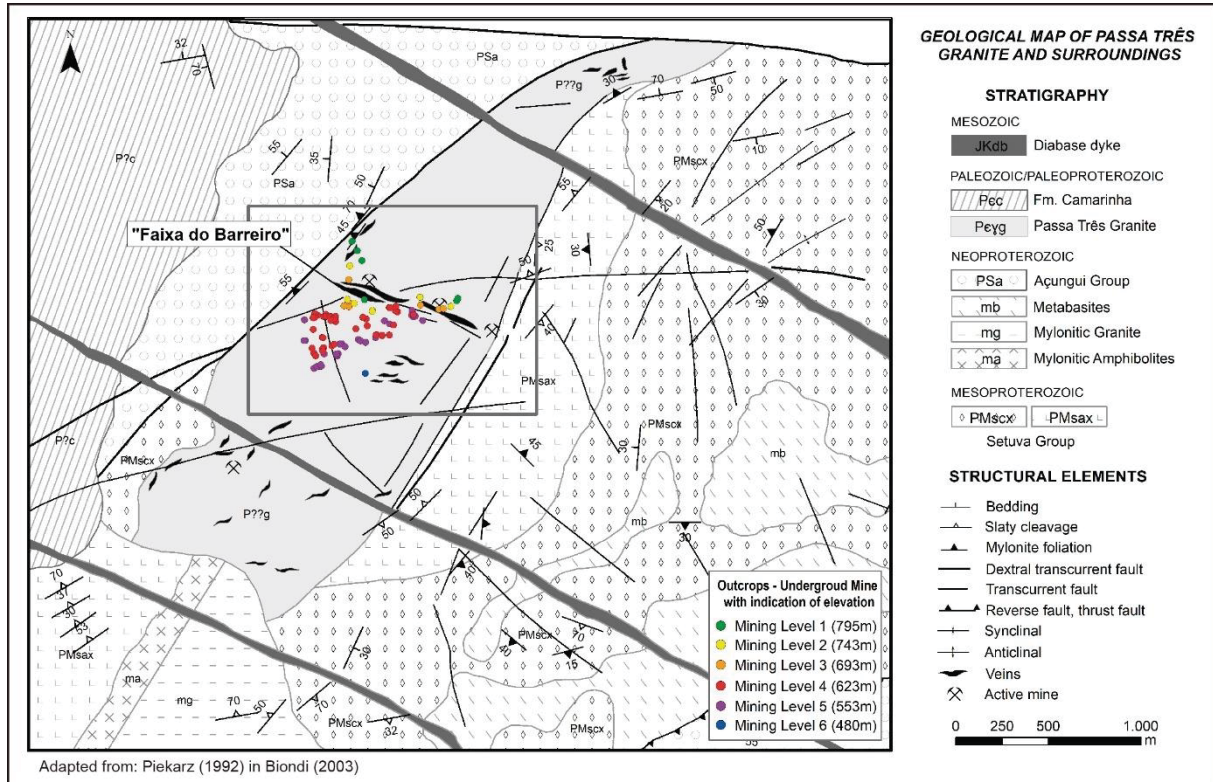


Figure 4.2 - Geologic map of the Passa Três granite and surrounding units. Different colours represent underground exposures of the mineralisation at different mine levels thus implying that gold-bearing structures dip southwards with moderate to high angles (40 to 60°). (Modified from PIEKARZ, 1992 in BIONDI, 2003)

4.3 METHODS

Petrographic studies were carried out at the Montpellier Géosciences Laboratory (Montpellier, France) on 68 representative samples from the mineralised veins, as well as from different granitic facies. The techniques used included scanning electron microscopy (SEM), electron microprobe (EPMA), laser ablation-inductively coupled plasma-mass spectrometry (LA-ICP-MS) for U-Pb and trace-element analyses, and multi-collector mass spectrometry for Ar-Ar geochronology.

Scanning electron microscopy (SEM) analyses were performed in a FEI Quanta 200 FEG SEM coupled to a Silicon Drift Detector (SDD) – X-Max^N for EDS analyses. Electron-microprobe analyses (EPMA) were performed on a Cameca SX100 Electron Microprobe Microanalyzer by wavelength dispersion spectrometry. Measurements were done at 20 kV with a beam current (cup reading) of 10 nA, using the following X-ray lines for the metallic minerals: S K α , Fe K α , Cu K α , Au L α , Mo L α , Pb L α , Ag L α , Zn L α , Ti K α , As L α , Bi L α . Analyses were performed on pyrite, chalcopyrite, gold and aikinite crystals.

For U-Pb analyses, zircon grains were separated using conventional techniques. After crushing and sieving, heavy minerals were concentrated by a gold panning kit (three sizes)

and subsequently processed by magnetic separation using a Frantz separator at the Laboratory of Isotopic Geology in UFRGS, Porto Alegre, Brazil. Zircon grains were handpicked from the non-magnetic fraction at 1.5 A intensity and the selected grains were then mounted on adhesive tape, and enclosed in epoxy resin at the Montpellier Géosciences Laboratory. U-Pb data were acquired at the University of Montpellier using a single collector, sector field ICP-MS (Element XR) coupled to a GEOLAS 193 nm excimer laser system (AETE-ISO regional facility of the OSU OREME). Analyses were performed using a 26 μm spot size, a 4 Hz repetition rate and an energy density of 12 J/cm^2 . For more details about the analytical procedures, see Bruguier et al. (2017) and Bosch et al. (2011). For concordant analyses, ages of zircons are expressed in terms of their $^{207}\text{Pb}/^{206}\text{Pb}$ ratios (grains older than 1 Ga) or their $^{206}\text{Pb}/^{238}\text{U}$ ratios (grains with Neoproterozoic age). Weighted mean ages and regressions were calculated using Isoplot (LUDWIG, 2012) and errors in the text and in the concordia diagram are quoted at the 2σ level.

For Ar-Ar analyses, muscovite crystals from 10 samples were separated from mineralised, transitional veins (with a K-feldspar border) and barren veins (see definition below). Samples were crushed, sieved, and single grains of micas were handpicked under a stereo microscope. The separates were washed repeatedly in an ultrasonic bath using distilled water and acetone. Samples were then irradiated for 40 hours in a reactor in Pavia, Italy. $^{40}\text{Ar}/^{39}\text{Ar}$ stepwise heating analyses were performed on an Argus VI multicollector (Thermo Scientific). Separated crystals were heated by an infrared laser (CO_2 , $\lambda = 10.600 \mu\text{m}$, $P = 30 \text{ W}$), and the polished sections were ablated with an ultraviolet laser (Spectron Laser Systems, $\lambda = 266\text{nm}$, $P = 240 \text{ mJ}$). The ArArCalc software© v. 2.5.2 by Koppers (2002) was used for data reduction and plotting. The plateau criteria involved at least 50% of the ^{39}Ar released in three or more contiguous steps with ages that agree within two sigma.

4.4 GEOLOGY OF THE DEPOSIT

4.4.1 Magmatic facies and alteration

In this study, we separated the Passa Três granite into three different granitic facies, called “medium-grained granite” (GEM), “microgranite” (GEF) and “white granite” (GEB), in addition to aplites and pegmatites. In terms of field relations, GEF and GEM facies appear to be contemporaneous and crop out within the entire intrusion. The leucocrate GEB facies was only recognized in drill cores. Aplites and pegmatites will be described in the next section (section 4.4.2).

The GEM facies is classified as a syenogranite and presents an igneous paragenesis composed of microcline, plagioclase, quartz and biotite (Figure 4.3a, b), and has a medium-

grained and isotropic texture. Zircon and apatite appear as accessories. Chlorite, sericite, carbonate, magnetite, hematite and chalcopyrite occur as alteration minerals. Magnetite is associated with well-crystallized sphalerite. Hematite is anhedral and occurs with magnetite, carbonate and sericite as aggregates. Carbonate veinlets are common and affect all the mineral phases. This facies is the most common and exhibits a typical and characteristic red colour (Figure 4.3a). Submagmatic fractures (BOUCHEZ et al., 1992) affect K-feldspar crystals and are filled by quartz (Figure 4.3c).

GEF is the same granite (syenogranite) and has a fine-grained isotropic texture (Figure 4.3d). The igneous paragenesis is composed of microcline, plagioclase, quartz and biotite, and accessory minerals such as apatite, zircon, and fluorite. Carbonate, chlorite, sericite, pyrite and sphalerite are observed and correspond to alteration products.

The GEB facies is a monzogranite composed of plagioclase, microcline and quartz (Figure 4.3e, f). The texture is medium grained and isotropic. Zircon, apatite and titanite occur as accessory minerals whereas sericite is very rare and corresponds to an alteration of feldspar. Chlorite crystals occur associated with the accessory minerals and are probably an alteration of biotite.

Four types of alteration were identified. The first one is a global red colour of the main granite, associated with hematite grains within K-feldspar (NAKANO et al., 2005; PUTNIS et al., 2007). The second is a muscovite-rich alteration. This one takes the form of millimetric muscovite grains mainly developed as large zones and within fractures with no clear orientation. Posterior to the muscovite, some fractures filled by sericite, carbonate, and some chlorite developed mainly parallel to the border of quartz veins. We associate to this event the systematic alteration of magmatic biotite into chlorite grains. Lastly, other alterations such as sodic (albite rim developed around magmatic K-feldspar) or potassic ones (clean K-feldspar border) are also suspected.

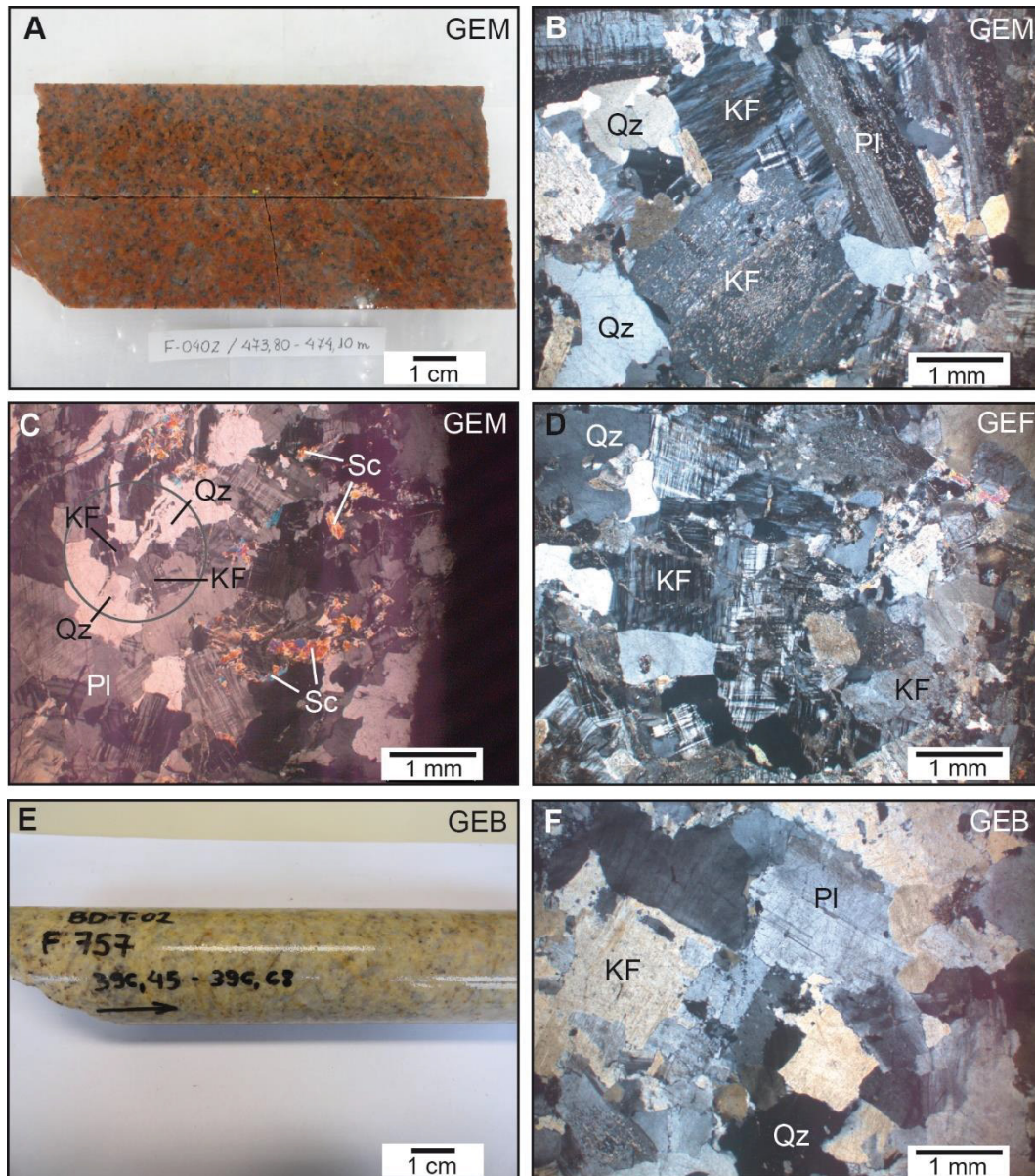


Figure 4.3 - Photographs of the three main facies of the Passa Três granite. A) Red coloured “medium grained granite” facies (GEM); B) Photomicrograph of the GEM facies; note sericitic alteration on plagioclase and K-feldspar crystals; C) K-feldspar with a submagmatic fracture filled by quartz (GEM); D) Photomicrograph of the microgranite facies (GEF); E) “White granite” facies (GEB); F) Photomicrograph of the GEB facies; note the absence of sericitic alteration. Sc: sericite; Qz: quartz; KF: K-feldspar; Pl: plagioclase.

4.4.2 Magmatic-hydrothermal transition

Within galleries and boreholes in the Passa Três granite, we observed rocks, textures and structures that clearly indicate the presence of magmatic-hydrothermal transitional features, such as aplites, pegmatites, UST (Unidirectional Solidification Texture, HÖNIG et al., 2010; SHAFAROUDI et al., 2015; YANG et al., 2016) and quartz veins with a K-feldspar border (herein denominated transitional veins) (Figures 4.4 and 4.5). All these features are intensively developed in the upper part of the granite body, and are described below.

Aplites mainly consist of quartz, K-feldspar, plagioclase and titanite, with no visible crystalline fabrics (Figure 4.4a-c). Contacts between these crystals are interdigitated, indicating fast cooling probably with little space available. At the borehole scale aplites seem to be abundant in zones surrounding the orebodies (Figure 4.4b). Even when hardly distinguishable from the red-coloured granite, aplites frequently border the low-angle dipping gold-bearing quartz veins that form the main orebodies. In the upper part of the granite body, they are also abundant and systematically associated with pegmatites.

Deformation is evidenced by fractured feldspar crystals, kink structures (plagioclase), and quartz crystals with undulose extinction and subgrain formation. Microfractures affecting plagioclase crystals and filled with magmatic quartz are indicative of submagmatic deformation (Figure 4.4d, BOUCHEZ et al., 1992). It is noteworthy that these structures are only found within aplite parallel to the orebodies and not in other intrusive facies. Some late minerals due to mineralisation and/or alteration are also present (pyrite, muscovite, chalcopyrite, gold, aikinite and carbonate). They affect mainly the fine matrix and can also be present as fracture infill. Pyrite crystals are euhedral to subhedral and are sometimes affected by the ongoing brittle deformation as expressed by brecciated pyrite minerals. Gold and aikinite are associated to the pyrite as fracture infill.

Pegmatites in the Passa Três granite occur mainly in the upper part of the body, sometimes associated with aplites, and occur in the form of scattered pockets exhibiting a final filling by large quartz grains. They are mainly composed of plagioclase, microcline, quartz, fluorite and hematite (Figure 4.4e), whereas alteration is expressed by carbonate and pyrite. When pegmatites are spatially associated with aplites, a gradual transition between them is observed. Submagmatic deformation is recorded by fractures filled by quartz in plagioclase crystal (Figure 4.4f).

Transitional veins are those composed of quartz, molybdenite, pyrite, chalcopyrite, muscovite and fluorite and characterized by the systematic occurrence of pink K-feldspar minerals all along the vein borders (Figure 4.4g, h). Such occurrences are considered as a marker of the transition between magmatic (GEM) to hydrothermal phases (quartz veins), that may contain the mineralisation.

USTs are constituted by parallel layers of quartz and K-feldspar (Figures 4.4i and 4.5) (HÖNIG et al., 2010; SHAFAROUDI et al., 2015; YANG et al., 2016). In detail, this texture consists in alternating crystallization of K-feldspar and quartz with some evidence of growth direction expressed by the fan shape of comb K-feldspars and quartz (Figure 4.5). Quartz crystals are vertically elongated (Figures 4.5b, c). A late assemblage composed of pyrite, chalcopyrite, molybdenite, fluorite, carbonate and white mica is expressed within fractures and/or veins (Figure 4.5c) and represents the mineralisation stage (see further in section 4.4.4)

thus providing a first piece of evidence for the link between magmatic and hydrothermal stages (Figure 4.5c).

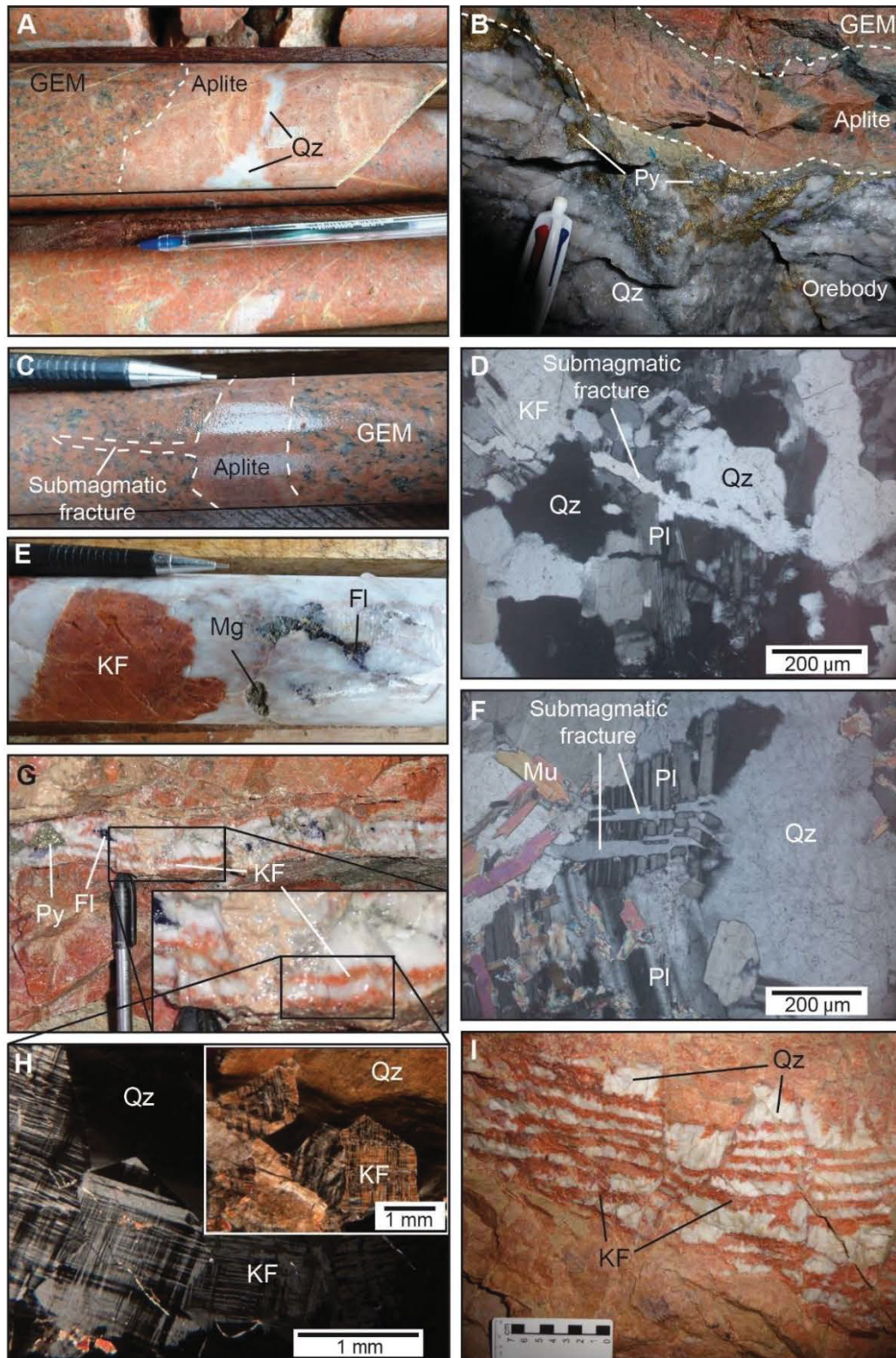


Figure 4.4 - Macroscopic and microscopic magmatic-hydrothermal transition features. A) Transition from GEM facies to aplite and quartz pockets interpreted as magmatic-hydrothermal transition; B) Mineralised vein hosted by granite (GEM facies) and bordered by aplite; C) Aplite filling a submagmatic fracture in GEM facies, in borehole drill; D) Aplite photomicrograph showing a K-feldspar crystal affected by a submagmatic fracture and filled by quartz (polarized light); E) Quartz-rich pegmatite pocket composed of quartz, K-feldspar, fluorite and magnetite; F) Plagioclase crystal with submagmatic fractures filled by

quartz in pegmatite pocket (polarized light); G) Transitional vein with K-feldspar borders composed of quartz, fluorite, chalcopryite, pyrite and molybdenite; and image showing in detail the K-feldspar and quartz bands; H) Details of K-feldspar crystals in the border of the transitional veins; I) UST-type texture observed at upper underground mine level, close to the surface. GEM: medium grain granite, Fl: fluorite, KF: K-feldspar, Mg: magnetite, Mu: muscovite, Pl: plagioclase, Qz: quartz, Py: pyrite.

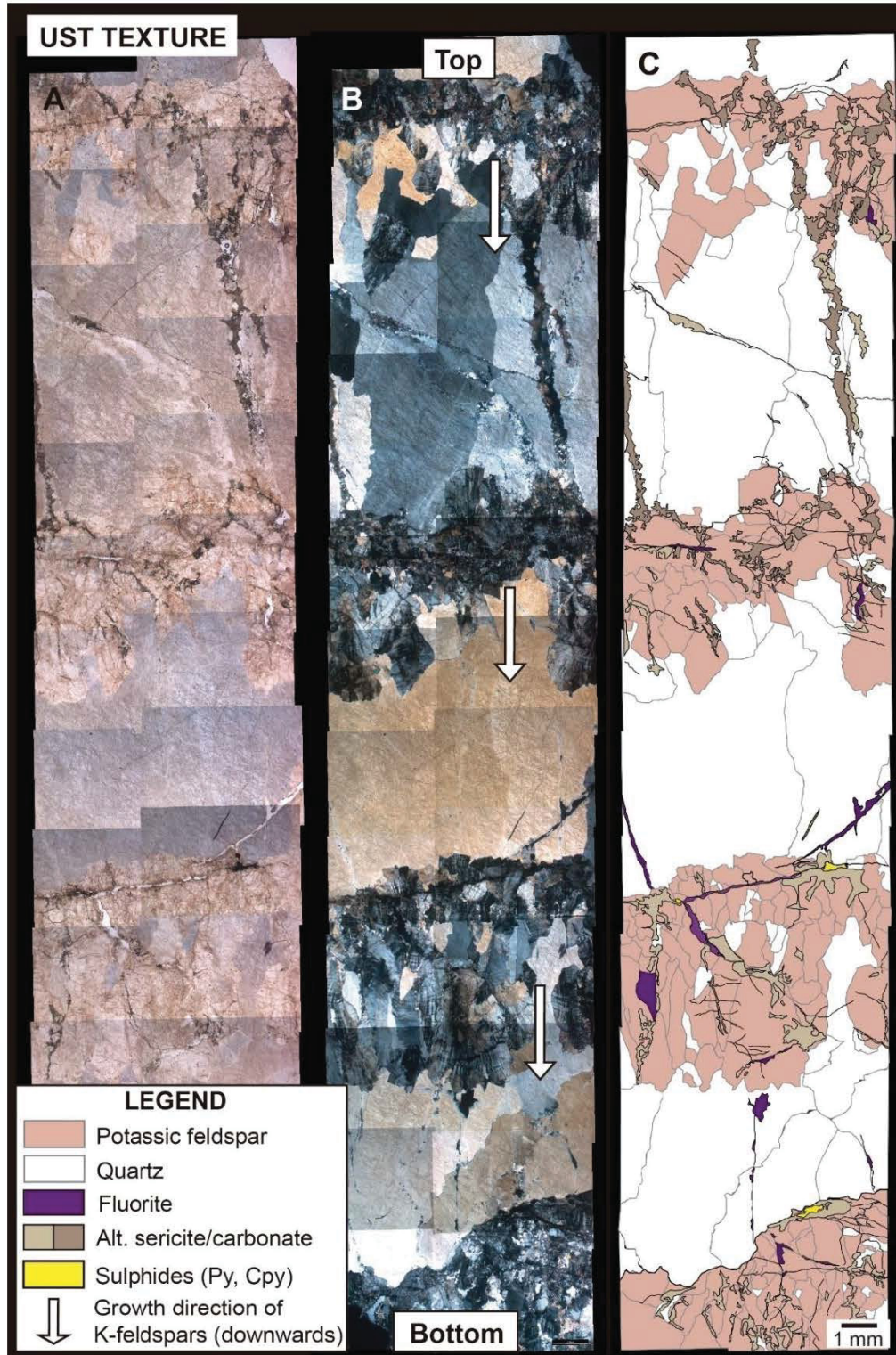


Figure 4.5 - Unidirectional Solidification Texture (UST) illustrated by photomicrographs mosaic (natural light) in A, photomicrographs mosaic (polarized light) in B and a schematic drawing in C. The texture is composed of alternating quartz and K-feldspar bands. Growing direction is indicated by K-feldspar grain shape and is downwards (indicated by arrows). This texture is affected by fractures filled by fluorite, pyrite and chalcopryite, and affected by alteration-related minerals (illite and sericite).

Barren veins are very abundant in the borehole drill. They occur near to and have the same direction as the mineralised body. They are only composed of quartz and are associated with muscovite alteration (Figure 4.6e). This muscovite was analysed by the Ar-Ar method (see section 4.5.2). Additionally, stockscheider structures (NESEN, 1980; CERNY, 1991) are well observed near the surface of the underground mine and are additional indicators that the cupola environment was a favourable site for mineralisation (Figure 4.6f).

4.4.3 Orebodies macroscopic features

Mineralised veins (or orebodies) are quartz pockets that have thicknesses between 30 cm and 3 m. The term “pocket” is herein used because these quartz-rich veins are not continuous and present a sigmoidal shape (Figure 4.6a), with internal massive, brecciated and/or sheared textures (Figure 4.6b). Other minerals such as sulphides (pyrite, chalcopyrite, aikinite, and molybdenite), fluorite, chlorite, muscovite, sericite, ankerite and calcite complete the paragenesis.

Two perpendicular vein systems (N-S and E-W trending with average dips of 60-75°W and 45-70°S, respectively) were described. From field observations, it was defined that the two systems present the same shape, the same size and the same internal texture, enabling them to be interpreted as contemporaneous. The sigmoidal shape of the orebodies is always associated with normal faults and extensional pull-aparts (Figure 4.6a). This configuration is observed at different scales, from exposure (Figures 4.6c and 4.9a) to thin-sections (section 4.4.4), and precursor barren quartz veins may also be observed (Figure 4.6d, e). The border low-angle faults, often underlined and re-used by late clay minerals (Figure 4.6g), are interpreted as “guide” levels allowing the filling of the open structure during formation of the mineralisation.

Besides the normal fault systems that contain the orebodies, several features evidence that deformation occurred after the mineralisation. In the field and also on thin-sections, a few reverse kinematic indicators, such as one fault system affecting the other one at the mine level and reverse faults (Figure 4.6h), were observed.

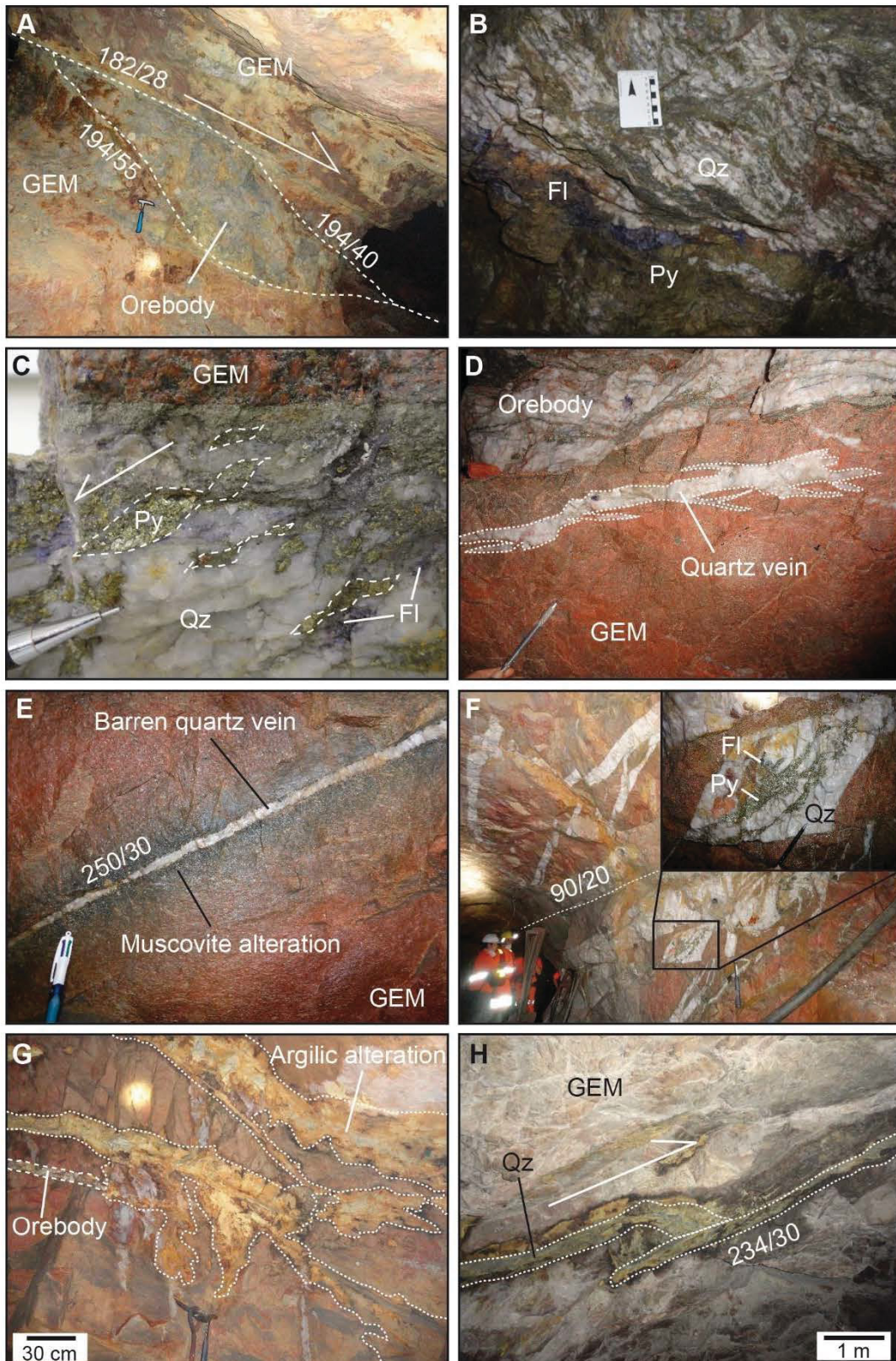


Figure 4.6 - Different textures and structures exhibited by the gold-mineralised veins: A) Orebody with a sigmoidal shape (i.e., extensional pull-apart); B) Mineralised vein with a sheared internal texture; C) Mineralised vein with pull-apart filled by pyrite at hand specimen scale; D) Earlier quartz vein with “en-échelon” fractures showing a very low-angle normal motion (Even if the normal motion is unclear, the quartz vein plane dip toward the south and the motion is toward the South); E) Early low-angle quartz veins observed within upper level of underground mine, with a centimetre-scale alteration halo; F) Intensive quartz vein system development indicator of a stockscheider environment and exhibiting pyrite

and fluorite minerals. Focus on an extensional pull-apart geometry associated with the emplacement of pyrite and fluorite; G) Low-angle faults filled by clay minerals posterior to the quartz veins, indicative of late argillic alteration; H) Reverse fault affecting a mineralised vein. Fl: fluorite, GEM: medium grain granite, Qz: quartz, Py: pyrite.

4.4.4 Microstructures and internal texture

Observations from field work, petrographic studies, and SEM analysis suggest a formation process divided in four phases, probably developed in continuity. These four phases are represented by the following paragenesis (first stage: quartz 1 and fluorite; second stage - divided in stage 2a and 2b, stage 2a: quartz 2 + pyrite 2a ± gold ± chalcopyrite ± aikinite ± fluorite ± sphalerite ± muscovite; stage 2b: quartz 2 + pyrite 2b + gold + chalcopyrite + aikinite + ankerite ± sphalerite ± fluorite ± muscovite; stage 3: quartz 3 + ankerite + calcite + molybdenite + aikinite + muscovite + fluorite). A paragenetic table is presented in Figure 4.7 and the hydrothermal phases, as well as the structural model, are presented in Figure 4.15.

STAGES MINERAL	Late magmatic stages				Early hydrothermal stages		Hydrothermal stages - Mineralisation Normal movement			Post-mineralisation	
	UST	Aplite	Pegmatite	Stockscheider	Vein (FK border)	Barren quartz veins	Stage 1	Stage 2		Stage 3	Reverse movement
								Phase 2a	Phase 2b		
Plagioclase											
K-Feldspar (magm.)											
Quartz (magm.)											
Muscovite											
Ankerite											
Fluorite											
Quartz 1 (hydr.)											
Illite											
Sericite											
Quartz 2 (hydr.)											
Pyrite 2a											
Pyrite 2b											
Chalcopyrite											
Gold											
Aikinite											
Sphalerite											
Molybdenite											
Calcite											
Quartz 3 (hydr.)											

Figure 4.7 - Global paragenetic evolution of the Passa Três gold deposit and relationships with different stages of the magmatic-hydrothermal transition. Gold occurs at Stage 2a as inclusions and at Stage 2b as native grain, forming an ore paragenesis with pyrite 2a, pyrite 2b, chalcopyrite, aikinite and rare sphalerite. Alteration minerals are not represented.

Pyrite 2a is anhedral and presents abundant inclusions, while pyrite 2b is euhedral, occurs at the borders of pull-aparts and fractures, presents very few inclusions and is very homogeneous (Figure 4.8c). Most of the gold is essentially associated with chalcopyrite, pyrite 2b and aikinite during stage 2b (Figure 4.8a-c). The two pyrite phases can be distinguished by the form of the crystals and the presence of inclusions. Pull-apart geometry was also suspected for the cavities that contain gold and associated sulphides, associated with quartz 2 (Figure 4.8d). SEM imagery demonstrates a gradual transition between the two pyrite phases (Figure

4.8e). Gold occurs mainly within fractures and geodic cavities in core of pyrite 2a, but everywhere associated with the pyrite 2b, aikinite and chalcopyrite (Figure 4.8e, f).

In the mineralised vein (Figure 4.9), quartz 1 presents undulose extinction, deformation planes with subgrain formation and recrystallization textures (new grains) (Figure 4.9c). Pyrite pockets are also affected by faulting (Figure 4.9d). The pull-apart structure filled with pyrite (stage 2a) is associated with the crystallization of quartz 2 and brecciation associated with faulting. Carbonate and/or quartz 3 veinlets are subsequent to quartz 1, ore paragenesis and breccia formation.

At the border of the orebodies, hosting granite (GEM) is brecciated (cataclasite and incohesive breccia). In these portions, K-feldspar, plagioclase, quartz and pyrite crystals are fractured and broken, and associated with a fine breccia matrix (Figure 4.9e). Quartz presents undulose extinction, fractures with subgrain formation, deformation lamellae and stretching. Fine matrix forms a deformation corridor, also affected by alteration minerals (muscovite, sericite, pyrite, illite, carbonate, chlorite), probably due to increased porosity (Figure 4.9f). Feldspar affected by faults and fractured pyrite pockets display a fracturing pattern that is consistent with normal kinematics. Specularite may be present in the deformation corridors, and fluorite may occur with quartz 1. As observed in some thin-sections, deformation (brecciation) may affect both vein and granite along the borders.

Inside the vein, portions of the hosting granite (enclaves) are found. These enclaves are deformed and can be classified as cohesive breccia. K-feldspar and plagioclase crystals are fractured and quartz presents undulose extinction, subgrains and new grains. In these portions, alteration is also present (sericite, carbonate, illite, pyrite) and conjugated normal fault systems are also recognized.

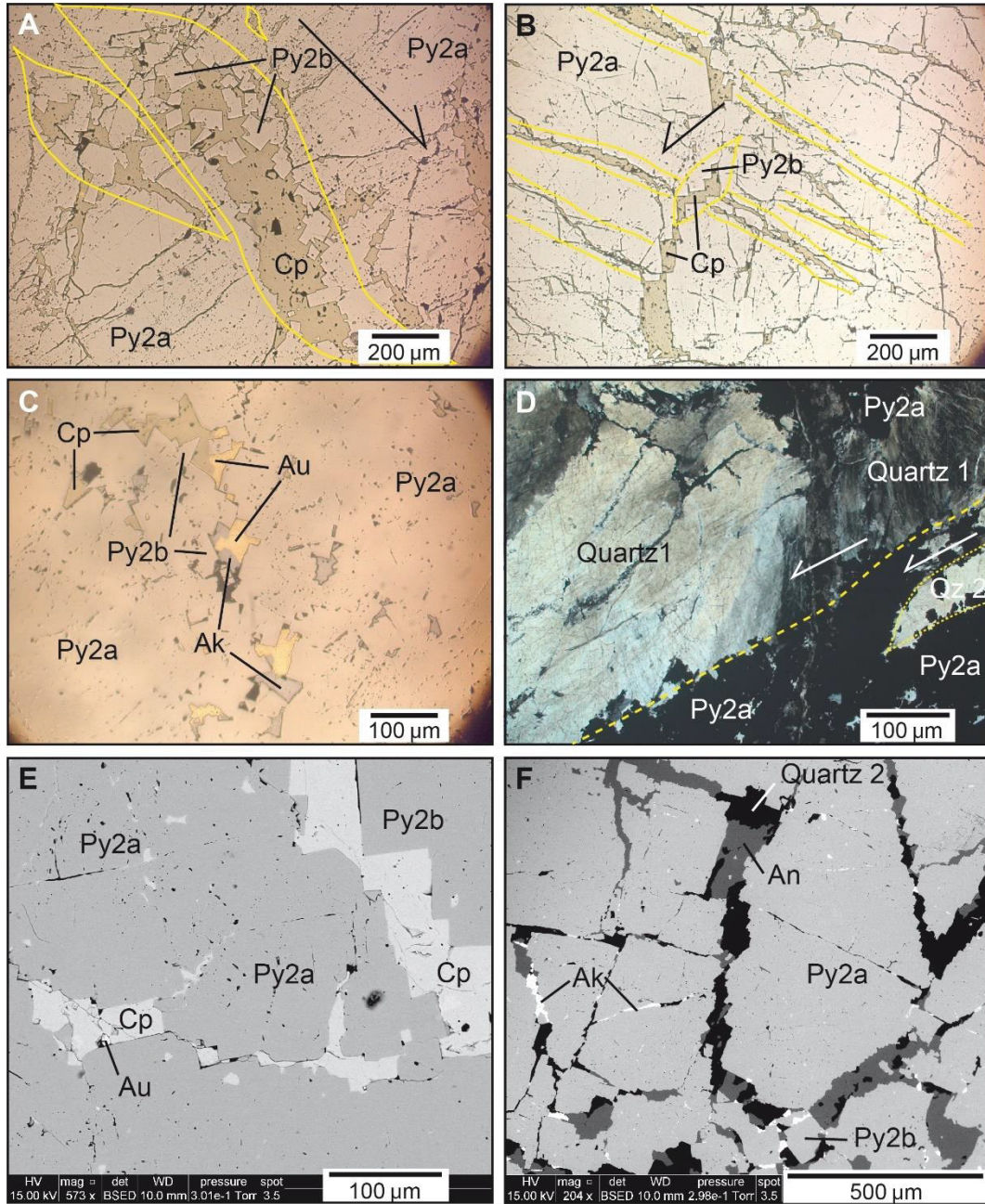


Figure 4.8 - Microscopic and SEM aspects of ore paragenesis. A) Supposed pull-apart site filled by ore paragenesis composed of chalcopyrite, gold, aikinite and pyrite 2b; B) Fractures associated to the main ore phase filled by chalcopyrite; C) Ore paragenesis composed of gold, aikinite and chalcopyrite; D) Pull-apart filled by quartz 2 in a pull-apart filled with pyrite 2a, next to quartz 1; E) Differences between pyrite 2a and pyrite 2b. Pyrite 2a presents inclusions and pyrite 2b is euhedral, with no inclusions. These images show the transitional limit between the two pyrites, indicating a progressive change of fluid composition and thus justifying their association within the same second event; F) Aikinite (white mineral) in equilibrium with chalcopyrite and pyrite 2b (light grey). Note the occurrence of ankerite and quartz as fracture infilling and related to the ore paragenesis (phase 2b). Ak: aikinite; An: ankerite; Au: native gold; Cp: chalcopyrite; Py2a: pyrite 2a; Py2b: pyrite 2b; Qz: quartz.

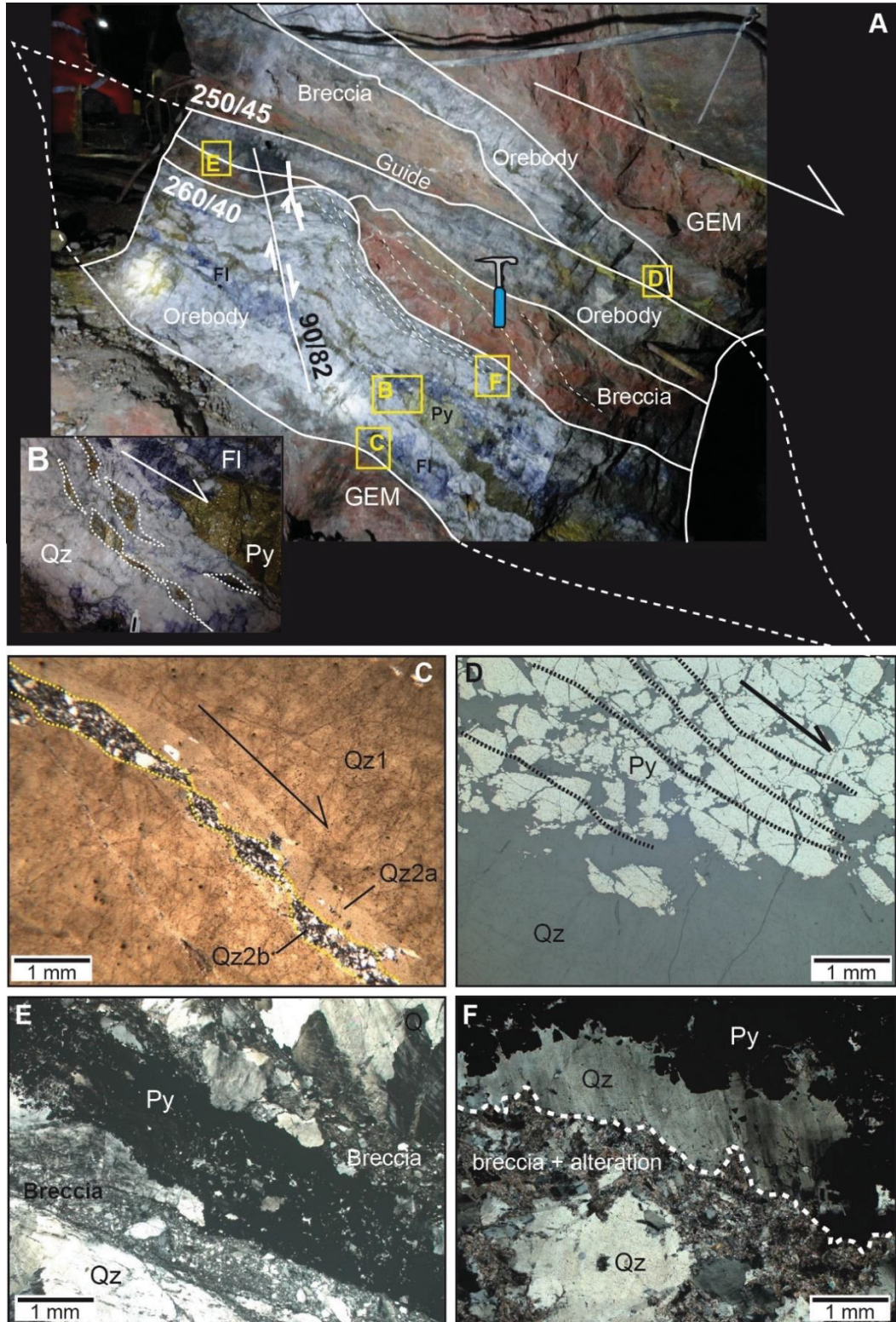


Figure 4.9 - Example of large scale gold-bearing pull-apart structure. A) The vein exhibits a banded structure underlined by pyrite (Py), fluorite (Fl) and portions of brecciated granite. The yellow squares indicate the location of Figures 4.9B, C, D, E and F; B) Extensional pull-apart filled with pyrite; C) Quartz 1 microtexture with pull-apart formed by recrystallized new grains and associated with normal movement; D) Pyrite layers affected by extensional fractures parallel to vein dipping; E) Breccia with fracture filled by pyrite, next to quartz 1 (orebody); F) Limit between granite and orebody marked by brecciated granite affected by alteration (sericite, carbonate) next to quartz 1 and pyrite (orebody). Fl: fluorite, GEM: medium grain granite, Py: pyrite, Qz: quartz. Orientations are indicated next to the structures in Figure A; Figures B, C, D, E, F are displayed in the same orientation in relation to the exposure view in Figure A.

Chemical analysis of minerals

Electron probe micro-analyser (EPMA) data indicate almost no difference in terms of composition between the different phases of pyrite and chalcopyrite (Appendix 4.A), although the detection limit does not allow one to be sure of the measurement significance. Nonetheless, this may indicate fluid homogeneity between stages 2a and 2b. Gold-bearing minerals are composed of Au (90,37–93,07%), Ag (7,71–12,13%) and traces of Cu, Fe and S (EPMA analyses, Appendix 4.A).

4.5 GEOCHRONOLOGY

In order to understand the transition between magmatic and hydrothermal phases and to define the timing of magmatism and mineralisation, U-Pb and Ar-Ar geochronological analyses were performed on zircon grains extracted from three samples (U-Pb) of the Passa Três granite (GEM, GEF and GEB) and on muscovite grains from hydrothermal veins (Ar-Ar), including mineralised veins, transitional veins (with a K-feldspar border) and barren quartz veins.

4.5.1 U-Pb zircon dating

U-Th-Pb analyses are reported in Appendix 4.B and the results are reported in Concordia diagrams (Figures 4.10 and 4.11). In all three facies, the zircon grains are euhedral, with sharp terminations.

Thirty grains were analysed from the granite sample GEM. Twelve analyses performed on zircon grains have concordant analytical points (Figure 4.10 and Appendix 4.B) and define a Concordia age of 611.9 ± 4.7 Ma (MSWD = 0.21; Probability of concordance = 0.64). This age is adopted as our best estimate of the age of the zircons and of the crystallization of the zircons from the granitic magma. The remaining eighteen analyses are significantly older, demonstrating that the granite zircon population has a significant inherited component. This inherited component includes Archean cores with $^{207}\text{Pb}/^{206}\text{Pb}$ ages around 3.0 Ga (2946 ± 49 Ma and 3013 ± 53 Ma) and as old as 3319 ± 59 Ma (2σ). Most cores are Paleoproterozoic in age (between 1.8 Ga and 2.2 Ga), with a maximum distribution at around 2.0 Ga (Appendix 4.C). Fifty-six grains were analysed from granite sample GEF. Overall, the distribution of the analyses is similar to that observed for the GEM sample (Figure 4.10). Eleven analyses performed on zoned grains or rims around visible cores cluster close to Concordia at c. 600 Ma. Among these, one result is significantly younger at 566 ± 22 Ma (2σ), whereas another one is significantly displaced to the right of the Concordia. The latter suggests that the analysis

includes a small proportion of inherited Pb or that the beam struck a common Pb-rich inclusion. Discarding these two results, the remaining nine data form a concordant group and provide a Concordia age of 611.9 ± 5.6 Ma (MSWD = 0.28; Probability of concordance = 0.60). This age is identical to that obtained for zircons from the GEM sample and is similarly interpreted as dating emplacement and crystallization of the granitic magma. Inherited components are dominated by Paleoproterozoic cores (with $^{207}\text{Pb}/^{206}\text{Pb}$ ages in the range 1953-2203 Ma) (Appendix 4.C), but also include a minor proportion of Archean cores with ages ranging from 3166 to 3196 Ma. In both samples, these inherited components are interpreted as inherited from the source rock(s) that melted to produce the granitic magma or as assimilated at depth during ascent and emplacement of the magma. Since both samples have the same age and were sampled from the same unit of the granite, it is justified to combine the twenty-one analyses concordant at c. 612 Ma to calculate a pooled Concordia age of 611.9 ± 3.6 Ma (MSWD = 0.01; Probability of concordance = 0.97). The age of 611.9 ± 3.6 Ma is thus taken as our best estimate for crystallization of the Passa Três granite.

Thirteen analyses were performed on zircon grains from the “white granite” (GEB sample). In the Concordia diagram (Figure 4.11), most analyses cluster close to Concordia at around 600 Ma, but are significantly displaced to the right suggesting the incorporation of variable amounts of common Pb. One analysis has older Pb/U and Pb/Pb ages indicating that this grain contains a component of inherited Pb with a minimum $^{206}\text{Pb}/^{238}\text{U}$ age of 839 Ma. The remaining analyses define a chord with a lower intercept of 592.8 ± 7.1 Ma (MSWD = 0.73; n = 12). This age is significantly younger than the 612 Ma age of the other two samples and is tentatively taken as dating a younger facies of the Passa Três granite, related to a late magmatic event.

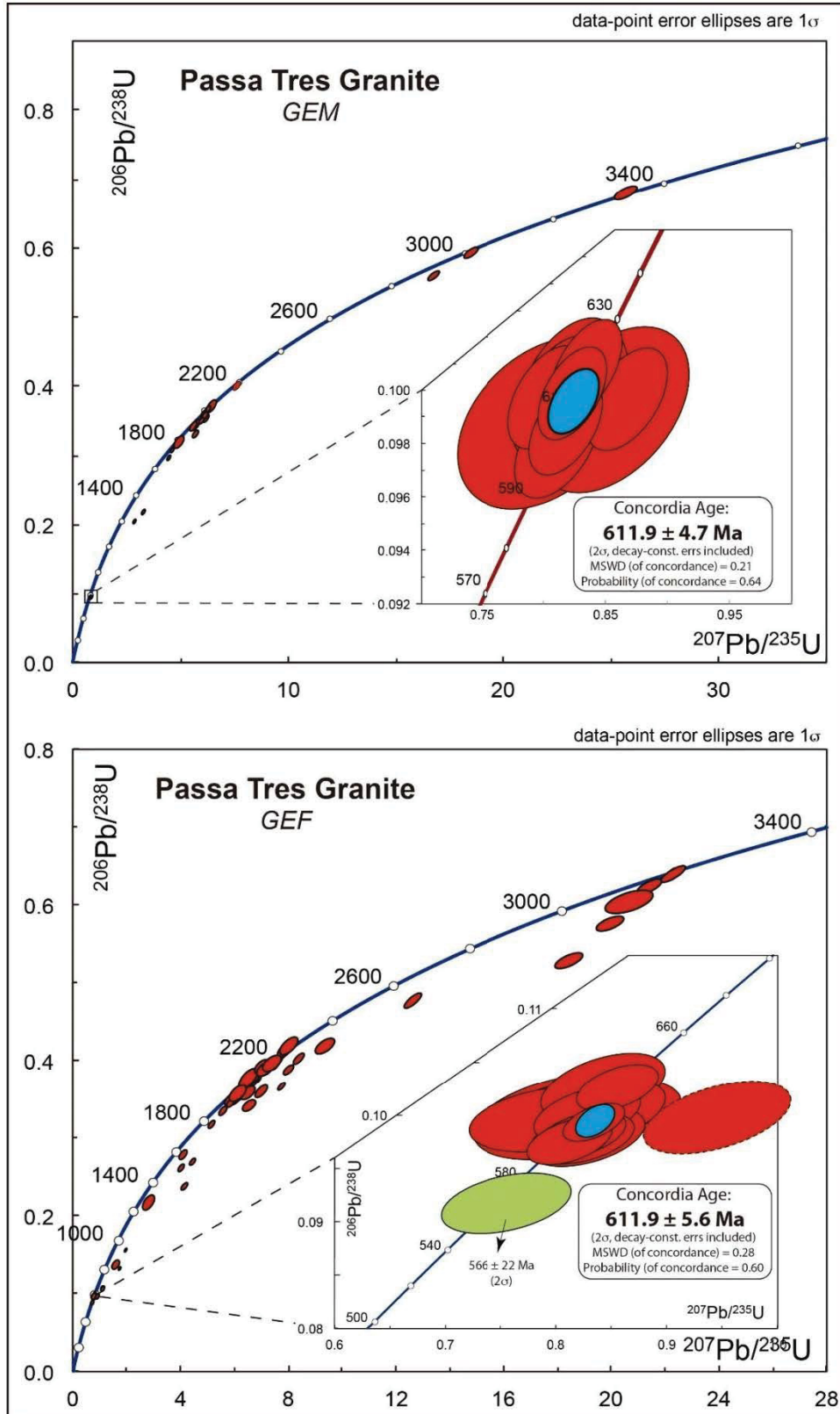


Figure 4.10 - U-Pb Concordia diagrams of two different facies of the Passa Trés granite: GEM (red colour, medium texture) and GEF (red colour, microgranite).

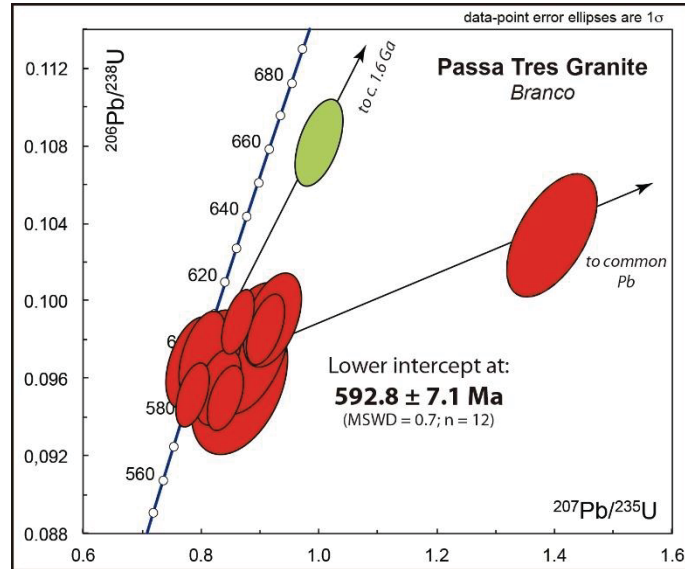


Figure 4.11 - U-Pb Concordia diagram of the white granite (GEB - Branco) facies of the Passa Três granite.

4.5.2 Muscovite Ar-Ar dating

Muscovite crystals were separated from the transitional veins (samples BD-83A and BD-83B), mineralised veins (samples BD-31B, BD-46 and BD-88) and barren veins (sample BD-85B). These samples were analysed by the stepwise heating method (Figure 4.12) and *in situ* analysis method (Figure 4.13). For the stepwise heating method, data are portrayed as age spectra on Figure 4.12 and a complete set of isotopic results is given in Appendix 4.D. For most samples, there is little evidence of significant age discordances on the age spectra that provided plateau ages for a large percentage of the ^{39}Ar released. Muscovite crystals from samples BD-83A and BD-83B (transitional veins) were separated into 250 micron and 500 micron fractions, and analysed separately. Sample BD-83A yields plateau ages of 612.2 ± 2 Ma (250 micron) and 608.8 ± 2 Ma (500 micron), and sample BD-83B yields plateau ages of 612.9 ± 2 Ma (250 micron) and 609 ± 2 Ma (500 micron). Muscovite samples from mineralised veins yield plateau ages of 608.8 ± 2 Ma (BD-46), 610.7 ± 2 Ma (BD-31B) and 611.7 ± 2 Ma (BD-88). The plateau age of sample BD-85B (barren vein) is 608.4 ± 2 Ma.

Using the stepwise heating method, the three types of veins analysed give a narrow range of muscovite ages between 613 ± 2 and 608 ± 2 Ma that can be interpreted to date cooling at about 450°C considering the large grain size of the dated micas (HARRISON et al., 2009). Since cooling rates in these veins were probably high, it is likely that these muscovite ages are close to their crystallization age.

Some of the same samples (BD-46, BD-85B and BD-88) were also chosen for *in situ* Ar-Ar laser probe analyses on muscovite and K-feldspar. These samples give a large spread of $^{40}\text{Ar}/^{39}\text{Ar}$ ages between 820 and 520 Ma (Figure 4.13 and Appendix 4.D). Ages between 610

and 600 Ma are consistent with those of the Passa Três granite emplacement as well as with those of the mineralisation. This is particularly evident for sample BD-88 for which a mean age of 610 ± 2 Ma was obtained from 14 spot fusions, in agreement with the plateau age of 611 ± 2 Ma reported above. In the same sample, K-feldspar provided apparent ages from 541 to 604 Ma that are interpreted to reflect different degrees of argon resetting during a late thermal event. This argon resetting is also recorded by samples BD-46 and BD-85B with ages that are respectively in the range 564-601 Ma and 554-597 Ma. For sample BD-46 (Figure 4.13), ages older than 610 Ma and up to 820 Ma are recorded within a quartz-carbonate-mica vein that are clearly indicative of the presence of excess argon in this vein, probably held by fluids. It is noteworthy that tiny micas surrounding a large carbonate crystal within this vein give ages of 554-573 Ma that together with the ages of sample BD-85B point to a minor heating event, associated to an event of reverse reactivation of faults observed in the mine, as well as in the thin sections.

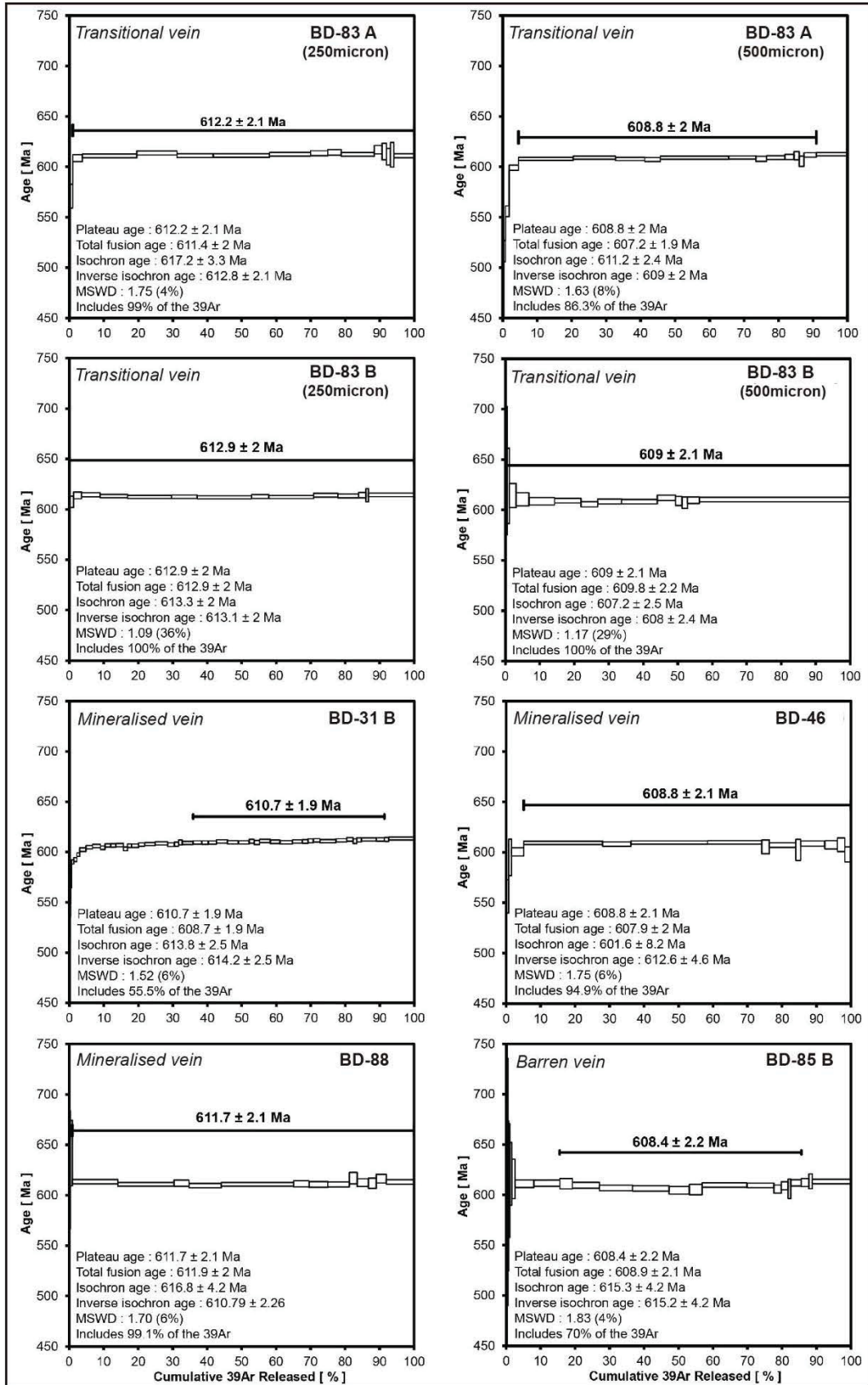


Figure 4.12 - ^{40}Ar - ^{39}Ar age spectra of muscovite crystals from transitional, mineralised and barren veins.

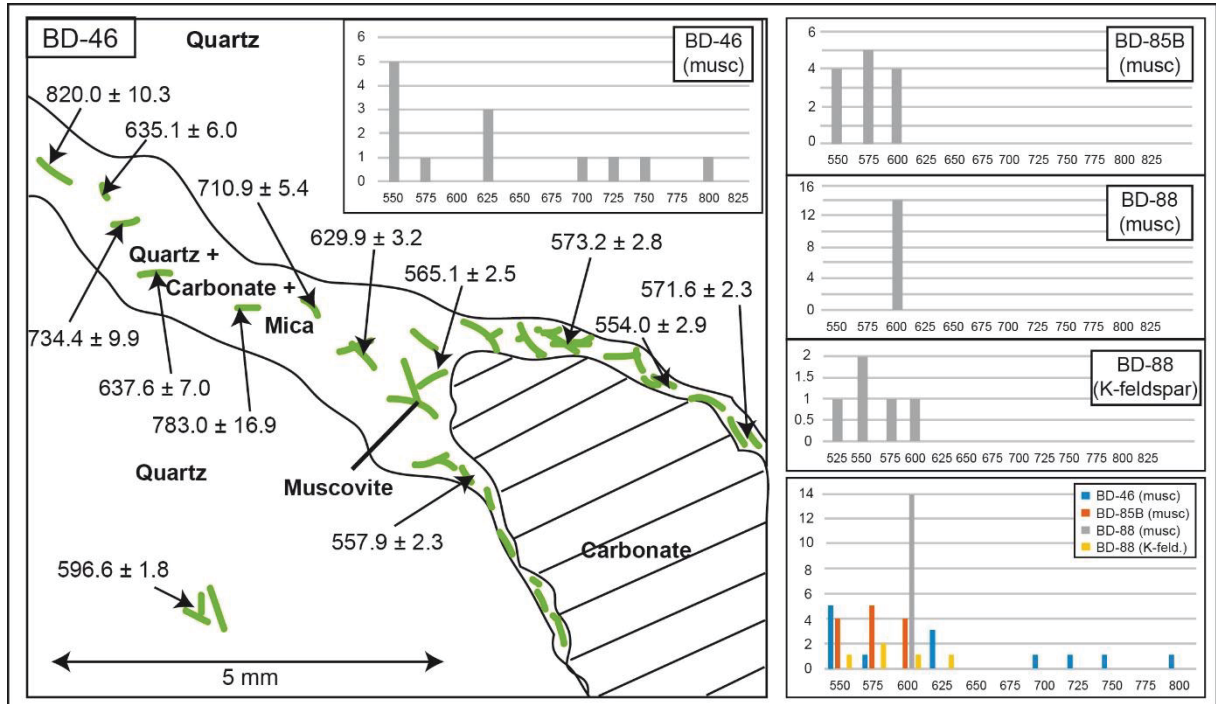


Figure 4.13 - ^{40}Ar - ^{39}Ar *in situ* ages of three muscovite samples and one K-feldspar sample. Ages older than 620 Ma for sample BD-46 are due to excess of argon. Ages younger than 600 Ma (samples BD-46 and BD-85b - muscovite, sample BD-88 - K-feldspar) are interpreted as partial resetting.

4.5.3 Geochronology integration

Geochronology data show that the Passa Três granite has an age of 611.9 ± 3.6 Ma (pooled age for the GEM and GEF facies). A less abundant, leucocratic facies (GEB sample) yields a significantly younger age of 592.8 ± 7.1 Ma. Ar-Ar analyses of muscovite grains provide three sets of ages for different quartz veins: veins with a K-feldspar border (612.9 ± 2 to 608.8 ± 2 Ma); mineralised veins (611.7 ± 2 to 608.8 ± 2 Ma); barren veins (608.4 ± 2 Ma). Therefore, despite the tightly clustered ages provided for different quartz veins by muscovite Ar-Ar analyses, it is possible to propose an order of crystallization, since the transitional veins are the oldest and the barren veins are the youngest, and the mineralised veins may be placed between them (Figure 4.14). Together with the ages for the granite facies, data show that the granite and the mineralisation occurred between 613 and 608 Ma (Figure 4.14).

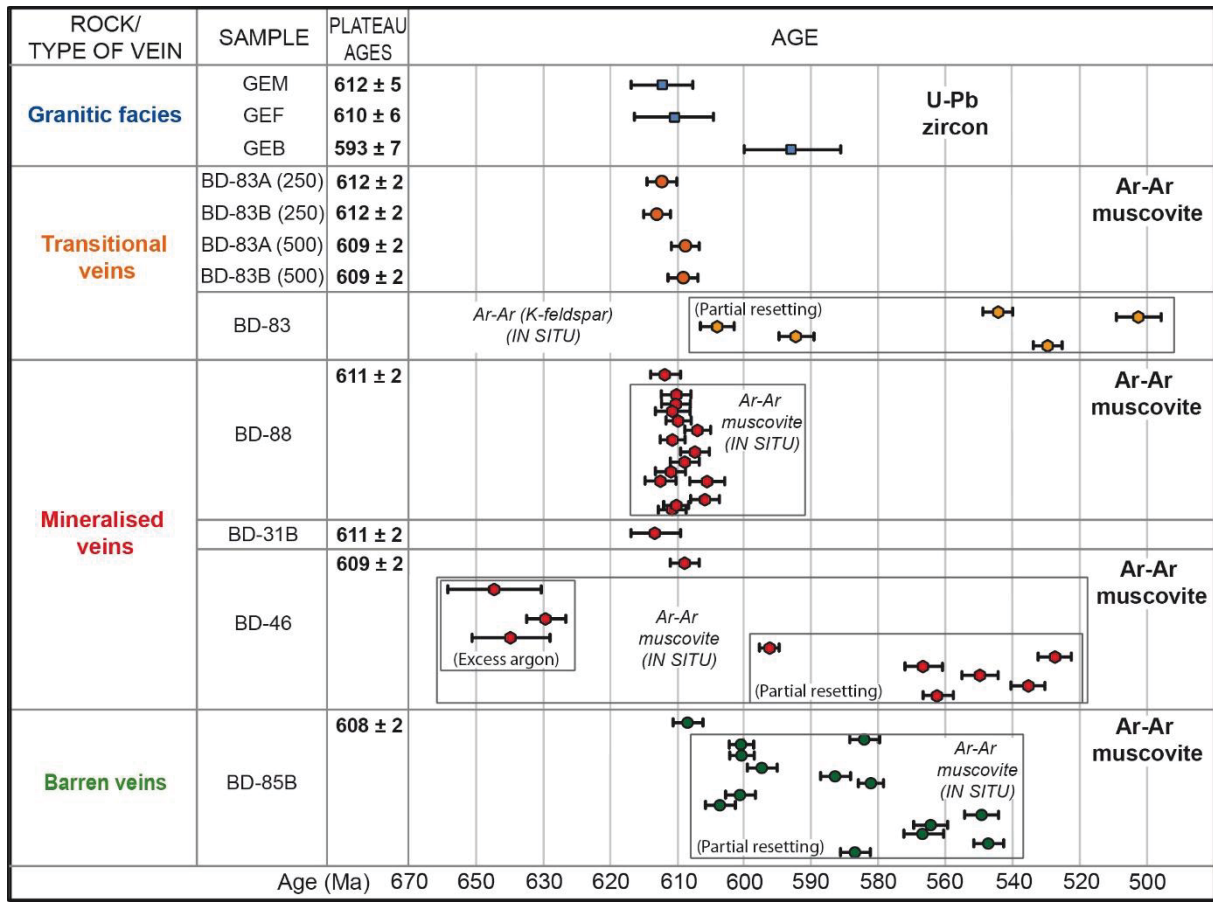


Figure 4.14 - Table showing the distribution of ^{40}Ar - ^{39}Ar and U-Pb ages obtained during this study for the Passa Três granite and gold mineralisation.

4.6 INTERPRETATION

Combining all these results, a four-stage global model for the formation of the gold mineralisation of the Passa Três granite is proposed (Figure 4.15). The definition of the ore paragenesis and vein infill succession, associated with the description of the magmatic, transitional and hydrothermal stages are presented in Figure 4.7, and all the minerals that characterize the late magmatic (aplitites, pegmatites, UST, stockscheider, transitional vein with a K-feldspar border), hydrothermal and post-mineralisation stages are indicated.

The data suggest that the granite was affected by low-angle shearing planes created in response to an extensional tectonics that may prevail during and after granite emplacement, as demonstrated by the presence of aplitic sills parallel to these planes (Figure 4.15a). Extensional features are abundant and the well-expressed structures are opening sites or pull-aparts filled by the different assemblages (Figure 4.15b, c, d). During the first stage, quartz 1 and sometimes fluorite represent the first filling stage of pull-aparts opened by normal fault systems. The second stage is divided into stage 2a and 2b. Stage 2a formed smaller pull-aparts inside the first ones (stage 1) and developed an assemblage composed of quartz 2 +

pyrite 2a ± gold ± chalcopyrite ± aikinite ± fluorite ± sphalerite ± muscovite. Stage 2b was only observed in thin sections and is represented by smaller pull-aparts and fractures that develop inside the structures of stage 2a. This stage contains native gold and is characterized by the following ore paragenesis: quartz 2 + pyrite 2b + gold + chalcopyrite + aikinite + ankerite ± sphalerite ± fluorite ± muscovite. These two earlier mineralisation stages are followed by stage 3 (not represented in Figure 4.15), characterized by the occurrence of quartz 3 + ankerite + calcite + molybdenite + aikinite + muscovite + fluorite. This stage displays a reverse character.

At mining scale, we suggest that low-angle shear zones developed following two orthogonal directions, N-S and E-W which are those recognized in underground works (Figure 4.16). As illustrated on the synthetic sketch of the drill holes, transitional features are mainly observed in the upper part of the drill holes (Figure 4.16) and also in upper levels of the mine. Aplites are frequently emplaced parallel to the plane of shearing and the deposit consists in a succession of meter-scale extensional pull-aparts that explain the plunging of the mineralised bodies towards the South and the East (Mining Geologists, personal communication). The succession of mineralised pockets is recognizable on the Surpac® model and consistent with the geological model.

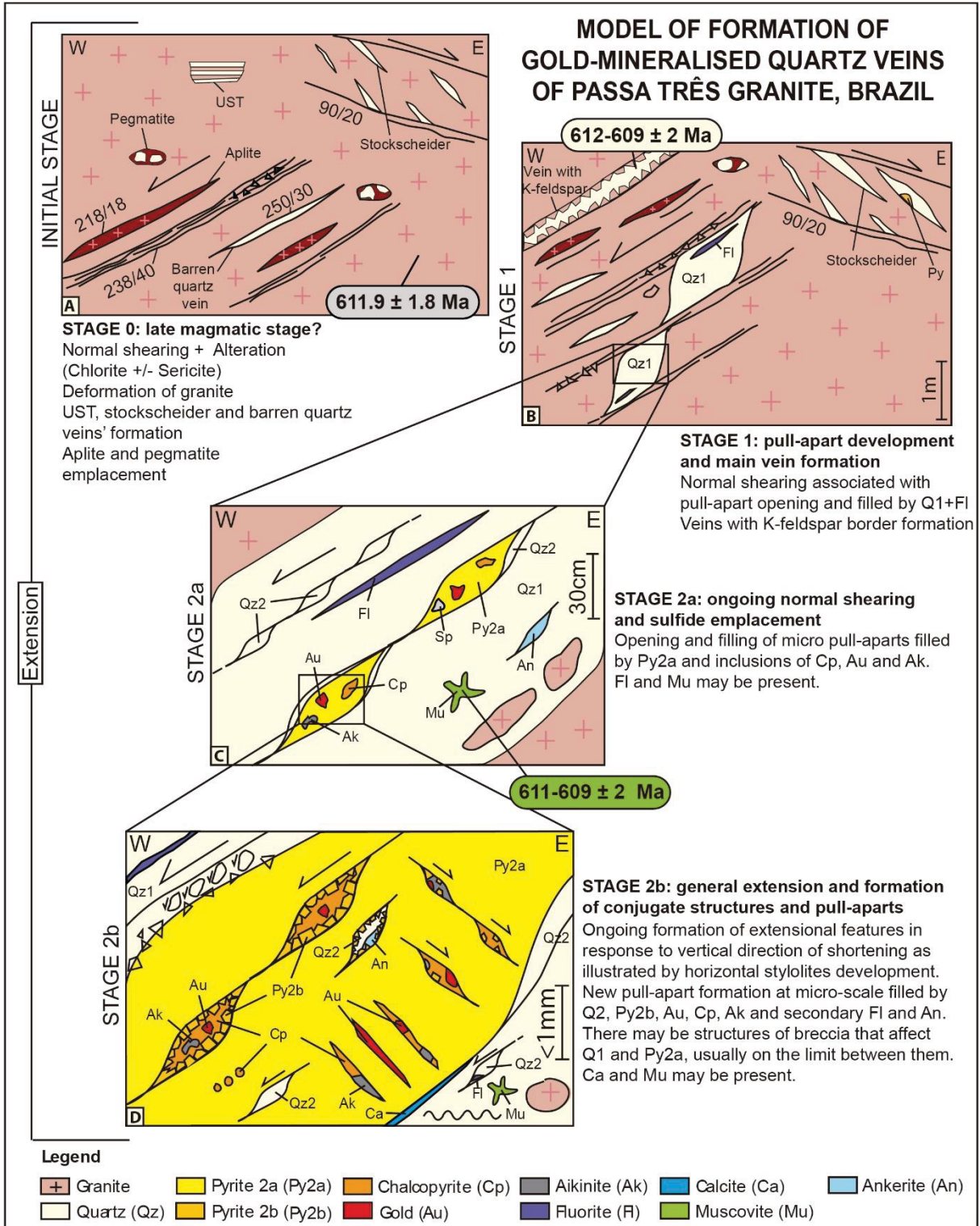


Figure 4.15 - Model of formation of the mineralised quartz veins of Passa Três granite, with the three stages considered as occurring within the errors of the zircon and muscovite ages (the fourth stage, interpreted as a reverse one, is not represented).

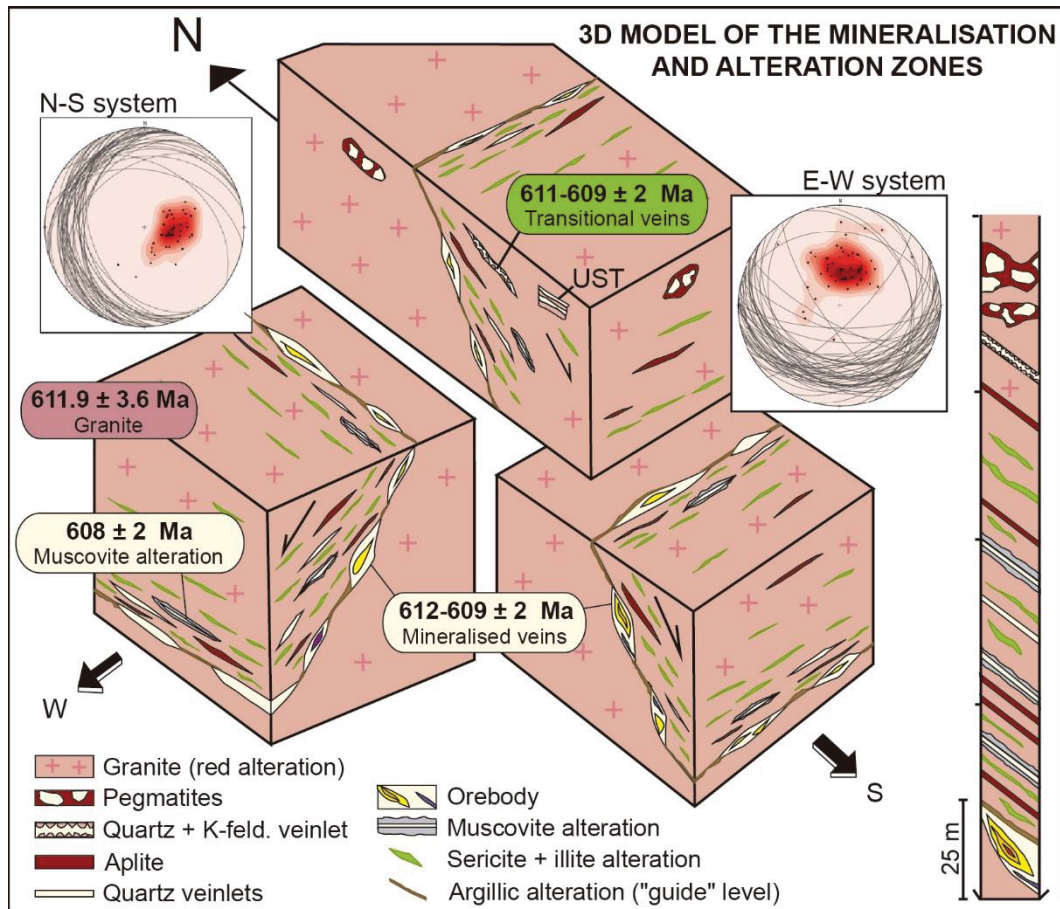


Figure 4.16 - Block-diagram of the Passa Três granite gold deposit with stereograms of the two normal fault systems (N-S and E-W) and ages for the granite facies, transitional veins, mineralised veins and non-mineralised veins. N-S stereogram: $n=45$, maximum density at 105/68 (pole), main plane at 285/22; E-W stereogram: $n=54$, maximum density at 12/63 (pole), main plane at 192/27.

4.7 DISCUSSION

4.7.1 Structural model

The structural model thus suggests an extensional context and the mineralised veins are related to the development of two normal fault systems, which created opening sites (pull-apart type). As there are two perpendicular systems, it is possible that extension occurred with a N230 direction (σ_3 orientation), with a vertical maximum stress σ_1 . In the mine level, we observe the two systems affecting each other, and there is no intermediary direction between them. However, according to Destro (1995), who studied sedimentary basins, two perpendicular normal fault systems may occur when sigma 2 is oscillatory, hence inducing a pressure release and an accommodation of the efforts. Even so, structurally controlled mineralisation was described in several gold deposits, such as the Scheelite Dome, Clear Creek and Dublin Gulch, at the Tombstone Gold Belt (Yukon, Canada) (STEPHENS et al., 2004). These deposits present auriferous veins inside the intrusions and also at the contact

with metasedimentary country rocks surrounding them. Nevertheless, the veins are believed to have originated from the granitic stocks, but controlled by regional scale structures, as well as structures developed inside the pluton, such as the case for the Scheelite Dome (STEPHENS et al., 2004). Because some granite-hosted sheeted veins have been interpreted as extensional veins, this possibility can also be considered for the Passa Três deposit, which is corroborated by the fact that fault-controlled features and pull-aparts have normal kinematics.

Gold-bearing veins can thus be compared to extensional veins developed in the core of the Passa Três granite controlled by a structural extensional context and occurring during the transition from magmatic to hydrothermal conditions. This interpretation is supported by the observation of tectonic control also within granitic features (submagmatic deformation, Figures 4.3c and 4.4c, d, f) and by the identical age of magmatic and hydrothermal structures (this study). A comparison can also be made with the Pogo deposit, in which ore-bearing veins are associated with brittle deformation and normal faults (RHYS et al., 2003) and the Scheelite Dome (Tombstone Gold Belt, Yukon, Canada), that displays several deformation phases with cementation and deposition of sulphide-rich assemblages (STEPHENS et al., 2004). Moreover, the roof zone of a pluton (as supported by several arguments at the Passa Três deposit) is associated to mechanical instability, and this has been recently illustrated in the case of some Variscan gold deposits (GLOAGEN et al., 2014).

4.7.2 Timing of granite emplacement and gold-mineralisation

The geochronological data obtained in this study for the Passa Três granite and other magmatic-hydrothermal features are synthesized on Figure 4.14. Apart from the GEB facies, the data show a remarkable coherence, demonstrating that Passa Três granite and quartz mineralisation were developed contemporaneously, exhibiting not only a spatial relationship, but also a temporal one. A review of the literature demonstrates that in many cases of gold deposits related to intrusions, the age difference between emplacement of a granite (magmatism) and its associated mineralisation (hydrothermalism) can be a few million years (from 1 to 4 Ma) (VIGNERESSE, 2007) or even with a shorter interval, ranging from 100,000 to 300,000 years (LI et al., 2013), in the cases where hydrothermal deposits consist of numerous short-lived hydrothermal pulses or are formed by short-lived hydrothermal systems.

Moreover, recent studies identified hydrothermal deposits with the same age as the related source granite and some mineralisations are considered as temporally, spatially, and probably genetically associated with the emplacement of the pluton, such as: the Jiepailing Sn-Be-F deposit (China) (U-Pb zircon, granite: 90.5 ± 0.9 Ma; Ar-Ar, mineralisation: 92.1 ± 0.7 Ma; YUAN et al., 2015), the Xitian W-Sn deposit in Southern China (U-Pb zircon, granite: 152

± 1.4 Ma; Re-Os molybdenite, mineralisation: 149.7 ± 0.9 Ma; Ar-Ar, ore-bearing greisen: 149.5 ± 1.5 Ma; LIANG et al., 2016), Mine granite in Morocco (Ar-Ar, Mine granite: 286 ± 0.4 Ma; Re-Os molybdenite, W-Mo mineralisation: 285 ± 0.5 Ma; MARCOUX et al., 2015), Fort Knox (Alaska, USA) (U-Pb zircon: 92.5 ± 0.2 Ma; Re-Os molybdenite: 92.4 ± 1.2 Ma; e.g., McCOY et al., 1997 in SELBY et al., 2002).

Our geochronological data revealed the existence of only one episode of magmatic-hydrothermal activity. As demonstrated in section 4.5.2 and in Figure 4.14, Ar-Ar ages of different quartz veins are concordant with the U-Pb zircon age (611.9 ± 3.6 Ma) of the Passa Três granite. This indicates that the gold deposit is temporally and spatially associated with the emplacement and crystallization of the granite. With these data we can assume a magmatic-hydrothermal activity bracketed between 613 and 608 Ma, with a maximum time interval of c. 9 Ma (considering error margins). The ages for the granite crystallization agree, within error margins, with data from Picanço (2000), who interpreted the final age for emplacement as 616 ± 36 Ma (Sm-Nd fluorite) and the tardi-magmatic processes as 604 ± 11 Ma (K-Ar muscovite in a pegmatite). Picanço (2000) also identified younger ages, such as 527 ± 10 Ma in sericite crystals found in fault zones (K-Ar sericite) and 510 ± 32 Ma (Rb-Sr pyrite) in pyrite concentrates. These ages could indicate remobilizations that could have been produced by the action of the shear zones, and also be associated with the younger ages obtained in this study, and may be responsible for the opening of the system of the K-feldspar and muscovite crystals, obtained during this study.

The short period between granite crystallization and ore formation observed in the Passa Três magmatic-hydrothermal system raises some questions about the temporal relation and the possible genetic association between magma and mineralisation. According to Vigneresse (2007), some I-type magmas having a low-fluid content can ascend to high crustal levels and keep their fluid content dissolved in the magma, with an interval of crystallization restricted to a short temperature range. Moreover, and according to Coulsen et al. 2001 (in LANG; BAKER, 2001), the igneous centres associated with intrusion-related gold systems can typically form multiphase complexes that were rapidly emplaced and cooled. In the case of the Passa Três granite, a rapid emplacement and cooling is consistent with the very short time interval between magmatic and hydrothermal stages. However, the occurrence of the younger GEB granitic facies also indicates that magmatic activity was still ongoing until c. 590 Ma. This late magmatic event was apparently not associated with the formation of additional mineralisation. Therefore, the cooling history at the Passa Três granite and associated mineralisation is represented by the granite crystallization (with high temperature K-feldspar), followed by the formation of the late magmatic features, such as UST, aplite, pegmatite and stockscheider. Finally, these features were followed by the hydrothermal stages (transitional vein - with a K-feldspar border - and the mineralised veins).

4.7.3 Magmatic-hydrothermal transition

The magmatic-hydrothermal transition is a key process in ore-forming systems related to igneous activity. Understanding and tracking the magmatic-hydrothermal evolution is thus very important in mineralised systems (GLOAGEN et al., 2014; ZENG et al., 2016). The potential link between magmatism and mineralisation represents a key point in our study case. In the Passa Três granite, the presence of i) K-feldspar crystals on the edge of some veins (transitional veins, Figure 4.4g), ii) aplitic sills parallel to the mineralised veins (Figures 4.4b, 4.15 and 4.16), iii) aplite-pegmatite pockets mainly observed in the upper part of drill holes (Figure 4.4a, c, e) and iv) UST-type structures (Figures 4.4i and 4.5) are strong arguments for the existence of this link.

The UST feature classically forms in the highest portions of a pluton and indicates fluid pressure fluctuations, typical of a magmatic-hydrothermal transition process (KIRWIN, 2005 in PIRAJNO, 2009). In the aplites and the aplite-pegmatite pockets, some portions present hydrothermal quartz with euhedral K-feldspar crystals as a transition between aplite and quartz. These observations, and the presence of K-feldspar crystals on the border of some veins, clearly illustrate the transition from the final stage of magmatism (euhedral K-feldspar crystallization) towards the formation of orebodies with the presence of fluorite and other sulphides (Figure 4.4g, h), and indicate that the mineralisation paragenesis is not entirely posterior to the magmatic stage but intimately related. Features like USTs and aplites were also observed in the Climax-Mo type deposit (mineralisation spatially and genetically related to felsic intrusions), where they occur in the cupola zone of small intrusions and may even contain the mineralisation (AUDETAT; LI, 2017). Although ore was not observed in this kind of features in the Passa Três deposit, the similarities with the Climax-Mo deposit type suggest the potential for containing a mineralisation even in the late magmatic stages in the studied mineralisation. Additionally, although miarolitic cavities were not found in the Passa Três granite, given the cupola zone context, it is possible that they occur and that they could even contain ore.

This group of evidence strongly suggests a *continuum* from late-stage magmatic features through hydrothermal veins. Based on field observations and ^{40}Ar - ^{39}Ar and U-Pb geochronology, we propose the following sequence of formation: granite emplacement (GEM and GEF facies: 611.9 ± 3.6 Ma), late-magmatic phases (aplite, pegmatite, UST, stockscheider), transitional veins with K-feldspar borders (612.9 ± 2 to 608.8 ± 2 Ma), mineralised quartz veins (611.7 ± 2 to 608.8 ± 2 Ma), and barren quartz veins (608.4 ± 2 Ma). Based on these data, the time interval between granite crystallization and formation of the mineralised veins is bracketed between 613 and 608 Ma. Therefore, the very narrow time interval between the ages of magmatism, hydrothermalism and mineralisation is a strong

argument for the link between them, leaving no space to believe that the mineralisation could originate from country rocks. Therefore, a magmatic influence for the nature of the fluid source can be reasonably suspected.

Indeed, the magmatic-hydrothermal transition observed at the Passa Três gold deposit can be compared to similar features described in the Timbarra (MUSTARD, 2001) and Fort Knox (BAKKE, 1995 in MUSTARD, 2001; McCOY et al., 1997 in THOMPSON et al., 1999) deposits. In these deposits it is possible to observe the lateral gradation between the mineralised veins and the more fractionated magmatic phases, leading to the genetic association between them and to the interpretation that ore fluids were emplaced among the late fluid phases of crystallizing intrusions (BAKKE, 1995 in MUSTARD, 2001; McCOY et al., 1997 in THOMPSON et al., 1999; MUSTARD, 2001). Unfortunately, in the Passa Três granite, it was not possible to observe a lateral gradation between the two end-member phases, except within transitional veins (with a K-feldspar border) that remain poorly developed. However, the close temporal relation strongly suggests a connection between the magmatic fluids and the hydrothermal ore fluids.

Except for aplitic dykes that essentially occur close to or along gold-bearing quartz veins, USTs, quartz veins with K-feldspar borders and aplite-pegmatite pockets are mainly concentrated in the upper levels of the underground works and in the upper parts of the drill hole (Figure 4.16). These features frequently occur within the roof of the granitic system (PIRAJNO, 2009) and in that case, the Passa Três deposit can be compared to other deposits recognized to have the mineralisation within the roof zone of small-scale intrusions, such as the Timbarra gold deposit in Australia (MUSTARD, 2001) or the syenite-associated gold deposits in the Abitibi greenstone belt in Canada (ROBERT, 2001). According to Lang et al. (2000 in MUSTARD, 2001) and Thompson et al. (1999), in intrusion-related environments, the most favourable areas for the formation of mineral deposits and especially gold deposits are apical portions of small intrusions, such as the Fort Knox deposit (BAKKE, 1995 in MUSTARD, 2001). Small stocks allow the focus of hydrothermal activity within a single area, representing a potential spot for the formation of intrusion-related deposits (MUSTARD, 2001).

Based on the data presented in this work, we suspect that the ore-forming process was the result of the fluid release that can occur during the transition from magmatic to hydrothermal stages, as demonstrated by the numerous structures observed in the studied area. The question as to whether gold came from the granite or from the surrounding rocks leached by the hot hydrothermal or magmatic-hydrothermal fluid will be discussed in future work presently in progress, concerning fluid inclusion and alteration characterization.

4.7.4 Implications for intrusion-related gold systems

The association of gold with Bi minerals has been frequently described (LANG; BAKER, 2001; THOMPSON et al., 1999) and is considered as an important feature in intrusion-related gold systems as observed in deposits such as Timbarra (Bi, As, Mo, Sn) (MUSTARD, 2001); Fort Knox (bismuthinite, Bi-Te sulphides, and molybdenite) (SELBY et al., 2002); Brués (Au, Bi, Te, W) (GLOAGEN et al., 2014); Tighza polymetallic district (Morocco) (Bi, As, W, Mo, Sb, Te) (MARCOUX et al., 2015); Linares (Bi, Te, S, Se) (CEPEDAL et al., 2013); and Dublin Gulch (MALOOF et al., 2001). Characteristics such as structurally controlled veins at the roof zone of a small granitic intrusion associated to the magmatic-hydrothermal transition, the metaluminous nature of the pluton, gold associated to Bi minerals and mineralisation coeval with granite crystallization are implications for an intrusion-related gold system classification, proposed by several authors (SILLITOE; THOMPSON, 1998; THOMPSON et al., 1999; LANG; BAKER, 2001), and, since the deposit is located at the pluton cupola, it could be more specifically compared to a granite-hosted gold deposit type.

At the Passa Três gold deposit, mineralisation occurs at the top of the pluton, as indicated by several textures found in the mine level, such as USTs and the presence of aplite and pegmatite veins. Notably, both aikinite and chalcopyrite are commonly found within, or in spatial association with, the same features that host gold, including transitional veins, USTs and mineralised quartz veins. Nevertheless, gold is associated with chalcopyrite and aikinite, suggesting a possible ore assemblage combining the following elements: Au, Bi and Cu. However, there exist other granite-related deposits, such as the Timbarra one, that are classified as magnetite- and ilmenite-bearing I-type granite, thus representing some exceptions to the general model (MUSTARD, 2001). While the Passa Três granite and its gold mineralisation share several similarities with intrusion-related gold systems, some divergences subsist that require complementary analyses, such as a fluid inclusion study and stable isotope analysis for $\delta^{34}\text{S}$ of sulphides in order to better characterize the source of ore fluids and to conclude about the type of deposit, granite-related or not.

4.8 CONCLUSIONS

The main results of this study can be summarized in five points:

- The Passa Três granite is formed by a very homogeneous magmatic facies that exhibits a systematic red colour (GEM and GEF), certainly related to a strong oxidation. Scant evidence of a leucocratic late granite was encountered within the drill holes (GEB facies);
- Gold-mineralised veins of Passa Três granite are associated to two main normal fault systems running N-S and E-W. Both fault systems present the same paragenesis and

deformation phases, and ore fluid input is considered as contemporaneous of the deformation and filling of extensional pull-aparts;

- The veins contain as ore paragenesis: pyrite + chalcopyrite + gold + aikinite + ankerite + quartz + sphalerite;
- Several features evidencing magmatic-hydrothermal transition conditions were encountered both within drill holes and underground outcrops. These structures are, by order of abundance, pegmatite-rich pockets with central hydrothermal quartz, quartz veins with a K-feldspar border, UST, barren quartz veins and aplite veins;
- Geochronology data show that the Passa Três granite has an age of 611.9 ± 4.7 and 611.9 ± 5.6 Ma (GEM and GEF facies, respectively). The GEB facies presents a younger age of 592.8 ± 7.1 Ma. Ar-Ar analyses on muscovite grains determined veins with a K-feldspar border: 612.9 ± 2 to 608.8 ± 2 Ma; mineralised veins: 611.7 ± 2 to 608.8 ± 2 Ma; barren vein: 608.4 ± 2 Ma.

This evidence suggests the existence of a magmatic-hydrothermal transition, strongly confirmed by U-Pb and ^{40}Ar - ^{39}Ar dating that indicate a granite emplacement, a magmatic-hydrothermal fluid release and the formation of gold-bearing quartz veins during a time lapse of approximately 5 Ma, between 613 and 608 Ma. Therefore, for exploration purposes, features indicative of magmatic-hydrothermal transition (such as the ones described in this work) may help the discovery of new prospective targets.

The Passa Três gold deposit represents a very particular deposit in which the transition from magmatic to hydrothermal stages seems to be demonstrated although a strong contrast subsists between i) the homogeneous quartz veins with, at least for the majority, no clear evidence of magmatic affinities and ii) the quasi-undeformed granite containing these meter-scale gold-bearing quartz veins.

ACKNOWLEDGEMENTS

The authors would like to thank the Laboratory of Analysis of Rocks and Minerals (LAMIR-UFPR, Brazil) for several analyses and sample preparation, and the Laboratory of Isotopic Geology (Institute of Geosciences, Federal University of Rio Grande do Sul – UFRGS, Brazil) for sample preparation for the U-Pb analysis. We sincerely thank Mineração Tabiporã and their staff for the field support and sampling assistance. Ms. Dressel would like to thank the CAPES Foundation (Ministry of Education of Brazil, Brasília - DF, 70.040-020, Brazil) for granting the scholarship CAPES-PDSE (Process n. 99999.006489/2015-00) and for the attribution of a 48-month PhD scholarship in Brazil. Johann TUDURI and an anonymous reviewer are acknowledged for their constructive and critical reviews.

5 HYDROTHERMAL EVOLUTION AND ORE GENESIS OF THE PASSA TRÊS' GRANITE GOLD MINERALISATION, NEOPROTEROZOIC: CONSTRAINTS FROM S ISOTOPE, FLUID INCLUSIONS AND HYDROTHERMAL ALTERATION

Bárbara Carolina Dressel* ^{1,2,5}; Alain Chauvet ¹; Barbara Trzaskos ²; Kalin Kouzmanov ³; Olivier Bruguier ¹; Patrick Monié ¹; Sandro Notto Villanova ⁴; José Bazille Newton ⁴

¹ CNRS-UMR 5243, Géosciences Montpellier, Université de Montpellier, cc60, 34095 Montpellier Cedex 5, France.

² Federal University of Paraná, Post-Graduation Program in Geology, Geology Department, Av. Coronel Francisco Heráclito dos Santos, 210, 81531-970, Curitiba - PR, Brazil.

³ University of Geneva - UNIGE, Department of Earth Sciences, 24 Rue du Général Dufour 1211, Genève, Switzerland.

⁴ Mineração Tabiporã, Rua Maria Aparecida de Oliveira, 803 - Lt. São Gerônimo, 83606-177, Campo Largo - PR, Brazil.

⁵ Capes-PDSE Scholarship Process n. 99999.006489/2015-00. CAPES Foundation, Ministry of Education of Brazil, Brasília - DF, 70.040-020, Brazil

*Corresponding author

Full postal address: Federal University of Paraná, Post-Graduation Program in Geology, Geology Department, Av. Coronel Francisco Heráclito dos Santos, 210, 81531-970, Curitiba -PR, Brazil

E-mail addresses: barbara.geologia@gmail.com, barbara.dressel@gm.univ-montp2.fr (Dressel, B.C.); alain.chauvet@gm.univ-montp2.fr (Chauvet, A.); barbaratzaskos@ufpr.br (Trzaskos, B.); kalin.kouzmanov@unige.ch (Kouzmanov, K.); olivier.bruguier@gm.univ-montp2.fr (Bruguier, O.); patrick.monie@gm.univ-montp2.fr (Monié, P.); notto@tabipora.com.br (Villanova, S.N.); josebazille@hotmail.com (Newton, J.B.)

5.1 INTRODUCTION

Emphasis on the need of describing intrusion-related gold deposits were highlighted by some authors (e.g. BAKER; LANG, 2001; HART, 2007; MARCOUX et al., 2015; TUDDURI et al., 2018) and intrusion-related deposits described in the literature were formed mainly during the Phanerozoic, usually in mid-Carboniferous age. The Passa Três deposit display several similarities with the intrusion-related gold systems (HART, 2007; LANG; BAKER, 2001; THOMPSON et al., 1999), such as mineralisation coeval to granite crystallisation, evidences for magmatic-hydrothermal transition (UST, stockscheider, quartz veins with K-feldspar borders), Au associated with Bi-bearing minerals, structurally controlled orebodies, and the mineralisation hosted at the cupola zone of a small granitic intrusion (DRESSEL et al., submitted - Chapter 4).

Previous studies at the Passa Três Granite dealt with preliminary data of the mineral composition, alteration, geochronology and some genetic aspects (PICANÇO, 2000; PIEKARZ, 1992), ore minerals and their textures, structural control and magmatic-hydrothermal transition (DRESSEL et al., submitted - Chapter 4). Nevertheless, some aspects of this gold deposits remain still poorly understood, like the composition of ore fluids, the characterization of the alteration related with the mineralisation and the source of the metals and ligands so necessary for the ore deposition.

Therefore, the aim of this paper is to present new observations of the orebodies of the Passa Três' gold deposit, fluid inclusions, hydrothermal alterations and $\delta^{34}\text{S}$ isotope data to identify the mineralisation events, to interpret the sources of the ore-forming fluids, and to provide a better insight into understanding the role of the ore fluid and ore genesis of the gold mineralisation of the Passa Três granite. Perhaps this deposit could be an example of granite-hosted gold deposit formed in the Neoproterozoic.

5.2 GEOLOGICAL SETTING

5.2.1 Regional geology

The Eastern Paraná state (Southern Brazil) is composed of four terranes presumably amalgamated during the Neoproterozoic, which include, from North to South, the Apiaí, Curitiba, Luís Alves and Paranaguá terranes (Figure 5.1), all representative of the Southern portion of the large-scale Ribeira Mobile Belt (HEILBRON et al., 2004). The Passa Três granite crops out within host rocks that mainly comprise the Mesoproterozoic Votuverava Group, of the Apiaí Terrane (Figure 5.1). The Votuverava Group is composed of a monotonous succession of meta-pelitic rocks (sericite schists, phyllites, slates), with subordinate intercalations of meta-arenites, rare carbonate rocks and meta-basites (BASEI et al., 2010).

Several studies demonstrated that the Southern part of the Apiaí Terrane is deformed and affected by extensive shearing events, involving thrust and strike-slip shear zones (BASEI et al., 2010; CAMPANHA; SADOWSKI, 1999; FIORI, 1992; SIGA JR. et al., 2009). These events were related to the oblique collision between the San Francisco, Congo and Paraná cratons during the Neoproterozoic (CAMPO NETO; FIGUEIREDO, 1995; FRAGOSO CESAR, 1993; ROGERS et al., 1995). This resulted in deformation of the sedimentary sequence under low to medium grade metamorphism (CAMPANHA; SADOWSKI, 1999).

Several authors agree on the existence of three main tectonic events that affected the rocks of the Precambrian terranes located in Eastern Paraná State. The first one is related to the thrust event (Açungui Thrust System), the second one is called the Apiaí Folding System, and the third one is associated to transcurrent shear deformation (dextral Lancinha Shear System, Figure 5.1) that delimitates the South-eastern contact of the Apiaí Terrane (CURY et al., 2002; FIORI, 1992, 1994; FIORI et al., 1987; FASSBINDER, 1996; KAULFUSS, 2001). Near the Passa Três granite, the third tectonic event is well illustrated by the Morro Grande and Lancinha faults, with the Passa Três granite being emplaced between these two structures (Figure 5.1).

Two main episodes of magmatism have been described. The first one, from 700 to 600 Ma, reflects the formation of a magmatic arc (Cordilleran type) and the production of extensive

calc-alkaline plutonism represented by I-type granites. Syn- to post-tectonic plutons were emplaced between 630 and 600 Ma (i.e., Cunhaporanga and Três Córregos batholiths) and are attributed to this first event (CAMPANHA; SADOWSKI, 1999; GIMENEZ FILHO et al., 2000; JANASI et al., 2001; PRAZERES FILHO, 2000; PRAZERES FILHO et al., 2003a). From 600 Ma onward, the Adamastor Ocean was completely consumed and most continental blocks were amalgamated. Then, the tectonics was characterized by the development of dextral shear zones related to some oblique collision and/or escape tectonics (e.g., Lancinha Shear System). In this context, pull-apart basins were created, filled by molasse sequences, and the regional units were intruded by post-tectonic granites that formed the second event between 590 and 560 Ma (A-type magmatism developing the Cerne, Passa Três, Piedade, Morro Grande and Varginha granites – Figure 5.1; CAMPANHA; SADOWSKI, 1999; PRAZERES FILHO et al., 2003b).

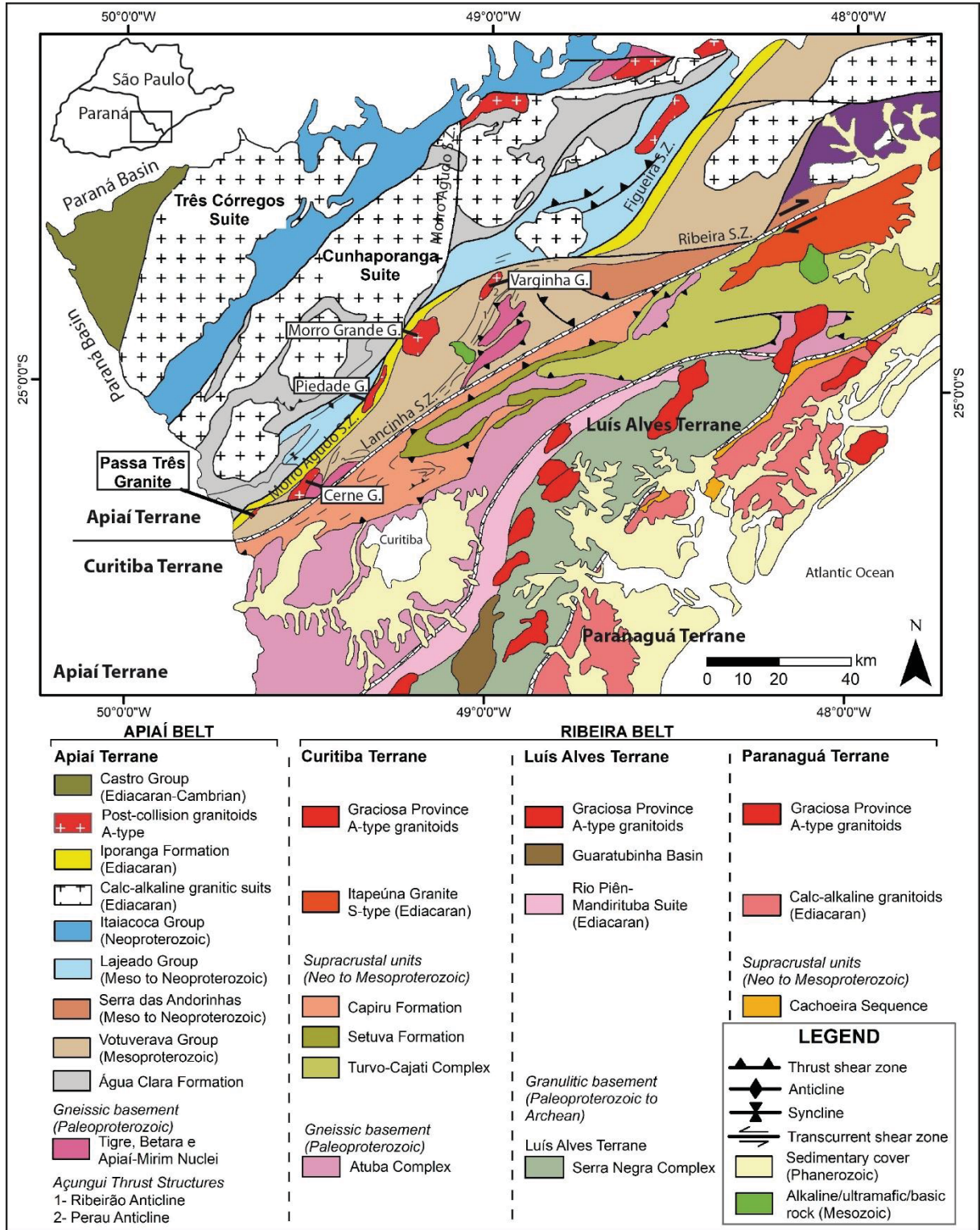


Figure 5.1 - Geological map with localisation of the Passa Três granite surrounded by its host rocks. The Apiaí, Curitiba, Luís Alves and Paranaguá terranes are also indicated. (Adapted from FALEIROS, 2008)

5.2.2 Local geology and characteristics of the Passa Três gold deposit

The Passa Três Granite is classified as I-type due to its metaluminous character and the type of its mineralisation associated with magnetite, titanite, apatite, amphibole, biotite and the absence of aluminous minerals (PIEKARZ, 1992). Classified as a shoshonite and belonging to the magnetite-granite series (PIEKARZ, 1992; PICANÇO, 2000), the Passa Três granite is considered post-collisional, such as other intrusions, like the Varginha, Morro Grande, Piedade and Cerne granites.

The Passa Três granite present gold-mineralised quartz veins with tabular and irregular shapes, ranging from millimetric to metric dimensions. These veins are constituted of quartz, sulphides (pyrite, chalcopyrite, aikinite, molybdenite), fluorite, muscovite, sericite, barite and carbonates. These veins infill pull-apart sites (extensional features) at two normal (contemporary and conjugated) fault systems of N-S and E-W direction, and dip angle of 60-75°W and 45-70°S, respectively, probably related to extensional tectonics during and after granite emplacement. Four phases of infilling and formation of pull-aparts were identified: first stage (quartz 1 + fluorite); stage 2a (quartz 2 + pyrite 2a ± gold ± chalcopyrite ± aikinite ± fluorite ± sphalerite ± muscovite); stage 2b (quartz 2 + pyrite 2b + gold + chalcopyrite + aikinite + ankerite ± sphalerite ± fluorite ± muscovite); stage 3 (quartz 3 + ankerite + calcite + molybdenite + aikinite + muscovite + fluorite) (DRESSEL et al., submitted - Chapter 4). PICANÇO (2000) also identified the presence of bornite, galena, covellite, chalcocite, digenite, arsenopyrite, iron oxides and clay minerals like illite, vermiculite and smectite.

Additionally, evidences like abundant aplites, pegmatites and quartz veinlets near the orebodies, veins with K-feldspar, *stockscheider* and unidirectional solidification textures (UST) suggest the existence of a magmatic-hydrothermal transition and are considered as a *continuum* from late-stage magmatic features through hydrothermal veins. This magmatic-hydrothermal transition was confirmed by U-Pb (LA-ICP-MS) and Ar-Ar geochronology data: Passa Três granite has an age of 611.9 ± 4.7 (medium texture facies), 611.9 ± 5.6 Ma (microgranite) and 592 ± 7 Ma (white granite facies); while Ar-Ar (muscovite) data indicate ages such as 612 to 608 ± 2 Ma for the transitional veins and of 611 to 608 ± 2 Ma for the orebodies. Based on these data, Dressel et al. (submitted - Chapter 4) considered the time interval from the granite crystallisation to the formation of the mineralised veins as bracketed between 613 and 608 Ma, representing a strong argument for the link among magmatism, hydrothermalism and mineralisation.

Hydrothermal alterations were observed by several authors and comprise biotite and amphibole alterations, microclinisation, sericite and muscovite alterations, argillic alteration, carbonation, silicification (PIEKARZ, 1992; PICANÇO, 2000), potassic alteration, phyllic alteration (TURINI NETO, 2012), epidotisation and saussuritisation (CURY, 2003). Piekarz

(1992) considers that the hydrothermal alteration would have acted in a pervasive way, but through selective fractures and/or veins in various physical-chemical stages.

Regarding the origin of the magma, the Passa Três Granite is considered as hybrid (crust and mantle origins), being intruded at a late-orogenic or late to post-collisional context related to the Três Córregos-Cunhaporanga magmatic arc (SOARES; GÓIS, 1987; CHIODI FILHO et al., 1989 in PIEKARZ, 1992; PIEKARZ, 1992). The emplacement of the Passa Três granite is also considered as sin to late-shear zones by Cury (2003), e.g., the Lancinha Shear Zone (FIORI, 1985b). Additionally, Cury (2003) suggests the possibility of crustal interaction as an important role in magma composition, as this pluton is considered very differentiated in relation to its sources indicated by the rare earth elements (REE) patterns and compares the Passa Três Granite to the A-type granites.

5.3 SAMPLING AND ANALYTICAL TECHNIQUES

The samples from hydrothermal altered rocks and orebodies were collected from different drill holes and inside the mine, approaching all the five levels of the mine. Polished thin sections were prepared to determine the paragenetic relationships of the ore minerals and to characterize the hydrothermal alteration assemblages. Analyses of thin sections were carried out on polarised-light microscopes.

Electron microprobe analyses (EPMA) and back-scattered electron imaging were done on carbon-coated polished sections with a Cameca X100 Electron Microprobe Microanalyzer by wave length dispersion spectrometry. Measurements were done at 20 kV with a beam current (cup reading) of 10 nA, using the following X-ray lines for silicates and carbonates: F K α , Al K α , Si K α , Ti K α , Na K α , Mg K α , Mn K α , Fe K α , K K α and Ca K α , and for the metallic minerals: S K α , Fe K α , Cu K α , Au L α , Mo L α , Pb M α , Ag L α , Zn L α , Ti K α , As L α , Bi L α .

For the fluid inclusions study, ten double polished thin sections were fabricated at the University of Montpellier, at the Geosciences Montpellier Laboratory. Among these thin sections, five ones were selected for microthermometry. Microthermometric measurements on doubly polished thin sections (100 μ m) were carried out using a Linkam heating and freezing stage at the Lamir Laboratory, Federal University of Paraná, Curitiba, Brazil. It has a temperature range from -180°C to +600°C.

Sulphur isotope was analysed from five pyrite samples (concentrate pulp) of the main mineralised veins and performed at the Actlab Laboratories at Ancaster, Canada. QemScan analysis determined major and trace elements by X-ray fluorescence (XRF) using a PANalytical AXIOS MAX with a Rhodium anode tube at 4 W at the University of Lausanne. SY-2, BHVO, NIM-N and NIM-G standards were used for quality control.

5.4 GOLD-MINERALISATION

The gold mineralisation at the Passa Três granite is composed of auriferous quartz veins concentrated in the granite. At the Faixa do Barreiro, the main mineralised vein zone in the Passa Três granite, where this study is focused, the orebodies are exposed in the underground mine and in the boreholes, and they are associated to two normal fault systems, of N-S and E-W orientations. Generally, the presence of cataclastic breccias and a fault gouge with sulphides is observed in the borders of these veins.

Gold mineralisation is represented by the quartz-sulfide veins, that occur in the pull-apart sites of the two normal fault systems (Figure 5.2a). As presented in the section 5.2.2, the orebodies were formed in four phases and gold occurs as native grains within fractures that affect pyrite, commonly associated with chalcopyrite and aikinite (Figure 5.2b).

Figure 5.3 displays SEM images of the ore paragenesis. On these images, one may observe homogeneity on the pyrite 2a, as well as the euhedral habit of pyrite 2b (Figure 5.3a, c). On the EDS mapping (Figure 5.3b, d), it is possible to observe the portions rich in Cu, represented by chalcopyrite, and portions rich in Pb, represented by aikinite. Late stage quartz-carbonate veins cut all other stages, and they are composed of quartz, ankerite and/or calcite, and are associated to late reverse movement.

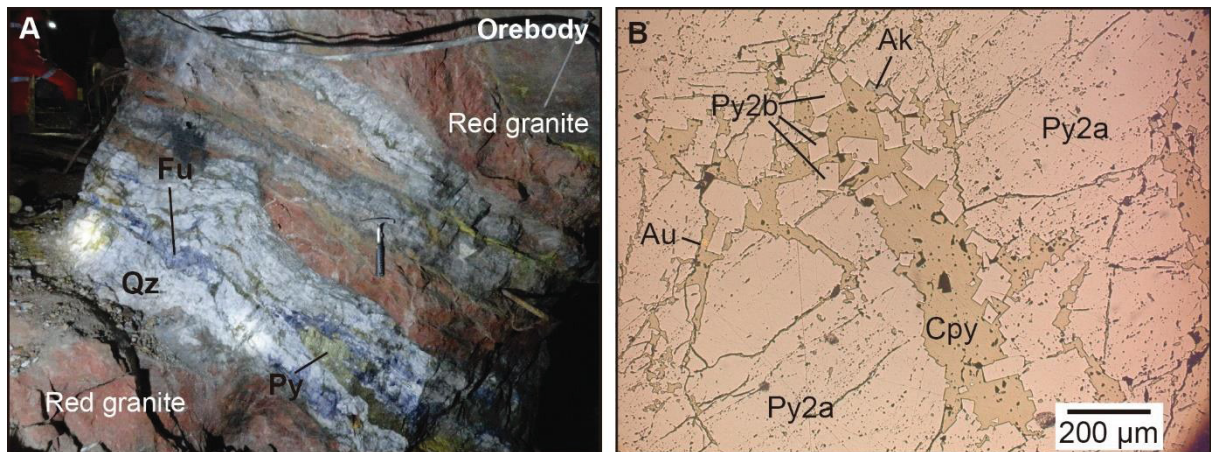


Figure 5.2 - A) Photograph of the orebody composed mainly of quartz, sulphides (pyrite, chalcopyrite) and fluorite; B) Detail of the ore paragenesis with two pyrite phases (Py2a, Py2b, see Dressel et al., submitted - Chapter 4), chalcopyrite, aikinite and gold in a pull-apart site.

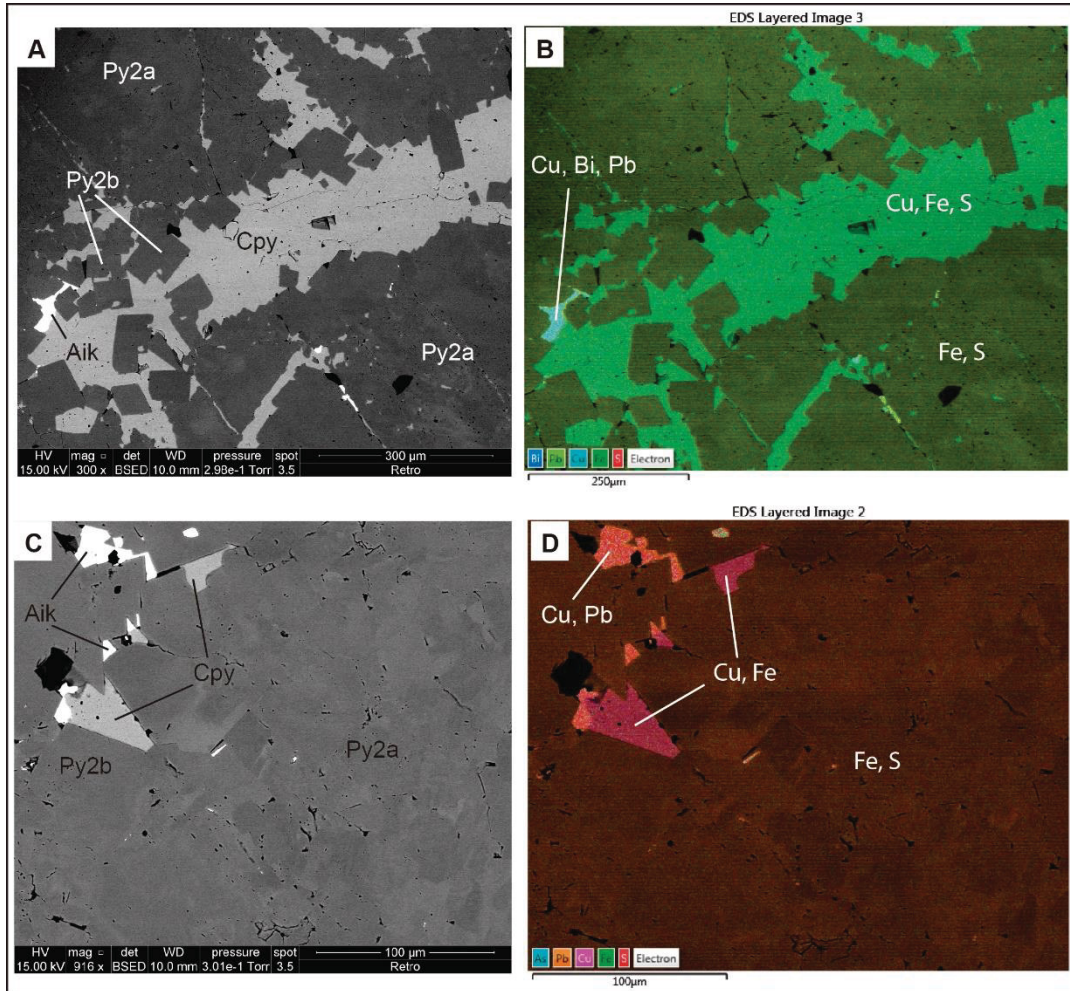


Figure 5.3 – SEM images of the ore paragenesis. Figures A and C show backscattering images, with indication of pyrite 2a, pyrite 2b, chalcopyrite, aikinite and gold. Figures B and D display the same images, but with an EDS chemical mapping, evidencing the presence of Cu, Pb and Bi.

5.4.1 Mineral chemistry (EPMA, LA-ICP-MS)

In order to verify the ore minerals, they were analysed by EPMA analysis. This technique identified that the gold alloy is composed of Au (90,37–93,07%) and Ag (7,71–12,13%), and also minor Cu, Fe and S (Figure 5.4). While Figure 5.5 displays analysis of aikinite, a sulfosalt of Pb, Cu and Bi, highlighting the close relation between Au and Bi.

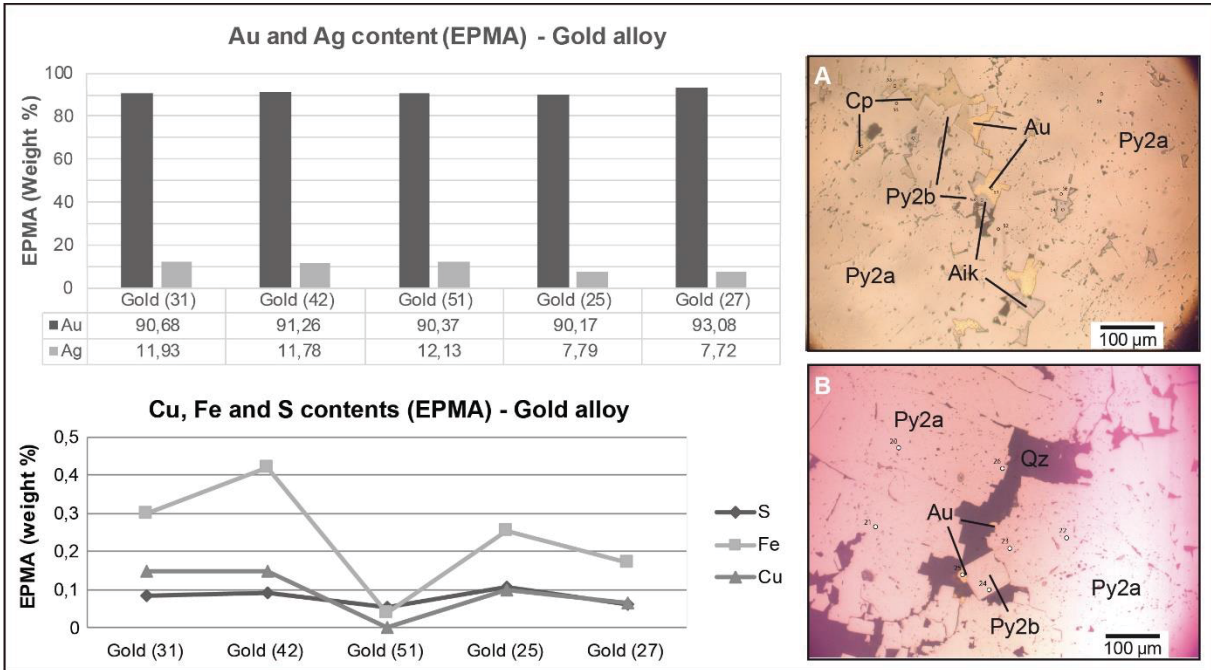


Figure 5.4 - EPMA analysis in gold next to pyrite 2a, pyrite 2b, chalcopyrite and aikinite.

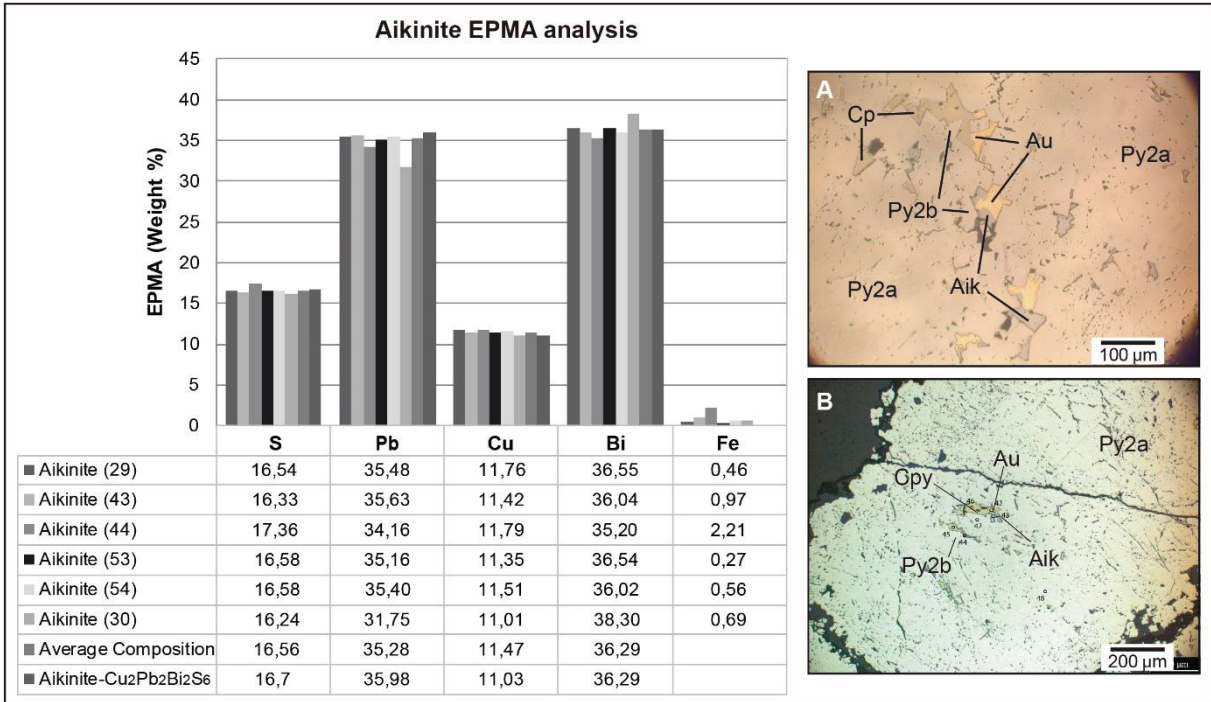


Figure 5.5 - EPMA analysis in crystals of aikinite, displaying its composition of Pb, Cu and Bi.

Due to the suspicion of the presence of invisible gold in pyrite 2a, LA-ICP-MS analysis were conducted (Figure 5.6). These analyses confirm the presence of invisible gold in pyrite 2a and also in pyrite 2b, and suggest its association with Cu, Ag, Sb, Pb and Bi, agreeing with the EPMA analysis (Figures 5.4 and 5.5). The presence of invisible gold in both pyrite phases may suggest that native gold was the result from remobilisation from pyrite 2a, possibly caused by deformation, as already observed at other gold deposits by Velásquez et al. (2014).

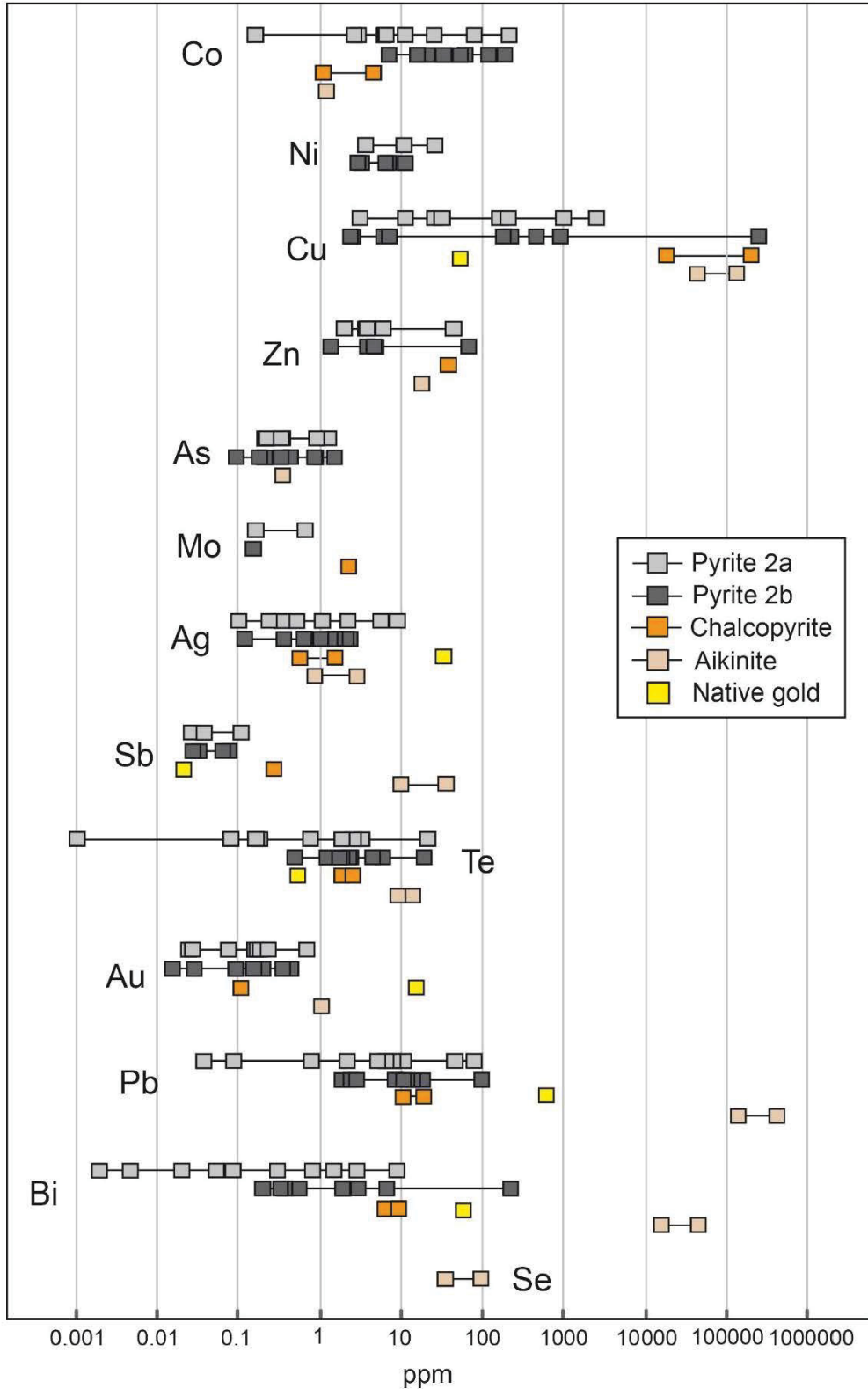


Figure 5.6 - Trace elements distribution by LA-ICP-MS analysis (Appendix 5.A) on the following minerals: pyrite 2a, pyrite 2b, chalcopyrite, aikinite and native gold. One may observe the concentration variation (ppm) of Co, Ni, Cu, Zn, As, Mo, Ag, Sb, Te, Au, Pb, Bi and Se. Concentration are displayed in logarithmic scale.

5.4.2 Fault gouge

The brown-coloured fault gouge occurs in the fault planes that shelter the orebodies, and at the borders of the veins with a thickness of millimetres to 1 centimetre. This fault gouge is probably due to the movements along the fault zones but also to their re-activation, which also led to brittle deformation and breccia formation in the border of the veins, in the host rock (red granite). It mainly consists of clay minerals and sulphur ones, mainly pyrite, and these minerals are interpreted as alteration posterior to the mineralisation. The fault gouge (or “guide”, as called by the mine geologists) is used as a guide for the mine geologists to find the orebodies, as it is present along the fault planes.

5.5 MINERALISATION RELATED HYDROTHERMAL ALTERATIONS

In the Passa Três gold deposit, there are different types of hydrothermal alteration, and its regular spatial distribution and vein minerals can be observed mainly in the drill holes (Figure 5.7). Based on investigations using optical microscopy, EPMA, XRF and SEM analysis, two main alteration assemblages were defined, associated to the mineralisation: a greisen-type and a phyllic-type alteration (Figure 5.7). The greisen-type alteration is associated to barren quartz veins during magmatic-hydrothermal transition, and it is observed in the drill holes and in the underground mine. The phyllic-type alteration is also observed, and is characterised by a greenish colour, occurring in a diffusive way and also in the border of the mineralised veins, associated to breccia. These alterations affect the red granite (host granite, GEM and GEF facies), considered as the least altered rock.

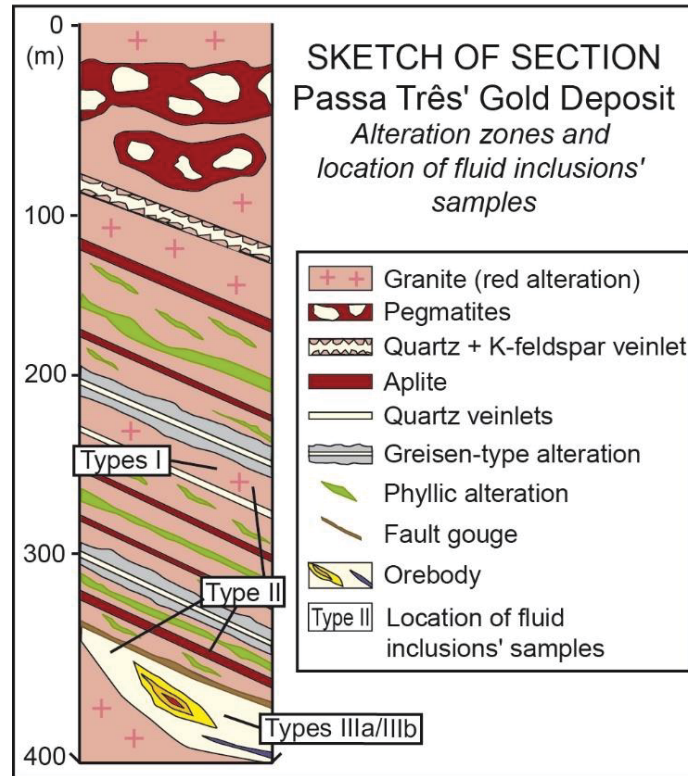


Figure 5.7 - Schematic sketch of the section showing the distribution of main alteration zones and veins near the main mineralisation at the “Faixa do Barreiro” pit.

5.5.1 Red Granite

In the Passa Três Granite, there are three different granitic facies, denominated “medium grain granite” (GEM), “microgranite” (GEF) and “white granite” (GEB), in addition to aplites and pegmatites. In terms of field relations, GEF and GEM facies appear to be contemporaneous and crop out at the whole length of the intrusion, however GEB seems to be posterior to GEM and GEF, and it is only seen at the drill cores. Here, we name the least altered rock as red granite, that represent both GEM and GEF facies (Figure 5.8a-d). The GEM facies is classified as a syenogranite and presents an igneous paragenesis composed of microcline, plagioclase, and quartz, and has a medium grain texture with isotropic structure. Zircon and apatite appear as accessories. The GEF facies is a syenogranite and has a fine-grain texture with isotropic structure. The igneous paragenesis is constituted of microcline, plagioclase and quartz, and the accessories: apatite, zircon, and fluorite. Chlorite (clinocllore, see section 5.5.4) occurs as an alteration of biotite and, possibly, amphibole (Figure 5.8c, d). K-feldspar present hematite inclusions (Figure 5.8e). Magnetite may occur associated with sphalerite, presenting well-formed crystals. Hematite is anhedral and also occurs with magnetite, carbonate and sericite as aggregates. A QemScam elemental map displays the distribution and percentage of the mafic minerals with concentration of Fe, Mg and Ca, and the

isotropic texture of the rock highlighted by quartz, plagioclase and microcline crystals (Figure 5.9). EPMA analysis suggests the presence of ankerite and calcite as carbonates associated with the red granite alteration (section 5.5.4), and carbonate was also identified as a major component of the alteration by the QemScan analyses.

GEM and GEF facies show the intense red colour over all the surface of the granite. This red colour is due to the presence of magnetite and hematite in porous of K-feldspar crystals, and in the rock matrix, as observed in SEM analyses (Figure 5.8e-g). This alteration is considered of high temperature and older than the mineralisation (NAKANO et al., 2005; PUTNIS et al., 2007), however Pirajno (2009) considers the hematite inclusions as a characteristic of potassic alteration. Among the common assemblages of potassic alteration, K-feldspar/chlorite is one of them, so it is possible to consider the red granite, including hematite inclusions in the K-feldspars, as a potassic alteration with the characteristic reddish colour.

The red granite is affected by two hydrothermal alterations: greisen-type and phyllic-type alterations (Figures 5.10 and 5.11). Unfortunately, it was not possible to find a sample without the red granite alteration, so this facies is considered further for the mass balance calculations as the least altered rock.

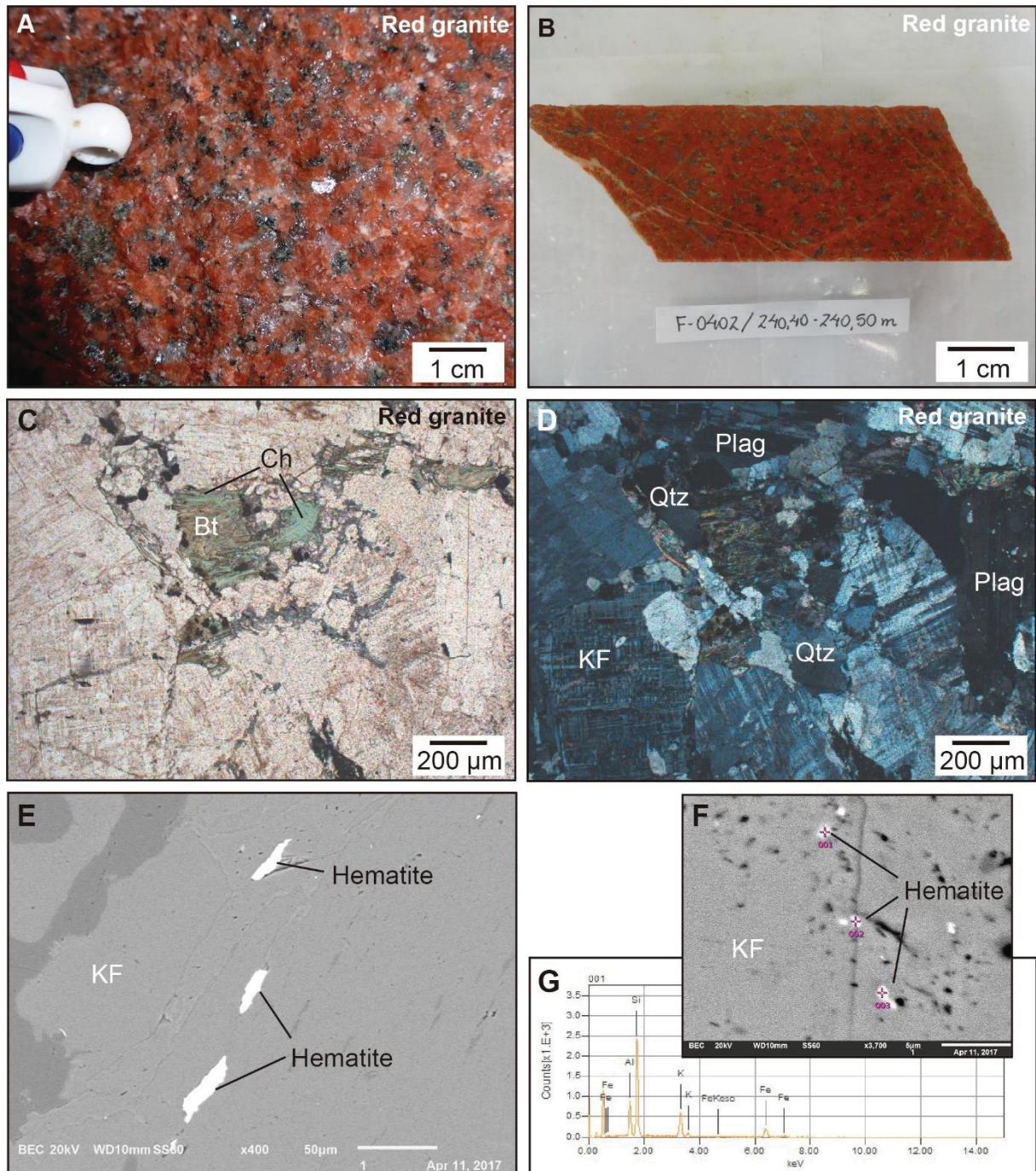


Figure 5.8 - Red granite's photographs (A, B), photomicrographs (C, D), SEM images (E, F) and SEM/EDS analyses (G). A and B Red granite with medium isotropic texture; biotite crystals are altered to chlorite; photograph in the underground mine (A) and in borehole (B); C) and D) Red granite with biotite crystal with chlorite alteration, in a medium isotropic texture; E) SEM image displaying hematite crystals in porous of a K-feldspar crystal; F) Hematite crystals in a K-feldspar pores and EDS analyses indicating presence of Fe. Bt: biotite, Ch: chlorite, FeO: Fe-oxide, Qz: quartz, KF: K-feldspar, Plag: plagioclase.

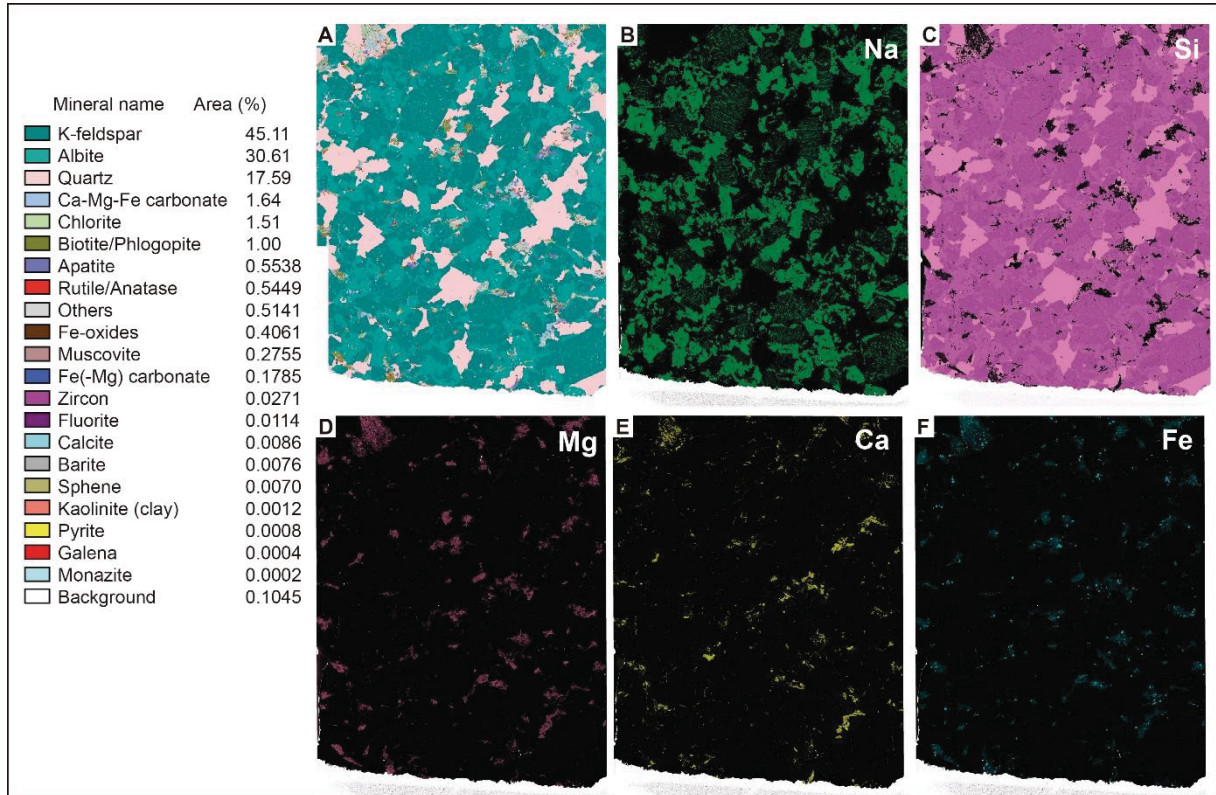


Figure 5.9 - A) QemScan map of the red granite. Distribution maps of X-ray elemental map of Na (B), Si (C), Mg (D), Ca (E) and Fe (F).

5.5.2 Greisen-type alteration

Greisen-type alteration in the Passa Três granite is composed of muscovite + quartz + chalcopyrite \pm pyrite, and present moderate intensity. This alteration is associated with the magmatic-hydrothermal transition, specifically with the many barren quartz veins (1 to 5 cm width) that preceded the emplacement of the mineralised veins (Figure 5.10a, b). It is characterised by a grey halo with 10 cm width in the border of the quartz veins (Figure 5.10a). These quartz veins are posterior to the aplites and pegmatites, forming after these late-magmatic phases and before the mineralisation. In the drill holes, they are near to the orebodies, and are more numerous as we approach the mineralised veins. Curiously, there are no quartz veins of this type deeper than the mineralisation in the drill holes.

Altered rocks are characterised by relict K-feldspar with partial transformation of K-feldspar and total transformation of plagioclase to muscovite (Figure 5.10c, d). The original igneous texture was largely obliterated, with muscovite replacing plagioclase, clinocllore, K-feldspar and biotite. Primary K-feldspar are anhedral, and quartz may present brittle deformation, such as fracturation. Secondary quartz occurs, and they present no deformation. Zircon, which are traditionally assumed to be resilient to hydrothermal alteration, is not

observed. Apatite and titanite also disappeared. Only limited sulphide minerals are associated with this alteration, occurring some sparse pyrite and chalcopyrite crystals.

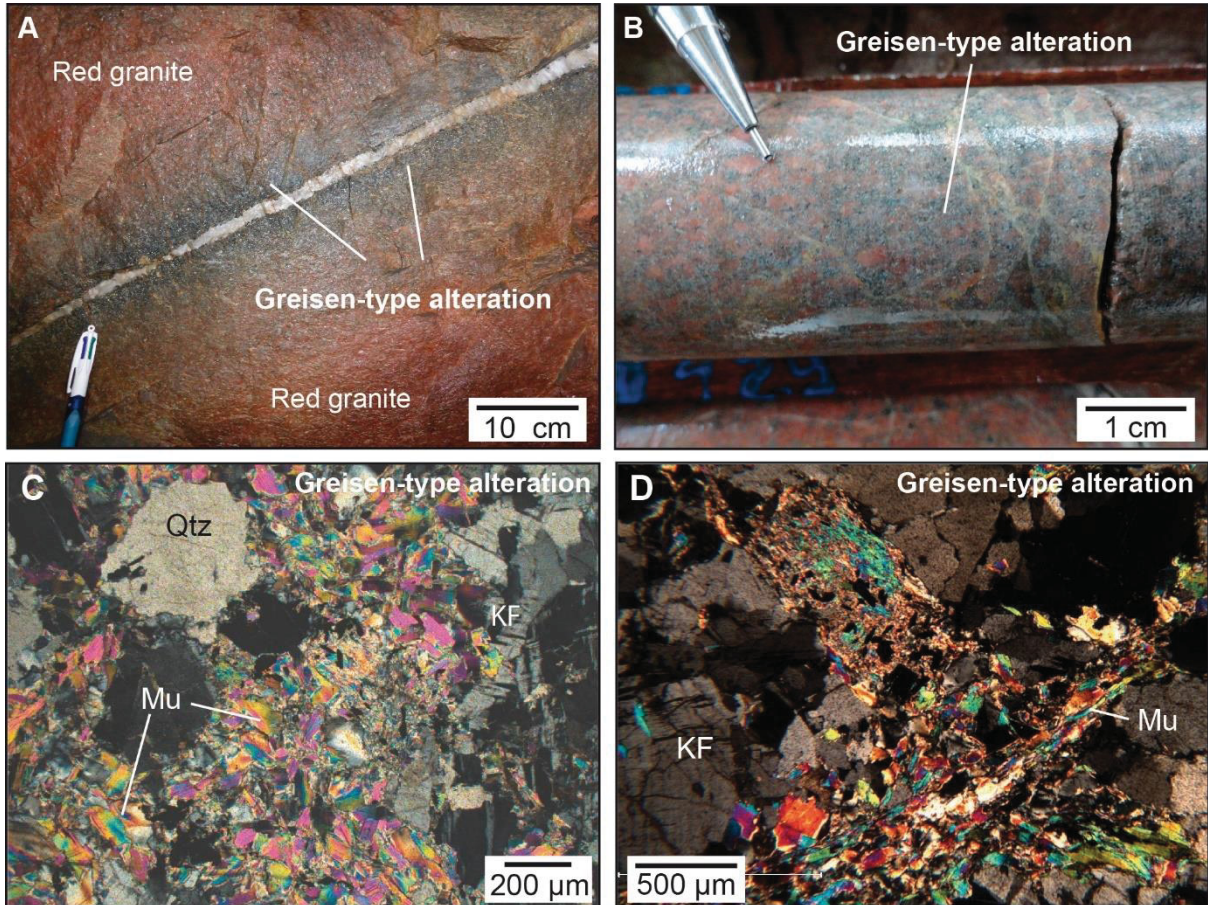


Figure 5.10 - Photographs of the greisen-type alteration related to the gold mineralisation. A) Greisen-type alteration in the border of a barren quartz vein, underground mine; B) Greisen-type alteration in borehole; the grey colour is very characteristic; C) Muscovite crystals as alteration of K-feldspar and plagioclase crystals, in a medium isotropic texture; D) Two fault planes with concentration of muscovite crystals.

5.5.3 Phyllic-type alteration

Phyllic-type alteration in the Passa Três deposit is weak to very weak and its assemblage is characterised by sericite + quartz + ankerite + rutile + siderite + pyrite clinocllore ± calcite. Small scale (up to 10 meters) diffusive phyllic alteration develop parallel to the fault systems that contain the mineralisation and is marked by a greenish colour (Figure 5.11a, b), and the details of the muscovite and carbonate crystals may be observed in Figure 5.11c, d. The intensity of this alteration varies greatly, presenting itself as very weak to moderate intensity, and may be related to the presence of breccia (Figure 5.11e-h). In the border of the mineralised veins, this alteration is very strong and related to breccia, where the original igneous texture is no longer observable (Figure 5.11e-h). On the microscope, we

observe alteration planes in the form of very small fractures that cut the earlier original igneous texture and may also affect the greisen alteration (Figure 5.11g, h). Figure 5.12 displays a QemScan elemental map showing the small fractures composed mainly of sericite + carbonate, that affect the red granite isotropic texture, and the alteration minerals concentrated in interstitial location, in the same position as the mafic minerals were in Figure 5.9, suggesting that most of the alteration replaced those minerals, forming the phyllic assemblage. Geometrically, in the drill holes, it presents a *zebra* pattern following planes parallel to the mineralised veins.

With weak diffusive alteration, biotite and chlorite (clinochlore) were partly or totally replaced by sericite, siderite and ankerite (see section 5.5.4), and plagioclase were transformed to sericite along hairline cracks (such as K-feldspar) or polysynthetic twinning and zoning. Regardless the intensity of the alteration, sericite and the other minerals also formed thin veinlets in micro-fractures with ankerite. A small amount of chalcopyrite occur as disseminated grains. Brittle deformation is represented by fracture in K-feldspar and plagioclase and undulose extinction in quartz crystals. On the micro-scale, it is clear that phyllic alteration overprints greisen alteration, as sericite/carbonate filled fractures affect the muscovite crystals of the greisen alteration.

At the border of the mineralised veins, strong phyllic alteration develop along cracks or other opens spaces of breccias (Figure 5.11e-h), and even in granite blocks that occurs inside the vein, which presents very strong alteration. This zone mainly comprises pyrite, carbonate and sericite. And most quartz and K-feldspar grains are broken, exhibiting irregular shapes and different sizes, indicating brittle deformation. Recrystallised quartz sub-grains may occur, and sericite may appear as fracture filling. Pyrite and chalcopyrite are the main sulphide minerals in this part and occur as subhedral/euhedral grains. During this work, gold was not observed in this alteration zone, although we cannot exclude the possibility that it may occur. Therefore, vein-related phyllic alteration shares similar alteration mineral assemblage with diffusive alteration, indicating that they were contemporaneous. This alteration is related with the mineralisation phase, being contemporary to the emplacement of the mineralised veins in the pull-apart sites of the normal faults (see DRESSEL et al., submitted - Chapter 4).

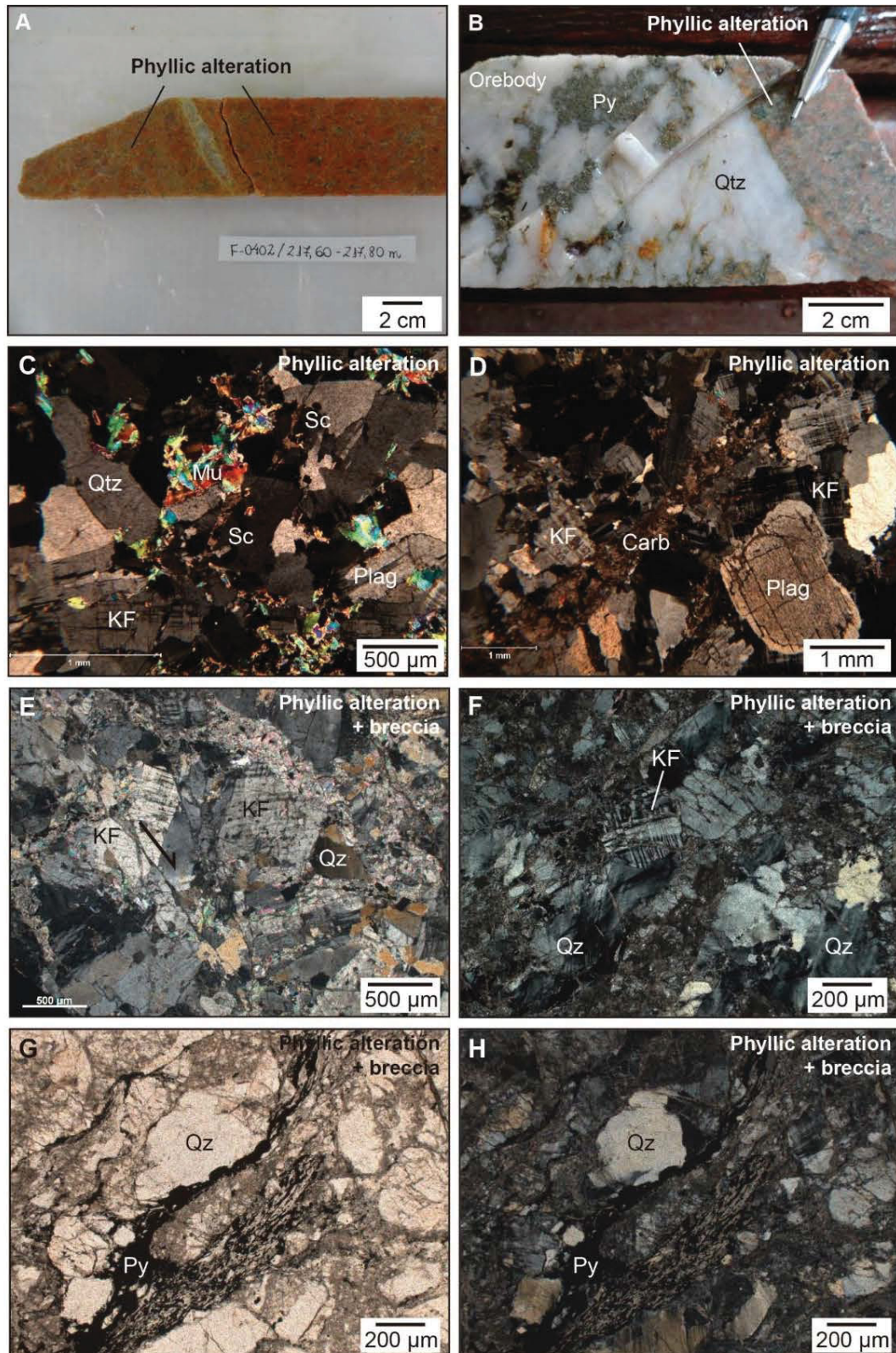


Figure 5.11 - Aspects of the phyllic-type alteration in the Passa Três deposit. A) Phyllic-type alteration in borehole; this alteration produces a greenish colour; B) Phyllic-type alteration in the border of an orebody (borehole); C) Phyllic-type alteration with sericite planes affecting the texture of the granite; D) Ankerite planes associated to the phyllic-type alteration; E to H) Phyllic-alteration superimposed to breccia (red granite) at the border of the orebody with details of normal faulting (E), fractured K-feldspar crystal (F) and strong alteration and py levels (G, H). Carb: carbonate, KF: K-feldspar, Mu: muscovite, Qz: quartz, Plag: plagioclase, Py: pyrite.

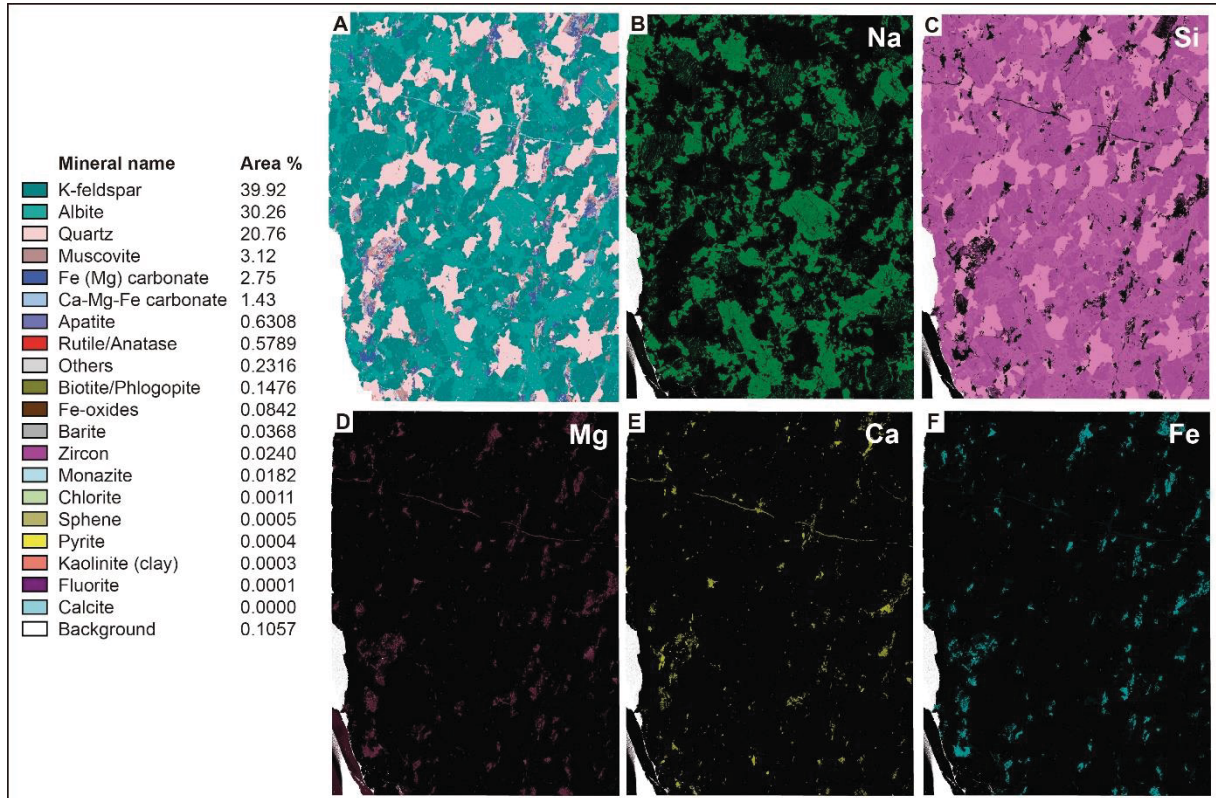


Figure 5.12 - A) QemScan map of the phyllic alteration. Distribution maps of X-ray elemental map of Na (B), Si (C), Mg (D), Ca (E) and Fe (F).

5.5.4 Mineral chemistry (EPMA)

In order to determine the minerals of the alteration assemblages of the red granite alteration and phyllic alteration, we carried out EPMA analysis to obtain the chemical compositions of feldspars, albite, chlorite, muscovite and carbonate. Figure 5.13 displays some analysed spots, and the results are presented on the Tables 5.1 to 5.8.

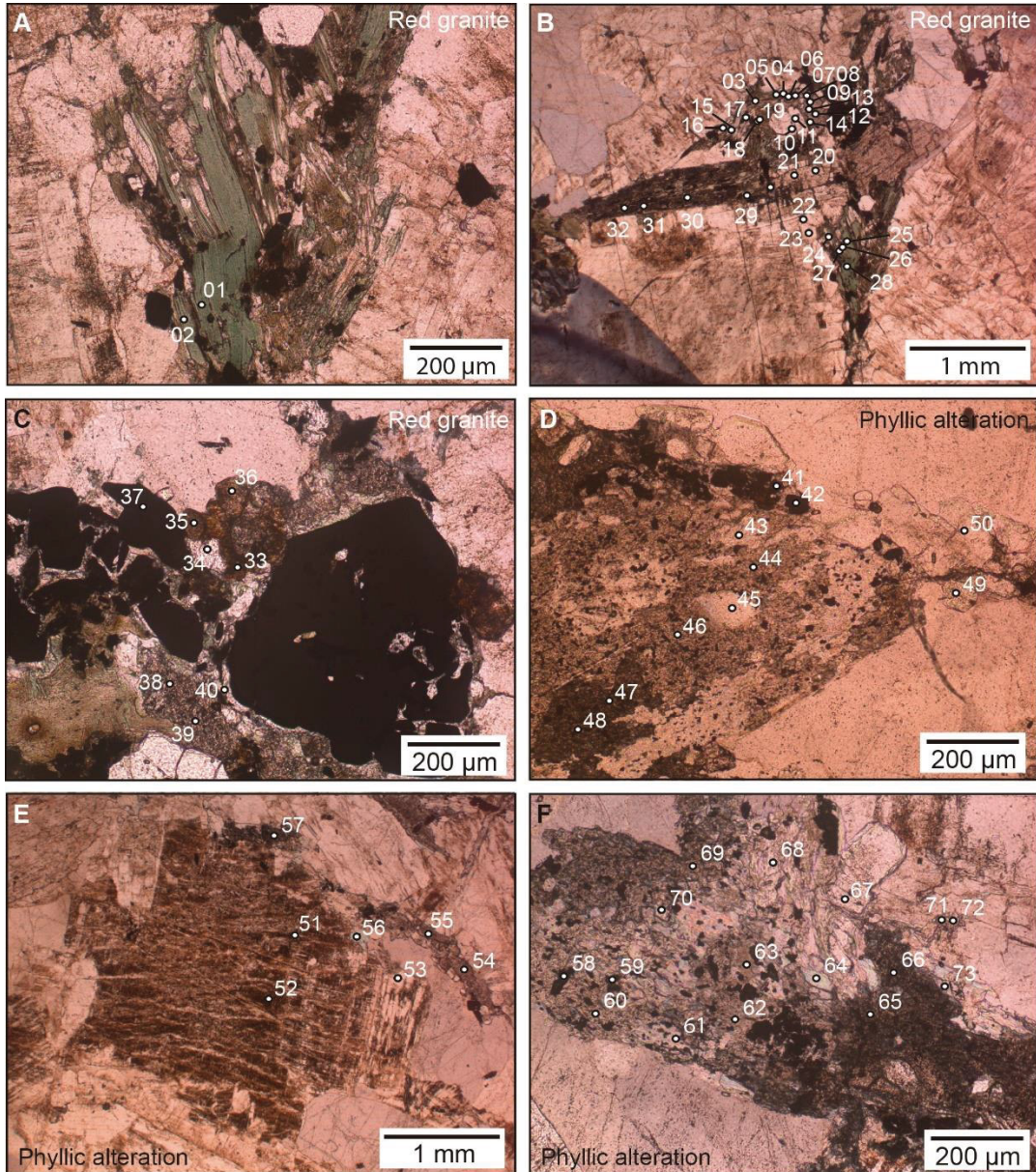


Figure 5.13 - Photograph of alteration minerals analysed in EPMA of red granite alteration and phyllic alteration in the thin sections. A) Chlorite crystals as alteration of biotite crystal, red granite alteration; B) Mafic aggregate in red granite formed by biotite, and possibly amphibole; as alteration minerals; analyses points indicate the presence of clinocllore, siderite, ankerite, calcite; quartz and albite are also identified; C) Localised alteration was observed in the red granite sample, with the presence of ankerite and siderite; D) Ancient titanite crystal altered by siderite, muscovite, ankerite and rutile, phyllic alteration; E) K-feldspar with Fe-oxide alteration; analysis spots indicate the strong presence of FeO; F) Phyllic alteration with indication of the analysed spots.

Feldspars

Table 5.1 display the EPMA results of feldspars. The analyses points on feldspar crystals of the GEM facies suggest an average formula $(K_{1.01}Na_{0.03})[Al_{1.00}Si_{2.97}O_8]$, indicating a potassic feldspar (DEER et al., 2010). This information, associated with the chess board texture observed by the petrographic analysis, we assume it to be microcline. In the same way, the analysis on feldspars on the edge of the transitional veins indicate an average formula

$(K_{1,03}Na_{0,03})[Al_{1,00}Si_{2,99}O_8]$, and also present chess board texture. Both feldspars with the same texture and very similar structural formulas suggest a similarity between magmatic K-feldspar and the feldspar in the border of early hydrothermal veins.

An EPMA analysis of feldspar associated to the red granite alteration indicate the presence of albite with an average structural formula $(K_{0,01}Na_{0,95})[Al_{1,01}Si_{2,98}O_8]$, and locally related to the phyllic alteration, with a structural formula $(K_{0,01}Na_{0,92})[Al_{1,04}Si_{2,96}O_8]$ (Table 5.1).

Muscovite

The Table 5.2 displays the results of the white mica associated to the greisen-type alteration, phyllic alteration and the transitional veins, associated with molybdenite. The analysis of white mica from the transitional vein indicate an average structural formula $(K_{2,03}Na_{0,03})(Fe_{0,59}Mg_{0,55}Al^{VI}_{2,92}Ti_{0,10})[Si_{6,81}Al^{IV}_{1,19}O_{20}](OH,F)_4$. While the analysis of the white mica crystals associated with greisen-type alteration indicate a structural formula $(K_{1,5}Na_{0,01})(Fe_{0,3}Mg_{0,59}Al^{VI}_{3,00}Ti_{0,03})[Si_{6,87}Al^{IV}_{1,13}O_{20}](OH_{3,61}F_{0,39})$, and those from the phyllic alteration suggest an average structural formula $(K_{1,53}Na_{0,02})(Fe_{0,33}Mg_{0,43}Al^{VI}_{3,10}Ti_{0,04})[Si_{6,70}Al^{IV}_{1,30}O_{20}](OH_{3,58}F_{0,42})$. These results point to a dioctahedral muscovite (DEER et al., 2010). In this way, these data indicate homogeneity among the muscovite compositions from the transitional veins and the greisen-type and phyllic alterations, that could suggest that their crystallisation was produced from a fluid with similar composition.

Chlorite

Tables 5.3a and 5.3b displays the results of chlorite crystals associated to the red granite alteration and phyllic alteration. The chlorite crystals related to the red granite alteration present an average structural formula $(K_{0,03}Na_{0,08}Mg_{4,47}Fe_{3,99}Al^{VI}_{2,11}Ti_{0,80})[(Si_{6,37}Al^{IV}_{1,69}O_{20}](OH_{3,47},F_{0,53})$. In the same way, the chlorite analysis related to phyllic alteration indicate an structural formula $(K_{0,01}Na_{4,41}Mg_{0,58}Fe_{0,40}Al^{VI}_{4,40}Ti_{3,97})[(Si_{7,31}Al^{IV}_{0,69}O_{20}](OH_{3,45},F_{0,55})$. These compositions and the diagram proposed by Bailey (1988) for classification of Fe-Mg chlorites (Figure 5.14) suggest a clinocllore composition, with the local presence of chamosite.

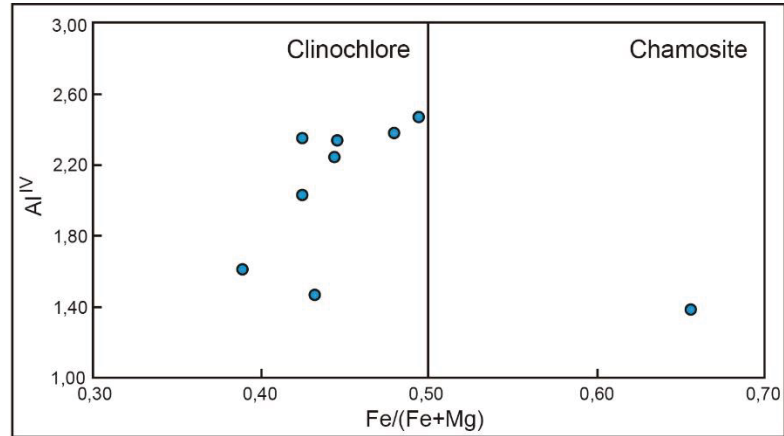


Figure 5.14 - Classification diagram for Fe-Mg chlorites proposed by Bailey (1988). Plotted points indicate the presence of clinochlore crystals, associated to the red alteration.

The Table 5.4 shows the analyses of biotite crystals of a GEM facies sample affected by the red granite alteration. These results suggest an average structural formula $(K_{1,75}Na_{0,01})(Fe^{II}_{0,06} Mg_{3,32})(Fe^{III}_{1,71}Al^{VI}_{0,00}Ti_{0,28})[Si_{5,48}Al^{IV}_{2,04}O_{20}](OH_{2,18},F_{1,82})$. Despite the presence of chlorite alteration related to the red granite alteration, these results show that some biotite may have been preserved in the red granite.

Carbonate

The EPMA analysis on carbonate crystals identified the presence of ankerite, calcite and siderite. Among these, related to the red granite alteration, we have ankerite and calcite, while associated with the phyllic alteration, we have both ankerite and calcite with the presence of siderite. The evidence for carbonate as alteration was also identified with QemScan analysis (Figures 5.9 and 5.12). Tables 5.5 and 5.6 show ankerite analysis and calculated structural formulas related to the red granite alteration and phyllic alteration, respectively. Table 5.7 displays results of the calcite analysis and calculated structural formula related to red granite and phyllic alterations. And, finally, Table 5.8 displays siderite analysis related to the phyllic alteration.

Table 5.1 - EPMA analysis and calculated structural formula for feldspars of granite (GEM facies, K-feldspar), transitional veins (K-feldspar), red granite alteration (albite) and phyllic alteration (albite).

	D-51 FK - GEM	D-52 FK - GEM	D-53 FK - GEM	BD-83-32 FK - Transitional vein	BD-83-34 FK - Transitional vein	BD-83-52 FK - Transitional vein	A-20 Albite Red granite	A-21 Albite Red granite	A-22 Albite Red granite	A-23 Albite Red granite	A-71 Albite Phyllic alt.
SiO2	63,74	63,76	63,19	63,74	63,12	63,08	68,97	68,91	67,86	68,09	67,32
Al2O3	18,15	18,17	18,24	17,83	17,91	18,08	19,94	19,90	19,60	19,46	20,01
TiO2	0,00	0,00	0,00	0,00	0,00	0,00	0,01	0,02	0,00	0,00	0,01
FeO	0,07	0,20	0,14	0,05	0,00	0,11	0,05	0,10	0,07	0,12	0,17
MnO	0,00	0,01	0,02	0,00	0,00	0,00	0,02	0,00	0,00	0,00	0,02
MgO	0,00	0,00	0,00	0,00	0,00	0,00	0,00	0,00	0,01	0,01	0,00
CaO	0,00	0,00	0,00	0,00	0,00	0,04	0,40	0,44	0,29	0,33	0,95
Na2O	0,20	0,16	0,60	0,23	0,23	0,47	11,13	11,05	11,29	11,47	10,84
K2O	17,55	16,96	16,46	17,39	17,26	16,75	0,08	0,12	0,10	0,10	0,17
Cr2O3	0,00	0,01	0,00	0,00	0,00	0,00	0,00	0,01	0,00	0,01	0,00
NiO	0,00	0,00	0,00	0,00	0,00	0,00	0,02	0,00	0,01	0,00	0,02
F	0,00	0,00	0,43	-	-	-	0,00	0,18	0,00	0,25	0,00
Cl	0,01	0,01	0,00	-	-	-	0,01	0,01	0,00	0,00	0,00
Total	99,72	99,30	99,07	99,24	98,53	98,53	100,64	100,73	99,23	99,84	99,52
Structural formula based on 8 oxygen atoms											
Site T											
Si	2,98	2,99	2,95	2,99	2,99	2,98	2,99	2,98	2,99	2,98	2,96
Al(IV)	1,00	1,00	1,00	0,99	1,00	1,01	1,02	1,01	1,02	1,00	1,04
Site M-I											
Na	0,02	0,01	0,05	0,02	0,02	0,04	0,94	0,93	0,96	0,97	0,92
K	1,05	1,01	0,98	1,04	1,04	1,01	0,00	0,01	0,01	0,01	0,01
F	0,00	0,00	0,06	-	-	-	0,00	0,02	0,00	0,00	0,00
Cl	0,00	0,00	0,00	-	-	-	0,00	0,00	0,00	0,00	0,00

Table 5.2 - EPMA results of white mica of transitional vein, greisen-type alteration and phyllic alteration.

	GEM-3 Musc. GEM	BD-83-42 Muscovite Transitional vein	BD-83-45 Muscovite Transitional vein	D-43 Muscovite Phyllic alt.	D-45 Muscovite Phyllic alt.	D-56 Muscovite Phyllic alt.	D-61 Muscovite Phyllic alt.	D-72 Muscovite Phyllic alt.
SiO ₂	52,76	50,42	48,7497	49,33	51,51	51,81	51,04	51,65
Al ₂ O ₃	26,87	25,17	25,5536	28,15	28,87	28,74	27,66	28,73
TiO ₂	0,07	0,27	0,225	0,10	0,07	0,09	0,14	0,11
FeO	2,75	4,46	5,8151	2,82	2,74	2,66	3,32	3,49
MnO	0,00	0,00	0,013	0,00	0,00	0,00	0,01	0,02
MgO	3,06	2,87	2,4796	2,16	2,20	2,25	2,33	2,15
CaO	0,06	0,00	0,0018	0,07	0,01	0,00	0,07	0,06
Na ₂ O	0,03	0,11	0,0884	0,07	0,05	0,04	0,16	0,07
K ₂ O	9,03	11,27	11,8707	9,47	8,67	9,01	8,76	9,80
Cr ₂ O ₃	0,03	0,00	0,0083	0,09	0,06	0,03	0,06	0,00
NiO	0,00	0,0055	0,0056	0,00	0,00	0,00	0,01	0,04
F	0,94	-	-	0,90	1,01	1,47	0,87	0,83
Cl	0,00	-	-	0,01	0,00	0,01	0,01	0,01
Total	95,61	94,58	94,81	93,17	95,20	96,10	94,43	96,97
Structural formula based on 22 oxygen atoms*								
Site T								
Si	6,87	6,89	6,73	6,65	6,72	6,68	6,76	6,71
Al(IV)	1,13	1,11	1,27	1,35	1,28	1,32	1,24	1,29
Site M-I								
Al(VI)	3,00	2,94	2,89	3,12	3,16	3,05	3,08	3,10
Ti	0,03	0,11	0,09	0,04	0,03	0,03	0,05	0,04
Fe	0,30	0,51	0,67	0,32	0,30	0,29	0,37	0,38
Mn	0,00	0,00	0,00	0,00	0,00	0,00	0,00	0,00
Mg	0,59	0,58	0,51	0,43	0,43	0,43	0,46	0,42
Site M-II								
Ca	0,00	0,00	0,00	0,00	0,00	0,00	0,00	0,00
Na	0,01	0,03	0,02	0,02	0,01	0,01	0,04	0,02
K	1,50	1,96	2,09	1,63	1,44	1,48	1,48	1,62
F	0,39	0,00	0,00	0,38	0,42	0,60	0,36	0,34
Cl	0,00	0,00	0,00	0,00	0,00	0,00	0,00	0,00

*Due to the impossibility of H₂O analysis by the EPMA, the calculus was based on 22 oxygen atoms

Table 5.3A - Chlorite analysis related to red granite alteration and phyllic alteration (Part A).

	A-1 Clinochlore Red granite	A-2 Clinochlore Red granite	A-4 Clinochlore Red granite	A-5 Clinochlore Red granite	A-6 Clinochlore Red granite	A-7 Clinochlore Red granite
SiO ₂	27,76	36,64	37,38	29,88	27,40	27,68
Al ₂ O ₃	18,69	16,47	13,96	17,55	17,80	17,68
TiO ₂	0,11	6,58	8,46	1,16	0,02	0,01
FeO	24,48	19,49	17,66	22,67	24,15	24,12
MnO	0,63	0,25	0,38	0,16	0,75	0,80
MgO	17,09	14,39	15,55	17,18	18,28	16,99
CaO	0,01	0,06	0,03	0,00	0,05	0,08
Na ₂ O	0,06	0,47	0,83	0,16	0,05	0,00
K ₂ O	0,01	0,09	0,12	0,05	0,01	0,02
Cr ₂ O ₃	0,04	0,03	0,02	0,02	0,02	0,03
NiO	0,01	0,03	0,02	0,03	0,03	0,04
F	0,69	2,00	3,97	0,83	0,45	0,61
Cl	0,00	0,01	0,00	0,01	0,00	0,01
Total	89,57	96,51	98,38	89,69	89,03	88,05
Structural formula based on 28 oxygen atoms*						
Site T						
Si	5,65	6,53	6,38	5,97	5,64	5,75
Al(IV)	2,35	1,47	1,62	2,03	2,36	2,25
Site M-I						
Al(VI)	2,14	1,99	1,19	2,11	1,96	2,08
Ti	0,07	3,53	4,35	0,70	0,01	0,01
Fe	4,17	2,90	2,52	3,79	4,16	4,19
Mn	0,00	0,00	0,00	0,00	0,00	0,00
Mg	5,19	3,82	3,96	5,12	5,61	5,26
Ca	0,00	0,00	0,00	0,00	0,00	0,00
Na	0,02	0,16	0,28	0,06	0,02	0,00
K	0,00	0,02	0,03	0,01	0,00	0,00
F	0,44	1,12	2,14	0,52	0,29	0,40
Cl	0,00	0,00	0,00	0,00	0,00	0,00

*Due to the impossibility of H₂O analysis by the EPMA, the calculus was based on 28 oxygen atoms

Table 5.3B - Chlorite analysis related to red granite alteration and phyllic alteration (Part B).

	A-25 Clinochlore Red granite	A-28 Clinochlore Red granite	A-29 Clinochlore Red granite	A-30 Clinochlore Red granite	A-33 Chamosite Red granite	A-59 Clinochlore Phyllic alt.
SiO ₂	26,55	27,14	46,63	40,28	30,19	44,60
Al ₂ O ₃	18,74	18,40	12,78	13,95	12,36	26,38
TiO ₂	0,00	0,16	0,02	0,05	0,03	8,06
FeO	27,11	26,43	22,31	19,52	34,44	2,94
MnO	1,14	1,05	0,05	0,38	0,32	0,01
MgO	15,61	16,11	10,60	14,46	10,14	2,37
CaO	0,01	0,02	0,25	0,11	0,56	0,10
Na ₂ O	0,03	0,02	0,33	0,20	0,26	13,88
K ₂ O	0,01	0,01	0,02	0,91	0,23	0,07
Cr ₂ O ₃	0,01	0,01	0,03	0,02	0,04	0,12
NiO	0,04	0,00	0,03	0,04	0,03	0,00
F	0,36	0,45	0,15	0,39	0,10	1,06
Cl	0,00	0,01	0,00	0,00	0,02	0,00
Total	89,61	89,81	93,18	90,29	88,73	99,59
Structural formula based on 28 oxygen atoms*						
Site T						
Si	5,53	5,61	8,62	7,74	6,61	7,31
Al(IV)	2,47	2,39	0,00	0,26	1,39	0,69
Site M-I						
Al(VI)	2,13	2,09	2,78	2,90	1,80	4,40
Ti	0,00	0,10	0,01	0,03	0,02	3,97
Fe	4,72	4,57	3,45	3,14	6,31	0,40
Mn	0,00	0,00	0,00	0,00	0,00	0,00
Mg	4,85	4,96	2,92	4,14	3,31	0,58
Ca	0,00	0,00	0,00	0,00	0,00	0,00
Na	0,01	0,01	0,12	0,08	0,11	4,41
K	0,00	0,00	0,00	0,22	0,07	0,01
F	0,24	0,29	0,09	0,23	0,07	0,55
Cl	0,00	0,00	0,00	0,00	0,00	0,00

*Due to the impossibility of H₂O analysis by the EPMA, the calculus was based on 28 oxygen atoms

Table 5.4 - EPMA analysis and calculated structural formula for biotite crystals (GEM facies).

	A-18 Biotite Red granite	A-19 Biotite Red granite
SiO ₂	40,35	39,70
Al ₂ O ₃	12,44	12,84
TiO ₂	0,67	0,70
FeO	14,92	15,82
MnO	0,36	0,39
MgO	16,69	15,82
CaO	0,04	0,02
Na ₂ O	0,04	0,07
K ₂ O	10,29	9,79
Cr ₂ O ₃	0,02	0,01
NiO	0,04	0,02
F	4,12	4,30
Cl	0,00	0,00
Total	100,00	99,47
Structural formula based on 22 oxygen atoms*		
Site T		
Si	5,51	5,45
Al(IV)	2,00	2,08
Site M-I		
Al(VI)	0,00	0,00
Ti	0,28	0,29
Fe ³⁺	1,70	1,71
Site M-II		
Fe ²⁺	0,00	0,11
Mn	0,00	0,00
Mg	3,40	3,24
Ca	0,00	0,00
Na	0,01	0,02
K	1,79	1,71
F	1,78	1,87
Cl	0,00	0,00

*Due to the impossibility of H₂O analysis by the EPMA, the calculus was based on 22 oxygen atoms

Table 5.5 - EPMA ankerite analysis related to the red granite alteration.

	A-12	A-13	A-14	A-15	A-16	A-17	A-24	A-26	A-32	A-34	A-38	A-39	A-40
	Ankerite Red granite	Ankerite Red granite	Ankerite Red granite	Ankerite Red granite	Ankerite Red granite	Ankerite Red granite	Ankerite Red granite	Ankerite Red granite	Ankerite Red granite	Ankerite Red granite	Ankerite Red granite	Ankerite Red granite	Ankerite Red granite
SiO2	0,09	0,08	0,10	0,06	0,19	0,07	0,12	1,08	0,27	0,46	0,11	0,13	0,08
Al2O3	0,01	0,00	0,01	0,00	0,07	0,00	0,01	0,65	0,15	0,22	0,01	0,01	0,00
TiO2	0,00	0,00	0,04	0,00	0,02	0,00	0,01	0,01	0,03	0,04	0,00	0,04	0,00
FeO	11,55	9,77	10,11	14,46	13,81	13,38	10,24	12,65	12,15	12,40	11,96	10,33	11,18
MnO	1,14	9,77	1,12	0,74	0,78	0,46	0,49	0,59	0,74	0,87	0,99	0,93	0,65
MgO	13,91	9,77	14,13	12,57	12,50	13,61	15,12	13,95	12,96	12,88	12,92	13,70	12,97
CaO	29,82	9,77	30,21	27,86	28,38	29,04	28,68	26,99	29,38	28,96	30,22	29,87	29,98
Na2O	0,02	9,77	0,02	0,02	0,01	0,00	0,00	0,02	0,02	0,02	0,00	0,00	0,01
K2O	0,00	9,77	0,00	0,01	0,03	0,01	0,02	0,04	0,00	0,04	0,04	0,03	0,00
Cr2O3	0,00	9,77	0,01	0,02	0,00	0,00	0,00	0,02	0,01	0,03	0,02	0,02	0,00
NiO	0,00	9,77	0,00	0,00	0,00	0,00	0,03	0,01	0,01	0,00	0,01	0,00	0,00
F	0,15	9,77	0,00	0,00	0,00	0,00	0,00	0,00	0,00	0,00	0,15	0,07	0,00
Cl	0,00	9,77	0,01	0,00	0,00	0,01	0,00	0,00	0,00	0,00	0,04	0,04	0,00
Total	56,69	9,77	55,77	55,74	55,80	56,58	54,71	56,00	55,73	55,92	56,46	55,17	54,87
Structural formula based on 6 oxygen atoms													
Fe	0,30	0,26	0,27	0,39	0,37	0,35	0,27	0,33	0,33	0,33	0,32	0,28	0,30
Mg	0,65	0,66	0,67	0,61	0,60	0,64	0,72	0,65	0,62	0,61	0,61	0,65	0,63
Mn	0,03	0,03	0,03	0,02	0,02	0,01	0,01	0,02	0,02	0,02	0,03	0,03	0,02
Ca	1,00	1,04	1,03	0,97	0,98	0,99	0,98	0,90	1,01	0,99	1,02	1,03	1,04
Na	0,00	0,00	0,00	0,00	0,00	0,00	0,00	0,00	0,00	0,00	0,00	0,00	0,00
K	0,00	0,00	0,00	0,00	0,00	0,00	0,00	0,00	0,00	0,00	0,00	0,00	0,00
Total	1,98	1,99	1,99	2,00	1,98	2,00	1,99	1,90	1,97	1,96	1,98	1,98	2,00
F	0,04	0,01	0,00	0,00	0,00	0,00	0,00	0,00	0,00	0,00	0,01	0,01	0,00

Table 5.6 - EPMA ankerite analysis associated with the phyllic alteration.

	D-42 Ankerite Phyllic alt.	D-54 Ankerite Phyllic alt.	D-62 Ankerite Phyllic alt.	D-63 Ankerite Phyllic alt.	D-68 Ankerite Phyllic alt.	D-70 Ankerite Phyllic alt.	D-47 Ankerite Phyllic alt.
SiO2	0,11	0,08	1,44	2,22	0,18	2,51	0,22
Al2O3	0,00	0,01	1,06	1,81	0,04	2,06	0,03
TiO2	0,44	0,01	0,01	0,06	0,01	0,02	0,00
FeO	12,98	9,79	12,75	11,80	12,87	11,92	47,36
MnO	1,06	1,09	0,12	0,09	0,67	0,08	0,28
MgO	12,43	14,60	14,61	14,87	13,36	15,15	13,34
CaO	29,80	30,21	28,09	26,54	29,36	27,35	0,37
Na2O	0,00	0,00	0,00	0,04	0,00	0,01	0,00
K2O	0,00	0,00	0,03	0,03	0,04	0,06	0,04
Cr2O3	0,02	0,00	0,04	0,00	0,01	0,01	0,02
NiO	0,00	0,01	0,00	0,01	0,01	0,02	0,02
F	0,00	0,23	0,00	0,00	0,04	0,00	0,00
Cl	0,06	0,00	0,07	0,00	0,00	0,00	0,00
Total	56,90	56,04	58,22	57,47	56,58	59,19	61,68
Structural formula based on 6 oxygen atoms							
Fe	0,34	0,26	0,32	0,29	0,34	0,28	1,31
Mg	0,59	0,68	0,65	0,65	0,63	0,64	0,66
Mn	0,03	0,03	0,00	0,00	0,02	0,00	0,01
Ca	1,01	1,01	0,89	0,83	0,99	0,83	0,01
Na	0,00	0,00	0,00	0,00	0,00	0,00	0,00
K	0,00	0,00	0,00	0,00	0,00	0,00	0,00
Total	1,97	1,97	1,86	1,78	1,98	1,76	1,98
F	0,00	0,02	0,00	0,00	0,00	0,00	0,00

Table 5.7 - EPMA calcite analysis related to the red granite and to the phyllic alterations.

	A-09 Calcite Red granite	A-10 Calcite Red granite	A-11 Calcite Red granite	A-27 Calcite Red granite	A-67 Calcite Red granite	A-50 Calcite Phyllic alt.
SiO2	0,41	0,29	0,42	0,37	0,36	0,26
Al2O3	0,00	0,02	0,00	0,03	0,00	0,00
TiO2	0,00	0,00	0,00	0,00	0,00	0,00
FeO	0,12	0,06	0,06	0,49	0,09	0,04
MnO	0,03	0,04	0,00	0,01	0,02	0,03
MgO	0,00	0,00	0,00	0,00	0,00	0,00
CaO	54,01	53,54	52,93	53,97	53,17	53,86
Na2O	0,17	0,11	0,22	0,24	0,21	0,07
K2O	0,00	0,00	0,00	0,02	0,01	0,00
Cr2O3	0,01	0,00	0,04	0,02	0,02	0,01
NiO	0,00	0,00	0,02	0,00	0,00	0,00
F	5,27	7,00	6,70	7,04	7,64	7,05
Cl	0,00	0,00	0,00	0,00	0,00	0,00
Total	60,02	61,06	60,39	62,18	61,52	61,32
Structural formula based on 6 oxygen atoms						
Fe	0,00	0,00	0,00	0,01	0,00	0,00
Mg	0,00	0,00	0,00	0,00	0,00	0,00
Mn	0,00	0,00	0,00	0,00	0,00	0,00
Ca	1,53	1,43	1,44	1,42	1,39	1,43
Na	0,01	0,01	0,01	0,01	0,01	0,00
K	0,00	0,00	0,00	0,00	0,00	0,00
Total	1,54	1,44	1,45	1,44	1,40	1,44
F	0,44	0,55	0,54	0,55	0,59	0,55

Table 5.8 - EPMA siderite analysis related to the red granite and phyllic alterations.

	D-35 Siderite Phyllic alt.	D-36 Siderite Phyllic alt.	D-44 Siderite Phyllic alt.	D-46 Siderite Phyllic alt.	D-48 Siderite Phyllic alt.	D-55 Siderite Phyllic alt.	D-57 Siderite Phyllic alt.	D-60 Siderite Phyllic alt.	D-65 Siderite Phyllic alt.	D-66 Siderite Phyllic alt.	D-69 Siderite Phyllic alt.
SiO2	0,30	0,27	0,24	0,13	0,14	0,12	1,28	0,11	0,13	0,10	0,27
Al2O3	0,06	0,07	2,59	0,04	0,05	0,02	0,56	0,00	0,11	0,01	0,00
TiO2	0,17	0,00	0,08	0,09	0,18	0,04	0,04	0,08	0,04	0,18	0,01
FeO	52,35	51,44	42,60	50,37	46,72	47,06	46,79	45,58	48,55	46,59	46,13
MnO	0,90	0,70	0,19	0,26	0,30	0,41	0,32	0,26	0,33	0,29	0,32
MgO	9,55	9,51	18,66	11,23	14,14	14,00	12,80	14,42	12,81	14,06	14,27
CaO	1,18	1,09	0,32	0,24	0,34	0,58	0,35	0,26	0,50	0,24	0,38
Na2O	0,05	0,03	0,01	0,02	0,01	0,01	0,04	0,02	0,01	0,00	0,00
K2O	0,00	0,00	0,49	0,01	0,04	0,01	0,28	0,04	0,03	0,01	0,02
Cr2O3	0,00	0,00	0,00	0,02	0,00	0,00	0,00	0,01	0,03	0,02	0,01
NiO	0,01	0,00	0,03	0,05	0,03	0,03	0,07	0,07	0,03	0,07	0,01
F	0,04	0,42	0,02	0,05	0,00	0,04	0,00	0,02	0,00	0,09	0,00
Cl	0,33	0,12	0,00	0,01	0,00	0,01	0,01	0,00	0,00	0,02	0,00
Total	64,93	63,65	65,21	62,52	61,94	62,32	62,54	60,88	62,59	61,69	61,42
Structural formula based on 6 oxygen atoms											
Fe	1,43	1,41	1,02	1,40	1,27	1,28	1,25	1,26	1,33	1,27	1,26
Mg	0,47	0,47	0,80	0,56	0,69	0,68	0,61	0,71	0,63	0,68	0,70
Mn	0,03	0,02	0,00	0,01	0,01	0,01	0,01	0,01	0,01	0,01	0,01
Ca	0,04	0,04	0,01	0,01	0,01	0,02	0,01	0,01	0,02	0,01	0,01
Na	0,00	0,00	0,00	0,00	0,00	0,00	0,00	0,00	0,00	0,00	0,00
K	0,00	0,00	0,02	0,00	0,00	0,00	0,01	0,00	0,00	0,00	0,00
Total	1,97	1,94	1,86	1,98	1,98	1,99	1,89	1,99	1,98	1,97	1,98
F	0,00	0,04	0,00	0,01	0,00	0,00	0,00	0,00	0,00	0,01	0,00

5.6 BULK-ROCK GEOCHEMISTRY AND MOBILIZATION OF ELEMENTS

In order to estimate the chemical changes associated with the main alteration assemblages (greisen and phyllic alterations), the major elements (Si, Al, Fe, Mg, Ca, Na, K and P), light-lithophile elements (LILEs; e.g., Cs, Rb, Sr, Ba, Pb and U, and trans-transition elements (TRTEs; e.g., Sc, V, Cr, Co, Ni, Cu, Zn and Bi) were analysed in representative samples of altered rocks and their equivalent, least altered "protolith" (red granite). The method of MacLean's (1990) was applied to calculate the mass balance between altered rocks and their protoliths. In this study, Al₂O₃ was chosen as the most immobile reference element the calculations. Element gains and losses on a weight basis were calculated with Al₂O₃ as immobile element, and following the equations: Change = A – F; EF = M_{precursor}/M_{altered}; RC = EF*component (A) wt% or ppm; MC = RC – precursor; MC = (MC*/F)*100, where A=altered rock element mass; F=fresh rock element mass; EF=enrichment factor; M=immobile element mass; RC= reconstituted composition; MC=mass change. Bulk rock analysis and mass balance calculations results are presented, respectively in Tables 5.9 and 5.10.

Table 5.9 - Major oxides (wt.%) and trace elements (ppm) for the Passa Três granite and altered samples.

Rock type	Red granite (least altered granite)	Greisen-type alteration		Phyllic-type alteration		Iron Oxides alteration	BD-GEM-Mafic
		355/17C	355/17F	355/17B	355/17D		
Sample	355/17A	355/17C	355/17F	355/17B	355/17D	355/17E	355/17H
SiO ₂	66,47	68,48	70,48	66,64	66,73	67,59	60,43
TiO ₂	0,61	0,54	0,49	0,63	0,57	0,59	0,84
Al ₂ O ₃	14,28	14,19	14,54	14,50	14,50	14,29	14,54
Fe ₂ O ₃	2,51	2,63	1,51	2,67	2,44	2,30	4,40
MnO	0,04	0,04	0,01	0,02	0,02	0,03	0,05
MgO	1,11	1,53	0,62	1,23	1,02	0,83	2,45
CaO	1,63	1,07	0,48	1,52	1,50	1,49	2,93
Na ₂ O	3,58	1,57	0,16	3,24	3,38	3,37	2,87
K ₂ O	6,64	7,05	9,76	6,56	6,43	6,71	6,09
P ₂ O ₅	0,31	0,29	0,23	0,33	0,32	0,31	0,59
Cr ₂ O ₃	0,00	0,00	0,00	0,00	0,00	0,00	0,01
NiO	0,00	0,00	0,00	0,00	0,00	0,00	0,01
LOI	2,00	2,53	1,63	2,33	2,96	2,48	4,54
TOTAL	99,17	99,92	99,90	99,68	99,87	100,00	99,75
Nb	12	11	9	12	11	11	11
Zr	304	270	325	317	277	304	338
Y	8	7	3	9	8	8	16
Sr	856	496	531	949	817	891	1091
U	8	11	7	8	7	7	8
Rb	159	191	238	151	145	155	133
Th	21	17	17	20	19	20	17
Pb	37	17	14	31	35	22	18
Ga	21	21	23	20	20	20	20

Zn	55	54	12	59	39	40	79
Cu	4	52	1022	3	4	11	5
Ni	13	11	10	13	13	10	34
Co	112	72	142	87	113	69	87
Cr	10	10	3	10	9	9	50
V	25	25	18	26	22	24	46
Ce	125	109	90	133	114	107	192
Nd	44	37	28	47	42	37	76
Ba	2820	2757	3511	2727	2687	2782	3407
La	82	67	59	84	64	75	114
Sc	3	3	<LLD	3	2	2	7
Mn	270	266	72	183	196	217	377
Ge	<LLD	<LLD	2	<LLD	<LLD	<LLD	<LLD
As	<LLD	<LLD	<LLD	<LLD	<LLD	<LLD	<LLD
Se	<LLD	<LLD	<LLD	<LLD	<LLD	<LLD	<LLD
Br	<LLD	<LLD	<LLD	<LLD	<LLD	<LLD	<LLD
Mo	<LLD	<LLD	5	<LLD	<LLD	<LLD	<LLD
Ag	<LLD	<LLD	<LLD	<LLD	<LLD	<LLD	<LLD
Cd	<LLD	<LLD	<LLD	<LLD	<LLD	<LLD	<LLD
Sn	6	4	5	4	5	4	5
Sb	<LLD	<LLD	<LLD	<LLD	<LLD	3	<LLD
Te	<LLD	<LLD	<LLD	<LLD	<LLD	<LLD	<LLD
I	<LLD	<LLD	<LLD	<LLD	<LLD	<LLD	<LLD
Cs	<LLD	3	<LLD	<LLD	<LLD	<LLD	<LLD
Sm	7	4	8	8	9	8	12
Yb	<LLD	<LLD	2	<LLD	3	<LLD	<LLD
Hf	<LLD	<LLD	<LLD	3	4	<LLD	<LLD
Ta	<LLD	<LLD	<LLD	<LLD	<LLD	<LLD	<LLD
W	506	406	712	443	533	362	389
Hg	<LLD	<LLD	<LLD	<LLD	<LLD	<LLD	<LLD
Tl	<LLD	<LLD	<LLD	<LLD	<LLD	<LLD	<LLD
Bi	<LLD	<LLD	<LLD	<LLD	<LLD	<LLD	<LLD

Table 5.10 - Calculated gains and losses for the different alteration zones.

	Greisen alteration	Phyllic alteration
SiO2	3,88	-0,01
TiO2	-15,92	0,09
Fe2O3	-18,05	0,04
MnO	-38,10	0,76
MgO	-3,51	0,12
CaO	-52,52	0,11
Na2O	-76,01	0,08
K2O	25,70	0,05
P2O5	-17,80	-0,03
Nb	-23,24	0,20
Zr	-2,57	0,13
Y	-41,11	0,09
Sr	-40,40	0,07
U	6,05	0,31
Rb	33,86	0,14
Th	-20,11	0,12

Pb	-59,39	0,08
Ga	4,42	0,02
Zn	-40,43	0,44
Cu	15149,29	-0,30
Ni	-19,82	0,07
Co	-5,27	-0,01
Cr	-34,23	0,13
V	-13,75	0,18
Ce	-20,93	0,13
Nd	-26,60	0,05
Ba	10,44	0,07
La	-23,68	0,33
Sc	-100,00	0,58
Mn	-37,86	0,41
Sn	-18,61	0,28
Sm	-17,90	-0,37
W	9,88	-0,08

5.6.1 Greisen-type alteration

Representative greisen alteration assemblages were analysed, with the Passa Três granite as their precursor (red granite). Loss and gain calculations for greisen-type alteration are presented in Table 5.9 and Figure 5.15a. Muscovitisation is characterised by strong gains of K₂O and LOI and loss of Na₂O and CaO, due to replacement of plagioclase by sericite. As expected, the breakdown of biotite and chlorite led to depletion of Fe₂O₃. In the muscovitisation zone, K₂O and Rb shows gain due to the recrystallisation of K-feldspar and Cu shows gain due to the crystallisation of chalcopyrite. Sr was lost due to the consumption of igneous plagioclase, whereas Ba shows a weak gain, which may be related to the recrystallisation of K-feldspar during muscovite alteration. U and Ga display slight gain. TiO₂ and P₂O₅ show loss, probably related to the consumption of titanite and apatite, respectively. Leaching of Nb is also observed, as it is contained in titanium minerals (e.g. titanite and ilmenite). Ga displays lower mobility, as the ionic radii of Al and Ga are very similar that most of the Ga is present in Al-bearing minerals, and Ga maintains similar immobility with Al. Slight gain was observed for W, and slight losses were also observed for MnO, Y, Pb, Zn, Ni, Cr, Nd, La, Sc.

5.6.2 Phyllic-type alteration

Representative phyllic alteration assemblages were analysed, with the Passa Três granite as their precursor (red granite). Loss and gain calculations for phyllic-type alteration are presented in Table 5.10 and Figure 5.15b. Losses of CaO and Na₂O indicate the consumption of plagioclase, and formation of sericite. Weak K₂O loss suggest that K-feldspar

was also altered, but sericite was crystallised. TiO₂ is related to the consumption of titanite, but some was kept in crystallisation of rutile. Despite the alteration of the chlorite crystals (clinochlore and chamosite), Fe₂O₃ and MgO were stable due to the crystallisation of siderite and ankerite. MnO loss probably is related to the alteration of magnetite, although Fe₂O₃ was immobile due to crystallisation of siderite. Small gain of Cu shows that some chalcopyrite has been crystallized, as also observed in the petrography.

Leaching of Nb is also observed, as it is contained in titanium minerals (e.g. titanite and ilmenite); U and Zr display slight loss, probably due to the consumption of zircon crystals. Yttrium, Sr, Cu and Sm display slight gain, and slight losses are shown by Rb, Th, Pb, Ga, Zn, Ni, Co, Cr, V, Ce, Ba, La, Sc, Mn, Sn, W.

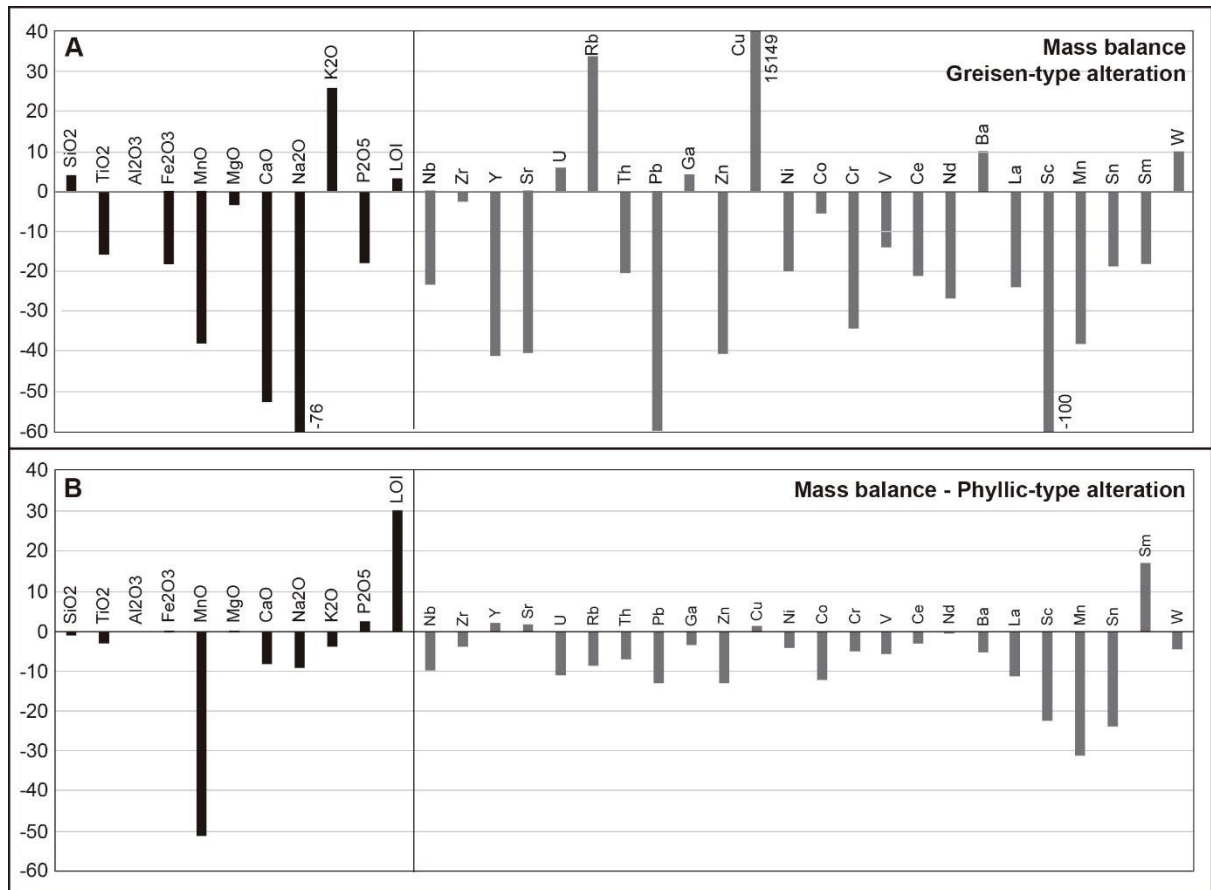


Figure 5.15 - Diagrams for mass balance calculations for greisen-type and phyllic-type alteration. Values that are greater than diagram boundaries are indicated next to the element.

5.6.3 Summary

The presence of mineralised bodies with very thin alteration margins indicates small scale and weak fluid-rock interaction. Nevertheless, even if mineralisation process may provoke the formations of alteration zones, gold precipitation was not observed in the alteration

halos, being concentration in the quartz veins. As shown in the previous section, some element concentrations are affected by mineral replacement reactions, mainly the greisen-type alteration, nevertheless, alteration zones may be used as a guide for localising the orebodies given its spatial relation with them.

5.7 SULPHUR ISOTOPES DATA

In order to verify the origin of gold, sulphur isotope ($\delta^{34}\text{S}$) was analysed in five samples of pyrite and one of barite (Table 5.11 and Figure 5.16). Samples were sent to Actlab Laboratory, in Canada. Pyrite crystals present $\delta^{34}\text{S}$ values between -0.1‰ and 1.1‰. These values are consistent with a magmatic origin for the sulphur minerals, and possibly with mantle contribution, indicating a very deep source. These results are coherent with chemical data already existent for the Passa Três Granite and interpreted as a mantle origin for the magma. On the other hand, the barite sample present a $\delta^{34}\text{S}$ value of 15.6. This range of value is associated to metamorphic and/or sedimentary rocks and could indicate a contamination by the country rocks (phyllites and marbles, in this case).

Table 5.11 - Sulphur isotopic data of sulphides from different pyrite and one of barityne crystals of Passa Três gold mineralisation.

Sample no.	Mineral	$\delta^{34}\text{S}$ /‰
BD-19a	Pyrite	0,65
BD-26a	Pyrite	0
BD-31a	Pyrite	0,7
BD-78a	Pyrite	1,1
BD-86b	Pyrite	-0,1
BD-31b	Barityne	15,6

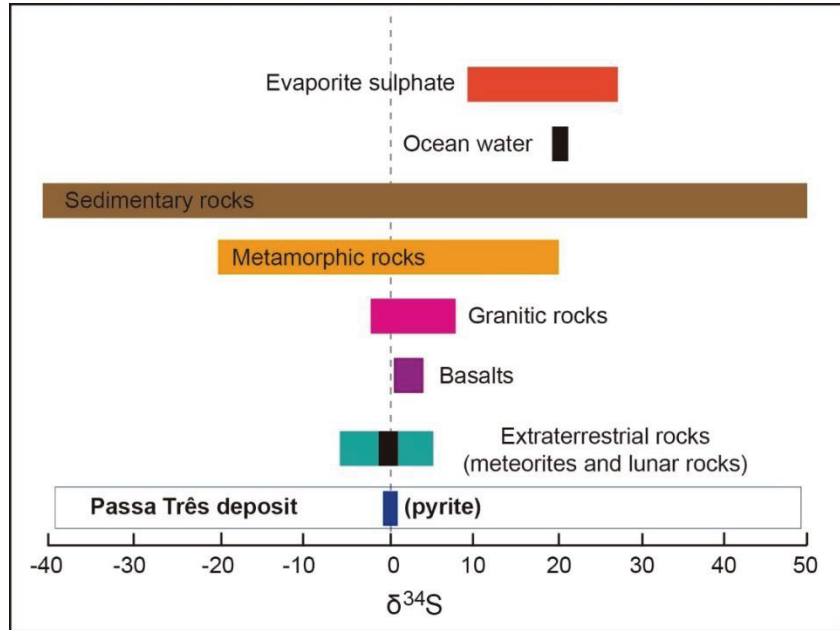


Figure 5.16 - Sulphur isotopic composition histograms of pyrite and barityne minerals from the Passa Três gold deposit.

5.8 FLUID INCLUSIONS

Quartz samples for fluid inclusions study were collected from the mineralised veins of levels 4 and 5 in the underground mine. Fluid inclusions from the host granite and aplites were also analysed. Fluid inclusions are hosted by quartz, which is the main gangue mineral in the deposit and associated with pyrite. Many of the collected samples did not contain inclusions of sufficient size and abundance to provide further study (difficulty also observed by Piekarz, 1992, and attributed to the brittle deformation of the orebodies), but still data was obtained. Unfortunately, fluid inclusions from the early hydrothermal veins (veins with K-feldspar borders) were too small to be analysed by microthermometry. Using the criteria for primary origin of Roedder (1984) all results are believed to have been obtained from primary and secondary fluid inclusions. The fluid inclusion assemblage (FIA) method (GOLDSTEIN; REYNOLDS, 1994) was applied in petrography study and microthermometry data analysis. A FIA considers that the inclusions are cogenetic, and formed at the same time and from the same fluid. Microthermometric data are summarised in Table 5.12 and Figures 5.17 to 5.21.

5.8.1 Petrography of fluid inclusions

Fluid inclusions are found on quartz and analysed samples include: red granite, aplite and mineralised veins (quartz 1 and quartz 3, see DRESSEL et al., submitted - Chapter 4). Four types of fluid inclusions are identified according to their optical characteristics at room temperature according to the criteria of Roedder (1984) and phase transitions during

microthermometric measurements (DIAMOND, 2001). They are: type I (primary origin), type II and types IIIa and IIIb. Type Ia is observed only in the granite sample; type II is observed in the granite, aplite and mineralised veins samples; and types IIIa and IIIb are observed in the mineralised veins (primary origin) and in the granite (secondary origin) (Figures 5.17 and 5.18). Fluid inclusions of type Ia are dominantly subhedral, elongate in the direction of growth, demonstrating that they are primary in origin (Figure 5.17a, b), whereas types II, IIIa and IIIb are secondary. Type Ia is two-phase with one liquid phase and a vapor phase (liquid H₂O + vapor CO₂), with sizes of 2-6 µm. Type II vary dramatically in shape, including rounded, oval, triangular and irregular, with sizes of 3-18 µm and variable vapor/liquid proportions (Figure 5.17c-f). This type represents inclusions with one vapor phase (vapor CO₂) and one (liquid H₂O) or two phases of liquid (liquid H₂O + liquid CO₂). They can be liquid-rich or vapor-rich, as vapor/liquid proportion is very variable. Type IIIa is round, occur as FIA in trails, and are bi-phase (vapor H₂O + liquid H₂O) (Figure 5.17g), while type IIIb is monophasic (liquid H₂O) and occur inside quartz 3 (Figure 5.17h), in paragenesis with gold bearing minerals (pyrite 2b, see DRESSEL et al., submitted - Chapter 4). Type IIIa present sizes of 4-9 µm and type IIIb of 4-7 µm.

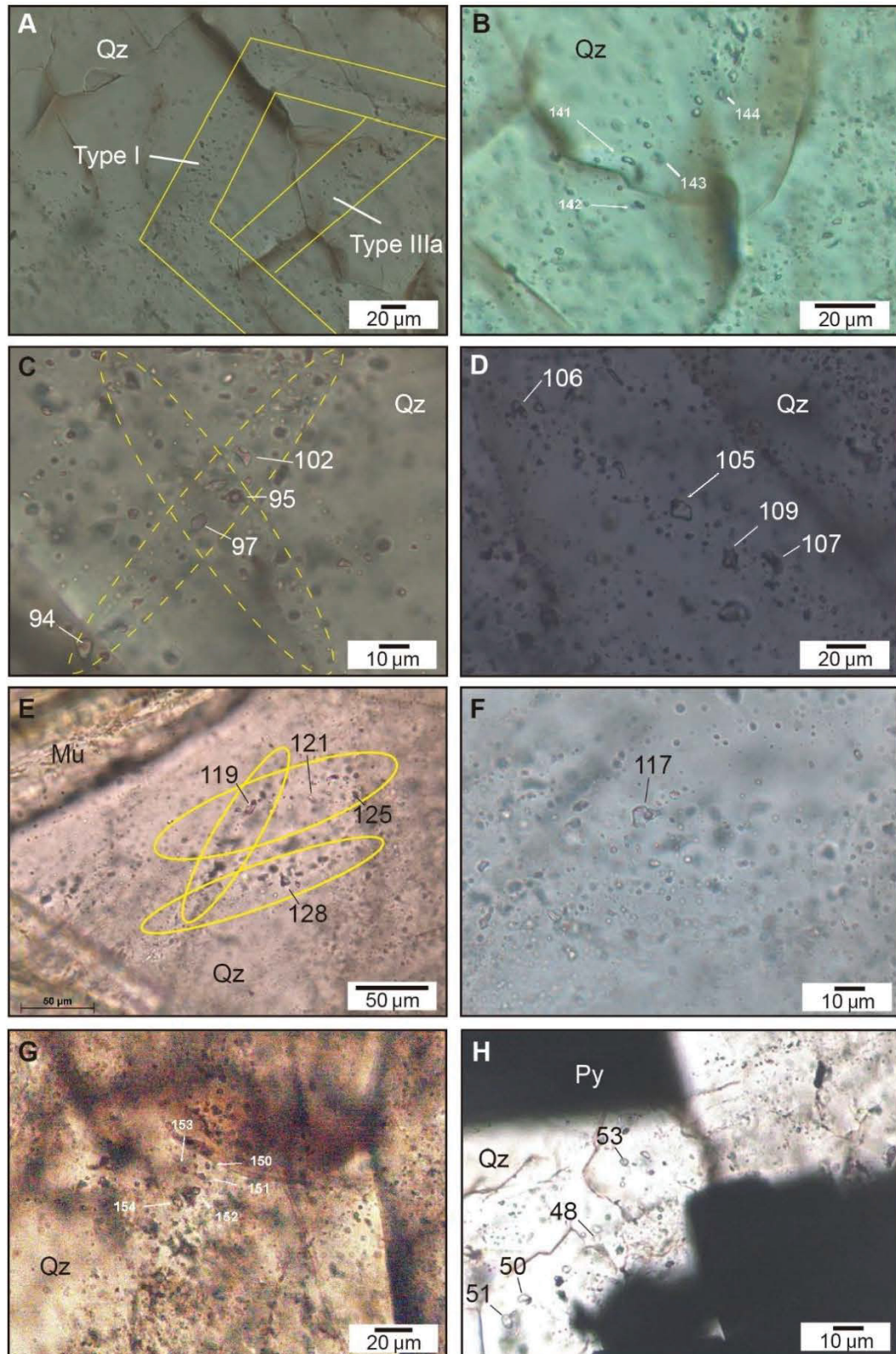


Figure 5.17 - Fluid inclusions in gold mineralisation in the Passa Três gold deposit. A) Primary H₂O-NaCl-CO₂ (type I) in growing planes in magmatic quartz and secondary H₂O-NaCl (type IIIa) as a trail, GEM facies; B) Detail of type IIIa fluid inclusions (liquid H₂O); C) Type II fluid inclusions showing different shapes and vapor/liquid rates, in granite sample; D) Type II fluid inclusions showing different shapes and vapor/liquid rates, in aplite sample; E) Type II fluid inclusions in quartz 1, mineralised vein; F) Detail of a type II fluid inclusion (liquid H₂O + vapor CO₂); G) Type IIIa fluid inclusions occurring in cluster in quartz 1, mineralised vein; H) Type IIIb fluid inclusions in quartz 3 near pyrite crystals, mineralised vein.

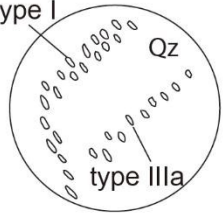
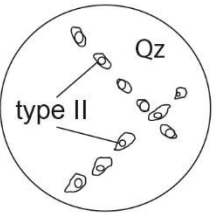
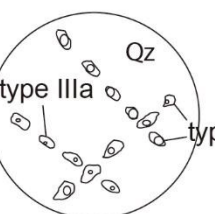
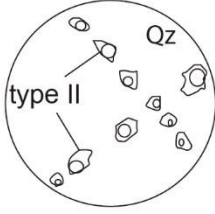
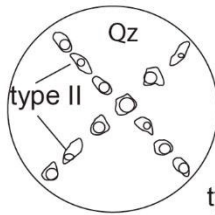
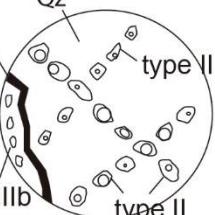
	Type I (H ₂ O-CO ₂ -NaCl) <i>Primary inclusions</i>	Type II (H ₂ O-CO ₂ -NaCl) <i>Related to Q1</i>	Type III (H ₂ O-NaCl) <i>Related to Q3</i>
GRANITE			
APLITE			
MINERALISED VEIN			

Figure 5.18 - Sketch of the different types of fluid inclusions. Primary fluid inclusions (type I) are found in magmatic quartz in the granite; type II fluid inclusions occur in the granite, in the aplites, as well as in the mineralised vein; types IIIa and IIIb are observed in the granite and in the mineralised vein.

5.8.2 Microthermometry

Some inclusions from all the identified types were selected for microthermometric study. Aqueous inclusions of type IIIa were selected for first melting (T_m), ice melting (T_{m-ice}) and total homogenisation (T_{h-tot}) temperatures testing, while aqueous-carbonic inclusions of types I and II were selected for the carbonic phase melting (T_{m-CO_2}), CO₂ clathrate melting ($T_{m-clath}$), partial homogenisation of CO₂ (T_{h-CO_2}), and final homogenisation temperatures (T_{h-tot}) determination. The microthermometric data of all types of fluid inclusions are listed in Table 5.12. Salinity and density were calculated with the CLATHRATE and FLUIDS package of Bakker (2003).

Within the CO₂-bearing fluid inclusions, the T_{m-CO_2} of type I range from -67.2 to -58.9°C, and of type II range from -72 to -56°C, which is slightly lower than the CO₂ triple point of -56.6 (FAN et al., 2003 in DENG et al., 2015). This discrepancy indicates that the carbonic phases may also include other volatiles, such as SO₂ (as indicated by Raman spectroscopy, see section 5.8.3). The $T_{m-clath}$ in the inclusions with CO₂ is between 4.5 and 14.7 °C (with an average value of 9.8 °C), below and upper the invariant point of pure CO₂ clathrate (10°C; HOLLISTER; BURRUS, 1976 in DENG et al., 2015), also indicating the probable presence of

other gases. Partial homogenisation of CO₂ liquid + CO₂ vapor to vapor CO₂, less commonly to liquid, is between 17.6 and 38.2 °C (with an average value of 30.1 °C), also suggesting the presence of other gases volatiles. Ice melting of CO₂ bearing inclusions is between -11.6 and -0.2°C (with an average value of -4.7 °C). Calculated salinities from type II vary from 0.04 to 9.77 wt.% NaCl eq. (with an average value of 2.45 wt.% NaCl eq.). Calculated densities from type II vary from 0.62 to 1.02 g/cm³ (with an average value of 0.89 g/cm³).

In the aqueous fluid inclusions, type IIIa presents ice melting ranging from -9.0 to -0.2°C and type IIIb from -6.4 to -0.7°C. The *Th*-tot of inclusions of type IIIa varies from 183 to 249°C (with an average value of 197 °C). The calculated salinities from types IIIa and IIIb varies from 0.35 to 12.84 wt.% NaCl eq. (with an average value of 4.61 wt.% NaCl eq.) and 2.4 to 9.7 wt.% NaCl eq. (with an average value of 4.88 wt.% NaCl eq.).

Diagrams showing values of *Tfm* vs. salinity (Figure 5.19a), *Th*-tot vs. salinity (Figure 5.19b), *Tfm* vs. *Th*-tot (Figure 5.19c) are presented next. The histograms of homogenisation temperatures and salinities are shown in Figure 5.20, respectively. And Figure 5.21 shows an isochore diagram. These data are discussed in sections 5.9.2 (Ore fluid composition), 5.9.3 (Sources of ore-forming fluids and materials) and 5.9.4 (Possible fluid processes).

Table 5.12 - Microthermometric results of fluid inclusions in the Passa Três gold deposit.

Sample no.	Mineral	Lithology	Type	Number	<i>Tfm</i> (oC)	<i>Tm</i> clath (oC) (average)	<i>Tm</i> -ice (oC)	<i>Th</i> -tot (oC) (average)	Salinity (wt.% NaCl eq.) (average)	Density (g/cm ³)
							(average)			(average)
GEF	Quartz	Granite	I	6	-67.2 to -61.4	4 to 16.4 (9.3)	-8.1 to -1.2 (-3.6)	431.7 to 112 (329.7)	0.04 to 10.63 (3.65)	0.74 to 0.94 (0.87)
GEF	Quartz	Granite	II	10	-67.6 to -56	4.5 to 14.7 (9.3)	-10.2 to -0.2 (-5)	150.1 to 452.8 (246.19)	0.4 to 9.77 (2.72)	0.62 to 1.02 (0.88)
BD-76d	Quartz	Aplite	II	14	-64.3 to -57.3	6.3 to 12.2 (9.4)	-11.6 to -1.6 (-6.3)	176.6 to 430 (301.1)	2.23 to 4.97 (2.64)	0.65 to 1.07 (0.93)
BD-26b	Quartz	Mineralised vein (Q1)	II	10	-62.5 to -57.3	8.4 to 15 (11.4)	-5.6 to -0.2 (-3.1)	146.8 to 430 (272.3)	0.81 to 2.74 (1.52)	0.71 to 0.92 (0.85)
BD-86a	Quartz	Mineralised vein (Q1)	IIIa	9	-31 to -22.6	-	-9 to -0.2 (-3.1)	183.4 to 249.8 (197.6)	0.35 to 12.84 (4.61)	0.81 to 1.01 (0.90)
BD-85b	Quartz	Mineralised vein (Q3)	IIIb	5	-27.5 to -24.1	-	-6.4 to -0.7 (-2.6)	-	2.4 to 9.7 (4.88)	-

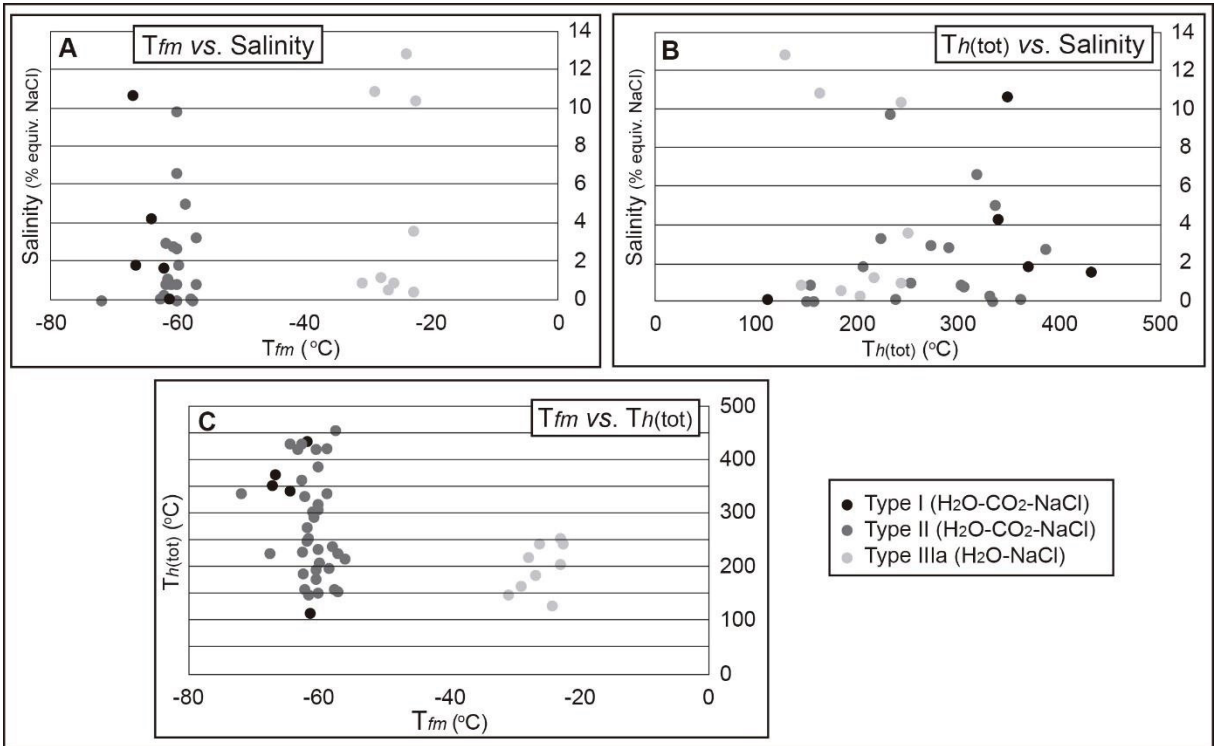


Figure 5.19 – A) Diagram with T_{fm} vs. salinity values for the fluid inclusions of the Passa Três gold deposit; B) Temperature (total homogenisation) vs. salinity plot of the fluid inclusions; C) Diagram with T_{fm} vs T_h-tot of various types of fluid inclusions of the Passa Três gold deposit. T_h (tot): total homogenisation temperature, T_{fm}: temperature of first melting, T_m ice: temperature of final ice melting.

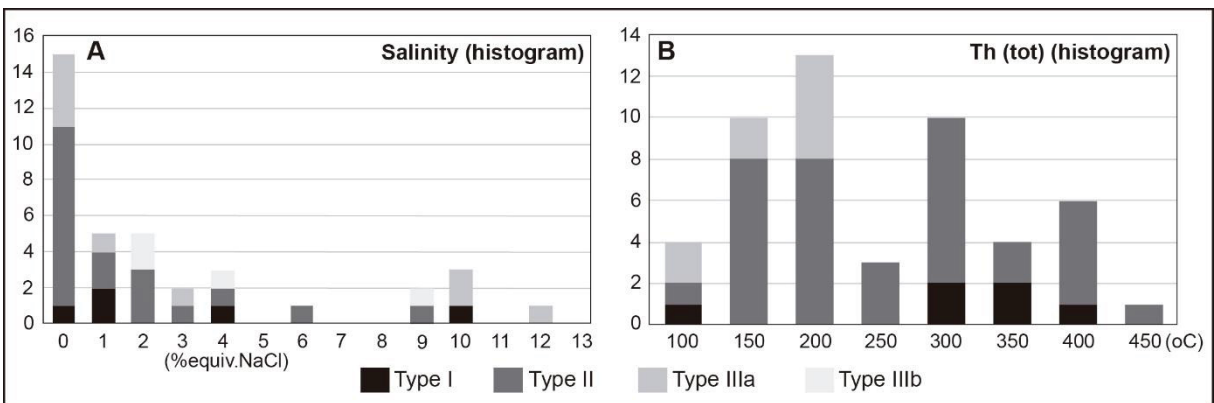


Figure 5.20 - A) Frequency histogram of salinities of the fluid inclusions types observed in the Passa Três deposit; B) Frequency histogram of total homogenisation temperatures (T_h-tot).

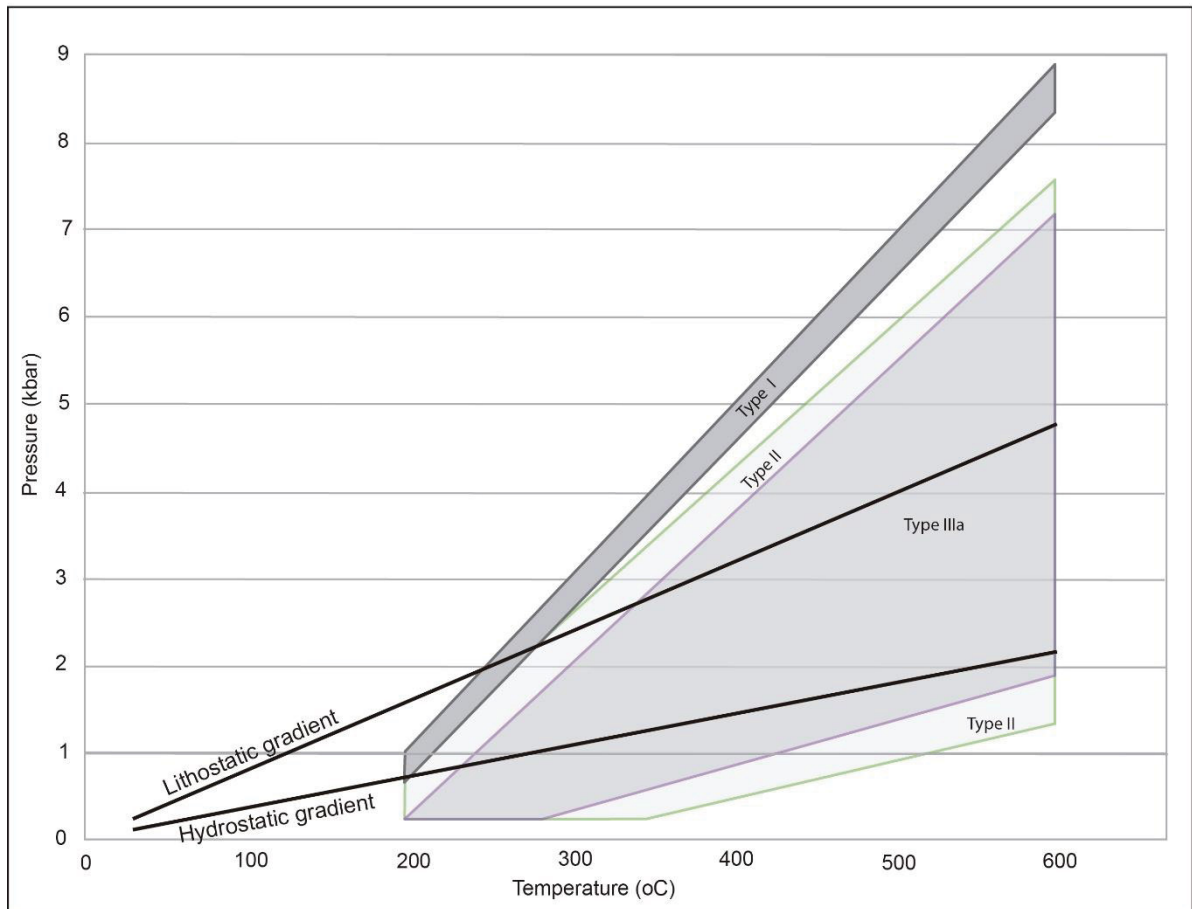


Figure 5.21 - P-T diagram based on fluid inclusion data (isochore) of the different types of fluid inclusions.

5.8.3 Laser Raman spectroscopy

The gas and liquid phases of types II and IIIa fluid inclusions were analysed by Laser Raman spectroscopy (Figure 5.22). Spectra of type II inclusions show the presence of CO_2 and SO_4 peaks, representing the main volatiles in these inclusions (Figure 5.22a-c). CO_2 peaks are observed around 1232 e 1355 cm^{-1} , and peaks for H_2O are also observed. Whereas for type IIIa fluid inclusions, peaks of SO_2 e H_2O occur, but only on the two CO_2 peaks are present (1233 cm^{-1}) (Figure 5.22d-f). No other gaseous phases were identified. These data are in coherence with microthermometric data, which indicate CO_2 first melting temperatures colder than $-56,6 \text{ }^\circ\text{C}$, triple point of pure CO_2 , suggesting the presence of other volatiles, what was confirmed by the presence of SO_2 . Unfortunately, it was not possible to analyse fluid inclusions of type I.

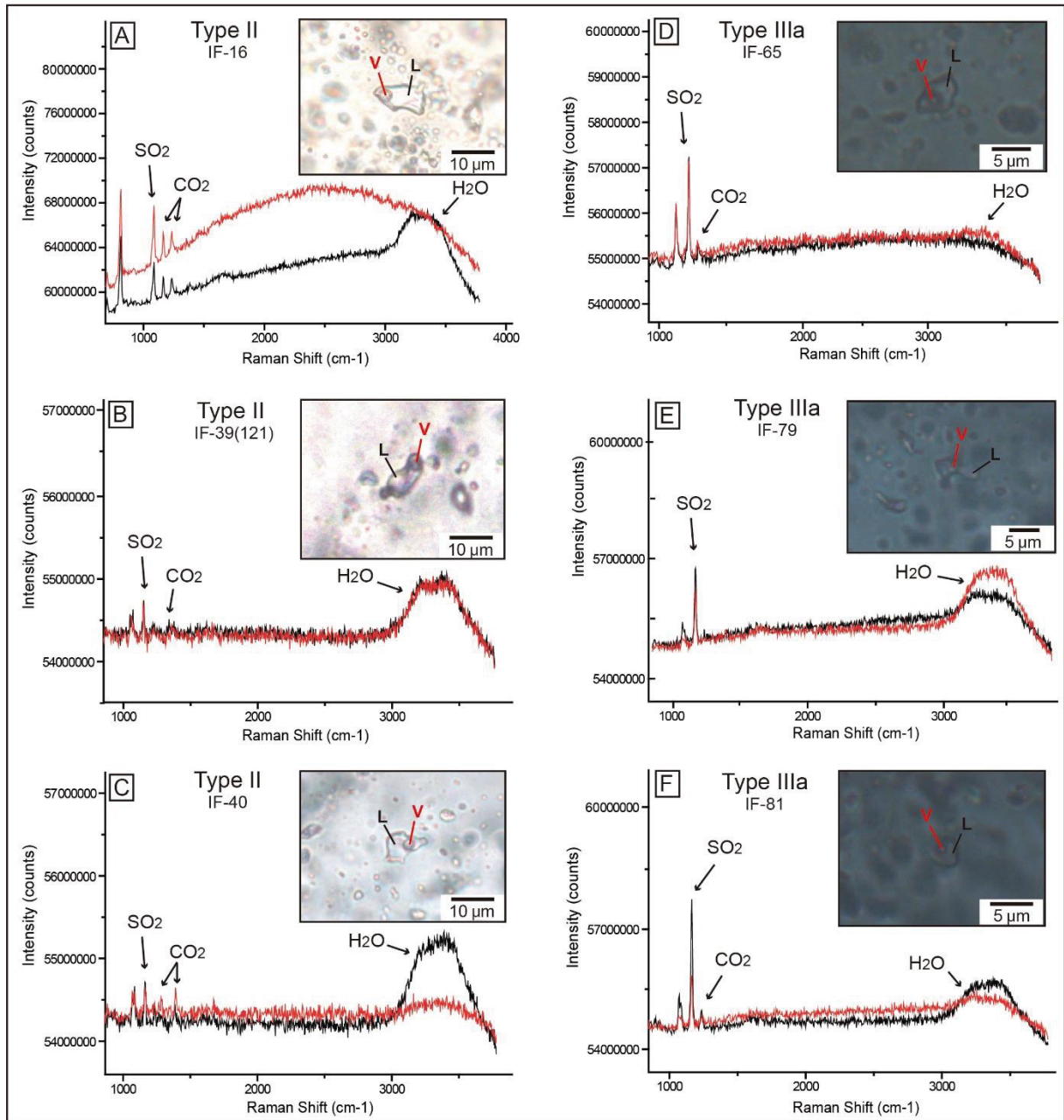


Figure 5.22 - Representative Raman spectra of fluid inclusions in the Passa Três deposit. A, B and C show the spectra of type II fluid inclusions, with the indication of the presence of CO₂, SO₂ and H₂O in vapor and liquid phases. Images D, E and F display spectra of type IIIa fluid inclusions and evidence the presence of SO₂ and minor presence of CO₂ in vapor and liquid phases.

5.9 DISCUSSION

5.9.1 Paragenetic sequence of alteration and mineralisation

Based on field, microscopic, SEM and XRD investigations, two stages of alteration assemblages were identified (Figures 5.10 and 5.11) and interpreted regarding the magmatic-hydrothermal transition. After the aplites, pegmatites, UST and stockscheider formation

(DRESSEL et al., submitted - Chapter 4), there were the early hydrothermal veins (with K-feldspar) and the barren hydrothermal quartz veins. Greisen-type alteration is related to this kind of vein, barren quartz veins that are very abundant in the drill holes near the orebody. With the development of the normal fault systems, fracturing occurred, also creating small fractured zones parallel to the main fault zones and allowing the hydrothermal fluids to infiltrate wall rocks in certain zones, leading to the phyllic-type alteration, and giving the greenish colour to the protolith red granite. With the development of the systems and formation of the main orebodies, activities on the normal fault systems created planes of brittle deformation and fracturing, allowing the formation of the fault gouge in the main fault planes. The paragenetic sequence of the alteration is displayed in Figure 5.23 and a schematic sketch of the magmatic-hydrothermal and alteration sequence is shown in Figure 5.24. Gold mineralisation was closely related to the phyllic-type alteration, as it affects the host rock (red granite) in the borders of the veins. Late quartz/ankerite veinlets also occur and are related to a late reverse movement (DRESSEL et al., submitted - Chapter 4).

Alteration Mineral	Red granite (least altered)	Greisen alteration	Phyllic alteration
Quartz	Thick solid line	Thin solid line	Thin solid line
K-feldspar	Thick solid line	Thin solid line	Thin solid line
Plagioclase	Thick solid line	Thin solid line	Thin solid line
Zircon	Thin solid line	Thin solid line	Thin solid line
Titanite	Thin solid line	Thin solid line	Thin solid line
Apatite	Thin solid line	Thin solid line	Thin solid line
Clinocllore	Thin solid line	Thin solid line	Thin solid line
Magnetite	Thin solid line	Thin solid line	Thin solid line
Pyrite	Thin solid line	Thin solid line	Thin solid line
Calcite	Thin solid line	Thin solid line	Thin solid line
Ankerite	Thin solid line	Thin solid line	Thin solid line
Muscovite	Thin solid line	Thin solid line	Thin solid line
Chalcopyrite	Thin solid line	Thin solid line	Thin solid line
Siderite	Thin solid line	Thin solid line	Thin solid line
Sericite	Thin solid line	Thin solid line	Thin solid line
Illite	Thin solid line	Thin solid line	Thin solid line
Rutile	Thin solid line	Thin solid line	Thin solid line

Figure 5.23 - Paragenetic sequence for the hydrothermal minerals of the Passa Trés gold deposit. The widths of the solid lines denote relative abundance of minerals.

and Dublin Gulch (quartz + K-feldspar + albite + muscovite + carbonate + disseminated sulphide, MALOOF et al., 2001). Additionally, alteration halos at the Passa Três deposit were also observed by Piekarcz (1992), following potassic alteration, and attributed to more acidic and hydrated conditions and lower temperatures (275 to 390°C), and was considered as endogene to the pluton. However, gold was not observed in this alteration zone.

Gold-mineralised quartz veins with neither intensive nor extensive alteration, confined to discrete envelopes along vein margins were considered by several authors (BAKER; LANG, 2001; HART, 2007; STEPHENS et al., 2004) as a characteristic for intrusion-related gold systems, where alteration halos are limited to 0.5 to 3 cm-wide halos adjacent to the veins. Considering sericite-dominant \pm pyrite \pm carbonate assemblage common in this classification of deposit, with chlorite alteration being more distal, we can assume a similarity of the alteration assemblages and occurrences of Passa Três deposit with other gold mineralisations, that are considered as intrusion-related gold deposits.

5.9.2 Ore fluid composition

Based on petrographic observations, both types II and III were dominant during the gold mineralisation stage, whereas type II is related to quartz 1 and types IIIa and IIIb are associated to quartz 3, in paragenesis with the gold bearing minerals. Based on the microthermometric and compositional test, it is shown that the ore fluid belongs to a medium-low temperature, moderate to low salinity and H₂O-NaCl-CO₂ fluid system (Figures 5.19 and 5.20).

Among the stages I to III, the salinities range between 0 and 4 wt.% NaCl eq., with some inclusions with higher salinities ranging from 9 to 12 wt.% NaCl eq. (Figure 5.20a). Homogenisation temperatures of type II range from 420 to 140 °C, whereas type IIIa range between 250 and 180°C, indicating the minimal temperatures of formation of the gold mineralisation (Figure 5.20b).

Type IIIa fluid inclusions homogenise into the liquid phase at 250 to 180°C, indicating that the magmatic fluid was trapped in the single state field (AUDÉTAT et al., 2008). Type II fluid inclusions ranges from 3 to 18 μ m and are frequently three-phased (LH₂O + LCO₂ + VCO₂), and generally by visual estimate, type II inclusions contain 45 to 96% vol. of aqueous liquid with respect to CO₂ phases (visual estimative). These CO₂-rich fluids are trapped in the quartz 1, that is coeval with the first phase of veins formation and precedes the main ore phase (stages 2a and 2b). Therefore, the spatial link of the gold mineralisation with the Passa Três granite strongly suggests that CO₂ was originated from felsic melts.

Fluid inclusion microthermometry indicates a magmatic fluid system with primary inclusions of H₂O-NaCl-CO₂ in the magmatic quartz (type I), that were also dominant during

the first stage of formation of the mineralised veins (type II, stage 2a). During the stage 2b (type III), where gold occurs in its native form with chalcopyrite and aikinite, the fluid is represented by a H₂O-NaCl composition and lower temperatures. Therefore, ore-forming fluid during stage 1 and 2a belongs to the H₂O-CO₂-NaCl system (with moderate temperature, enrichment of CO₂ and medium-low salinity), and during stage 2b, ore-forming fluids present H₂O-NaCl composition, showing lower temperatures, low salinity, and no CO₂ in the late stages of the mineralisation (as also observed by WEN et al., 2016 in the Sanshandao deposit, China). This interpretation is in accord with the work of Piekarz (1992), who suggested that the fluids responsible for the gold deposition are represented by aqueous fluid inclusions (5 to 9 mol%CO₂), low salinity (0.1 to 7 wt.% NaCl eq.), associated to the final stages of deformation, during brittle conditions, with gold deposition related to temperatures higher than 280°C and pressures higher than 1100 bars.

Our fluid inclusions data may be compared with gold deposits of Yukon deposits (e.g. Fort Knox, Dublin Gulch, Scheelite Dome and Clear Creek), that developed from fluids with low to moderate salinity (≤ 12 wt.% NaCl eq.), temperatures of 290°C to 380°C, CO₂-rich (5-14%), aqueous carbonic fluids (GOLDFARB et al., 2007; HART, 2007). Pressures from 1 to 2 kilobars (kbar), or 3.5 to 7 km depth were estimated for those deposits (GOLDFARB et al., 2007).

5.9.3 Sources of ore-forming fluids and materials

The $\delta^{34}\text{S}$ values of pyrite from the Faixa do Barreiro site have a narrow range from -0.1‰ to 1.1‰, which correspond to magmatic systems (ASSUNÇÃO; KLEIN, 2014; BIONDI, 2015; HEDENQUIST; LOWERSTERN, 1994). This suggest that the sources of sulphur in the Passa Três deposit were most likely derived from the magmatic sulphur, as already observed by Picanço (2000).

The close association of the orebodies with magmatic-hydrothermal transition and the H₂O-CO₂-NaCl ore fluid composition, combined with $\delta^{34}\text{S}$ isotope data, indicates that the ore-forming fluids could have been mainly derived from the magmatic fluids, with the sulphides origin being the magma itself (AUDÉTAT et al., 2008; HEDENQUIST; LOWERSTERN, 1994; WEN et al., 2016).

Commonly, gold is dissolved and transported in the form of gold bisulphide [Au(HS)₀, Au(HS)₂-] and gold chloride [AuCl₂-] (BIONDI, 2015; PIRAJNO, 2009; WEN et al., 2016). Our fluid inclusion study indicates that the ore fluid belongs to a H₂O-CO₂-NaCl system, with moderate salinities and *T_{h-tot}* temperatures between 400 and 150°C (moderate temperatures) at the Passa Três deposit. This, combined with the close association of gold with sulphides in

orebodies, suggests that gold was most likely transported as a gold bisulphide complex (LI et al., 2013; WEN et al., 2016).

5.9.4 Possible fluid processes

The formation of magmatic-hydrothermal ore deposits results from different processes, such as the formation of an upper crustal magma chamber, fractional crystallisation of mafic and felsic magmas, exsolution of aqueous fluids into a confined volume, vapor-brine immiscibility, magma mixing, cooling and the precipitation of ore minerals (AUDÉTAT et al., 2008; FOURNIER, 1999; HART, 2007; HEDENQUIST; LOWERSTERN, 1994; PIRAJNO, 2009). Orebodies in the Passa Três granite are placed in pull-apart sites in two normal fault systems located at the cupola zone of the pluton, as indicated by several features, such as USTs, stockscheider and other structures described by Dressel et al. (submitted - Chapter 4), tracing the magmatic-transition for this deposit.

Fluid inclusions change from the primary fluid inclusions hosted by magmatic quartz in the granite, to the first stage and the third mineralisation stage, and this change can be caused by various processes, such as immiscibility and fluid rock interaction (FOURNIER, 1999; HURAI et al., 2015; WILKINSON, 2001). Our data show that alteration is weak and concentrated at discrete halos around orebodies, therefore fluid unmixing is considered to have occurred (although we may not exclude alteration processes). In some analysed samples, the coexisting two-phase liquid-rich and vapor-rich fluid inclusions share variable Th -tot (Figure 5.19b) and behave oppositely during homogenisation, suggesting unmixing occurred locally, and even maybe boiling (FAN et al., 2005 in DENG et al., 2015). In the main mineralisation stage, the fluid inclusions are dominated by H₂O-NaCl-CO₂ composition (first phase), followed by a H₂O-NaCl composition (third stage), what could also be produced by unmixing from a parental homogeneous fluid (FALEIROS et al., 2014). Type II fluid inclusions in this case is represented by fluid inclusions with the association of a wide range of salinities, Th -tot temperatures, vapor-rich constituents and densities (Figures 5.19 and 5.20 and Table 5.12), which could be related to unmixing, progressive decompression processes and the formation of “steam” (FOURNIER, 1999; HURAI et al., 2015; WILKINSON, 2001). In our study, the isochore diagram (Figure 5.21) shows a drop among the isochores of types II and among the isochores of type IIIa, that could be explained by the fault-valve model (BOULLIER; ROBERT, 1992; SIBSON, 2000; FAMIN et al., 2005; FALEIROS et al., 2014).

So, considering the ore-controlling conditions in the Passa Três deposit and the location of the mineralisation (limited to the cupola zone, 100 to 200 m at the carapace of this pluton, and probably immediately above the zone of volatile saturation, AUDÉTAT et al., 2008) and the fluid inclusion study, we could assume that decompression related with fault-valve

process in the context of extension and the development of the normal fault systems, involving a change from lithostatic pressure to hydrostatic pressure could have occurred (BOULLIER; ROBERT, 1992; SIBSON, 2000; FAMIN et al., 2005; FALEIROS et al., 2014). In this scenario, a sudden decrease from lithostatic to hydrostatic pressure could induce a transition from a steam-dominated fluid to a brittle-plastic transition, indicating a depth of 2 to 3 km (FOURNIER, 1999). However, the absence of stockwork in intrusion-hosted deposits is associated with a deeper level of emplacement (5-9 km, BAKER; LANG, 2001), as the increased confining pressure prevents rapid fluid exsolution and explosive pressure release and favours the structural control of the orebodies in the carapace zone (FOURNIER, 1999; STEPHENS et al., 2004), favouring the channelling of the ore fluids in the normal faults systems. Therefore, cooling associated to fault-valve process and decompression, might also be responsible for the ore deposition (FOURNIER, 1999; BAKER; LANG, 2001), as well as fluid focusing, a role played by the development of the normal faults systems.

Therefore, the succession in time and space from the deformation textures observed close to the magmatic conditions (submagmatic fractures filled by quartz) to the ductile-brittle deformation conditions (e.g. undulose quartz, pull-apart opening, fracturation of sulphides and gold emplacement – DRESSEL et al., submitted - Chapter 4) agrees with the existence of a continuous and progressive event that resulted in the formation of the gold deposit.

5.9.5 Implications for ore formation in the Passa Três gold deposit

The obtained data suggest that the ore-forming fluids derived from the magmatic fluid. After tracing the magmatic-hydrothermal transition with the description of aplites, pegmatites, UST's and *stockscheider* structures, the hydrothermal stages of the deposit were identified. These stages include early hydrothermal veins (with K-feldspar border), barren quartz veins and the orebodies, marked by the association Au-Bi-Mo. Alteration styles comprise greisen-type (associated with barren quartz veins) and a phyllic-type alteration (associated with the orebodies and related fractures systems), occurring as discrete envelopes. With the presence of a H₂O-CO₂-NaCl fluid composition and the evidences for decompression process, we assume that the mineralisation was emplaced in an extensional context with the formation of the normal fault systems, accompanied by brittle deformation and the development of greisen-type and phyllic alteration. The fluid would unmix caused by decompression and be channeled in the fault systems, resulting in the weak development of the alteration halos and alteration zones. The formation of the granite related to a strike-slip fault, and the development of normal fault systems in the cupola zone of this pluton are coherent with an extensional geodynamic setting.

Mineralisation (611 to 608 Ma) coeval to granite crystallisation (612 to 610 Ma), association of gold with Bi minerals, low-sulphide character, structurally controlled veins, fluid inclusions with CO₂ and low salinities, narrow alteration envelopes and magmatic-hydrothermal transition features at the roof of a small granitic intrusion in post-collisional setting suggest that the Passa Três gold deposit shares several similarities with intrusion-related gold deposits, more specifically with granite-hosted gold deposit type (GOLDFARB et al., 2007; HART, 2007; LANG; BAKER, 2001; THOMPSON et al., 1999).

According to Hart (2007), most of the IRGRS deposits were formed during the Phanerozoic, especially during the Cretaceous and the mid-Paleozoic. So the Passa Três gold deposit could be a Proterozoic example of this kind of deposit.

5.10 CONCLUSIONS

Main results of this study can be summarised in four points:

- In the Passa Três granite, there are three alteration zones: a red granite alteration, represented by the GEM and GEF facies (magmatic stage); a greisen-type alteration, related to barren quartz veins (during magmatic-hydrothermal transition); and, finally, a phyllic alteration, very weak, but associated with the ore formation (hydrothermal stage).
- The $\delta^{34}\text{S}$ values of pyrite crystals from the Passa Três deposit are similar to those of the magmatic systems, indicating that the sulphur in this deposit have magmatic origin.
- Petrographic observations and microthermometric data analysis show that the fluid inclusions of the Passa Três deposit suggest an ore fluid with H₂O-CO₂-NaCl composition, with moderate to high temperatures (400 to 100°C) and low to moderate salinities (0.04 to 12.84 wt.% NaCl eq.).
- Ore fluid is derived from the magmatic fluid, with silica and metals concentration in the late magmatic stages (aplites, pegmatites, UST, stockscheider), followed by early hydrothermal stages (early hydrothermal veins with K-feldspar border, barren quartz veins), with the ore concentrated in the hydrothermal stages (mineralised quartz veins). Processes like decompression, unmixing and cooling are also considered responsible for ore deposition at some extent.

The geological evidence, fluid inclusion and alteration characteristics data indicate that the Passa Três gold deposit exhibits the characteristics of intrusion-related gold systems, with an intimate relationship with Passa Três granite (granite-hosted deposit).

ACKNOWLEDGEMENTS

The authors would like to thank the Laboratory of Analysis of Rocks and Minerals (LAMIR-UFPR, Brazil) for several analysis and sample preparation. We sincerely thank Mineração Tabiporã and their staff for the field support and sampling assistance. Ms. Dressel would like to thank CAPES Foundation (Ministry of Education of Brazil, Brasilia - DF, 70.040-020, Brazil) for granting the scholarship CAPES-PDSE (Process n. 99999.006489/2015-00) and for the concession of a 48 months PhD scholarship in Brazil.

6 DISCUSSÕES

Em escala da mina dois sistemas de falhas normais, desenvolvidos seguindo direções ortogonais, N-S e E-W, podem ser observados. Feições de transição magmato-hidrotermal são observadas na parte superior dos testemunhos de sondagem e também nos níveis superiores da mina subterrânea, indicando a transição entre as fases magmáticas (granito), tardi-magmáticas (aplitos, pegmatitos, veios de transição com borda de K-feldspato, *stockscheider*), até as fases hidrotermais (veios de quartzo estéreis e veios de quartzo mineralizados).

Os dados sugerem que o granito teria sido afetado pela formação de dois planos de falha originados em resposta à tectônica distensional atuante durante e após a colocação do Granito Passa Três, como indicado pela presença de aplitos paralelos a esses planos. Feições distensionais são abundantes, principalmente representadas pelos sítios de abertura ou *pull-aparts* dos sistemas de falhas normais, preenchidos por diferentes assembleias. Os corpos mineralizados seriam formados em quatro etapas. Durante o primeiro estágio, quartzo 1 e fluorita constituem o preenchimento dos *pull-aparts* abertos nesse estágio. O segundo estágio é dividido nos estágios 2a e 2b. O estágio 2a caracteriza os *pull-aparts* menores desenvolvidos dentro dos *pull-aparts* do primeiro estágio e consiste da assembleia quartzo 2 + pirita 2a ± ouro ± calcopirita ± aikinita ± fluorita ± esfalerita ± muscovita. O estágio 2b foi somente observado em *pull-aparts* menores e fraturas desenvolvidos dentro dos *pull-aparts* do estágio 2a. Esse estágio contém grãos de ouro nativo e é caracterizado pela seguinte paragênese de minério: quartzo 2 + pirita 2b + ouro + calcopirita + aikinita + ankerita ± esfalerita ± fluorita ± muscovita. Esses estágios são seguidos pelo estágio 3, caracterizado pela ocorrência de quartzo 3 + ankerita + calcita + molibdenita + aikinita + muscovita + fluorita, que apresenta caráter reverso.

Dessa forma, o depósito consiste em uma sucessão de *pull-aparts* distensionais de escala métrica dentro de dois sistemas de falhas ortogonais, o que explica o mergulho dos corpos mineralizados para Sul e para Leste.

Em relação às alterações hidrotermais, duas assembleias relacionadas ao evento de mineralização foram identificadas: alteração do tipo *greisen* e alteração fílica. A primeira ocorre na forma de halos de cor cinza em torno dos veios de quartzo estéreis e é definida pela paragênese (muscovita + quartzo + pirita ± calcopirita), enquanto que a segunda apresenta aspecto esverdeado e é composta pela assembleia (sericita + quartzo + ankerita + rutilo + siderita ± pirita ± clinocloro ± calcita). Essa alteração é associada aos veios mineralizados, ocorrendo tanto em suas bordas, como em faixas paralelas a esses, como evidenciado nos testemunhos de sondagem. Além disso, tem-se *gouge* de falha nas bordas dos veios, acompanhando os planos de falha, com argila e sulfetos associados. A presença de alteração

potássica é suspeitada, embora seja anterior à mineralização e considerada como autometassomatismo de alta temperatura relacionada à evolução do granito.

Os dados de isótopo de enxofre ($\delta^{34}\text{S}$) indicam proveniência dos sulfetos a partir dos próprios fluidos magmáticos, enquanto que os dados de inclusões fluidas sugerem a composição $\text{H}_2\text{O}-\text{CO}_2-\text{NaCl}$ para os fluidos mineralizadores, com salinidades baixas a moderadas.

6.1 TRANSIÇÃO MAGMATO-HIDROTHERMAL E RELAÇÃO TEMPORAL

A transição magmato-hidrotermal é um processo-chave na formação de sistemas minerais associados a intrusões. A definição e a compreensão da evolução magmato-hidrotermal é, portanto, de grande importância para sistemas mineralizados (GLOAGUEN et al., 2014; ZENG et al., 2016). Dessa forma, o elo potencial entre o magmatismo e a mineralização representa o ponto chave nesse estudo. No Granito Passa Três, a presença de cristais de K-feldspato na borda de alguns veios (veios de quartzo transicionais), *sills* de aplito paralelos aos veios mineralizados, bolsões de aplito-pegmatito observados nas porções superiores dos testemunhos de sondagem, estruturas do tipo UST e ambiente *stockscheider* são fortes argumentos para a existência desse elo.

Feições do tipo UST se formam tipicamente nas porções superiores dos plútons e indicam flutuações de pressão durante o processo de cristalização, típico de processos de transição magmato-hidrotermal (KIRWIN, 2005 in PIRAJNO, 2009). Nos bolsões de aplitos e de pegmatitos, algumas porções apresentam cristais de K-feldspato euédricos como transição entre a matriz aplítica e o quartzo hidrotermal. Essas observações claramente ilustram a transição magmato-hidrotermal e indicam que a paragênese de mineralização não é inteiramente posterior ao estágio magmático, mas intimamente associado. Os cristais de feldspato potássico na borda de alguns veios podem ser interpretados da mesma forma e nesse caso, pode-se observar a transição do estágio final do magmatismo (cristalização de K-feldspato) para a formação dos veios mineralizados com a presença de fluorita e sulfetos. Essas feições, como UST's e aplitos foram observadas também no depósito do tipo Clímax-Mo (mineralização espacialmente e geneticamente associada a intrusões félsicas), também na zona de cúpula de *stocks* graníticos, podendo até mesmo conter alguma mineralização (AUDÉTAT; LI, 2017). Embora esse tipo de estrutura mineralizada não tenha sido observado no depósito do Granito Passa Três, as similaridades com esse tipo de depósito indicam o potencial da mineralização ser encontrada em feições de transição magmato-hidrotermal, incluindo possíveis cavidades miarolíticas.

De fato, a transição magmato-hidrotermal observada no depósito aurífero do Granito Passa Três pode ser comparada a feições similares descritas nos depósitos de Timbarra

(Australia, MUSTARD, 2001) e Fort Knox (Alaska, USA; McCOY et al., 1997 in THOMPSON et al., 1999; BAKKE, 1995 in MUSTARD, 2001). Nesses depósitos, é possível observar a gradação lateral entre os veios mineralizados e as fases magmáticas mais fracionadas. Essa gradação foi interpretada como transição magmato-hidrotermal, e, portanto, convergindo para a interpretação da associação genética entre os fluidos mineralizadores hidrotermais e a colocação do plúton, onde os fluidos mineralizadores seriam posicionados entre as fases tardias de granitos em cristalização (THOMPSON et al., 1999; MUSTARD, 2001). Embora não tenha sido observada a gradação lateral entre as duas fases finais no Granito Passa Três, a forte relação temporal e espacial ainda sugere a conexão entre os fluidos magmáticos e os fluidos hidrotermais mineralizadores.

Com exceção dos diques aplíticos, que ocorrem próximo ou ao longo de veios de quartzo auríferos, UST's, veios de quartzo com borda de K-feldspato e bolsões aplito-pegmatíticos se concentram principalmente nos níveis superiores tanto da mina subterrânea quanto nos testemunhos de sondagem. Essas feições ocorrem com frequência na zona de cúpula de sistemas graníticos (PIRAJNO, 2009), assim como em outras associações ígneas, tais como o depósito de ouro Timbarra na Austrália (MUSTARD, 2001) ou o depósito de ouro associado a sienito no *greenstone belt* de Abitibi no Canadá (ROBERT, 2001). De acordo com Lang et al. (2000 in MUSTARD, 2001) e Thompson et al. (1999), em ambientes associados a intrusões, as áreas mais favoráveis para a formação de depósitos minerais, particularmente de ouro, são porções apicais de pequenas intrusões. O depósito de Fort Knox, por exemplo, está alojado na porção apical de uma pequena intrusão, de cerca de 1.100 por 600 m de área de superfície com contatos verticais (BAKKE, 1995 in MUSTARD, 2001). Dessa forma, fatores como intrusões de pequeno tamanho e contatos verticais são parâmetros considerados significantes para o foco da atividade hidrotermal para produzir um depósito do tipo *intrusion-related* em potencial (MUSTARD, 2001).

No Granito Passa Três, a relação temporal entre a formação do granito e a mineralização pôde ser constatada pelos dados geocronológicos obtidos no presente estudo. Com exceção da fácies “granito branco” (GEB), os dados mostraram a contemporaneidade entre o Granito Passa Três e a mineralização de ouro, exibindo, dessa forma, não somente uma relação espacial, mas também temporal. Assim, as evidências de transição magmato-hidrotermal, somadas aos dados geocronológicos, sugerem fortemente um *continuun* desde os estágios tardi-magmáticos até os veios hidrotermais e, conseqüentemente, o intervalo estreito entre as idades de magmatismo e aquelas dos veios mineralizados é um forte argumento para o elo entre magmatismo, hidrotermalismo e mineralização. Baseando-se nas observações de campo e nos dados geocronológicos, a seguinte sequência de formação foi proposta: colocação do granito (fácies GEM e GEF: $611,9 \pm 3,6$ Ma), fases tardi-magmáticas (aplito, pegmatito), veios transicionais com borda de K-feldspato ($612,9 \pm 2$ a $608,8 \pm 2$ Ma),

veios de quartzo mineralizados ($611,7 \pm 2$ a $608,8 \pm 2$ Ma), e veios de quartzo estéreis ($608,4 \pm 2$ Ma). Com base nesses dados, o intervalo de tempo entre a cristalização do granito e a formação dos veios mineralizados pôde ser posicionada entre 613 e 608 Ma, corroborando assim a relação entre o magmatismo e a mineralização. Essas idades de cristalização concordam, dentro das margens de erro, com os dados propostos por Picanço (2000), que interpretou a idade final de colocação de 616 ± 36 Ma (Sm-Nd fluorita) e os processos tardi-magmáticos como 604 ± 11 Ma (K-Ar muscovita em pegmatito).

Além do Granito Passa Três, vários depósitos auríferos associados a intrusões apresentam diferença de idade de poucos milhões de anos entre a colocação do granito (magmatismo) e a mineralização associada (hidrotermalismo). De acordo com Li et al. (2013) e Vignerresse (2007), certos depósitos hidrotermais podem ser formados por vários pulsos hidrotermais ou por sistemas hidrotermais de vida curta, com intervalos de formação entre 100 mil a 300 mil anos. Nesse contexto, estudos recentes identificaram depósitos hidrotermais com idades semelhantes às fontes graníticas associadas, incluindo mineralizações consideradas como temporal, espacial e, provavelmente, geneticamente associadas à colocação do plúton. Exemplos dessa situação abrangem os seguintes casos: o depósito de Sn-Be-F de Jiepailing (China) (U-Pb zircão, granito: 90.5 ± 0.9 Ma; Ar-Ar, mineralização: 92.1 ± 0.7 Ma) (YUAN et al., 2015), o depósito W-Sn de Xitian no sul da China (U-Pb zircão, granito: 152 ± 1.4 Ma; Re-Os molibdenita, mineralização: 149.7 ± 0.9 Ma; Ar-Ar, *greisen* mineralizado: 149.5 ± 1.5 Ma; LIANG et al., 2016), o granito Mine no Marrocos (Ar-Ar, Granito Mine: 286 ± 0.4 Ma; Re-Os molibdenita, W-Mo mineralização: 285 ± 0.5 Ma) (MARCOUX et al., 2015), Fort Knox (Alaska, USA) (U-Pb zircão: 92.5 ± 0.2 Ma; Re-Os molibdenita: 92.4 ± 1.2 Ma) (e.g., McCOY et al., 1997 in SELBY et al., 2002). No Granito Passa Três, os dados geocronológicos obtidos nesse estudo revelam a existência de apenas um episódio de atividade hidrotermal.

6.2 FLUIDO MINERALIZADOR: COMPOSIÇÃO, FONTES E ALTERAÇÕES HIDROTERMAIS

Para caracterizar o fluido mineralizador, foram realizados estudos de inclusões fluidas, de alterações hidrotermais e de isótopo $\delta^{34}\text{S}$. Os dados obtidos nesse estudo são discutidos a seguir.

As análises microtermométricas e de composição (espectroscopia Raman) indicam que as inclusões fluidas teriam pertencido a um sistema de fluido de temperatura média a baixa, baixa salinidade e de composição $\text{H}_2\text{O}-\text{CO}_2-\text{NaCl}$. Durante o estágio de mineralização, as inclusões fluidas dominantes teriam sido os tipos II e III, sendo que o tipo II seria relacionado ao quartzo 1 e tipos IIIa e IIIb seriam relacionados ao quartzo 3, em paragênese com os minerais de minério. Entre os estágios I e III, as salinidades variam geralmente entre

0 e 4 wt.% NaCl eq., localmente com salinidades entre 9 e 12 wt.% NaCl eq., identificadas em algumas inclusões.

Inclusões fluidas do tipo I homogenizam para o líquido em temperaturas em torno de 420°C, assim como as do tipo IIIa (de 250 a 180°C), sugerindo que o fluido teria sido aprisionado de forma homogênea (AUDÉTAT et al., 2008). Já as inclusões fluidas do tipo II apresentam tamanhos entre 3 e 18 µm, são geralmente trifásicas (LH₂O + LCO₂ + VCO₂), contendo (por estimativa visual) 45 a 96% de volume de líquido em relação às fases de CO₂, e apresentam temperaturas de homogeneização entre 420 e 150°C, podendo homogeneizar tanto para o líquido quanto para o vapor. Esses fluidos ricos em CO₂ teriam sido aprisionados no quartzo 1, sendo contemporâneos com a primeira fase de formação dos veios e precede a fase principal de mineralização (estágios 2a e 2b). Assim sendo, a ligação espacial da mineralização com o Granito Passa Três sugere que o CO₂ teria sido proveniente das fases líquidas do magma. Em algumas amostras analisadas, a coexistência de inclusões fluidas bifásicas ricas em líquido e outras ricas em vapor com temperaturas de homogeneização variáveis e comportamentos opostos durante a homogeneização, sugerem a possibilidade de imiscibilidade (*unmixing*), pelo menos, localmente (FAN et al., 2005 in DENG et al., 2015) em inclusões do tipo II.

Em relação aos processos de fluidos, as análises microtermométricas indicam um fluido com inclusões primárias de composição H₂O-NaCl-CO₂ no quartzo magmático (tipo I), composição que dominaria o fluido também no primeiro estágio de formação dos veios (tipo II, fase 2a). Durante o estágio 2b, onde o ouro ocorre na sua forma nativa com calcopirita e aikinita, o fluido é representado pela composição H₂O-NaCl e temperaturas mais baixas. Dessa forma, o fluido mineralizador durante os estágios 2a e 2b pertenceria a um sistema H₂O-CO₂-NaCl (com temperatura moderada, enriquecimento de CO₂ e salinidade moderada a baixa), e durante o estágio 2b, o fluido apresentaria composição H₂O-NaCl, com temperaturas mais baixas, salinidades baixas e sem a presença de CO₂ nos últimos estágios da mineralização, o que também foi observado por Wen et al. (2016) no depósito de Sanshandao (Província Aurífera de Jiaodong, China). Nas inclusões do tipo II, as análises de espectroscopia Raman também indicam a presença de SO₂. A presença de outros voláteis já havia sido suspeitada pelas temperaturas mais baixas de fusão inicial (mais frias que -56,6°C, temperatura de fusão inicial do CO₂ puro) nas inclusões de H₂O-CO₂-NaCl (tipo II), sendo justificadas pela presença de SO₂.

Essa interpretação está de acordo com o trabalho de Piekarcz (1992), que sugeriu que os fluidos responsáveis pela precipitação do ouro seriam representados por inclusões fluidas aquosas (5 a 9 mol%CO₂), de baixa salinidade (0,1 a 7 wt.% NaCl eq.), associadas aos estágios finais de deformação, durante condições rúpteis, e com a deposição do ouro ocorrendo em temperaturas entre 265 e 280°C e pressões na ordem de 1240 bar. Além disso,

os dados de inclusões fluidas desse trabalho podem ser comparados aos dos depósitos auríferos de Yukon (tais como Fort Knox, Dublin Gulch, Scheelite Dome e Clear Creek), os quais se desenvolveram a partir de fluidos aquo-carbônicos de salinidade baixa a moderada (≤ 12 wt.% NaCl eq.), temperaturas de 290 a 380°C, ricos em CO₂ (5-14%) (GOLDFARB et al., 2007; HART, 2007). Pressões entre 1 e 2 kilobars (kb) ou profundidades entre 3 e 9 km são estimadas para esses depósitos de Yukon (GOLDFARB et al., 2007; HART, 2007).

Em relação a fontes de materiais, os valores $\delta^{34}\text{S}$ de pirita da Faixa do Barreiro (Granito Passa Três) apresentam faixa estreita, entre -0.1‰ e 1.1‰, e correspondem aos valores de sistemas magmáticos (ASSUNÇÃO; KLEIN, 2014; BIONDI, 2015; HEDENQUIST; LOWERSTERN, 1994). De fato, a associação dos corpos mineralizados com a transição magmato-hidrotermal e composição do fluido mineralizador H₂O-CO₂-NaCl, combinada com os dados isotópicos de $\delta^{34}\text{S}$, indicam que os fluidos mineralizadores poderiam ter sido derivados dos fluidos magmáticos, com os sulfetos tendo origem no próprio magma do Granito Passa Três (AUDÉTAT et al., 2008; HEDENQUIST; LOWERSTERN, 1994; WEN et al., 2016).

Nesse contexto, durante as condições magmáticas a *subsolidus*, alguns minerais que seriam estáveis sob condições magmáticas podem se tornar instáveis e ser transformados em outros minerais, causando redistribuição de metais e íons entre os minerais e os fluidos aquosos exsolvidos. Assim, sulfetos magmáticos podem ser recristalizados como óxidos de Fe durante a fase de perda de voláteis e resfriamento do corpo intrusivo, disponibilizando enxofre, cobre, ouro e outros elementos calcófilos, e anfibólios e biotita magmática são substituídos por biotita e clorita secundárias (AUDÉTAT et al., 2008). Esses processos podem explicar a origem do S e do Fe e adição desses aos fluidos mineralizadores.

De acordo com Hart (2007), em geral plútons com mineralização do tipo IRGD apresentam valores isotópicos que indicam derivação crustal, como é o caso das intrusões de Yukon e Alaska, com razões iniciais de Sr acima de 0,71 e epsilon Nd de -7 a -15 (MAIR, 2005 in HART, 2007). Esses dados podem ser comparados com os dados de Cury (2003), os quais apontaram valores de epsilon Nd entre -13 e -16 para o Granito Passa Três.

Quanto ao transporte do ouro, ele geralmente é dissolvido e transportado na forma de bissulfeto [Au(HS)₀, Au(HS)₂-] ou cloreto [AuCl₂-] (BIONDI, 2015; PIRAJNO, 2009; WEN et al., 2016). O estudo de inclusões fluidas sugere um sistema H₂O-CO₂-NaCl para o fluido mineralizador, com salinidades moderadas e temperaturas mínimas entre 400 e 150°C (temperaturas moderadas) no Granito Passa Três. Esses dados, combinados com a relação próxima do ouro com sulfetos nos corpos mineralizados, são fatores sugestivos que o ouro teria sido transportado provavelmente por complexo bissulfetado (LI et al., 2013; WEN et al., 2016).

Em relação às alterações hidrotermais, no Granito Passa Três foi constatada a presença de alterações do tipo *greisen* (associadas a veios de quartzo estéreis) e do tipo filica

(relacionada aos veios mineralizados), além da alteração vermelha (possivelmente potássica), considerada como alteração de alta temperatura (autometassomatismo) e anterior à mineralização. Com exceção dessa alteração, essas alterações ocorrem como envelopes estreitos na forma de halos adjacentes aos veios mineralizados e veios de quartzo estéreis. Considerando o fluido mineralizador resultante da evolução do próprio fluido magmático, interpreta-se que a alteração seria, portanto, endógena ao sistema de transição magmato-hidrotermal, onde o próprio fluido hidrotermal alteraria as rochas graníticas que o deram origem. Esses tipos de alteração foram atribuídos por Piekarz (1992) a condições mais ácidas e hidratadas e de baixas temperaturas (275 a 390°C).

A presença de zonas de alteração hidrotermal fracas também foi observada em outros depósitos, tais como Emerald Lake (quartzo + muscovita + carbonato - BAKER; LANG, 2001) e Dublin Gulch (quartzo + K-feldspato + albita + muscovita + carbonato + sulfeto disseminado - MALOOF et al., 2001). Além disso, veios de quartzo auríferos com alterações pouco intensas, restritas a envelopes discretos ao longo das margens dos veios (espessuras de 0,5 a 3cm) foram considerados por diversos autores como característica de sistemas auríferos do tipo *intrusion-related* (BAKER; LANG, 2001; STEPHENS et al., 2004; HART, 2007). Dessa forma, considerando a assembleia sericita ± pirita ± carbonato como comum na classificação desses depósitos, com a alteração clorítica sendo mais distal, pode-se assumir a similaridade das assembleias de alteração e as ocorrências no depósito do Granito Passa Três com tais mineralizações.

6.3 CONTROLE ESTRUTURAL E PROCESSOS DE FORMAÇÃO DA MINERALIZAÇÃO

Depósitos minerais magmato-hidrotermais podem ser formados por diferentes processos, envolvendo a formação da câmara magmática supracrustal, cristalização fracionada de magmas félsicos e máficos, exsolução de fluidos aquosos e canalização em espaço confinado, imiscibilidade vapor-salmoura, mistura de magma, resfriamento e precipitação do minério (HEDENQUIST; LOWERSTERN, 1994; FOURNIER, 1999; HART, 2007; PIRAJNO, 2007; AUDÉTAT et al., 2008).

No Granito Passa Três, o modelo estrutural sugere a formação de veios mineralizados em contexto distensional associados à formação de dois sistemas de falhas normais, os quais criaram sítios de abertura (*pull-aparts*). A presença de dois sistemas perpendiculares indica possível direção N230 (orientação para sigma 3), com stress vertical máximo em sigma 1. No nível da mina é possível observar um sistema cortando o outro e ausência de veios de direção intermediária entre os dois sistemas. Segundo Destro (1995), a formação de sistemas normais

ortogonais pode ser desenvolvida quando σ_2 é oscilatório, o que geraria alívio de pressão e acomodação dos esforços.

O controle estrutural de corpos mineralizados foi observado em diversos depósitos auríferos, incluindo Scheelite Dome, Clear Creek e Dublin Gulch, no Cinturão Aurífero de Yukon (Yukon, Canadá) (STEPHENS et al., 2004). Embora esses depósitos contenham veios auríferos alojados tanto na intrusão, como nos contatos com as rochas encaixantes dos plútons, considera-se que os veios teriam se originado a partir dos *stocks* graníticos, mas controlados por estruturas tanto de escala regional como por estruturas desenvolvidas dentro do plúton. Esse é o caso de diversos depósitos, como Scheelite Dome, onde os veios mineralizados são controlados por sistemas de falhas dentro da intrusão hospedeira (STEPHENS et al., 2004) e o depósito de Pogo, onde os veios mineralizados estão associados com deformação rúptil e falhas normais (RHYS et al., 2003). Além disso, a zona de cúpula de um granito é associada com instabilidade mecânica, como tem sido documentado em alguns depósitos de ouro variscanos (GLOAGUEN et al., 2014) e facilitaria o desenvolvimento de estruturas de tendência rúptil. Dessa forma, feições de controle estrutural (como deformação submagmática) e *pull-aparts* de cinemática normal indicam contexto distensional para a formação dos veios auríferos do Granito Passa Três, durante condições de transição magmato-hidrotermal.

Conforme discutido na seção 6.2, a composição das inclusões fluidas é alterada desde as inclusões da fase magmática (tipo I, H₂O-CO₂-NaCl), primeira fase hidrotermal (tipo II, H₂O-CO₂-NaCl) para a terceira fase de mineralização (tipo III, H₂O-NaCl), e essa mudança poderia ter sido causada por vários processos, tais como imiscibilidade de fluidos ou interação com a rocha encaixante (FOURNIER, 1999; HURAI et al., 2015; WILKINSON, 2001). Os dados desse trabalho mostram que a alteração (interação com as rochas encaixantes) é de intensidade fraca e concentrada em discretos halos ao longo dos corpos mineralizados, assim sendo, a imiscibilidade (*unmixing*) pode ser considerada como um fator, embora não seja possível excluir o processo de interação. No estágio principal de mineralização, as inclusões fluidas são dominadas pela composição H₂O-NaCl-CO₂, enquanto que no terceiro estágio, as inclusões são dominadas por um fluido H₂O-NaCl, o que poderia ser produzido a partir da imiscibilidade (*unmixing*) de um mesmo fluido parental (FALEIROS et al., 2014). As inclusões de tipo II, nesse caso, são representadas por inclusões fluidas com intervalo considerável de salinidades, constituintes ricos em vapor e densidade, o que poderia ser relacionado à imiscibilidade (*unmixing*), descompressão progressiva e à formação de vapor (FOURNIER, 1999; HURAI et al., 2015; WILKINSON, 2001). Nesse estudo, o diagrama de isócoras (Figura 5.21) mostra grandes variações entre isócoras de um mesmo tipo (tipo II e tipo IIIa), o que poderia ser explicado pelo modelo de falha-válvula (BOULLIER; ROBERT, 1992; SIBSON, 2000; FAMIN et al., 2005; FALEIROS et al., 2014).

Considerando que as condições de controle da mineralização no depósito do Granito Passa Três e a localização da mineralização (limitado à zona de cúpula, 100 a 200m abaixo da carapaça do plúton, e provavelmente abaixo da zona de saturação de voláteis, AUDÉTAT et al., 2008), e as evidências das inclusões fluidas, pode-se sugerir descompressão associada à um processo do tipo falha-válvula num contexto de distensão e desenvolvimento dos sistemas de falhas normais, envolvendo mudança de pressão litostática para pressão hidrostática (BOULLIER; ROBERT, 1992; SIBSON, 2000; FAMIN et al., 2005; FALEIROS et al., 2014). Nesse cenário, a mudança repentina de pressão litostática para hidrostática poderia induzir o escape do fluido dominado por vapor durante a transição rúptil-plástica, indicando profundidade de 2 a 3 km (FOURNIER, 1999). Entretanto, a ausência de *stockwork* em depósito do tipo *intrusion-hosted* é associado com níveis mais profundos de colocação (5-9 km, BAKER; LANG, 2001), considerando que o aumento da pressão confinante previne a rápida exsolução e o alívio de pressão explosivo e favorece o controle estrutural dos corpos mineralizados na zona da carapaça (FOURNIER, 1999; STEPHENS et al., 2004), favorecendo portanto a canalização dos fluidos mineralizadores nos sistemas de falhas normais. Assim sendo, o resfriamento, associado com processo de falha-válvula e descompressão, pode ter sido também responsável pela mineralização (FOURNIER, 1999; BAKER; LANG, 2001), assim como a canalização dos fluidos mineralizadores, papel exercido pelo desenvolvimento dos sistemas de falhas normais. Dessa forma, considera-se que a profundidade de formação do depósito seria de 3,5 a 4 km, e pressão na ordem de ~1240 bar.

Em relação à concentração de metais, estes podem ser intruduzidos à fases magmáticas por uma série de caminhos, entretanto, os cátions e ânions necessários para a mineralização podem ser mobilizados totalmente a partir das fases magmáticas em depósitos magmato-hidrotermais (HEDENQUIST; LOWERSTERN, 1994). Dessa forma, os processos magmáticos operantes nas fases finais de cristalização, como a diferenciação magmática, são necessários para a concentração do minério, onde os elementos incompatíveis pode ser concentrados no final da história de cristalização do fluido magmático (HART, 2007).

A coexistência de deformação dúctil em quartzo (extinção ondulante) e deformação rúptil em feldspato nas rochas alteradas próximas aos veios mineralizados sugere que a deformação e, conseqüentemente, a mineralização, teria ocorrido em temperaturas na ordem de 300-400°C (SCHOLZ, 1988 in LI et al., 2013). A Figura 6.1 ilustra esse aspecto, onde os veios do Granito Passa Três podem ser comparados aos veios de Au-Bi-Te, formados entre 300 e 350°C.

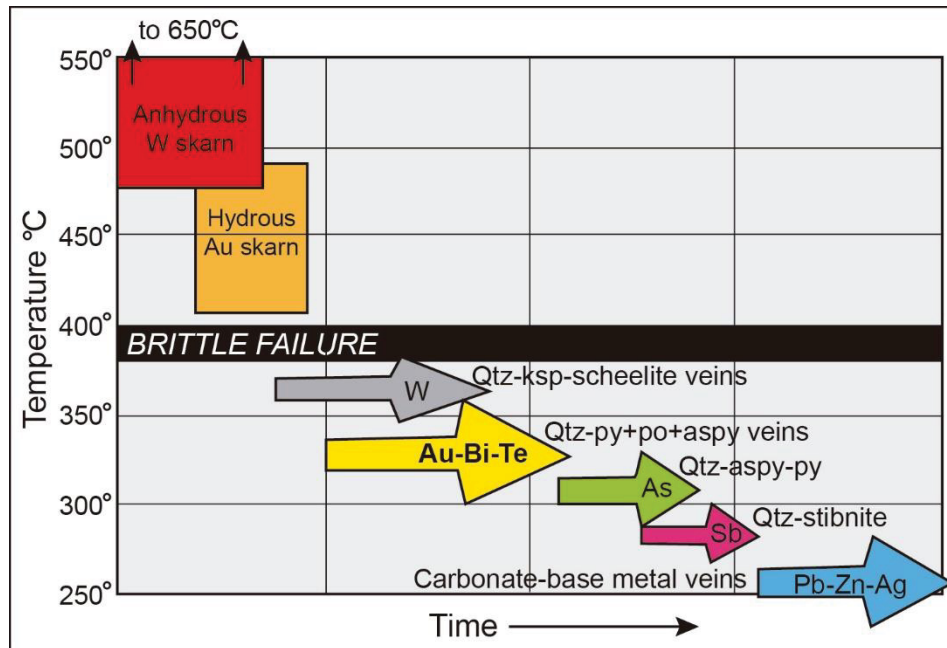


Figura 6.1 - Paragéneses esquemáticas dos tipos e associações minerais associadas ao sistema típico RIRGS. Assim como o tempo, o eixo inferior poderia representar também a distância a partir da fonte granítica, tanto que os veios de As, Sb e Pb-Zn-Ag estão praticamente fora do plúton (HART, 2007).

O curto período entre a cristalização do granito e a mineralização observados no sistema magmato-hidrotermal do Granito Passa Três podem trazer algumas questões acerca da relação temporal e a possível relação genética entre magma e mineralização. De acordo com Vignerresse (2007), alguns magmas do tipo I com baixo teor de fluido dissolvido podem ser aptos a acender a altos níveis crustais e manter seu conteúdo de fluido dissolvido no magma, com cristalização restrita a um intervalo curto de temperatura. Além do mais, segundo Coulsen et al. (2001 in LANG; BAKER, 2001), centros ígneos associados com sistemas do tipo IRGD podem ser formados a partir de complexos multifásicos que foram colocados e cristalizados rapidamente. No caso do Granito Passa Três, a colocação e o resfriamento rápidos são consistentes com o intervalo de tempo curto entre os estágios magmáticos e hidrotermais. No entanto, a ocorrência da fácies GEB pode indicar que a atividade magmática tenha persistido até cerca de 590 Ma. Esse evento tardi-magmático aparentemente não teve relação com algum episódio adicional de mineralização.

Sendo assim, a sucessão temporal e espacial a partir das texturas de deformação submagmáticas observadas próximas a condições magmáticas (fraturas submagmáticas preenchidas por quartzo), até as condições dúcteis-rúpteis (e.g. quartzo ondulante, abertura de pull-aparts, faturamento de sulfetos e precipitação do ouro – DRESSEL et al., submetido, Capítulo 4), está em acordo com a existência de um evento contínuo e progressivo que teria resultado na formação do depósito aurífero.

6.4 SÍNTESE DOS PROCESSOS DE FORMAÇÃO DO DEPÓSITO

A Figura 6.2 exibe um desenho esquemático da formação do depósito aurífero do Granito Passa Três. Os dados obtidos sugerem que os fluidos mineralizadores evoluíram a partir de fluido magmático, seguido de transição magmato-hidrotermal com a formação de aplitos, pegmatitos, UST's e *stockscheider*, chegando aos estágios hidrotermais do depósito. Esses estágios incluem veios hidrotermais preliminares (com borda de K-feldspato), veios de quartzo estéreis e os corpos mineralizados, caracterizados pela associação Au-Bi-Cu±Mo. Os sulfetos seriam provenientes do próprio fluido magmático, como indicado pelos valores de $\delta^{34}\text{S}$. A presença de fluido de composição $\text{H}_2\text{O}-\text{CO}_2-\text{NaCl}$ e evidências de decompressão acompanham a formação desses corpos mineralizados em contexto distensional com o desenvolvimento de sistemas de falhas normais, acompanhado de deformação rúptil e alterações do tipo *greisen* e filica. Nessas condições, o fluido seria canalizado em sistemas de falhas (*pull-aparts*), resultando em fraco desenvolvimento de halos e zonas de alteração. A colocação do plúton granítico associada à zona de transcorrência, e o desenvolvimento de sistemas de falhas normais na zona de cúpula desse granito são coerentes com o contexto geodinâmico distensional, possivelmente associado ao alívio pós-colisional.

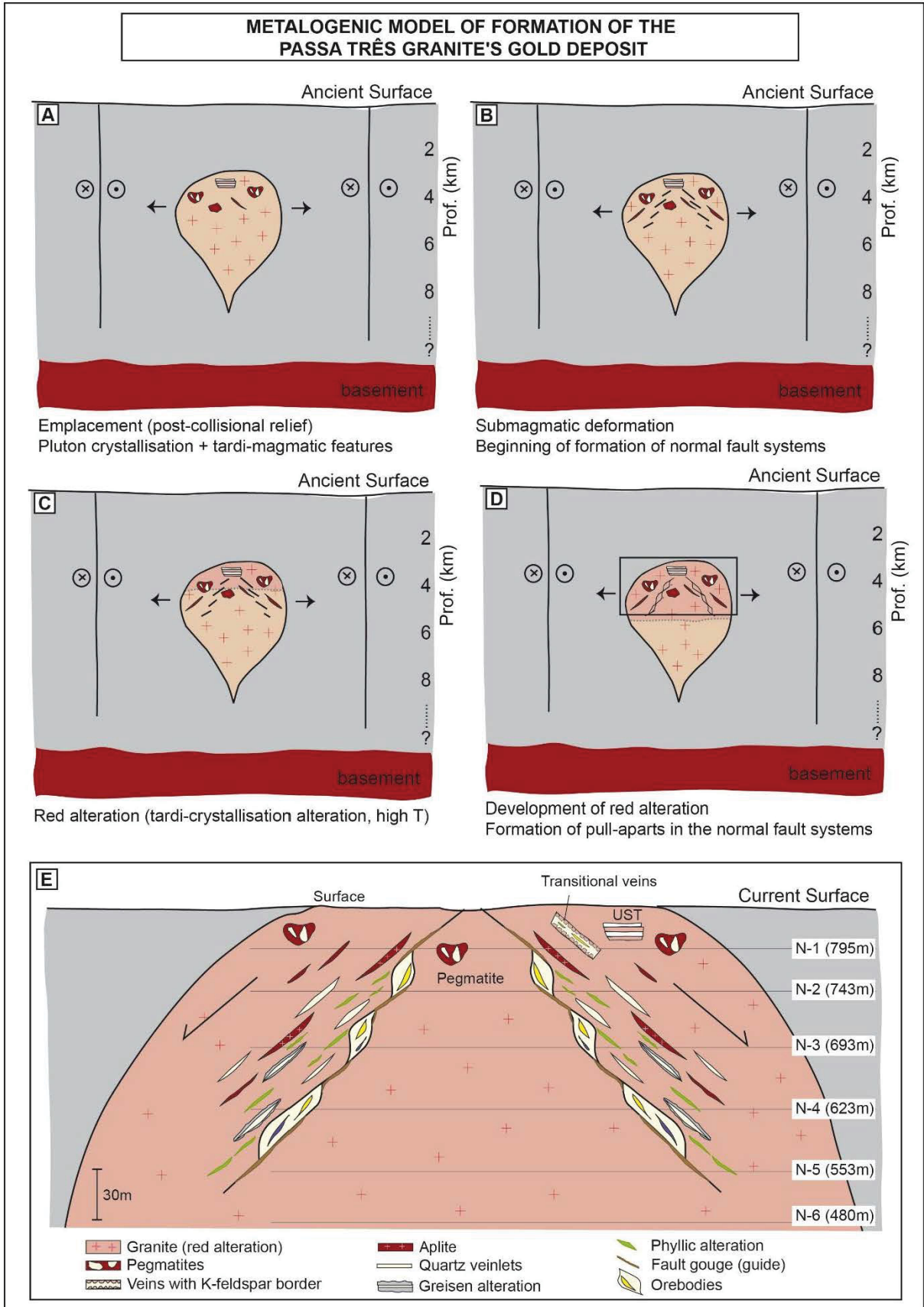


Figura 6.2 - Modelo metalogenético proposto para a mineralização aurífera do Granito Passa Três.

6.5 MODELO METALOGENÉTICO E COMPARAÇÃO COM SISTEMAS DO TIPO *INTRUSION-RELATED* (IRGD)

A associação de ouro com minerais de bismuto foi frequentemente descrita (LANG; BAKER, 2001; THOMPSON et al., 1999) e é considerada um fator importante em sistema do tipo *intrusion-related*, como observado nos depósitos de Timbarra (Bi, As, Mo, Sn) (MUSTARD, 2001); Fort Knox (bismutinita, sulfetos de Bi-Te, e molibdenita) (SELBY et al., 2002); Brués (Au, Bi, Te, W) (GLOAGUEN et al., 2014); distrito polimetálico de Tighza (Morocco) (Bi, As, W, Mo, Sb, Te) (MARCOUX et al., 2015); Linares (Bi, Te, S, Se) (CEPEDAL et al., 2013); e Dublin Gulch (MALOOF et al., 2001). Notavelmente, ambas a aikinita e a calcopirita são encontradas dentro ou em associação espacial com estruturas que contém ouro, incluindo veios hidrotermais, UST's e veios de quartzo mineralizados. Assim sendo, o ouro está associado com calcopirita e aikinita, sugerindo possível assembleia mineral de afinidade Au-Bi-Cu±Mo.

O Quadro 6.1 compara características dos depósitos do tipo *intrusion-related* com as da mineralização do Granito Passa Três. Assim sendo, características como a mineralização (611 a 608 Ma) coeva à cristalização do granito (612 a 610 Ma), associação com minerais de Bi, baixo conteúdo de sulfetos, veios estruturalmente controlados, inclusões fluidas com CO₂ e baixas salinidades, zonas de alteração restritas e evidências de transição magmato-hidrotermal na zona de cúpula de um *stock* granítico em contexto pós-colisional mostram que o depósito de ouro do Granito Passa Três compartilha diversas semelhanças com os depósitos do tipo *intrusion-related*, mais especificamente com os depósitos do tipo *granite-hosted* (GOLDFARB et al., 2007; HART, 2007; LANG; BAKER, 2001; THOMPSON et al., 1999).

Segundo Hart (2007), a maioria dos depósitos IRGRS foram formados durante o Fanerozoico, especialmente durante o Cretáceo e o Paleozoico. Nesse contexto, o Granito Passa Três poderia ser um exemplo raro desse tipo de depósito originado no Proterozoico.

Quadro 6. 1 - Comparação entre os modelos de depósitos do tipo *intrusion-related* (conforme proposto por LANG; BAKER, 2001; THOMPSON et al., 1999) e o depósito aurífero do Granito Passa Três.

	IRGD	Passa Três
<i>Contexto tectônico</i>	Margem continental antiga atrás de orógenos acrescionários ou colisionais e arcos magmáticos relacionados à subducção; contexto pós-deformacional	Contexto pós-orogênico, de alívio pós-colisional
	Rochas encaixantes metassedimentares	Idem
	Intrusões não tão deformadas, sendo que intrudiram milhões de anos após a deformação regional	Não se observa deformação no Granito Passa Três
<i>Intrusões</i>	Intrusões metaluminosas e subalcalinas de composições intermediárias a félsicas, posicionadas entre as séries da ilmenita e da magnetita; composição cálcio-alcalina	Plúton cálcio-alcalino, metaluminoso, de composição félsica
	Feições físicas e suporte geoquímico deveriam existir para alto conteúdo de voláteis; exsolução de fluidos; processo de fracionamento rápido; plútons zonados; texturas porfíricas; presença de aplitos e pegmatitos; veios de quartzo e turmalina; alteração do tipo <i>greisen</i> ; cavidades miarolíticas e/ou UST's, geralmente na região apical dos plútons	Presença de aplitos, pegmatitos, UST's, <i>stock scheider</i> ; exsolução de fluidos
	Plútons mineralizados apresentam características muito evidentes de geração de fluidos hidrotermais	Evidência de transição magmato-hidrotermal, sugerindo que os fluidos hidrotermais originaram a partir do magma
	Profundidades de 5 a 7 km	Em torno de 3,5 a 4 km
<i>Mineralização</i>	Assembleia metálica envolvendo a associação do ouro com teores elevados de Bi, W, As, Mo, Te e/ou Sb e baixos teores de metais base	Assembleia metálica do ouro associado a Bi, Cu e Pb, afinidade Au-Bi±Cu
	Baixo teor de sulfetos, abaixo de 5% em volume; assembleia mineral reduzida, tipicamente envolvendo arsenopirita, pirrotita e pirita, e ausência de óxidos de ferro	Baixo teor de sulfeto em volume; assembleia reduzida composta por pirita, calcopirita, aikinita, molibdenita
<i>Teor de ouro</i>	Geralmente baixo, de 0,8 a 1,5 g/ton	Teor médio de 0,6 g/ton
<i>Mineralizações associadas e zoneamento mineral</i>	Localização em províncias magmáticas conhecidas pela presença de depósitos de tungstênio e/ou estanho	
	Gradientes termais em torno dos plútons são bruscos e resultam em zonas concêntricas dependentes da temperatura se formando ao redor dos plúton atingindo alguns quilômetros de distância, ou somente auréola termal; mineralização aurífera proximal pode estar associada com Bi, Te e W alojada na auréola termal com teores de As ou Sb, e mineralização distal pode ser associada com Ag-Pb-Zn	
<i>Fluidos</i>	Fluidos hidrotermais aquo-carbônicos; baixa salinidade; 300-450oC (variável)	Fluidos aquo-carbônicos, de salinidade baixa a moderada e temperaturas entre 420 e 180oC
<i>Alteração hidrotermal</i>	Fraca	Fraca e localizada
<i>Tipos de depósito e estruturas</i>	Uma grande gama de estilos de mineralização pode se formar dentro da intrusão: skarn, substituições, disseminações, <i>stock works</i> e veios	Mineralização é constituída por veios
	Veios bandados -> o estilo mais característico da mineralização aurífera são feixes de veios de quartzo paralelos (0,1 a 5cm de espessura), com baixo teor de sulfetos, geralmente na porção mais apical e rígida do plúton, entre dezenas e centenas de metros abaixo da cúpola da intrusão	
	Os tipos reduzidos diferenciam-se dos oxidados pela associação com W e ausência de teores anômalos de Cu	
<i>Relação temporal</i>	Depósitos do tipo <i>intrusion-related</i> são contemporâneos com o seu plúton causativo (± 2 Ma)	Mineralização é contemporânea ao Granito Passa Três

7 CONCLUSÕES

Os principais resultados desse trabalho podem ser sumarizados nos seguintes pontos:

- O Granito Passa Três é formado por fácies magmática bastante homogênea, a qual exibe cor vermelha característica (fácies GEM e GEF). Poucas evidências da presença de granito leucocrático de cor branca foram encontradas nos testemunhos de sondagem (fácies GEB);
- Os veios mineralizados do Granito Passa Três estão associados a dois sistemas de falhas normais, de direções N-S e E-W. Ambos os sistemas apresentam a mesma paragênese e fases de deformação, e o aporte de fluido mineralizador é considerado contemporâneo à deformação e ao preenchimento dos *pull-aparts* distensionais;
- A mineralização apresenta afinidade Au-Bi-Cu±Mo;
- Os veios contêm como paragênese de minério: pirita + calcopirita + ouro + aikinita + ankerita + quartzo + esfalerita;
- Diversas evidências de transição magmato-hidrotermal foram encontradas tanto nos testemunhos de sondagem como na mina subterrânea. Essas estruturas incluem, em ordem de abundância: bolsões de pegmatito ricos em quartzo, veios de quartzo com borda de K-feldspato, UST, veios de quartzo estéreis e veios aplíticos;
- Os dados de geocronologia indicam que o Granito Passa Três possui idade de $611,9 \pm 4,7$ e $611,9 \pm 5,6$ Ma (fácies GEM e GEF, respectivamente). A fácies GEB apresenta idade mais jovem de $592,8 \pm 7,1$ Ma. Análises Ar-Ar em muscovita determinaram as seguintes idades: veios com borda de K-feldspato: $612,9 \pm 2$ a $608,8 \pm 2$ Ma; veios mineralizados: $611,7 \pm 2$ a $608,8 \pm 2$ Ma; veios estéreis: $608,4 \pm 2$ Ma;
- No Granito Passa Três há três zonas de alteração: alteração de cor vermelha (fácies GEM e GEF, estágio magmático); alteração do tipo *greisen*, relacionada a veios de quartzo estéreis (durante a transição magmato-hidrotermal); e, finalmente, alteração filica, muito fraca, mas associada à mineralização (estágio hidrotermal);
- Os valores $\delta^{34}\text{S}$ analisados em cristais de pirita dos corpos mineralizados são similares àqueles de sistemas magmáticos, indicando que o enxofre presente no depósito foi derivado de fontes magmáticas;
- Observações petrográficas e análises microtermométricas sugerem que as inclusões fluidas do depósito do Granito Passa Três pertencem a um fluido de composição $\text{H}_2\text{O}-\text{CO}_2-\text{NaCl}$, com temperaturas altas a moderadas (400 a 100°C) e salinidades baixas a moderadas (0,04 a 12,84 wt.% NaCl eq.).
- O fluido mineralizador teria sido derivado do fluido magmático, com a concentração de sílica e metais nos estágios tardi-magmáticos (aplitos, pegmatitos, UST, *stockscheider*),

seguidos pelos estágios hidrotermais preliminares (veio hidrotermal preliminar com borda de K-feldspato, veios de quartzo estéreis). Processos como descompressão, *unmixing* e resfriamento são considerados como atuantes e responsáveis pela formação do depósito em algum nível.

Essas evidências sugerem a existência da transição magmato-hidrotermal, confirmada pelas datações U-Pb e Ar-Ar, indicando que a colocação, a liberação do fluido magmato-hidrotermal e a formação dos veios de quartzo auríferos ocorreram em intervalo de aproximadamente 5 Ma, entre 613 e 608 Ma. Tais dados, associados às evidências de inclusões fluidas e de alteração hidrotermal e afinidade com Bi são características de sistemas do tipo *intrusion-related*, onde a mineralização se encontra alojada no próprio *stock* granítico, indicando, portanto, modelo do tipo *granite-hosted* para o Granito Passa Três.

Além de tudo, para fins de exploração, as evidências indicativas de transição magmato-hidrotermal, tais como as descritas nesse trabalho, podem auxiliar na descoberta de novos alvos prospectivos.

REFERÊNCIAS

- ASSUNÇÃO, R.F.S.; KLEIN, E.L. The Moreira Gomes deposit of the Caiú-Caiú goldfield: Fluid inclusions and stable isotope constraints and implications for the genesis of granite-hosted gold mineralization in the Tapajós Gold Province, Brazil. **Journal of South American Earth Sciences**, v. 49, p. 85-105 2014.
- AUDÉTAT, A.; LI, W. The genesis of Climax-type porphyry Mo deposits: Insights from fluid inclusions and melt inclusions. **Ore Geology Reviews**, v. 88, p. 436–460, 2017.
- AUDÉTAT, A.; PETTKE, T.; HEINRICH, C.A.; BODNAR, R.J. The Composition of Magmatic-Hydrothermal Fluids in Barren and Mineralized Intrusions. **Economic Geology**, v. 103, n. 5, p. 877–908, 2008.
- BAILEY S.W. Chlorites: structures and crystal chemistry. In: Bailey S.W. (ed.). *Hydrous Phyllosilicates (Exclusive of micas)*. **Reviews in Mineralogy**, v.19, p. 347-403, 1988.
- BAKER, T.; LANG, J. Fluid inclusion characteristics of intrusion-related gold mineralization, Tombstone - Tungsten magmatic belt, Yukon Territory, Canada. **Mineralium Deposita**, v. 36, p. 563-582, 2001.
- BAKKER, R.J. Package *FLUIDS 1*. Computer programs for analysis of fluid inclusion data and for modelling bulk fluid properties. **Chemical Geology**, v. 194, p. 3-23, 2003.
- BASEI, M.A.S.; BRITO NEVES, B.B.; SIGA JUNIOR, O.; BABINSKI, M.; PIMENTEL, M.M.; TASSINARI, C.C.G.; HOLLANDA, M.H.B.; NUTMAN, A.; CORDANI, U.G. Contribution of SHRIMP U–Pb zircon geochronology to unravelling the evolution of Brazilian Neoproterozoic fold belts. **Precambrian Research**, v. 183, p. 112-144, 2010.
- BIONDI, J.C. **Processos metalogenéticos e os depósitos minerais brasileiros**. São Paulo: Oficina de Textos, 2003.
- BIONDI, J.C. **Processos metalogenéticos e os depósitos minerais brasileiros**. 2 ed. São Paulo: Oficina de Textos, 2015.
- BORGO, A. **Depósito de ouro do Tocantinzinho (Província Aurífera do Tapajós):** Relação entre deformação, hidrotermalismo e mineralização. 226 f. Tese (Doutorado) - Setor de Ciências da Terra, Universidade Federal do Paraná, Curitiba, 2017.
- BOSCH, D.; GARRIDO, C.J.; BRUGUIER, O.; DHUIME, B.; BODINIER, J.L.; PADRON-NAVARTA, J.A.; GALLAND, B. Building an island-arc crustal section: Time constraints from a LA-ICP-MS zircon study. **Earth and Planetary Science Letters**, v. 309, p. 268–279, 2011.
- BOUCHEZ, J.L.; DELAS, C.; GLEIZES, G.; NEDELEC, A.; CUNEY, F. M. Submagmatic microfractures in granites. **Geology**, v. 20, p. 35-38, 1992.
- BOULLIER, A.M.; ROBERT, F. Palaeoseismic events recorded in Archaean gold-quartz vein networks, Val d'Or, Abitibi, Quebec, Canada. **Journal of Structural Geology**, v. 14, n. 2, p. 161-179, 1992.
- BRUGUIER, O., BOSCH, D., CABY, R., VITALE-BROVARONE A., FERNANDEZ L., HAMMOR D., LAOUAR, R., OUABADI, A., ABDALLAH, N., AND MECHATI, M. Age of UHP metamorphism in the Western Mediterranean: Insight from rutile and zircon inclusions in a

diamond-bearing garnet megacryst (Edough Massif, NE Algeria) **Earth and Planetary Science Letters**, v. 474, p. 215- 225, 2017.

CAMPANHA, G.A.C.; SADOWSKI, G.R. Tectonics of the southern portion of the Ribeira Belt (Apiáí Domain). **Precambrian Research**, v. 98, p. 31-51, 1999.

CAMPOS NETO, M.C.; FIGUEIREDO, M.C.H. The Rio Doce Orogeny, Southeastern Brazil. **Journal of South American Earth Sciences**, v. 8, n. 2, p. 143-162, 1995.

CEPEDAL, A.; FUERTES-FUENTE, M.; MARTÍN-IZARD, A.; GARCÍA-NETO, J.; BOIRON, M.C. An intrusion-related gold deposit (IRGD) in the NW of Spain, the Linares deposit: Igneous rocks, veins and related alterations, ore features and fluids involved. **Journal of Geochemical Exploration**, v. 124, p. 101-126, 2013.

CERNY, P. Rare-element granitic pegmatites. Part 1: Anatomy and internal evolution of pegmatite deposits. **Geosciences Canada**, v. 18, n. 2, p. 49-67, 1991.

CURY, L.F. **Geocronologia e litogeoquímica dos stocks graníticos da porção sudeste da Faixa Apiáí, Estado do Paraná**. 125 f. Dissertação (Mestrado) – Instituto de Geociências, Universidade de São Paulo, São Paulo, 2003.

CURY, L.F.; KAULFUSS, G.A.; SIGA JR., O.; BASEI, M.A.S.; HARARA, O.M.; SATO, K. Idades U-Pb (Zircões) de 1.75 Ga em granitóides alcalinos deformados dos núcleos Betara e Tigre: Evidências de regimes extensionais do Estateriano na Faixa Apiáí. **Geologia USP, Série Científica**, v. 2, p. 95-108, 2002.

CURY, L.F.; SIGA JR., O.; HARARA, O.M.M.; PRAZERES FILHO, H.J.; BASEI, M.A.S. Aspectos tectônicos das intrusões dos Granitos do Cerne, Passa Três e Rio Abaixo, Sudeste do Pré-Cambriano Paranaense. Estudo baseado em datações ^{39}Ar - ^{40}Ar em micas. **Geologia USP, Série Científica**, v. 8, n. 1, p. 87-104, 2008.

DEER, W.A.; HOWIE, R.A.; ZUSSMAN, J. **Minerais constituintes das rochas**. 4 ed. Lisboa: Fundação Calouste Gulbenkian, 2010.

DENG, J.; LIU, X.; WANG, Q.; PAN, R. Origin of the Jiaodong-type Xinli gold deposit, Jiaodong Peninsula, China: Constraints from fluid inclusion and C–D–O–S–Sr isotope compositions. **Ore Geology Reviews**, v. 65, p. 674–686, 2015.

DESTRO, N. Release fault: A variety of cross fault in linked extensional fault systems, in the Sergipe-Alagoas Basin, NE Brazil. **Journal of Structural Geology**, v. 17, n. 5, p. 615-629, 1995.

DIAMOND, L. W. Review of the systematics of CO₂–H₂O fluid inclusions. **Lithos**, v. 55, p. 69-99, 2001.

DRESSEL, B. C.; CHAUVET, A.; TRZASKOS, B.; BIONDI, J. C.; BRUGUIER, O.; MONIÉ, P.; VILLANOVA, S. N.; NEWTON, J. B. **The Passa Três lode gold deposit (Paraná State, Brazil): An example of structurally-controlled mineralisation formed during magmatic-hydrothermal transition and hosted within granite**. No prelo.

FALEIROS, A. M.; CAMPANHA, G. A. C.; FALEIROS, F. M.; BELLO, R. M. S. Fluid regimes, fault-valve behavior and formation of gold-quartz veins - The Morro do Ouro Mine, Ribeira Belt, Brazil. **Ore Geology Reviews**, v. 56, p. 442–456, 2014.

- FALEIROS, F.M. **Evolução de terrenos tectono-metamórficos da Serrania do Ribeira e Planalto Alto Turvo (SP, PR)**. 318 f. Tese (Doutorado) – Instituto de Geociências, Universidade de São Paulo, São Paulo, 2008.
- FAMIN, V.; HÉBERT, R.; PHILIPPOT, P.; JOLIVET, L. Ion probe and fluid inclusion evidence for co-seismic fluid infiltration in a crustal detachment. **Contributions to Mineralogy and Petrology**, v.150, p. 354-367, 2005.
- FASSBINDER, E. **A unidade Água Clara no contexto do Grupo Açungui: um modelo transpressivo de colisão oblíqua no Neoproterozóico paranaense**. 207 f. Tese (Doutorado) – Instituto de Geociências, Universidade de São Paulo, São Paulo, 1996.
- FIORI, A.P. A Falha da Lancinha no Pré-Cambriano paranaense: reflexo de uma falha profunda? **Boletim Paranaense de Geociências**, v. 36, p. 3-14, 1985a.
- FIORI, A.P. Aplicação do modelo de cisalhamento simples na análise da deformação dúctil de alguns granitos paranaenses. **Boletim Paranaense de Geociências**, v. 36, p. 31-40, 1985b.
- FIORI, A.P. Tectônica e estratigrafia do Grupo Açungui – PR. **Boletim IG-USP, Série Científica**, v. 23, p. 55-74, 1992.
- FIORI, A.P. Evolução geológica da Bacia Açungui. **Boletim Paranaense de Geociências**, Curitiba, v. 42, p. 7-27, 1994.
- FIORI, A.P.; FASSBINDER, E.; GÓIS, J.R.; FUMAGALLI, C.E. Compartimentação tectônica do Grupo Açungui a norte de Curitiba. In: SIMPÓSIO SUL-BRASILEIRO DE GEOLOGIA, 3., 1987, Curitiba. **Atas...** Curitiba: SBG, 1987. v. 1, p. 183-196.
- FOURNIER, R.O. Hydrothermal processes related to movement of fluid from plastic into brittle rock in the magmatic-epithermal environment. **Economic Geology**, v. 94, n. 8, p. 1193-1211, 1999.
- FRAGOSO CESAR, A.R.S. As placas brasileiras do sul e sudeste da Plataforma Sul-Americana. In: SIMPÓSIO NACIONAL DE ESTUDOS TECTÔNICOS, 4., 1993, Belo Horizonte. **Atas...** Belo Horizonte: SBG, 1993.
- GIMENEZ FILHO, A.G.; JANASI, V.A.; CAMPANHA, G.A.C.; TEIXEIRA, W.; TREVIZOLI JR., L.E. U-Pb dating and Rb-Sr isotope geochemistry of the Eastern portion of the Três Córregos Batolith Ribeira Fold Belt, São Paulo, Brazil. **Revista Brasileira de Geociências**, v. 30, n. 1, p. 45-50, 2000.
- GIMENEZ FILHO, A.; TEIXEIRA, W.; FIGUEIREDO, M. C. H.; TREVIZOLI JR., L. Geologia, petrografia e litogeoquímica do Complexo Granítico Três Córregos na região de Barra do Chapéu e Ribeirão Branco, SP. **Revista Brasileira de Geociências**, v. 25, n. 2, p. 92-106, 1995.
- GLOAGUEN, E.; BRANQUET, Y.; CHAUVET, A.; BOUCHOT, V.; BARBANSON, L.; VIGNERESSE, J.J. Tracing the magmatic/hydrothermal transition in regional low-strain zones: the role of magma dynamics in strain localization at pluton roof, implications for intrusion-related gold deposits. **Journal of Structural Geology**, v. 58, p. 108-121, 2014.
- GOLDFARB, R.J.; MARSH, E. E., HART, C.J.R.; MAIR, J.L.; MILLER, M.L.; JOHNSON, C. Geology and Origin of Epigenetic Lode Gold Deposits, Tintina Gold Province, Alaska and Yukon. In: GOUGH, L. P.; DAY, W. C. (Eds.). **Recent U.S. Geological Survey Studies in the Tintina Gold Province, Alaska, United States, and Yukon, Canada - Results of a 5-Year**

Project. Scientific Investigations Report. U.S. Department of the Interior U.S. Geological Survey. 2007.

GOLDFARB, R.J.; GROVES, D.I.; GARDOLL, S. Orogenic gold and geologic time: a global synthesis. **Ore Geology Reviews**, v. 18, p. 1-75, 2001.

GOLDSTEIN, R. H.; REYNOLDS, T. J. **Systematics of fluid inclusions in diagenetic minerals.** Society for Sedimentary Geology, Society of Economic Paleontologists and Mineralogists, Short Course 31, 199 p., 1994.

GROVES, D.I.; GOLDFARB, R.J.; GEBRE-MARIAM, M.; HAGEMANN, S.G.; ROBERT, F. Orogenic gold deposits: a proposed classification in the context of their crustal distribution and relationship to other gold deposit types. **Ore Geology Reviews**, v. 13, p. 7-27, 1998.

HARRISON, T.M.; CÉLÉCIER, J.; AIKMAN, A.B.; HERMANN, J.; HEIZLER, M.T. Diffusion of ^{40}Ar in muscovite. **Geochimica et Cosmochimica Acta**, v. 73, p. 1039-1051, 2009.

HART, C.J.R. Reduced intrusion-related gold systems. In: GOODFELLOW, W.D. (ed.) **Mineral deposits of Canada: A synthesis of major deposit types, district metallogeny, the evolution of geological provinces, and exploration methods.** Geological Association of Canada, 2007. Special Publication n. 5, p. 95-112.

HEDENQUIST, J.W.; LOWENSTERN, J. B. The role of magmas in the formation of hydrothermal ore deposits. **Nature**, v. 370, p. 519-527, 1994.

HEILBRON, M.; PEDROSA-SOARES, A.C.; CAMPOS NETO, M. DA C.; SILVA, L.C. DA; TROUW, R.A.J.; JANASI, V. A. Província Mantiqueira. In: MANTESO-NETO, V. *et al.* (Orgs.). **Geologia do continente sul-americano: evolução da obra de Fernando Flávio Marques de Almeida.** São Paulo: Deca, 2004. p. 203-234.

HÖNIG, S.; LEICHMANN, J.; NOVÁK, M. Unidirectional solidification textures and garnet layering in Y-enriched garnet-bearing aplite-pegmatites in the Cadomian Brno Batholith, Czech Republic. **Journal of Geosciences**, v. 55, p. 113-129, 2010.

HURAI, V.; HURAIÓVÁ, M.; SLOBODNI'K, M.; THOMAS, R. **Geofluids Developments in Microthermometry, Spectroscopy, Thermodynamics, and Stable Isotopes.** Amsterdam: Elsevier, 2015.

JANASI, V.A.; LEITE, R.J.; VAN SCHMUS, W.R. U-Pb chronostratigraphy of the granitic magmatism in the AgudosGrandes Batholith (west of São Paulo) – implications for the evolution of the Ribeira Belt. **Journal of South American Earth Sciences**, v. 14, p. 363-376, 2001.

KAULFUSS, G.A. **Geocronologia dos Núcleos de Embasamento Setuva, Betara e Tigre, Norte de Curitiba-PR.** 115 f. Dissertação (Mestrado) – Instituto de Geociências, Universidade de São Paulo, São Paulo, 2001.

KOPPERS, A.P. ArArCALC software for $^{40}\text{Ar}/^{39}\text{Ar}$ age calculations. **Computers & Geosciences**, v. 28, p. 605-619, 2002.

LANG, J.R.; BAKER, T. Intrusion-related gold systems: the present level of understanding. **Mineralium Deposita**, v. 36, p. 477-489, 2001.

LI, J.; QIN, K.; LI, G.; XIAO, B.; ZHAO, J.; CHEN, L. Magmatic-hydrothermal evolution of the Cretaceous Duolong gold-rich porphyry copper deposit in the Bangongco metallogenic belt,

Tibet: evidence from U-Pb and $^{40}\text{Ar}/^{39}\text{Ar}$ geochronology. **Journal of Asian Earth Sciences**, v. 41, p. 525-536, 2013.

LIANG, X.; DONG, C.; JIANG, Y.; WU, S.; ZHOU, Y.; ZHU, H.; FU, J.; WANG, C.; SHAN, Y. Zircon U-Pb, molybdenite Re-Os and muscovite Ar-Ar isotopic dating of the Xitian W-Sn polymetallic deposit, eastern Hunan Province, South China and its geological significance. **Ore Geology Reviews**, v. 78, p. 85-100, 2016.

LUDWIG, K.R. Isoplot 3.75 – A geochronological toolkit for Microsoft Excel. **Berkeley Geochronology Center Special Publication**, n. 5, 2012. Available on: http://www.bgc.org/isoplot_etc/isoplot.html

MACLEAN, W. H. Mass change calculations in altered rock series. **Mineralium Deposita**, v. 25, n. 1, p. 44-49, 1990.

MALOOF, T.L.; BAKER, T.; THOMPSON, J.F.H. The Dublin Gulch intrusion-hosted gold deposit, Tombstone plutonic suite, Yukon Territory, Canada. **Mineralium Deposita**, v. 36, p. 583-593, 2001.

MARCOUX, E.; NERCI, K.; BRANQUET, Y.; RAMBOZ, C.; RUFFET, G.; PEUCAT, J.J.; STEVENSON, R.; JÉBRAK, M. Late-Hercynian intrusion-related gold deposits: An integrated model on the Tighza polymetallic district, central Morocco. **Journal of African Earth Sciences**, v. 107, p. 65-88, 2015.

MINEROPAR. **Mapa Geológico do Estado do Paraná**. Curitiba: MINEROPAR, 2006. Escala 1:250.000.

MUSTARD, R. Granite-hosted gold mineralization at Timbarra, northern New South Wales, Australia. **Mineralium Deposita**, v. 36, p. 542-562, 2001.

NAKANO, S.; AKAI, J.; SHIMOBAYASHI, N. Contrasting Fe-Ca distributions and related microtextures in syenite alkali feldspar from the Patagonian Andes, Chile. **Mineralogical Magazine**, v. 69, n. 4, p. 521-535, 2005.

NESEN, G. The tin-tungsten mine of Santa-Comba - An example of an endogranite with a stockscheider set in a lineament (Galicia, NW Spain). **Comptes Rendus Hebdomadaires des Séances de l'Académie des Sciences, Serie D**, v. 291, p. 17-20, 1980.

PICANÇO, J.L. **Composição isotópica e processos hidrotermais associados aos veios auríferos do maciço granítico Passa Três, Campo Largo, PR**. 175 f. Tese (Doutorado) – Instituto de Geociências, Universidade de São Paulo, São Paulo, 2000.

PIEKARZ, G.F. **O Granito Passa Três – PR e as mineralizações auríferas associadas**. 221 f. Dissertação (Mestrado) – Instituto de Geociências, Universidade Estadual de Campinas, Campinas, 1992.

PIRAJNO, F. **Hydrothermal processes and mineral systems**. Springer & Geological Survey of Western Australia, 2009.

PRAZERES FILHO, H.J. **Litogeoquímica, geocronologia (U-Pb) e geologia isotópica dos complexos graníticos Cunhaporanga e Três Córregos, Estado do Paraná**. 180 f. Dissertação (Mestrado) – Instituto de Geociências, Universidade de São Paulo, São Paulo, 2000.

PRAZERES FILHO, H.J.; BASEI, M.A.S.; PASSARELLI, C.R.; HARARA, O.M.M.; SIGA JR., O. U-Pb Zircon ages of post-orogenic granitic magmatism in Apiaí Folded Belt (Paraná State, Southern Brazil): Petrological and geotectonic significance. In: SOUTH AMERICAN SYMPOSIUM ON ISOTOPE GEOLOGY, 4., 2003, Salvador. **Short papers**. Salvador: CBPM, 2003a.

PRAZERES FILHO, H.J.; HARARA, O.M.; BASEI, M.A.S.; PASSARELLI, C.R.; SIGA JR., O. Litogeoquímica, geocronologia U-Pb e geologia isotópica (Sr-Nd-Pb) das rochas graníticas dos batólitos Cunhaporanga e Três Córregos na porção sul do Cinturão Ribeira, Estado do Paraná. **Geologia USP, Série Científica**, v. 3, p. 51-70, 2003b.

PUTNIS, A.; HINRICHS, R.; PUTNIS, C.V.; GOLLA-SCHINDLER, U.; COLLINS, L.G. Hematite in porous red-clouded feldspars: Evidence of large-scale crustal fluid-rock interaction. **Lithos**, v. 95, p. 10-18, 2007.

REIS NETO, J. M. **Faixa Itaiacoca: registro de uma colisão entre dois blocos continentais no Neoproterozóico**. 253 f. Tese (Doutorado em Geologia) – Instituto de Geociências da Universidade de São Paulo, São Paulo, 1994.

RHYS, D.; DIMARCHI, J.; SMITH, M.; FRIESEN, R.; ROMBACH, C. Structural setting, style and timing of vein-hosted gold mineralization at the Pogo deposit, east central Alaska. **Mineralium Deposita**, v. 38, p. 863-875, 2003.

ROBERT, F. Syenite-associated disseminated gold deposits in the Abitibi greenstone belt, Canada. **Mineralium Deposita**, v. 36, p. 503-516, 2001.

ROEDDER, E. Fluid inclusions. **Reviews in mineralogy**, v. 12, 644 p., 1984.

ROGERS, J.J.W.; UNRUG, R.; SULTAN, M. Tectonic assembly of Gondwana. **Journal of Geodynamics**, v. 19, n. 1, p. 1-34, 1995.

SADOWSKI, G. R.; MOTIDOME, M. J. Brazilian Megafaults. **Revista Geologia do Chile**, v. 31, p. 61-75, 1987.

SALAMUNI, E.; FIORI, A.P.; WERNICK, E. Evolução tectônica e estruturação do Núcleo Betara, arredores de Curitiba - PR. In: CONGRESSO BRASILEIRO DE GEOLOGIA, 37., 1992, São Paulo. **Anais...** São Paulo: SBG, 1992. v. 1, p. 280.

SELBY, D.; CREASER, R.A.; HART, C.J.R.; ROMBACH, C.S.; THOMPSON, J.F.H.; SMITH, M.T.; BAKKE, A.A.; GOLDFARB, R.J. Absolute timing of sulfide and gold mineralization: a comparison of Re-Os molybdenite and Ar-Ar mica methods from the Tintina Gold Belt, Alaska. **Geology**, v. 30, n. 9, p. 791-794, 2002.

SHAFAROUDI, A.M.; KARIMPOUR, M.H.; STERN, C.R. The Khopik porphyry copper prospect, Lut Block, Eastern Iran: Geology, alteration and mineralization, fluid inclusion, and oxygen isotope studies. **Ore Geology Reviews**, v. 65, p. 522-544, 2015.

SIBSON, R. H. Fluid involvement in normal faulting. **Journal of Geodynamics**, v. 29, p. 469-499, 2000.

SIGA JR., O. **Domínios tectônicos do sudeste do Paraná e nordeste de Santa Catarina: geocronologia e evolução crustal**. Tese (Doutorado) – Instituto de Geociências, Universidade de São Paulo, São Paulo, 1995.

SIGA JR., O.; BASEI, M.A.S.; PASSARELLI, C.R.; SATO, K.; CURY, L.F.; MCREATH, I. Lower and Upper Neoproterozoic magmatic records in Itaiacoca Belt (Paraná-Brazil): Zircon ages and lithostratigraphy studies. **Gondwana Research**, v. 15, p. 197-208, 2009.

SILLITOE, R.H.; THOMPSON, J.F.H. Intrusion-Related Vein Gold Deposits: types, tectono-magmatic settings and difficulties of distinction from orogenic gold deposits. **Resource Geology**, v. 48, n. 2, p. 237-250, 1998.

SOARES P.C., GÓIS J.R. Geologia do Granito Passa Três (Paraná) e suas mineralizações auríferas. In: SIMPÓSIO SUL-BRASILEIRO DE GEOLOGIA, 3., Curitiba. **Anais...** Curitiba: SBG, 1987. v. 2, p. 497.

SOARES, P. C.; REIS NETO, J. Um estudo de caracterização termo-dinâmica de micro-estruturas dos Grupos Açungui e Setuva (PR). In: SIMPÓSIO SUL-BRASILEIRO DE GEOLOGIA, 3., 1987, Curitiba. **Anais...** Curitiba: SBG, 1987. v. 1. p. 147-165.

STEPHENS, J.L.; MAIR, J.L.; OLIVER, N.H.S.; HART, C.J.R.; BAKER, T. Structural and mechanical controls on intrusion-related deposits of the Tombstone Gold Belt, Yukon, Canada, with comparisons to other vein-hosted ore-deposit types. **Journal of Structural Geology**, v. 26, p. 1025-1041, 2004.

THEODOROVICZ, A.; CÂMARA, M. M.; TAKAHASHI, A. T.; MORAES, S. M.; GODOY, H. K. Geologia do Pré-Cambriano das folhas Engenheiro Maia e Ribeirão Branco, São Paulo. In: CONGRESSO BRASILEIRO DE GEOLOGIA, 35., 1988, Belém. **Anais...** Belém: SBG, 1988. v. 6, p. 2713-2726.

THOMPSON, J.F.H.; SILLITOE, R.H.; BAKER, T.; LANG, J.R.; MORTENSEN, J.K. Intrusion-related gold deposits associated with tungsten-tin provinces. **Mineralium Deposita**, v. 34, p. 323-334, 1999.

TUDDURI, J.; CHAUVET, A.; BARBANSON, L.; LABRIKI, M.; DUBOIS, M.; TRAPY, P.H.; LAHFIDA, A.; POUJOL, M.; MELLETON, J.; BRADA, L.; ENNACIRID, A.; MAACHA, L. Structural control, magmatic-hydrothermal evolution and formation of hornfels-hosted, intrusion-related gold deposits: Insight from the Thaghassa deposit in Eastern Anti-Atlas, Morocco. **Ore Geology Reviews**, v. 97, 2018. Disponível em: <<https://doi.org/10.1016/j.oregeorev.2018.04.023>>. Acesso em: 03 junho 2018.

TURINI NETO, G. **Estudos geoquímicos da mineralização aurífera do Granito Passa Três – PR**. 47 f. Monografia (Trabalho de Conclusão de Curso) – Instituto de Geociências, Universidade de São Paulo, São Paulo, 2012.

VELÁSQUEZ, G.; BÉZIAT, D.; SALVI, S.; SIEBENALLER, L.; BORISOVA, A. Y.; POKROVSKI, G. S.; PARSEVAL, P. Formation and deformation of pyrite and implications for gold mineralization in the El Callao District, Venezuela. **Economic Geology**, v. 109, p. 457-486, 2014.

VIGNERESSE, J.L. The role of discontinuous magma inputs in felsic magma and ore generation. **Ore Geology Reviews**, v. 30, n. 3-4, p. 181-216, mar. 2007.

WEN, B.J.; FAN, H.R.; HU, F.F.; LIU, X.; YANG, K.F.; SUN, Z.F.; SUN, Z.F. Fluid evolution and ore genesis of the giant Sanshandao gold deposit, Jiaodong gold province, China: Constrains from geology, fluid inclusions and H–O–S–He–Ar isotopic compositions. **Journal of Geochemical Exploration**, v. 171, p. 96–112, 2016

WERNICK, E.; RIGO JR., L.; GALEMBECK, T. M. B.; DIEFENBACH, K. W. Os complexos granitóides Cunhaporanga e Três Córregos (PR): zoneamento magmático e implicações geotectônicas. **Geociências**, v. 9, p. 67-85, 1990.

WILKINSON, J.J. Fluid inclusions in hydrothermal ore deposits. **Lithos**, v. 55, p. 229–272, 2001.

WILSON, S. A.; RIDLEY, W. I.; KOENIG, A. E. Development of sulfide calibration standards for the laser ablation inductively-coupled plasma mass spectrometry technique. **Journal of Analytical Atomic Spectrometry**, v. 17, p. 406-409, 2002.

YANG, Z.; CHANG, Z.; HOU, Z.; MEFFRE, S. Age, igneous petrogenesis, and tectonic setting of the Bilihe gold deposit, China, and implications for regional metallogeny. **Gondwana Research**, v. 34, p. 296-314, 2016.

YUAN, S.; MAO, J.; COOK, N.J.; WANG, X.; LIU, X.; YUAN, Y. A Late Cretaceous tin metallogenic event in Nanling W–Sn metallogenic province: Constraints from U–Pb, Ar–Ar geochronology at the Jiepailing Sn–Be–F deposit, Hunan, China. **Ore Geology Reviews**, v. 65, p. 283-293, 2015.

ZENG, L.; BAO, Z.; SHAN, Q.; YANG, W.; ZHAO, Y.; LI, N. Magmatic–hydrothermal evolution of highly fractionated granites: Evidence from the Kuiqi miarolite in Fujian province, SE China. **Journal of Asian Earth Sciences**, v. 123, p. 100-110, 2016.

APÊNDICES

Appendix 4.A - EPMA major elements concentrations (in wt. %) of pyrite 2a and 2b, chalcopyrite, aikinite, molybdenite and native gold.

Appendix 4.B - Laser ablation U-Th-Pb analyses for zircon grains from the Passa Três granitoids, South Brazil. Analyses marked with * indicate grains used in age calculation.

Appendix 4.C - Scanning Electron Microscope (SEM) Cathodoluminescence images of zircon grains from the Passa Três granitoids. A) Euhedral zircon grain from the GEM granite, showing an euhedral, oscillatory zoned overgrowth surrounding a euhedral, unzoned Paleoproterozoic core; B) Euhedral to subhedral zircon grains from the GEF granite displaying inherited cores. The grain on the left has a high-U core of Paleoproterozoic age; C) Euhedral grain with a fine oscillatory zoning of magmatic origin surrounding a zoned core of Paleoproterozoic age. The last growth band appears darker which indicates a U enrichment in the late stage of the magmatic evolution; D) Euhedral zircon grains with cores. The grain in the upper part displays a Paleoproterozoic core wrapped by a Neoproterozoic, zoned, overgrowth of magmatic origin. Circles correspond to the laser spots (26 μm). Errors are ± 2 sigma.

Appendix 4.D - ^{40}Ar - ^{39}Ar stepwise heating analytical data for eight muscovite samples from the Passa Três gold deposit, South Brazil. Data in red represent negative values.

Appendix 5.A - LA-ICP-MS analyses of selected pyrite, chalcopyrite, aikinite and native gold from the Passa Três Granites's gold deposit.

Appendix 4.A - EPMA major elements concentrations (in wt. %) of pyrite 2a and 2b, chalcopyrite, aikinite, molybdenite and native gold.

Sample		S	Fe	Cu	Au	Mo	Pb	Ag	Zn	Ti	As	Bi
12 / 1	Pyrite 2a	52,14	45,99	<0,07				<0,05	<0,11	<0,03		<0,53
13 / 1	Pyrite 2a	52,36	45,68					<0,05	<0,12	<0,03		
22 / 1	Pyrite 2a	52,78	46,30		<0,29			<0,05		<0,03		
23 / 1	Pyrite 2a	52,22	45,96	<0,07					<0,12	<0,03		<0,51
24 / 1	Pyrite 2a	52,33	46,46	<0,07				<0,05	<0,12			
26 / 1	Pyrite 2a	52,78	46,08	<0,06							<0,06	
41 / 1	Pyrite 2a	52,30	45,95	<0,07				<0,05		<0,03		<0,51
59 / 1	Pyrite 2a	52,20	46,35	<0,07					<0,12	<0,03	<0,06	
47 / 1	Pyrite 2a	52,04	45,94	<0,07				<0,05	<0,13	<0,03	<0,06	
48 / 1	Pyrite 2a	52,22	45,96	<0,07	<0,3			<0,05	<0,12	<0,03		<0,52
20 / 2	Pyrite 2a	51,39	46,23	<0,06	<0,28			<0,05		<0,03		<0,50
21 / 2	Pyrite 2a	51,36	45,93								<0,06	
22 / 2	Pyrite 2a	51,91	46,02	<0,06				<0,05	<0,12			
23 / 2	Pyrite 2a	51,44	45,78	<0,07				<0,05		<0,03	<0,06	
28 / 2	Pyrite 2a	51,78	46,01		<0,29					<0,03		
56 / 2	Pyrite 2a	51,49	46,06	<0,07				<0,05			<0,06	<0,52
1 / 1	Pyrite 2b	52,62	46,51					<0,05	<0,12			<0,50
2 / 1	Pyrite 2b	52,04	45,99	<0,07				<0,05		<0,03		
3 / 1	Pyrite 2b	52,42	46,58	<0,06				<0,05			<0,06	
4 / 1	Pyrite 2b	52,67	46,48					<0,05	<0,12		<0,06	<0,51
5 / 1	Pyrite 2b	52,27	46,39	<0,07				<0,06	<0,12		<0,06	
6 / 1	Pyrite 2b	52,48	46,15	<0,07				<0,05		<0,03	<0,06	<0,53
7 / 1	Pyrite 2b	52,08	46,14		<0,30			<0,05	<0,12	<0,03		
8 / 1	Pyrite 2b	52,84	46,01							<0,03		<0,52
9 / 1	Pyrite 2b	51,65	45,48	<0,06	<0,30					<0,03		<0,51
10 / 1	Pyrite 2b	52,64	46,20	<0,06				<0,05	<0,12	<0,03	<0,06	
11 / 1	Pyrite 2b	52,54	45,88	<0,07					<0,12	<0,03	<0,07	
18 / 1	Pyrite 2b	52,09	46,08	<0,07	<0,30					<0,03	<0,06	
19 / 1	Pyrite 2b	52,63	45,93	0,15				<0,05			<0,06	<0,50
20 / 1	Pyrite 2b	52,66	46,03	<0,07				<0,05		<0,03	<0,06	
21 / 1	Pyrite 2b	51,99	46,31	0,18					<0,13	<0,03		
25 / 1	Pyrite 2b	52,28	46,58	0,13				<0,05		<0,03		
27 / 1	Pyrite 2b	52,69	46,48	0,22	<0,28			<0,05	<0,12			
28 / 1	Pyrite 2b	51,50	46,36	0,56				<0,05		<0,03		
32 / 1	Pyrite 2b	52,68	46,11	0,15	<0,30						<0,06	<0,54
33 / 1	Pyrite 2b	51,97	46,42	0,21						<0,03		
49 / 1	Pyrite 2b	51,53	44,39	<0,07				<0,05			<0,06	<0,54
52 / 1	Pyrite 2b	52,71	46,14	<0,06				<0,05	<0,12	<0,03	<0,06	<0,50
56 / 1	Pyrite 2b	52,55	46,11	0,09								
58 / 1	Pyrite 2b	52,12	45,70	<0,07					<0,12			<0,53
24 / 2	Pyrite 2b	51,47	46,02	<0,07					<0,11		<0,06	<0,51

26 / 2	Pyrite 2b	51,24	46,00	<0,06				<0,05			<0,06	
31 / 2	Pyrite 2b	51,66	45,94	<0,06					<0,11	<0,03	<0,06	<0,48
58 / 2	Pyrite 2b	51,45	45,62	<0,07				<0,05		<0,03		
55 / 2	Py (remob)	51,11	45,66	<0,07				<0,05				
15 / 2	Py (remob)	51,05	46,16	<0,06				<0,05	<0,12	<0,03		<0,48
16 / 2	Py (remob)	50,94	46,07						<0,11	<0,03	<0,06	<0,52
17 / 2	Py (remob)	51,35	45,93					<0,05	<0,12		<0,06	<0,49
18 / 2	Py (remob)	51,56	46,22	<0,07				<0,05	<0,12		<0,06	
19 / 2	Py (remob)	51,21	46,04	<0,06	<0,28			<0,05	<0,11			
44 / 2	Py (remob)	51,35	45,65	<0,07				<0,05				<0,52
50 / 2	Py (remob)	51,54	45,91		<0,28			<0,05	<0,11	<0,03		
34 / 1	Chalcopyrite	34,24	29,55	35,34				<0,05			<0,08	<0,53
35 / 1	Chalcopyrite	34,06	29,09	35,36	<0,32				<0,16	<0,03	<0,08	
36 / 1	Chalcopyrite	34,03	29,56	35,76	<0,30			<0,05	<0,16	<0,03	<0,08	<0,53
37 / 1	Chalcopyrite	33,96	29,64	35,52				<0,05		<0,03		
38 / 1	Chalcopyrite	34,35	29,65	36,30	<0,30			<0,05	<0,16			
39 / 1	Chalcopyrite	34,16	29,59	35,84	<0,30				<0,17	<0,03		
40 / 1	Chalcopyrite	34,44	29,65	36,30				<0,06	<0,16	<0,03	<0,08	<0,53
45 / 1	Chalcopyrite	33,99	29,49	35,42				<0,05	<0,16	<0,03	<0,08	<0,54
46 / 1	Chalcopyrite	34,34	29,86	35,46	<0,30					<0,03	<0,07	
55 / 1	Chalcopyrite	34,24	29,81	34,98	<0,30				<0,16	<0,03		<0,53
57 / 1	Chalcopyrite	32,71	29,53	34,40				<0,05	<0,15	<0,03		
29 / 2	Chalcopyrite	33,60	29,63	35,10								
49 / 2	Chalcopyrite	34,00	29,19	35,24				<0,05	<0,15			<0,51
39 / 2	Chalcopyrite	33,70	29,61	35,48	<0,31			<0,05			<0,08	
35 / 2	Chalcopyrite	33,71	29,09	34,67	<0,29			<0,05	<0,15	<0,03		
36 / 2	Chalcopyrite	33,42	28,95	34,92				<0,05	<0,15		<0,08	<0,53
14 / 1	Cpy (remob)	34,87	30,03	35,34				<0,05			<0,07	<0,52
15 / 1	Cpy (remob)	34,61	29,23	35,31				<0,05				<0,54
17 / 1	Cpy (remob)	34,06	29,36	35,04				<0,05	<0,17		<0,08	
60 / 2	Cpy (remob)	33,69	28,99	34,69	<0,29				<0,16		<0,07	
31 / 1 .	Native gold	0,08	0,30	0,15	90,68			11,93			<0,07	<0,70
42 / 1 .	Native gold	0,09	0,42	0,15	91,26			11,78				<0,69
51 / 1 .	Native gold	0,05	<0,06		90,37	0,08		12,13		<0,05	<0,07	
25 / 2 .	Native gold	0,11	0,26	0,10	90,17			7,79		<0,04		
27 / 2 .	Native gold	0,06	0,17	<0,09	93,08			7,72		<0,05	<0,07	<0,71
29 / 1 .	Aikinite	16,55	0,46	11,76			35,48	<0,07				36,55
43 / 1 .	Aikinite	16,34	0,97	11,42			35,63					36,04
44 / 1 .	Aikinite	17,36	2,21	11,79	<0,38		34,16	<0,07				35,20
53 / 1 .	Aikinite	16,58	0,27	11,35			35,16		<0,14	<0,05		36,54
54 / 1 .	Aikinite	16,58	0,56	11,51	<0,38		35,40		<0,14	<0,05		36,02
30 / 2 .	Aikinite	16,25	0,69	11,01			31,75		<0,29		<0,13	38,30
40 / 2 .	Molybdenite	39,10	<0,05	<0,07	0,05	52,22		<0,06	0,15			<0,55
41 / 2 .	Molybdenite	39,58	<0,05	<0,07		52,04			0,15		<0,05	<0,56

Appendix 4.B - Laser ablation U-Th-Pb analyses for zircon grains from the Passa Três granitoids, South Brazil. Analyses marked with * indicate grains used in age calculation.

Sample	Pb* (ppm)	Th (ppm)	U (ppm)	Th/U	208Pb/206Pb	207Pb/206Pb	± (1s)	207Pb/235U	± (1s)	206Pb/238U	± (1s)	Apparent ages (Ma)			Disc. (%)		
												206Pb/238U	± (1s)	207Pb/206Pb		± (1s)	
Passa Três Granite																	
GEIM																	
aa_1	17,0	57,9	34,6	1,67	0,45	0,1244	0,0040	6,4051	0,1883	0,3736	0,0076	0,69	2046,2	35,5	2019,5	55,8	-1,3
aa_2	13,1	33,8	51,7	0,65	0,24	0,1069	0,0026	3,2683	0,0701	0,2217	0,0031	0,65	1290,9	16,2	1747,5	43,6	26,1
aa_3*	13,7	134,9	108,6	1,24	0,39	0,0631	0,0017	0,8672	0,0216	0,0997	0,0013	0,51	612,5	7,4	711,6	57,1	13,9
aa_4*	13,2	93,4	117,7	0,79	0,25	0,0602	0,0016	0,8181	0,0195	0,0987	0,0012	0,50	606,5	6,9	608,9	55,6	0,4
aa_5*	8,6	88,6	66,3	1,33	0,41	0,0600	0,0020	0,8256	0,0250	0,0998	0,0013	0,44	613,4	7,8	602,8	69,0	-1,8
aa_6	6,9	2,8	19,7	0,14	0,04	0,1188	0,0035	5,6780	0,1541	0,3468	0,0063	0,67	1919,1	30,1	1937,7	52,3	1,0
aa_7*	4,2	30,3	36,3	0,83	0,26	0,0625	0,0032	0,8551	0,0412	0,0993	0,0020	0,43	610,2	12,0	690,1	106,1	11,6
aa_8*	3,1	20,4	28,3	0,72	0,22	0,0588	0,0036	0,8007	0,0463	0,0988	0,0021	0,37	607,3	12,4	559,2	127,3	-8,6
aa_9	77,2	89,9	104,6	0,86	0,32	0,2154	0,0033	16,6615	0,2186	0,5611	0,0057	0,77	2871,2	23,4	2946,3	24,7	2,5
aa_10* r	15,6	169,9	122,0	1,39	0,40	0,0584	0,0017	0,8032	0,0209	0,0998	0,0013	0,49	612,9	7,5	544,9	61,0	-12,5
aa_11* c	16,7	124,1	135,2	0,92	0,29	0,0590	0,0019	0,8132	0,0234	0,0999	0,0014	0,49	613,9	8,3	568,3	67,1	-8,0
aa_12* r	8,1	63,5	68,0	0,93	0,29	0,0597	0,0024	0,8213	0,0310	0,0998	0,0017	0,45	613,3	9,9	591,8	85,6	-3,6
aa_13	22,4	62,1	47,9	1,30	0,36	0,1253	0,0027	6,1541	0,1158	0,3562	0,0046	0,69	1964,3	22,1	2032,9	37,1	3,4
aa_14	43,5	41,9	130,3	0,32	0,10	0,1074	0,0019	4,6027	0,0716	0,3110	0,0033	0,68	1745,5	16,2	1754,9	32,4	0,5
aa_15	47,7	48,2	149,8	0,32	0,10	0,1075	0,0019	4,4395	0,0677	0,2994	0,0031	0,68	1688,4	15,4	1758,1	31,9	4,0
aa_16	58,7	32,6	82,3	0,40	0,11	0,2245	0,0038	18,3873	0,2675	0,5941	0,0065	0,75	3006,2	26,2	3012,9	26,7	0,2
aa_17	32,8	107,2	61,1	1,75	0,51	0,1226	0,0025	6,2360	0,1116	0,3690	0,0045	0,68	2024,5	21,2	1994,1	35,6	-1,5
aa_18*	30,6	372,4	219,0	1,70	0,50	0,0598	0,0015	0,8235	0,0183	0,0999	0,0011	0,51	613,8	6,7	595,1	52,8	-3,1
aa_19*	18,3	33,4	184,3	0,18	0,06	0,0600	0,0015	0,8347	0,0190	0,1008	0,0012	0,52	619,3	7,0	604,6	53,6	-2,4
aa_20	25,5	35,6	63,0	0,56	0,16	0,1211	0,0026	6,0554	0,1127	0,3625	0,0046	0,68	1994,2	21,6	1973,1	37,0	-1,1
aa_21	27,8	197,7	30,4	6,51	1,92	0,1171	0,0032	5,5665	0,1357	0,3448	0,0055	0,65	1909,6	26,3	1912,3	47,6	0,1
aa_22	26,2	84,6	110,0	0,77	0,22	0,0995	0,0022	2,8547	0,0557	0,2081	0,0025	0,62	1218,5	13,5	1615,0	40,7	24,6

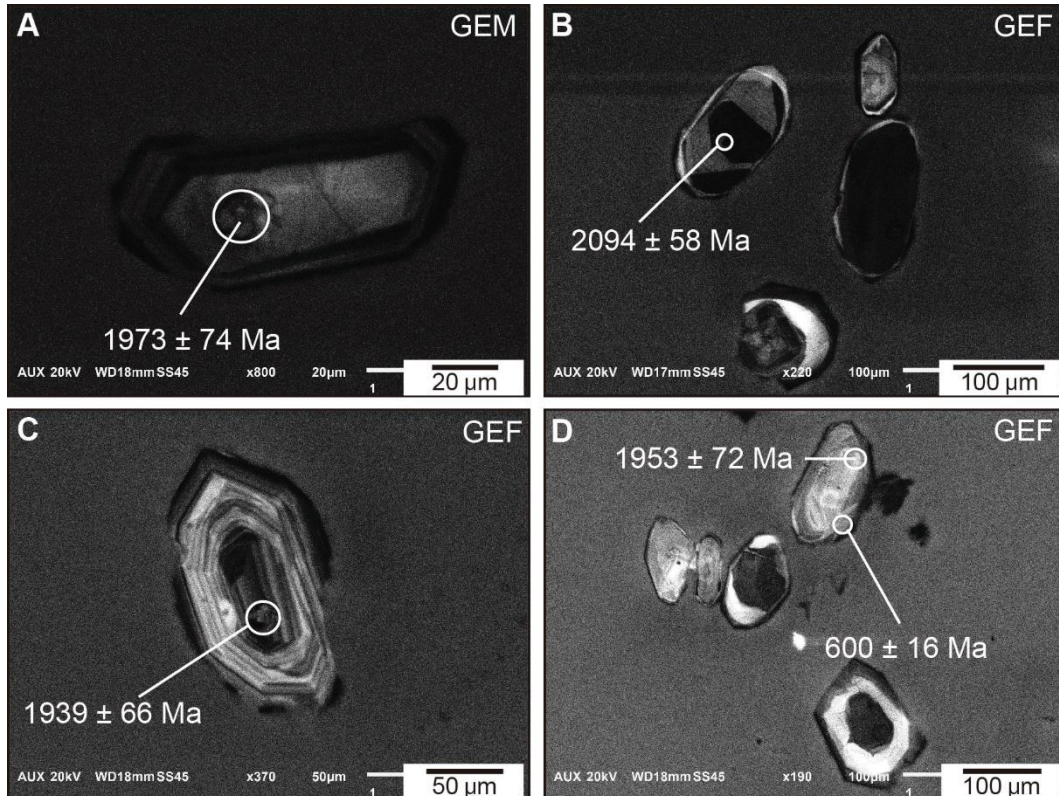
aa_23*	13,8	136,2	107,6	1,27	0,38	0,0593	0,0021	0,8208	0,0264	0,1004	0,0015	0,47	616,7	9,0	578,2	74,2	-6,7
aa_24	4,2	1,8	12,9	0,14	0,04	0,1105	0,0045	4,9065	0,1847	0,3221	0,0073	0,60	1800,1	35,7	1807,1	72,2	0,4
aa_25	72,7	75,5	154,5	0,49	0,14	0,1363	0,0027	7,5735	0,1313	0,4030	0,0047	0,68	2182,7	21,7	2180,8	34,0	-0,1
aa_26	65,5	190,2	131,0	1,45	0,42	0,1228	0,0028	6,0898	0,1214	0,3596	0,0047	0,66	1980,4	22,5	1997,5	39,4	0,9
aa_27	40,0	80,9	92,2	0,88	0,30	0,1232	0,0028	5,6673	0,1142	0,3337	0,0044	0,66	1856,5	21,4	2002,5	39,9	7,3
aa_28	201,9	142,9	214,6	0,67	0,21	0,2723	0,0052	25,5587	0,4280	0,6808	0,0081	0,71	3347,3	31,0	3319,3	29,6	-0,8
aa_29*	17,0	129,2	149,6	0,86	0,26	0,0600	0,0018	0,8112	0,0225	0,0980	0,0013	0,49	602,8	7,8	604,3	64,5	0,2
aa_30	129,7	122,9	335,9	0,37	0,10	0,1223	0,0024	5,9463	0,0990	0,3528	0,0037	0,64	1947,7	17,8	1989,4	33,8	2,1
GEF																	
aa_31	3,3	17,4	20,9	0,83	0,20	0,0837	0,0051	1,6215	0,0905	0,1404	0,0038	0,49	847,2	21,6	1286,3	113,1	34,1
aa_32	26,2	75,2	52,3	1,44	0,41	0,1239	0,0031	6,2524	0,1375	0,3661	0,0052	0,64	2010,9	24,4	2012,7	43,0	0,1
aa_33	96,0	106,3	221,4	0,48	0,14	0,1279	0,0026	6,6359	0,1167	0,3762	0,0041	0,63	2058,6	19,4	2069,6	35,2	0,5
aa_34	61,0	57,7	92,1	0,63	0,16	0,2516	0,0053	18,3710	0,3378	0,5296	0,0066	0,68	2739,6	28,0	3194,8	32,8	14,2
aa_36	53,1	157,4	112,6	1,40	0,37	0,1227	0,0029	6,0036	0,1246	0,3548	0,0046	0,62	1957,6	21,9	1996,1	41,1	1,9
aa_37*	7,2	30,7	72,6	0,42	0,11	0,0613	0,0027	0,8283	0,0343	0,0980	0,0018	0,44	602,6	10,6	650,1	92,9	7,3
aa_38	31,3	69,1	95,3	0,72	0,20	0,1061	0,0028	4,1090	0,0969	0,2809	0,0040	0,61	1595,8	20,3	1733,4	47,7	7,9
aa_39	124,9	542,3	191,8	2,83	0,78	0,1285	0,0029	6,7546	0,1324	0,3811	0,0046	0,61	2081,6	21,3	2078,0	38,8	-0,2
aa_40	6,9	80,3	58,3	1,38	0,40	0,0597	0,0032	0,7555	0,0387	0,0918	0,0019	0,40	566,4	11,0	591,6	113,6	4,3
ab_1*	4,0	32,4	32,5	1,00	0,30	0,0599	0,0042	0,8283	0,0557	0,1003	0,0022	0,33	616,1	12,9	600,4	144,6	-2,6
ab_2	47,0	160,1	172,7	0,93	0,28	0,1255	0,0027	4,1589	0,0792	0,2404	0,0031	0,67	1389,0	16,1	2035,5	37,9	31,8
ab_3	73,7	122,9	170,2	0,72	0,22	0,1218	0,0025	6,0575	0,1084	0,3606	0,0044	0,68	1985,2	20,9	1983,4	35,6	-0,1
ab_4	20,6	47,6	76,5	0,62	0,17	0,1109	0,0023	4,0356	0,0744	0,2639	0,0032	0,65	1510,0	16,1	1814,4	37,4	16,8
ab_5	72,7	172,0	148,9	1,16	0,31	0,1243	0,0029	6,2535	0,1289	0,3649	0,0052	0,68	2005,3	24,3	2019,1	40,3	0,7
ab_6	119,4	86,9	160,4	0,54	0,15	0,2480	0,0042	21,3359	0,3092	0,6241	0,0066	0,72	3126,1	26,0	3172,1	26,2	1,5
ab_7	223,9	269,2	481,4	0,56	0,16	0,1347	0,0023	7,2395	0,1084	0,3898	0,0040	0,68	2122,1	18,5	2160,3	29,9	1,8
ab_8*	4,6	36,4	39,1	0,93	0,28	0,0579	0,0037	0,7955	0,0486	0,0997	0,0020	0,33	612,5	11,9	525,4	134,1	-16,6
ab_9	188,0	227,2	368,4	0,62	0,18	0,1375	0,0027	7,7830	0,1361	0,4106	0,0050	0,69	2217,8	22,7	2195,9	34,0	-1,0
ab_10	103,1	150,4	246,1	0,61	0,18	0,1278	0,0023	6,4832	0,1004	0,3680	0,0038	0,67	2019,8	18,1	2068,2	31,1	2,3
ab_11	23,4	65,3	51,3	1,27	0,42	0,1401	0,0034	6,9917	0,1498	0,3621	0,0054	0,69	1992,3	25,3	2227,9	40,9	10,6
ab_13	52,6	93,3	135,4	0,69	0,21	0,1201	0,0024	5,5763	0,0970	0,3368	0,0039	0,66	1871,4	18,5	1957,8	34,9	4,4

ab_14	24,3	68,8	46,7	1,47	0,42	0,1239	0,0042	6,0726	0,1882	0,3555	0,0074	0,67	1960,9	35,3	2013,4	59,0	2,6
ab_15	71,6	75,0	174,0	0,43	0,14	0,1257	0,0025	6,2774	0,1120	0,3623	0,0043	0,66	1993,0	20,2	2038,7	35,3	2,2
ab_16	10,2	31,4	20,0	1,57	0,44	0,1250	0,0038	6,2528	0,1755	0,3629	0,0065	0,64	1995,9	30,8	2028,8	53,3	1,6
ab_17*	10,3	109,1	78,6	1,39	0,42	0,0611	0,0024	0,8242	0,0308	0,0979	0,0016	0,43	601,9	9,2	642,8	83,6	6,4
ab_18*	14,1	157,3	103,9	1,51	0,45	0,0608	0,0021	0,8234	0,0263	0,0982	0,0014	0,45	604,1	8,4	632,5	72,4	4,5
ab_19	108,8	161,3	250,6	0,64	0,20	0,1309	0,0026	6,8139	0,1175	0,3777	0,0042	0,64	2065,4	19,4	2109,9	34,0	2,1
xb_1	90,7	111,4	222,7	0,50	0,19	0,1523	0,0022	7,7400	0,0893	0,3685	0,0033	0,77	2022,4	15,4	2372,1	23,9	14,7
xb_2	25,9	80,7	151,6	0,53	0,16	0,0908	0,0015	1,9898	0,0281	0,1590	0,0015	0,68	951,1	8,5	1441,7	31,6	34,0
xb_4	133,3	224,1	280,1	0,80	0,22	0,1355	0,0019	7,5116	0,0865	0,4020	0,0035	0,76	2178,3	16,1	2170,6	24,3	-0,4
xb_5	10,6	73,5	79,6	0,92	0,30	0,0732	0,0020	1,1178	0,0279	0,1108	0,0015	0,54	677,4	8,6	1018,5	55,2	33,5
xb_6	20,3	29,7	43,1	0,69	0,20	0,1340	0,0024	7,3037	0,1124	0,3953	0,0045	0,73	2147,2	20,6	2151,4	30,7	0,2
xb_7	52,4	39,0	140,5	0,28	0,07	0,1908	0,0036	12,5868	0,2085	0,4786	0,0064	0,80	2521,1	27,7	2748,7	30,7	8,3
xb_8	123,7	89,7	301,5	0,30	0,09	0,1311	0,0018	6,7646	0,0767	0,3744	0,0032	0,74	2049,9	14,8	2112,3	24,2	3,0
xb_9	143,4	176,9	314,8	0,56	0,16	0,1378	0,0020	7,5072	0,0881	0,3952	0,0034	0,74	2147,0	15,9	2199,4	24,6	2,4
xb_10	36,4	25,7	47,2	0,54	0,15	0,2518	0,0039	22,2249	0,2978	0,6403	0,0069	0,80	3190,2	27,1	3195,9	24,5	0,2
xb_11	23,9	20,5	49,6	0,41	0,19	0,1503	0,0027	8,3753	0,1321	0,4043	0,0047	0,74	2188,6	21,6	2349,0	30,8	6,8
xb_12	22,2	40,3	114,7	0,35	0,14	0,0947	0,0018	1,7682	0,0293	0,1355	0,0015	0,65	819,0	8,2	1521,5	35,8	46,2
xb_13	12,3	36,9	27,2	1,36	0,38	0,1198	0,0025	5,7971	0,1058	0,3511	0,0044	0,68	1939,9	20,9	1952,6	36,4	0,7
xb_14*	8,0	90,2	63,2	1,43	0,44	0,0604	0,0020	0,8126	0,0253	0,0976	0,0015	0,48	600,5	8,5	617,2	71,4	2,7
xb_15*	18,0	164,8	146,3	1,13	0,35	0,0609	0,0015	0,8345	0,0183	0,0994	0,0012	0,54	610,8	6,8	636,0	51,7	4,0
xb_16*	8,7	75,5	71,3	1,06	0,34	0,0605	0,0019	0,8556	0,0243	0,1026	0,0014	0,49	629,7	8,4	620,7	65,5	-1,4
xb_17*	8,2	63,6	71,9	0,88	0,32	0,0687	0,0035	0,9452	0,0437	0,0998	0,0022	0,49	613,4	13,1	889,0	100,4	31,0
xb_18	99,8	261,8	211,4	1,24	0,36	0,1297	0,0021	6,7662	0,0953	0,3784	0,0037	0,68	2068,9	17,1	2093,8	28,7	1,2
xb_19	70,8	164,7	155,6	1,06	0,30	0,1260	0,0021	6,4589	0,0923	0,3719	0,0036	0,68	2038,4	17,0	2042,4	29,1	0,2
xb_20	42,9	64,9	127,8	0,51	0,14	0,1170	0,0021	5,1566	0,0805	0,3196	0,0033	0,67	1787,9	16,3	1911,2	31,9	6,5
xb_21	63,2	100,7	141,5	0,71	0,23	0,1488	0,0026	7,9985	0,1229	0,3899	0,0040	0,67	2122,4	18,7	2332,0	30,0	9,0
xb_22*	8,7	140,2	61,2	2,29	0,64	0,0600	0,0025	0,8285	0,0316	0,1001	0,0017	0,45	615,1	10,2	604,3	86,5	-1,8
xb_23	123,5	29,7	357,5	0,08	0,03	0,1248	0,0022	6,2036	0,0937	0,3606	0,0036	0,65	1985,2	16,9	2025,4	30,5	2,0
xb_24	178,0	294,2	460,4	0,64	0,19	0,1265	0,0022	6,1823	0,0940	0,3544	0,0035	0,65	1955,4	16,7	2050,4	30,6	4,6
xb_25	58,2	63,8	208,7	0,31	0,12	0,1189	0,0022	4,4553	0,0726	0,2718	0,0029	0,65	1550,1	14,5	1939,3	33,0	20,1

xb_26	72,4	130,6	189,5	0,69	0,21	0,1225	0,0023	5,8626	0,0985	0,3471	0,0037	0,64	1920,6	17,8	1993,0	33,5	3,6
xb_27	129,0	211,4	296,8	0,71	0,20	0,1324	0,0025	7,1070	0,1159	0,3893	0,0040	0,63	2119,7	18,6	2129,8	32,1	0,5
xb_28	98,3	51,9	154,3	0,34	0,09	0,2500	0,0047	19,8899	0,3327	0,5769	0,0063	0,65	2936,2	25,6	3184,9	29,6	7,8
xb_29	38,0	10,5	94,2	0,11	0,03	0,1367	0,0028	7,5643	0,1391	0,4013	0,0047	0,64	2175,2	21,8	2185,6	35,4	0,5
xb_30	7,3	39,8	36,0	1,10	0,49	0,0752	0,0033	1,1397	0,0461	0,1098	0,0022	0,50	671,8	12,8	1075,0	85,9	37,5
xa_13*	18,7	165,3	154,4	1,07	0,32	0,0612	0,0028	0,8452	0,0353	0,1003	0,0020	0,47	616,0	11,6	644,5	94,5	4,4
xa_14	77,8	108,2	162,3	0,67	0,20	0,1375	0,0037	7,8771	0,1896	0,4157	0,0064	0,64	2241,0	29,0	2195,4	45,9	-2,1
xa_15*	17,9	208,9	130,2	1,60	0,48	0,0595	0,0028	0,8426	0,0368	0,1027	0,0021	0,47	630,2	12,2	586,3	99,5	-7,5
xa_16	21,8	44,6	47,4	0,94	0,29	0,1248	0,0047	6,5112	0,2265	0,3786	0,0086	0,65	2069,5	40,1	2025,5	65,4	-2,2
xa_17	36,9	46,1	76,6	0,60	0,19	0,1381	0,0042	8,0092	0,2209	0,4208	0,0074	0,64	2264,0	33,7	2203,2	51,9	-2,8
xa_18	144,6	209,0	308,6	0,68	0,22	0,1289	0,0035	7,0046	0,1711	0,3943	0,0058	0,60	2142,8	26,6	2082,5	47,3	-2,9
xa_19	65,2	52,7	145,7	0,36	0,10	0,1612	0,0045	9,3420	0,2359	0,4205	0,0066	0,62	2262,7	29,9	2467,9	46,8	8,3
xa_20	7,6	10,1	33,3	0,30	0,10	0,0935	0,0052	2,8337	0,1445	0,2198	0,0063	0,56	1280,6	33,4	1498,7	101,1	14,6
xa_21	203,3	381,6	523,1	0,73	0,21	0,1381	0,0038	6,5442	0,1600	0,3438	0,0047	0,56	1904,7	22,7	2203,4	47,0	13,6
xa_22*	8,2	90,8	66,3	1,37	0,39	0,0587	0,0042	0,8089	0,0550	0,0999	0,0027	0,39	614,0	15,6	556,5	149,5	-10,3
xa_24	87,6	178,0	215,7	0,83	0,23	0,1308	0,0040	6,4915	0,1788	0,3601	0,0057	0,58	1982,4	27,2	2108,5	52,8	6,0
xa_27	184,1	128,5	277,2	0,46	0,13	0,2470	0,0077	20,5924	0,5804	0,6047	0,0098	0,57	3048,8	39,2	3165,6	48,8	3,7
xa_28	267,2	361,9	610,6	0,59	0,17	0,1323	0,0042	7,1332	0,2016	0,3912	0,0060	0,54	2128,2	27,9	2128,4	54,1	0,0
xa_29	143,4	135,2	328,6	0,41	0,13	0,1345	0,0045	7,3875	0,2249	0,3984	0,0069	0,57	2161,5	31,6	2157,7	57,7	-0,2
xa_30	65,6	82,100	160,3	0,51	0,12	0,1236	0,0046	6,1249	0,2065	0,3594	0,0070	0,58	1979,4	33,4	2009,0	64,4	1,5
BRANCO (White Granite)																	
ab_21*	15,3	122,2	132,0	0,93	0,28	0,0642	0,0021	0,8412	0,0251	0,0951	0,0014	0,48	585,5	8,0	747,8	67,0	21,7
ab_22*	19,8	245,5	155,5	1,58	0,45	0,0599	0,0019	0,7858	0,0231	0,0952	0,0013	0,48	586,5	7,9	598,4	67,6	2,0
ab_23*	2,9	23,6	26,2	0,90	0,26	0,0656	0,0053	0,8648	0,0665	0,0957	0,0029	0,39	589,2	16,9	792,2	161,8	25,6
ab_25*	42,7	753,6	258,4	2,92	0,92	0,0632	0,0018	0,8625	0,0224	0,0990	0,0014	0,53	608,5	7,9	715,3	59,7	14,9
ab_26*	11,7	159,4	89,4	1,78	0,47	0,0629	0,0026	0,8295	0,0315	0,0956	0,0016	0,44	588,8	9,3	705,5	84,3	16,5
ab_27*	6,5	60,9	56,6	1,07	0,32	0,0613	0,0030	0,8218	0,0379	0,0973	0,0019	0,42	598,5	11,1	649,2	102,3	7,8
ab_28*	18,0	209,3	149,1	1,40	0,40	0,0588	0,0029	0,7849	0,0362	0,0969	0,0019	0,43	596,2	11,3	558,6	104,0	-6,7
ab_29*	21,6	238,4	163,2	1,46	0,46	0,0669	0,0021	0,9090	0,0264	0,0986	0,0015	0,52	606,2	8,7	834,3	65,2	27,3
ab_30*	16,6	182,1	118,8	1,53	0,46	0,0657	0,0044	0,8836	0,0552	0,0976	0,0028	0,45	600,5	16,2	795,7	134,9	24,5

ab_31	34,0	294,3	279,0	1,05	0,41	0,0670	0,0024	0,9995	0,0330	0,1082	0,0018	0,51	662,1	10,6	839,0	73,5	21,1
ab_32*	10,6	87,1	74,0	1,18	0,45	0,0977	0,0049	1,3932	0,0623	0,1034	0,0026	0,56	634,4	15,1	1581,3	90,2	59,9
ab_33*	14,0	89,4	125,9	0,71	0,20	0,0599	0,0026	0,8027	0,0326	0,0973	0,0019	0,47	598,4	10,9	598,8	92,4	0,1
ab_34*	15,4	112,6	122,1	0,92	0,31	0,0674	0,0032	0,9206	0,0401	0,0991	0,0020	0,46	609,0	11,5	850,4	94,6	28,4

Appendix 4.C - Scanning Electron Microscope (SEM) Cathodoluminescence images of zircon grains from the Passa Tres granitoids. A) Euhedral zircon grain from the GEM granite, showing an euhedral, oscillatory zoned overgrowth surrounding a euhedral, unzoned Paleoproterozoic core; B) Euhedral to subhedral zircon grains from the GEF granite displaying inherited cores. The grain on the left has a high-U core of Paleoproterozoic age; C) Euhedral grain with a fine oscillatory zoning of magmatic origin surrounding a zoned core of Paleoproterozoic age. The last growth band appears darker which indicates a U enrichment in the late stage of the magmatic evolution; D) Euhedral zircon grains with cores. The grain in the upper part displays a Paleoproterozoic core wrapped by a Neoproterozoic, zoned, overgrowth of magmatic origin. Circles correspond to the laser spots (26 μm). Errors are ± 2 sigma.



Appendix 4.D - ⁴⁰Ar-³⁹Ar stepwise heating analytical data for eight muscovite samples from the Passa Três gold deposit, South Brazil. Data in red represent negative values.

Sample	Step	³⁶ Ar [fA]	³⁷ Ar [fA]	³⁸ Ar [fA]	³⁹ Ar [fA]	⁴⁰ Ar [fA]	40(r)/39(k)	± 2s	Age ± 2s (Ma)	40Ar(r) (%)	39Ar(k) (%)
BD-31B Muscovite	1	0,2006977	0,1284294	0,151714	0,3099	66,60	23,59276	± 3,53036	157,89	10,98	0,02
	2	0,0635131	0,1980817	0,107576	0,4429	55,57	83,14744	± 4,57444	504,17	± 24,21	66,25
	3	0,0412435	0,0864731	0,124791	0,6581	61,08	74,31184	± 3,35292	456,80	± 18,21	80,06
	4	0,0220427	0,6136075	0,068212	1,1086	94,38	79,32434	± 1,89249	483,82	± 10,13	93,14
	5	0,0052310	0,0931431	0,083308	1,3256	117,00	87,10393	± 2,71563	524,98	± 14,21	98,68
	6	0,0043249	0,0220108	0,018347	1,7380	165,12	94,25993	± 1,85062	562,03	± 9,48	99,21
	7	0,0065637	0,1590566	0,037667	2,3223	211,81	90,37414	± 1,25914	542,01	± 6,52	99,08
	8	0,0163523	0,0680698	0,044046	3,7312	361,20	95,49690	± 0,75563	568,36	± 3,86	98,65
	9	0,0122250	0,0475215	0,162701	13,0609	1307,02	99,78553	± 0,37634	590,13	± 1,90	99,71
	10	0,1940953	0,1141084	0,235711	15,9755	1658,96	100,24358	± 0,37250	592,44	± 1,88	96,53
	11	0,0373593	0,2870251	0,244968	16,6419	1695,71	101,22377	± 0,36686	597,37	± 1,84	99,34
	12	0,0470770	0,1716602	0,491155	34,4026	3530,24	102,20237	± 0,33405	602,29	± 1,67	99,60
	13	0,0184522	0,1136399	0,486684	35,6912	3671,01	102,69275	± 0,33656	604,74	± 1,68	99,84
	14	0,0212647	0,2524388	0,551945	43,3262	4466,04	102,92565	± 0,34128	605,91	± 1,71	99,85
	15	0,0176051	0,0067693	0,332157	25,1086	2581,75	102,60645	± 0,35267	604,31	± 1,77	99,79
	16	0,0204029	0,5207910	0,447191	29,7283	3070,16	103,06440	± 0,34385	606,60	± 1,72	99,80
	17	0,0265778	0,2895553	0,424341	30,3186	3132,83	103,06289	± 0,35847	606,59	± 1,79	99,74
	18	0,0124175	0,5037747	0,557988	40,9040	4221,57	103,10937	± 0,33702	606,83	± 1,68	99,90
	19	0,1922141	0,0746752	0,356528	21,9387	2302,64	102,36003	± 0,36191	603,08	± 1,81	97,52
	20	0,0071189	0,2410039	0,318990	22,5294	2323,06	103,01121	± 0,36560	606,34	± 1,83	99,90
	21	0,0105209	0,0750370	0,535714	37,7923	3896,27	103,00538	± 0,34616	606,31	± 1,73	99,91
	22	0,0125918	0,3961364	0,475160	33,9618	3509,83	103,22896	± 0,34522	607,42	± 1,73	99,89
	23	0,0506663	0,0796052	0,809243	58,7216	6082,81	103,32240	± 0,31621	607,89	± 1,58	99,74
	24	0,0350358	0,0320194	0,961560	67,9315	7040,50	103,47923	± 0,31869	608,67	± 1,59	99,84
	25	0,0123834	0,0035644	0,562120	36,4403	3764,70	103,20151	± 0,37265	607,29	± 1,86	99,89
	26	0,0091397	0,3693064	0,436579	24,0374	2485,63	103,28734	± 0,39934	607,72	± 2,00	99,88
	27	0,0044689	0,0834069	0,460202	19,0469	1975,67	103,64760	± 0,46408	609,52	± 2,32	99,92
	28	0,0417714	0,3615366	0,545981	59,4748	6171,58	103,55173	± 0,30986	609,04	± 1,55	99,79
	29	0,0185162	0,0789264	0,503990	48,6538	5048,24	103,63655	± 0,33019	609,46	± 1,65	99,88

30	0,0122558	0,2170791	0,260952	34,6861	3598,26	103,62451	± 0,34983	609,40	± 1,75	99,89	1,83
31	0,0166987	0,2345436	0,431358	45,1060	4679,72	103,63104	± 0,32621	609,43	± 1,63	99,89	2,38
32	0,0172586	0,0240688	0,681616	60,0168	6238,52	103,85164	± 0,32351	610,53	± 1,61	99,91	3,17
33	0,0187086	0,5774339	0,678966	59,8050	6207,37	103,69293	± 0,31757	609,74	± 1,59	99,90	3,16
34	0,0196209	0,3770655	0,731375	59,4418	6169,02	103,67633	± 0,31731	609,66	± 1,58	99,90	3,14
35	0,0065571	0,2643185	0,339783	26,9266	2799,67	103,89407	± 0,39053	610,75	± 1,95	99,92	1,42
36	0,0065061	0,1262397	0,420255	30,1336	3125,53	103,64937	± 0,40702	609,52	± 2,03	99,93	1,59
37	0,0146661	0,2238422	0,695995	58,7507	6112,31	103,95531	± 0,31952	611,05	± 1,59	99,92	3,10
38	0,0143945	0,3048220	0,715606	53,5151	5558,26	103,77512	± 0,32489	610,15	± 1,62	99,91	2,83
39	0,0178198	0,2830751	0,906087	68,4671	7104,92	103,68530	± 0,30958	609,70	± 1,55	99,92	3,62
40	0,0115741	0,3158443	0,737775	54,1016	5621,55	103,83537	± 0,31956	610,45	± 1,59	99,93	2,86
41	0,0075725	0,1559292	0,471743	31,7986	3305,15	103,86083	± 0,36484	610,58	± 1,82	99,92	1,68
42	0,0062157	0,3590297	0,375047	27,7561	2887,96	103,97383	± 0,38698	611,14	± 1,93	99,93	1,47
43	0,0064250	0,2361470	0,542262	36,5943	3810,26	104,06116	± 0,34242	611,58	± 1,71	99,94	1,93
44	0,0196508	0,6809171	1,178571	88,9444	9250,81	103,93290	± 0,31638	610,94	± 1,58	99,93	4,70
45	0,0131440	0,3518036	0,798628	58,5346	6095,48	104,05958	± 0,31333	611,57	± 1,56	99,93	3,09
46	0,0070229	0,1647668	0,447069	34,9410	3645,14	104,25444	± 0,35985	612,54	± 1,79	99,93	1,85
47	0,0033048	0,0283599	0,238528	20,1477	2094,59	103,90357	± 0,45106	610,79	± 2,25	99,94	1,06
48	0,0051816	0,2455969	0,327376	25,0566	2611,52	104,15211	± 0,39531	612,03	± 1,97	99,93	1,32
49	0,0160038	0,0063179	1,008685	82,2643	8579,99	104,23070	± 0,30323	612,42	± 1,51	99,94	4,35
50	0,0089353	0,4165996	0,616918	44,3457	4625,42	104,23304	± 0,33951	612,44	± 1,69	99,93	2,34
51	0,0048717	0,1309955	0,275061	23,9567	2499,42	104,25986	± 0,40182	612,57	± 2,00	99,93	1,27
52	0,1092976	0,0608260	1,712012	139,7040	14619,44	104,40484	± 0,29780	613,29	± 1,48	99,77	7,38
Total											
age:											
1	0,4799275	0,2305539	0,1053692	1,86867	315,891	93,12453	± 3,21137	556,20	± 16,51	55,09	0,81
2	0,0026812	0,0932024	0,0000539	1,69156	171,237	100,74338	± 3,58068	594,96	± 18,02	99,52	0,73
3	0,0161416	0,1596780	0,1525883	8,16370	836,231	101,83601	± 0,79625	600,45	± 3,99	99,42	3,54
4	0,0273325	0,2140569	0,6891490	52,70319	5469,840	103,62215	± 0,31461	609,39	± 1,57	99,84	22,85
5	0,0061125	0,0339740	0,2961685	19,06259	1972,761	103,38400	± 0,44355	608,20	± 2,22	99,90	8,27
6	0,0200911	0,1033065	0,6613881	51,24673	5319,842	103,68320	± 0,31645	609,69	± 1,58	99,88	22,22
7	0,0112680	0,0268765	0,4909752	36,29008	3767,761	103,72191	± 0,34152	609,89	± 1,70	99,90	15,74
8	0,0017354	0,1115889	0,0033698	4,94908	509,417	102,81479	± 1,33831	605,35	± 6,70	99,89	2,15
9	0,0069972	0,0094422	0,2562967	17,82425	1841,499	103,18869	± 0,45428	607,22	± 2,27	99,88	7,73

BD-46
Muscovite

10	0,0002459	0,0909477	0,0297797	3,13850	320,981	102,23486	± 2,09104	602,45	± 10,48	99,97	1,36
11	0,0040089	0,0810951	0,2361291	16,23582	1681,692	103,49737	± 0,51854	608,77	± 2,59	99,92	7,04
12	0,0029640	0,0600866	0,1346717	8,38438	866,492	103,23086	± 0,82530	607,43	± 4,12	99,89	3,64
13	0,0018362	0,0415308	0,1119089	4,86862	503,200	103,23650	± 1,32695	607,46	± 6,63	99,88	2,11
14	0,0039072	0,03775209	0,0343179	4,18335	425,009	101,32387	± 1,48196	597,88	± 7,45	99,73	1,81
Total											608.85 ± 2.10
age:											38,23
BD-83A											± 26,46
1	0,2649301	0,2497536	0,0662635	0,61004	126,786	79,43359	± 4,94628	484,41	± 11,82	98,96	0,71
2	0,0052361	0,1797045	0,0316120	1,55605	150,980	96,00616	± 2,31787	570,96	± 3,46	98,60	2,78
3	0,0299956	0,0688765	0,0646365	6,08270	638,429	103,49309	± 0,69291	608,74	± 1,85	99,64	15,83
4	0,0429310	0,0453353	0,4576990	34,61605	3609,917	103,90809	± 0,37142	610,82	± 1,96	99,89	11,58
5	0,0093177	0,0633777	0,3517901	25,33475	2650,695	104,50892	± 0,39397	613,81	± 1,91	99,85	10,51
6	0,0112266	0,1906956	0,2507851	22,98253	2393,254	103,98095	± 0,38285	611,18	± 1,82	99,88	16,32
7	0,0134744	0,0519279	0,4418879	35,68638	3715,943	104,00672	± 0,36519	611,31	± 1,89	99,90	11,95
8	0,0084978	0,3170266	0,3317172	26,14573	2728,498	104,25353	± 0,37854	612,54	± 2,41	99,91	4,96
9	0,0031511	0,1744081	0,1751747	10,83901	1133,424	104,47089	± 0,48337	613,62	± 2,75	99,90	3,92
10	0,0028914	0,2482573	0,1551178	8,57420	897,979	104,62587	± 0,55309	614,39	± 1,92	99,93	9,58
11	0,0046789	0,0112844	0,2665781	20,94217	2184,214	104,22160	± 0,38611	612,38	± 4,08	99,96	2,26
12	0,0005162	0,2261311	0,0743849	4,93928	519,618	105,15336	± 0,81997	617,02	± 8,28	99,92	1,29
13	0,0006847	0,0671356	0,0396163	2,82588	296,312	104,77919	± 1,66413	615,16	± 8,22	99,84	1,13
14	0,0012422	0,1674356	0,0481175	2,47900	257,613	103,74962	± 1,64651	610,02	± 12,18	99,85	0,99
15	0,0011227	0,0547884	0,0654331	2,16210	225,541	104,15725	± 2,44287	612,06	± 2,10	99,91	5,92
16	0,0037546	0,1523332	0,2190673	12,94031	1346,354	103,94628	± 0,42190	611,01			
Total											612.15 ± 2.06
age:											18,82
BD-83A											± 24,64
1	2,2519380	0,2404632	0,4302982	2,38737	819,678	64,60610	± 4,39447	404,25	± 10,63	96,44	0,50
2	0,0387563	0,3156353	0,0348843	3,65495	323,170	85,26389	± 2,01645	516,52	± 5,31	95,49	1,06
3	0,1145208	0,2929378	0,0680364	7,74306	752,815	92,83853	± 1,03049	556,01	± 2,58	96,00	2,71
4	0,2821817	0,1957209	0,3009445	19,79924	2089,501	101,31163	± 0,51269	599,17	± 1,50	98,47	15,86
5	0,6234888	0,1105701	1,5864509	115,73131	12111,929	103,05408	± 0,29876	607,92	± 1,53	99,90	12,28
6	0,0296280	0,1593670	1,1534964	89,63376	9267,500	103,28588	± 0,30656	609,08	± 1,64	99,90	8,42
7	0,0190913	0,3838097	0,7813679	61,45860	6338,603	103,03567	± 0,32716	607,83	± 1,95	99,90	4,56
8	0,0100491	0,2190719	0,4688695	33,28370	3428,832	102,92054	± 0,38883	607,25			

9	0,0416055	0,4658489	1,8881692	144,66638	14954,394	103,27743	± 0,29927	609,04	± 1,50	99,91	19,83	
10	0,0166358	0,0665507	0,7508302	57,21513	5917,014	103,32153	± 0,32952	609,26	± 1,65	99,91	7,84	
11	0,0078394	0,1089943	0,2995331	22,67121	2338,909	103,05539	± 0,48060	607,93	± 2,41	99,89	3,11	
12	0,0077384	0,2321289	0,5086973	38,95473	4027,354	103,31806	± 0,37876	609,24	± 1,90	99,93	5,34	
13	0,0041202	0,4582806	0,3042572	19,20333	1987,549	103,43106	± 0,52178	609,81	± 2,61	99,93	2,63	
14	0,0011844	0,4456208	0,1533946	10,97478	1138,264	103,68125	± 0,82749	611,06	± 4,14	99,96	1,50	
15	0,0018686	0,1092882	0,1371090	10,02021	1028,568	102,58640	± 1,00906	605,58	± 5,06	99,94	1,37	
16	0,0051494	0,2527580	0,3468984	26,13583	2715,645	103,83872	± 0,43280	611,85	± 2,16	99,94	3,58	
17	0,0170809	0,0833805	0,8501882	66,08999	6878,565	103,99291	± 0,32083	612,62	± 1,60	99,92	9,06	
Total age: 608,80 ± 1,99												
BD-83B	1	0,3182592	0,0952629	0,1334262	5,23073	632,665	102,95962	± 1,12047	607,45	± 5,61	85,13	1,21
Muscovite	2	0,0518620	0,0786123	0,1526680	10,18967	1077,423	104,22441	± 0,65873	613,78	± 3,29	98,57	2,35
(250	3	0,0873875	0,0322274	0,2793344	23,26589	2453,823	104,34887	± 0,41846	614,40	± 2,09	98,94	5,37
micron)	4	0,0948978	0,0997826	0,4850324	34,55700	3625,369	104,08916	± 0,34891	613,10	± 1,74	99,22	7,97
	5	0,0993582	0,3362629	0,6647829	55,32578	5779,995	103,93065	± 0,32117	612,31	± 1,61	99,48	12,77
	6	0,0458001	0,0634346	0,3994182	32,09184	3350,211	103,96337	± 0,34692	612,47	± 1,73	99,59	7,40
	7	0,0611608	0,0921077	0,8523601	68,44167	7126,422	103,85048	± 0,31447	611,91	± 1,57	99,74	15,79
	8	0,0172732	0,0318864	0,3046835	21,63853	2255,995	104,01245	± 0,39599	612,72	± 1,98	99,76	4,99
	9	0,0224133	0,0286480	0,7458820	56,27520	5854,481	103,90577	± 0,31113	612,18	± 1,56	99,88	12,98
	10	0,0181791	0,2293025	0,3725967	30,52183	3188,353	104,27692	± 0,38520	614,04	± 1,92	99,82	7,04
	11	0,0149562	0,0459650	0,3458039	26,02318	2714,012	104,11286	± 0,40666	613,22	± 2,03	99,83	6,00
	12	0,0062607	0,0642244	0,1473621	9,25290	966,789	104,27440	± 0,54714	614,03	± 2,73	99,80	2,14
	13	0,0024856	0,1212319	0,0478706	3,07752	321,679	104,27058	± 1,31435	614,01	± 6,56	99,76	0,71
	14	0,0262160	0,1588687	0,7411136	57,49914	6007,759	104,33945	± 0,36447	614,35	± 1,82	99,86	13,27
Total age: 612,96 ± 1,95												
BD-83B	1	0,0625620	0,0177459	0,0669668	0,19480	34,603	82,71909	± 71,18152	500,73	± 376,38	46,57	0,05
Muscovite	2	0,0066717	0,1996893	0,0010225	0,52979	56,660	103,15774	± 32,43683	605,69	± 161,84	96,48	0,14
(500	3	0,0038998	0,1219546	0,0171463	1,40806	155,877	109,88993	± 13,01174	638,98	± 63,74	99,26	0,37
micron)	4	0,0054169	0,4604797	0,0232281	2,36221	254,051	106,82864	± 7,56225	623,92	± 37,35	99,35	0,61
	5	0,0203723	0,2639360	0,1129987	7,54681	797,668	104,89430	± 2,41286	614,34	± 11,98	99,24	1,96
	6	0,0437694	0,0426178	0,2456012	14,40210	1513,072	104,15106	± 1,29835	610,64	± 6,46	99,14	3,74
	7	0,0394040	0,1566603	0,4347394	28,54726	2973,388	103,74006	± 0,74042	608,60	± 3,69	99,60	7,41

8	0,0205704	0,1549141	0,4340943	29,60154	3080,875	103,86408	± 0,46009	609,22	± 2,29	99,79	7,69
9	0,0214139	0,2741091	0,2833600	18,61464	1926,507	103,14699	± 0,52554	605,64	± 2,62	99,66	4,83
10	0,0283495	0,2398966	0,4095537	26,59701	2766,347	103,68660	± 0,47674	608,33	± 2,38	99,69	6,91
11	0,0330390	0,2644723	0,6247126	39,76208	4132,258	103,67055	± 0,44393	608,25	± 2,21	99,76	10,32
12	0,0128824	0,0785976	0,3047686	20,42688	2137,156	104,42932	± 0,53779	612,03	± 2,67	99,81	5,30
13	0,0059579	0,0151361	0,0811519	7,33653	763,458	103,81251	± 0,89250	608,96	± 4,45	99,76	1,91
14	0,0024823	0,0691822	0,0222726	6,07220	628,937	103,44779	± 1,12879	607,14	± 5,63	99,87	1,58
15	0,0075900	0,4618967	0,1934958	13,21793	1376,254	103,94656	± 0,63664	609,63	± 3,17	99,83	3,43
16	0,1215332	0,5257430	2,2802260	168,49807	17576,541	104,09071	± 0,44910	610,34	± 2,23	99,79	43,75
Total											
age:											
609.03 ± 2.08											
BD-85B	1	0,0218520	0,4317501	0,0834516	0,07242	7,492	± 63,90575	101,01	± 421,50	14,34	0,01
Muscovite	2	0,0087641	0,0380316	0,1542256	0,14970	4,599	± 29,59946	91,62	± 196,24	43,86	0,03
	3	0,0126615	0,0984303	0,1986928	0,13699	8,605	± 52,35077	232,85	± 321,01	56,70	0,03
	4	0,0159656	0,1380733	0,2641701	0,14598	10,453	± 52,99594	256,20	± 320,79	55,07	0,03
	5	0,0043919	0,0067818	0,1978771	0,12961	6,879	± 64,06985	278,20	± 383,14	81,24	0,03
	6	0,0362555	0,0293813	0,2418494	0,42849	51,394	± 38,69444	564,23	± 197,54	79,16	0,08
	7	0,0026683	0,1776213	0,0220396	0,58880	61,425	± 30,63527	605,01	± 152,91	98,73	0,11
	8	0,0033747	0,1419305	0,0113593	0,38866	40,918	± 46,44201	603,72	± 231,97	97,58	0,08
	9	0,0057984	0,0288477	0,0059352	0,74374	79,505	± 24,73490	612,83	± 122,93	97,84	0,15
	10	0,0030615	0,0113215	0,0322207	1,19760	122,852	± 14,86014	598,98	± 74,42	99,25	0,23
	11	0,0708341	0,1838815	0,0045062	1,60406	189,206	± 11,40568	614,25	± 56,64	88,92	0,31
	12	0,0073286	0,2452390	0,0629549	2,93993	314,418	± 6,29194	620,88	± 31,13	99,31	0,57
	13	0,0145487	0,1368833	0,0166621	4,64051	492,541	± 3,97181	615,85	± 19,71	99,12	0,90
	14	0,0365398	0,0763141	0,3916880	28,12754	2943,017	± 0,74967	611,08	± 3,73	99,62	5,48
	15	0,0295677	0,0432041	0,5176737	38,49419	4025,238	± 0,61292	611,54	± 3,05	99,77	7,51
	16	0,0085597	0,0508567	0,2133694	18,92752	1975,748	± 1,03555	611,09	± 5,15	99,86	3,69
	17	0,0274611	0,1904185	0,5520149	40,15227	4180,784	± 0,59603	609,45	± 2,97	99,80	7,83
	18	0,0404375	0,3259939	0,7323424	49,21222	5100,498	± 0,55552	606,86	± 2,77	99,76	9,60
	19	0,0474089	0,5725434	0,8314305	54,16307	5608,565	± 0,52699	606,32	± 2,63	99,74	10,56
	20	0,0349277	0,0508991	0,4978213	30,12323	3111,130	± 0,75431	604,55	± 3,77	99,66	5,87
	21	0,0155944	0,0168288	0,2931394	18,98413	1961,658	± 1,01681	605,30	± 5,07	99,76	3,70
	22	0,0320023	0,0588337	0,9176749	66,87503	6964,209	± 0,46396	609,83	± 2,31	99,86	13,04
	23	0,0270968	0,4520289	0,5248340	40,13195	4178,362	± 0,46134	609,43	± 2,30	99,80	7,83

24	0,0104325	0,0088077	0,1350829	10,82734	1120,276	103,17284	± 0,81487	605,77	± 4,07	99,72	2,11
25	0,0069652	0,0264163	0,1535926	10,19644	1060,889	103,83403	± 0,81464	609,07	± 4,06	99,80	1,99
26	0,0024607	0,0224004	0,0494843	4,01710	415,439	103,22612	± 1,94708	606,04	± 9,71	99,82	0,78
27	0,0056364	0,0232827	0,1758377	15,63557	1634,238	104,40408	± 0,64963	611,90	± 3,23	99,89	3,05
28	0,0026377	0,1737536	0,1714127	11,25756	1176,855	104,46273	± 0,79695	612,19	± 3,96	99,93	2,20
29	0,0006351	0,0379489	0,1275206	5,04157	528,163	104,71637	± 1,48838	613,45	± 7,39	99,96	0,98
30	0,0212665	0,0658148	0,7595234	57,52698	6029,073	104,68517	± 0,43944	613,30	± 2,18	99,89	11,22
Total											608.38 ± 2.25
BD-88	1	0,1077370	0,2701927	0,1507952	0,63983	100,144	± 11,863	625,31	± 58,71	68,23	0,32
Muscovite	2	0,0042883	0,2752588	0,0508556	1,18249	131,523	± 6,625	641,86	± 32,48	99,05	0,60
	3	0,0604046	0,1805189	0,3796371	26,06905	2740,977	± 0,433	613,52	± 2,16	99,34	13,19
	4	0,0152679	0,2435111	0,4054728	32,21856	3352,401	± 0,380	610,79	± 1,90	99,86	16,30
	5	0,0030345	0,0000000	0,1175031	8,52015	888,150	± 0,617	611,90	± 3,07	99,89	4,31
	6	0,0074612	0,1959836	0,2783326	18,55117	1925,126	± 0,441	609,51	± 2,20	99,88	9,39
	7	0,0140516	0,1439971	0,5264048	41,42175	4308,574	± 0,379	610,81	± 1,89	99,89	20,96
	8	0,0032859	0,0616718	0,0972350	8,81603	918,048	± 0,628	611,35	± 3,13	99,89	4,46
	9	0,0041464	0,1664649	0,1598868	10,72911	1116,021	± 0,565	610,76	± 2,82	99,88	5,43
	10	0,0044667	0,0000000	0,1580463	12,36398	1285,930	± 0,509	610,71	± 2,54	99,89	6,26
	11	0,0014976	0,0000000	0,0765499	4,49780	473,507	± 1,134	617,05	± 5,64	99,89	2,28
	12	0,0013146	0,0000000	0,0869541	6,42477	670,243	± 0,770	612,49	± 3,84	99,93	3,25
	13	0,0008459	0,1633338	0,0476829	4,46971	465,592	± 1,006	611,80	± 5,01	99,94	2,26
	14	0,0002710	0,2102901	0,0323015	5,82031	611,496	± 0,848	616,48	± 4,22	99,98	2,95
	15	0,0203854	0,1366760	0,2917910	15,88653	1664,573	± 0,457	613,23	± 2,28	99,63	8,04
Total											611.92 ± 2.03

Appendix 5.A - LA-ICP-MS analyses of selected pyrite, chalcopyrite, aikinite and native gold from the Passa Três Granites's gold deposit.

Mineral type	Co (ppm)	Ni (ppm)	Cu (ppm)	Zn (ppm)	As (ppm)	Se (ppm)	Mo (ppm)	Ag (ppm)	Sb (ppm)	Te (ppm)	Au (ppm)	Pb (ppm)	Bi (ppm)
Pyrite 2a	6,02	<2,17	1009,66	3,83	1,28	<2,42	<0,04	9,24	0,11	20,80	0,67	81,25	8,98
Pyrite 2a	0,16	3,68	26,64	45,44	0,35	<2,61	<0,05	0,52	0,04	2,56	0,03	7,99	0,82
Pyrite 2a	25,79	<2,51	11,73	3,74	<0,07	<2,91	<0,06	<0,03	<0,02	0,08	0,02	0,04	0,00
Pyrite 2a	208,83	10,84	32,88	6,19	0,22	<2,94	<0,06	0,10	<0,02	0,18	<0,01	0,78	0,05
Pyrite 2a	11,41	<2,49	3,11	<1,43	0,21	<2,92	<0,06	<0,03	0,03	<0,06	<0,01	0,09	0,00
Pyrite 2a	6,48	26,58	165,74	<4,55	0,91	<12,55	0,64	2,16	<0,09	3,22	0,18	46,55	2,91
Pyrite 2a	6,99	<3,43	214,56	1,98	0,29	<4,3	<0,11	1,06	<0,02	1,85	0,17	10,70	1,48
Pyrite 2a	79,67	<3,46	161,32	<1,76	0,32	<4,31	<0,10	0,24	<0,03	0,16	0,07	5,29	0,02
Pyrite 2a	2,63	<3,24	2567,88	<1,64	0,22	<4,17	0,16	5,54	<0,03	<0,081	0,23	2,18	0,09
Pyrite 2a	2,98	<9,32	215,04	<4,39	<0,29	<13,34	<0,35	0,34	<0,08	0,75	0,16	6,70	0,30
Pyrite 2b	116,94	7,24	6,13	3,82	0,09	<2,82	<0,06	0,12	0,03	1,69	0,02	1,86	0,55
Pyrite 2b	59,68	3,28	220,99	<1,35	0,87	<2,99	<0,07	1,02	0,06	5,86	0,15	12,26	1,91
Pyrite 2b	16,01	6,53	907,09	5,02	1,50	<4,29	<0,10	2,34	0,08	18,76	0,09	98,41	221,74
Pyrite 2b	33,33	11,56	467,78	<1,75	0,42	<3,95	0,15	0,35	<0,02	2,32	0,03	8,60	1,88
Pyrite 2b	186,41	11,37	2,54	<1,32	<0,058	<2,35	<0,04	2,12	<0,01	2,24	0,35	2,45	0,36
Pyrite 2b	20,60	3,01	2,45	<1,38	0,20	<2,46	<0,05	1,54	<0,01	1,85	0,43	2,78	0,34
Pyrite 2b	52,40	11,59	7,31	1,35	0,17	<2,48	<0,04	0,12	<0,01	0,48	<0,01	13,88	0,20
Pyrite 2b	7,12	<2,37	179,27	4,77	0,33	<2,69	<0,05	1,31	0,03	4,40	0,19	11,11	2,92
Pyrite 2b	1,12	<23,51	247859,81	67,86	0,88	<30,47	<0,78	0,64	<0,20	1,18	<0,19	18,48	6,59
Chalcopyrite	1,08	<18,43	18842,54	<8,99	<0,52	<24,35	2,27	0,56	<0,16	1,87	<0,15	10,45	6,32
Chalcopyrite	4,68	<11,66	205120,09	38,68	<0,34	<14,01	<0,32	1,55	0,27	2,51	0,11	18,85	9,54
Aikinite	<0,56	<11,31	43622,75	<5,38	0,35	34,12	<0,43	2,79	10,08	13,94	1,05	143622,59	16413,98
Aikinite	1,19	<26,22	132715,64	18,60	<0,771	96,69	<0,75	0,87	35,78	9,11	<0,19	419886,28	45934,55
Native gold	<0,02	<0,37	53,99	<0,18	<0,01	<0,51	<0,01	34,32	0,02	0,52	15,68	614,08	58,57